Supporting Information

Flexible Biguanide Mono- and Bimetallic Zinc Complexes for the Ring-Opening (Co)polymerization of Lactides

Benjamin Théron,[a†] Lukáš Vlk,[a‡] Tomáš Chlupatý,[‡] Marie-José Penouilh,[†] Eliška Procházková,[I] Raluca Malacea-Kabbara,[†] Pierre Le Gendre*,[†] Aleš Růžička[‡]**

[†]Univ. Bourgogne Europe, Institut de Chimie Moléculaire de l'Université de Bourgogne (ICMUB), UMR CNRS 6302, 9 Avenue Alain Savary, 21078 Dijon, France

[‡]Department of General and Inorganic Chemistry, Faculty of Chemical Technology, University of Pardubice, Studentská 573, CZ-532 10, Pardubice, Czech Republic.

[I]Institute of Organic Chemistry and Biochemistry, Czech Academy of Sciences, Flemingovo nám. 2, Prague 160 00, Czech Republic

[a] these authors contributed equally

e-mails: tomas.chlupaty@upce.cz, pierre.le-gendre@u-bourgogne.fr, ales.ruzicka@upce.cz

TABLE OF CONTENTS

Synthetic Aspects and Structural Investigation of 1

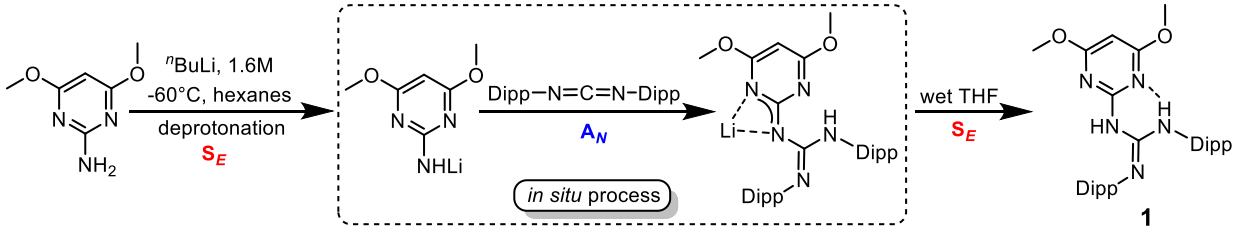

Scheme S1. Synthesis of **1**.

The protoligand **1** was prepared, in a high overall yield of 95 %, by a simple several-step one-pot procedure (Scheme ***S1***S1) where lithium 4,6-dimethoxypyrimidin-2-amide undergoes nucleophilic addition to cumulated multiple CN bonds of bis(2,6-diisopropylphenyl)carbodiimide[1]. In the final step, the reaction mixture was quenched by wet THF to give **1**.

NMR analysis of **1** helped to understand significant information about the shape, electronic behavior, and mutual orientation of **1** as well as further reactivity and structure of metal complexes. The stability of the N_5C_2 central system was corroborated by heating of **1** in Tol-d_8 in a vacuum-sealed NMR tube for 24 hours at 150°C with no effect on the structure or purity observed by spectroscopic methods. Structurally diverse hydrogen atoms of *NH* groups (for N*H*^{Dipp} 9.84 ppm in C_6D_6/9.66 ppm in THF-d_8; for N*H*^{Prm} 7.13 ppm in C_6D_6/6.75 ppm in THF-d_8 – Figures S2-S5) in central biguanide-like skeleton of **1**, and its signals absence after reactions with zinc reagents, allowed an easy evaluation of synthetic progress as well as probable structure estimation of formed zinc complexes. The ^{13}C NMR chemical shift values of central carbon atoms of N_5C_2 biguanide can serve as diagnostic tool for described synthetic and structural investigation (for pyrimidine - Ar_q^{Prm} 158.1 ppm at C_6D_6/158.4 ppm at THF-d_8; for guanidine - Ar_q^{Gua} 143.6 ppm at C_6D_6/143.7 ppm at THF-d_8).

On the other hand, possible appearance of different tautomers of **1** (see Figure 3 in the Main text) in C_6D_6 solution and more likely in THF-d_8, complicates the structure analysis. Based on the observation of two distinct sets of signals (an additional, very minor, set is visible at low temperature (Figure S4) in ^{1}H NMR spectra, one can predict that two dominant tautomers (Figure S1) are present. Both have strong intramolecular hydrogen bonds between N*H* groups and donor atoms, which can be assumed on the basis of lower field signals observed in ^{1}H NMR spectra at various temperatures. For minor tautomer **1B**, the proton of original N*H*^{Prm} is moved closer to Dipp moiety and observed at 5.72 ppm (C_6D_6) or 6.24 ppm (THF-d_8). This prototropic tautomerism in solution is reflected in values of

1. Chlupatý, T.; Nevoralová, J.; Ružičková, Z.; Ružička, A. Lithium and Dilithium Guanidinates, a Starter Kit for Metal Complexes Containing Various Mono- and Dianionic Ligands. *Inorg. Chem*. **2020**, *59*, 10854–10865. DOI : 10.1021/acs.inorgchem.0c01362.

other significant parameters, such as N*H*^{Dipp} (11.98 in C_6D_6 or 11.64 ppm in THF-d_8) and Ar*H*^{Prm} (5.20 in C_6D_6 or 5.48 ppm in THF-d_8) signals of **1B** in both deuterated solvents and has further been confirmed with the help of NOESY experiments (see Figure S48–S50) and VT ^{1}H NMR measurements in THF-d_8 in the range of 213–328 K (see spectra in Figure **S2** S2–S5).

The major/minor tautomer population of 89:11 mol % (see Figure S1) observed at room temperature changes gradually with decreasing the temperature to 213 K (66:34). The presence of two different species is also reflected in characteristic ^{13}C NMR parameters of **1** in THF-d_8 (δ(Ar_q^{Gua}/Ar_q^{Prm}) 143.7/158.4 for major **1A** and δ(Ar_q^{Gua}/Ar_q^{Prm}) 157.1/166.6 for minor tautomer **1B**). Purity of **1** was also confirmed by C, H, N-analysis.

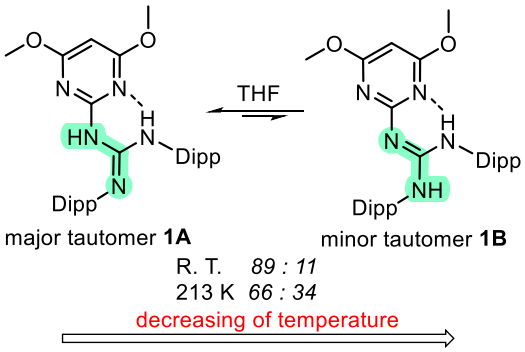

Figure S1. Prototropic guanidine tautomerism of **1** in THF-d_8 solution.

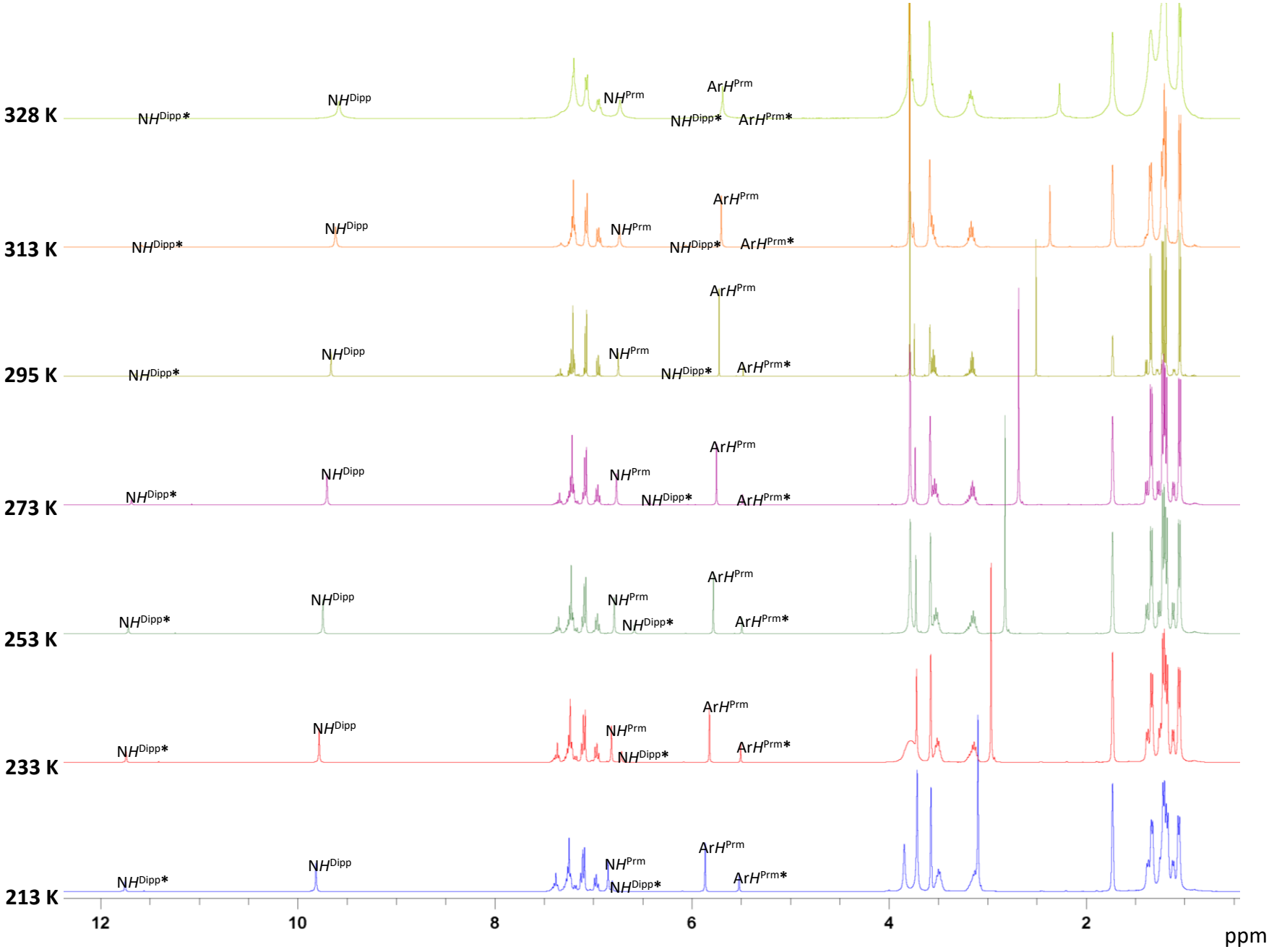

Figure S2. VT ^{1}H NMR spectra of **1** in THF-d_8, 213–328 K. Significant signals of minor tautomer are marked with asterisks.

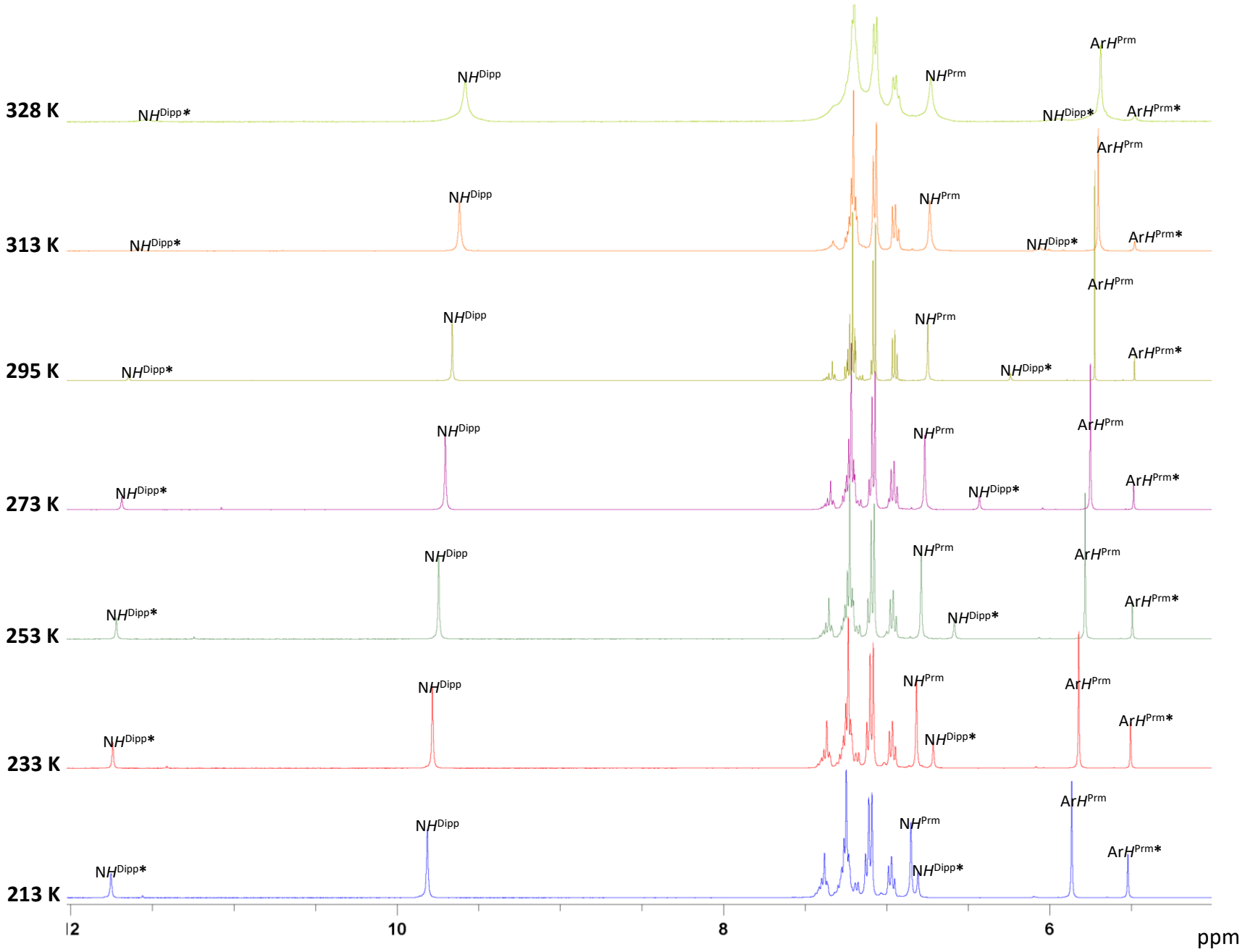

Figure S3. Detail of VT ^{1}H NMR spectra of **1** in THF-d_8, 213–328 K. Significant signals of minor tautomer are marked with asterisks.

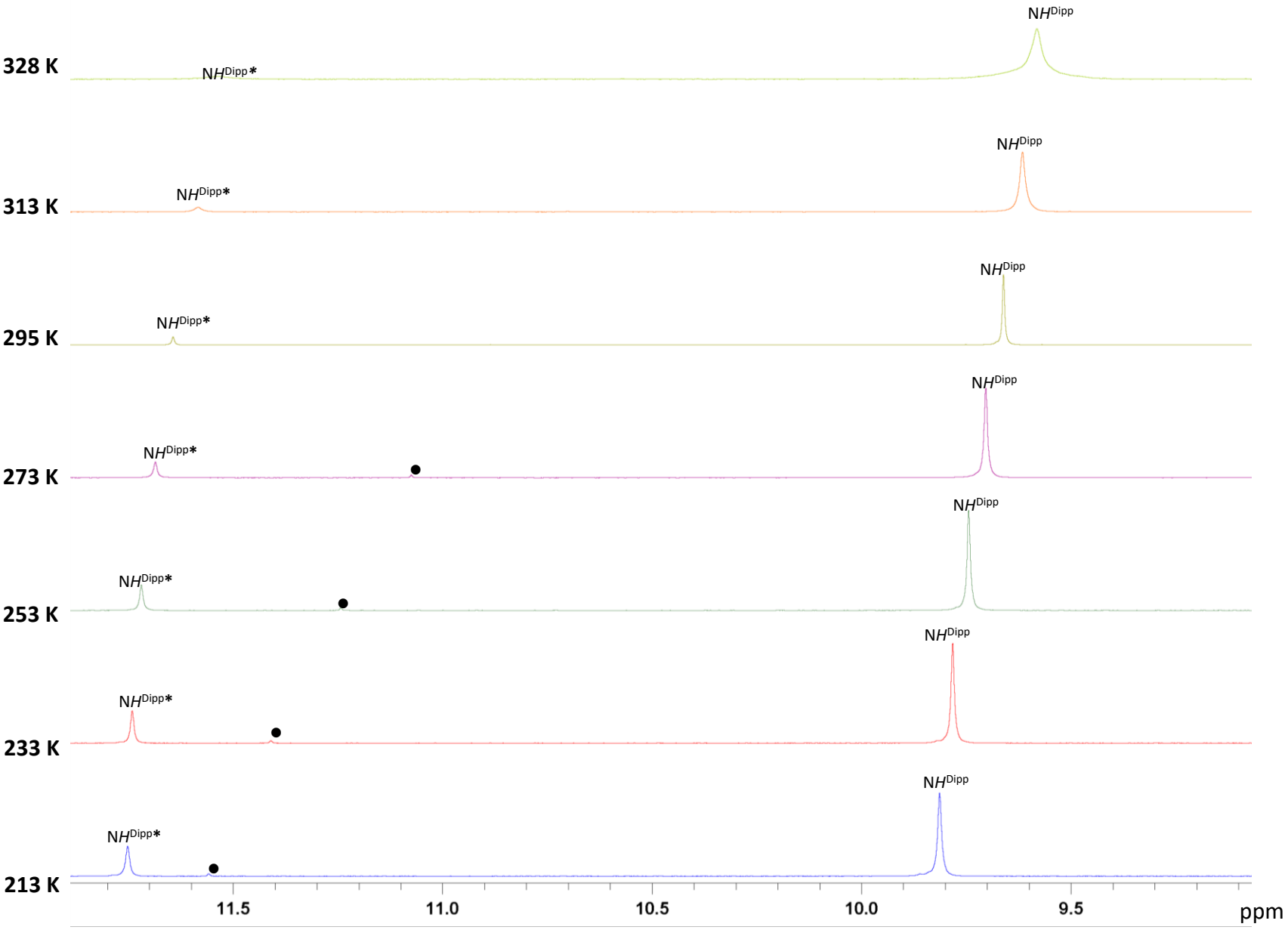

Figure S4. Detail of VT ^{1}H NMR spectra of **1** in THF-d_8, 213–328 K. Significant signals of minor tautomer are marked with asterisks. Most probably the signal of very minor isomer is marked with black dot. Relative intensities are 11/0/89 at 295 K and 34/0.08/66 at 213 K, respectively.

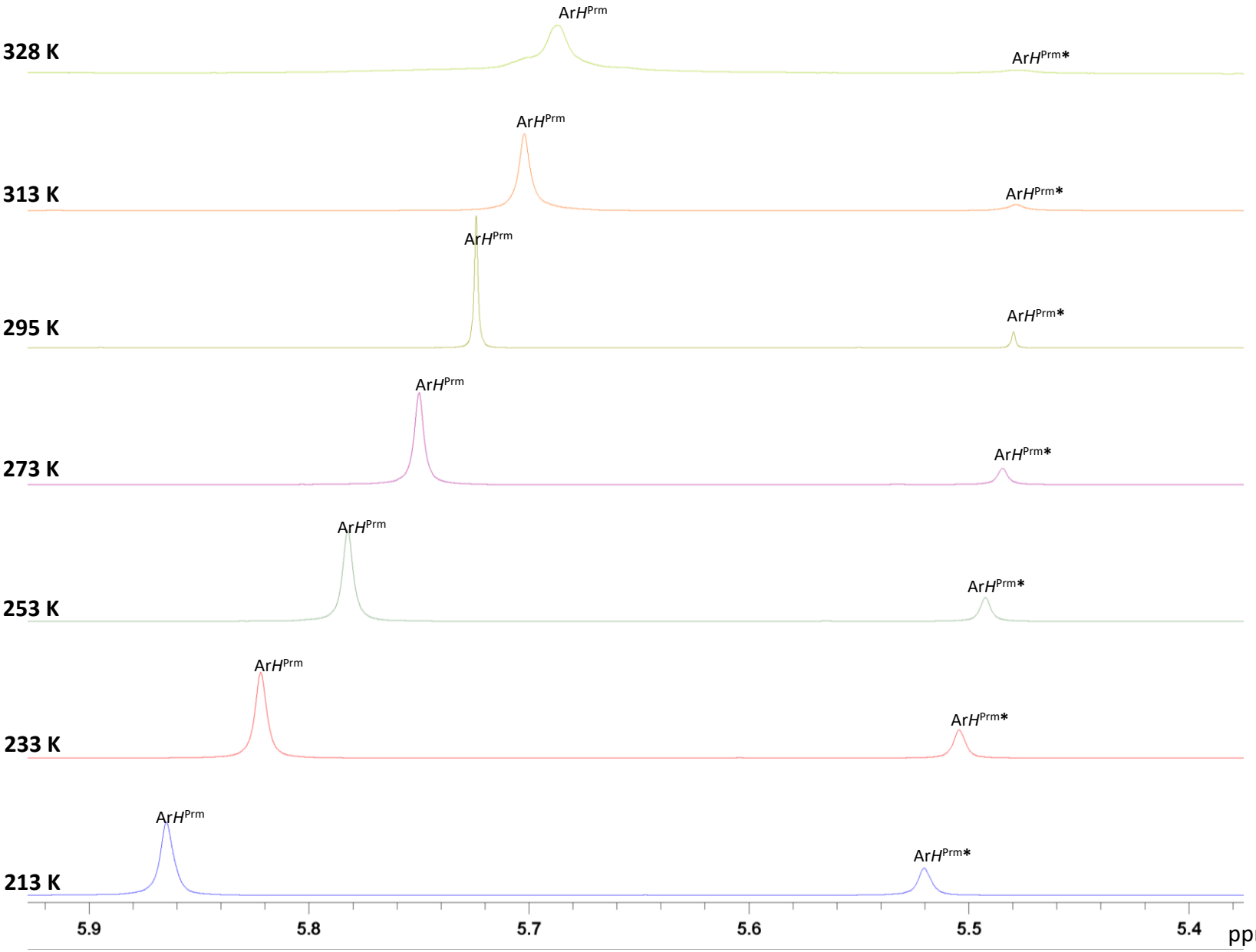

Figure S5. Detail of VT ^{1}H NMR spectra of **1** in THF-d_8, 213–328 K. Significant signals of minor tautomer are marked with asterisks.

In order to investigate tautomeric equilibria of **1** isomers in more details, theoretical calculations were performed. First, structures of possible isomers were optimized and DFT-calculated (B3LYP-D3/6-311+g(d,p)+CPCM(THF)) relative Gibbs' free energies mutually compared (Figure S6).

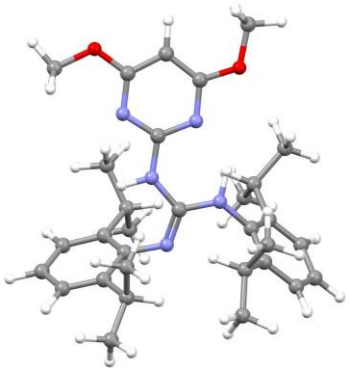

1A) observed in solid state as well as major isomer in solution in THF and even more dominant species in benzene

0 kcal.mol^{-1} in THF
2.92 kcal.mol^{-1} in C_6H_6

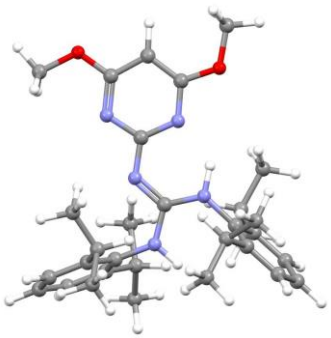

1B) observed as minor isomer in solution in THF, very minor in benzene (see text above)

0.18 kcal.mol^{-1} in THF
3.82 kcal.mol^{-1} in C_6H_6

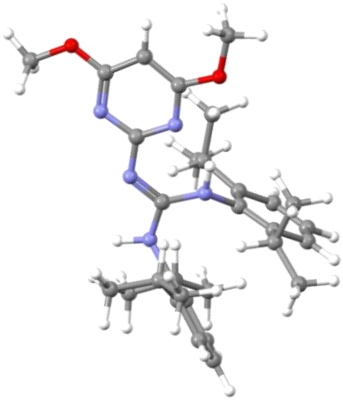

1C) most probably observed in THF solution at lower temperature as very minor isomer; similar arrangement as in some complexes

4.34 kcal.mol^{-1} in THF

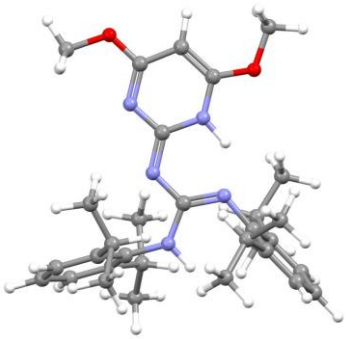

1D) not observed

7.79 kcal.mol^{-1} in THF

Figure S6. Optimized structures of possible tautomers/isomers of **1** along with relative Gibbs' free energies.

Results of DFT calculations for possible forms showed, two of them (**1A** and **1B**) are close in energy, while remaining two of them are higher by 4.34 and 7.79 kcal.mol^{-1}, respectively, which according to Boltzmann distribution means, their presence in lower than 1% and thus under the detection limit of NMR spectra. For most energetically relevant isomers of **1** (Figure S6 – **1A** and **1B**) the NMR spectra parameters were calculated by GIAO method (B3LYP/6-311+g(d,p)/D3/CPCM(THF)). Calculated ^{1}H NMR chemical shifts (calibrated to Me_4Si) for signals of hydrogen atoms involved in intramolecular H-bond agreed well for both isomers – δ 9.66 (meas. **1A**), 9.70 (calcd. **1A**), 11.65 (meas. **1B**), 11.71 (calcd. **1B**) – while the values for the second N*H* groups are a bit underestimated but reasonable in trends – δ 6.75 (meas. **1A**), 6.27 (calcd. **1A**), 6.24 (meas. **1B**), 4.55 (calcd. **1B**) – the value is maybe influenced by small residual amount of water. However indisputable is the fact the calculated chemical shielding values for signals in ^{13}C NMR spectra perfectly correlate with the experimental values of chemical shifts for each isomer (Table S1, Figure S7).

Table S1. List of measured ^{13}C NMR chemical shifts and its calculated chemical shieldings for major **1A** and minor **1B** tautomers of **1**

	major tautomer 1A			***minor tautomer 1B***		
carbon atom	**measured δ(^{13}C) [ppm]**	**calculated shielding [ppm]**	**calculated δ(^{13}C) [ppm]**	**measured δ(^{13}C) [ppm]**	**calculated shielding [ppm]**	**calculated δ(^{13}C) [ppm]**
Ar_q^{OMe}	173.0	4.68	172.2	172.1	5.14	172.0
Ar_q^{Prm}	158.4	19.60	157.8	166.6	11.82	165.5
Ar_q^{Gua}	143.7	33.80	144.1	157.1	22.89	154.8
Ar_q	148.3	27.75	149.9	148.9	26.57	151.2
Ar_q	143.5	32.62	145.2	147.6	27.27	150.6
Ar_q	141.6	35.31	142.6	134.4	44.27	134.1
Ar_q	134.5	42.14	136.0	132.9	44.35	134.0
ArH	128.4	49.75	128.7	129.9	48.62	129.9
ArH	124.1	54.94	123.6	128.1	49.34	129.2
ArH	123.9	55.59	123.0	125.0	54.23	124.4
ArH	123.8	55.65	123.0	123.7	55.18	123.5
ArH^{Prm}	83.7	102.14	78.0	81.6	104.07	76.1
OCH_3	54.8	126.97	54.1	53.8	127.83	53.1
CH^{iPr}	29.7	148.45	33.3	29.8	148.76	32.8
CH^{iPr}	28.8	150.16	31.7	29.7	148.82	32.7
CH_3^{iPr}	26.2	156.59	25.5	26.2	156.67	25.1
CH_3^{iPr}	24.7	157.28	24.8	24.7	157.32	24.5
CH_3^{iPr}	24.3	158.87	23.3	24.1	158.76	23.1
CH_3^{iPr}	23.2	160.07	22.1	22.8	159.28	22.6

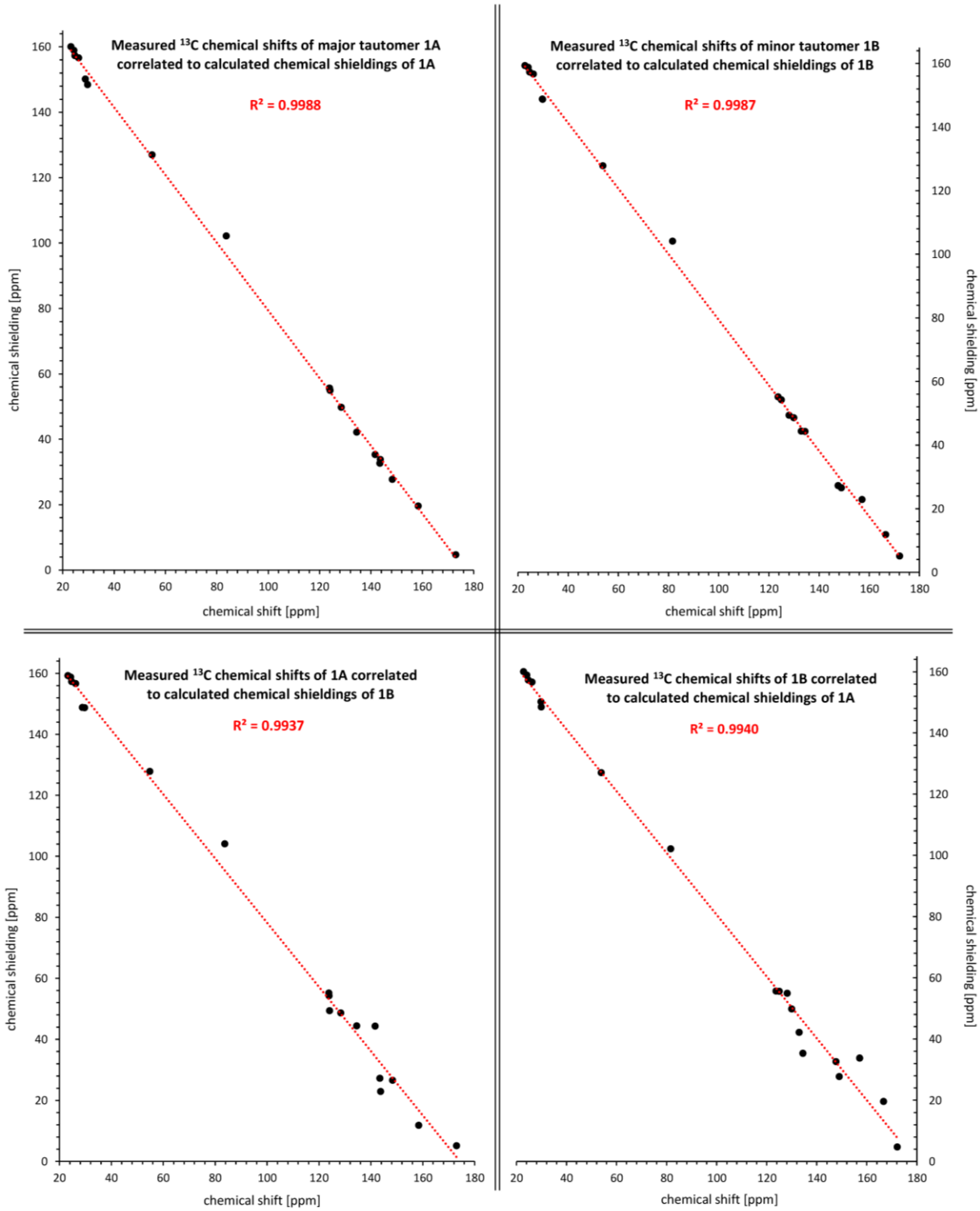

Figure S7. Correlation (including coefficient of determination R^2) of measured ^{13}C NMR chemical shifts and its calculated chemical shieldings for major **1A** and minor **1B** tautomers of **1**.

As the optimized structure for **1** - tautomer **1A** perfectly matches the solid-state structure of **1** (Figure S9) and also the ^{13}C NMR spectra parameters measured in solution agree well with calculation

results, we performed the topological analysis of optimized isomers **1A** and **1B** by QTAIM method (Figure S8).

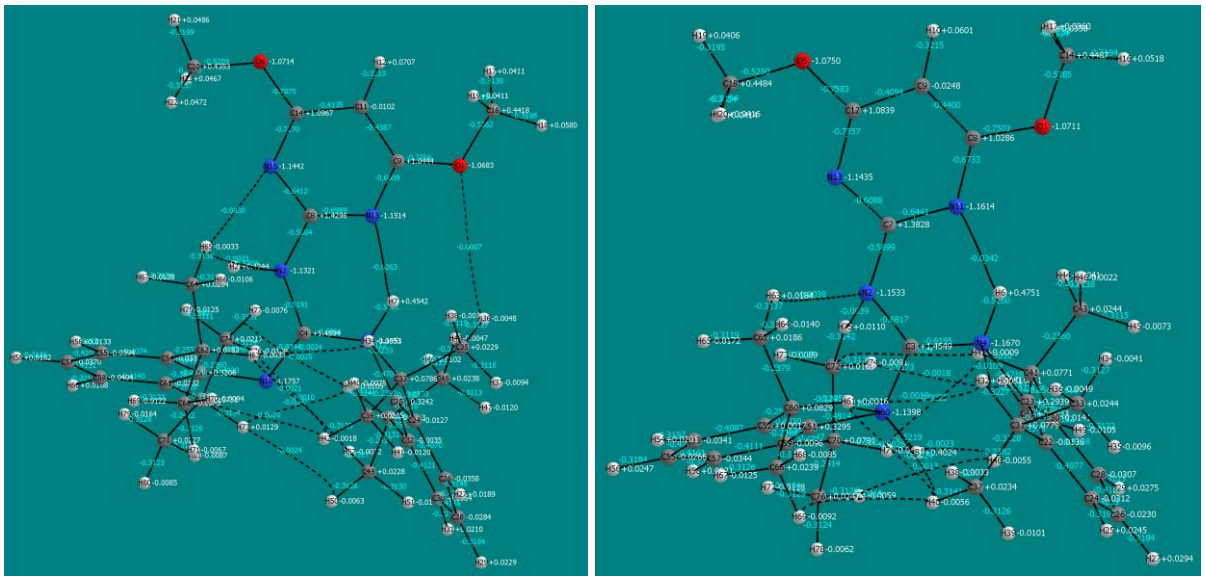

Figure S8. The topological analysis of isomers **1A** (left)and **1B** (right) by QTAIM method.

Based on the topological analysis results, we can approve the information seen from NMR spectra in solution and solid state XRD results, the only one of the N*H* group in each structure is involved in strong intramolecular H-bonding, remaining short contacts are of negligible strength. In addition, one can admit, calculated bond dissociation energy of H-bonding interaction in **1A** and even more in **1B** is quite strong (8.25 and 10.73 kcal.mol^{-1} – according the Espinosa's equation[2]). The value for the **1B**, compared to **1A**, could be the reason of fairly low field ^{1}H NMR shift for that hydrogen (see above).

The solid-state structure of **1** (Figure S9) resembles the structures of many guanidines and biguanides.[3, 4] The biguanide system together with the pyrimidine ring is perfectly planar due to high conjugation of π-electrons and interlocking by rather strong H-bond N1-H1···N5 (2.709(2) Å). Only the C1–N3 bond (1.403(2) Å) is a bit elongated due to localization of π-electron density between the neighboring C1–N2 atoms (1.283(2) Å). The C1–N3–C2 angle is quite wide (131.76(16) °), which is paradoxically a consequence of the mentioned H-bond.

2. Espinosa, E.; Molins, E.; Lecomte, C. Hydrogen bond strengths revealed by topological analyses of experimentally observed electron densities. *Chem. Phys. Lett.* **1998**, *285*, 170–173. DOI : 10.1016/S0009-2614(98)00036-0.

3. Tan, C. H.; Coles, M. The Chemistry of Guanidine, Guanidinium, and Guanidinate Compounds. *Aust. J. Chem.* **2014**, *67*, 963–964. DOI: 10.1071/CH14384.

4. Kurzer, F.; Pitchfork, E. D. *Biguanides*. Springer-Verlag Berlin Heidelberg GmbH, Berlin, **1968**.

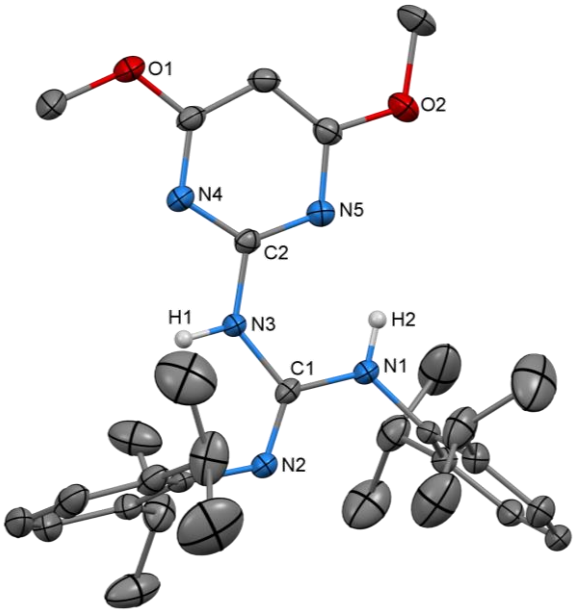

Figure S9. The ORTEP view 50% probability level of molecular structure of **1**. Selected bond lengths (Å) and angles (°): C1–N1 1.355(2), C1–N2 1.283(2), C1–N3 1.402(2), C2–N3 1.387(2), C2–N4 1.342(2), C2–N5 1.323(2), C1–N3–C2 131.90(16), N1–N5 2.710(2).

Synthetic Aspects of 2 - 3 and Structural Investigation of 2 - 5

The reaction time ideal for maximizing the conversion of **1** to dinuclear bis(ethylzinc) biguanide **3** was experimentally determined to 7 hours (see NMR spectra in Figures S10–S21). This period seems to be the best compromise between the conversion and relatively fast decomposition of **3** to **2** and some unidentified ethylzinc moiety in solution as well as in the solid state.

Note, **3** was obtained in 95+% of purity only. A kinetic protection effect of a high excess (6 or 20 equivalents) of diethylzinc can be used in order to proceed the formation of **3** from monometalic complex intermediate **2** faster (see NMR spectra in Figures S12–S15) than the **3** decomposition. For 20 eq. of Et_2Zn the maximum conversion was 97 % after 25 hours (Figures S14–S15). While for the reaction of **2** with 2 or 6 eq. of Et_2Zn the best protocol needs 7 hours (for 2 eq. of 89 % and for 6 eq. 90 %).

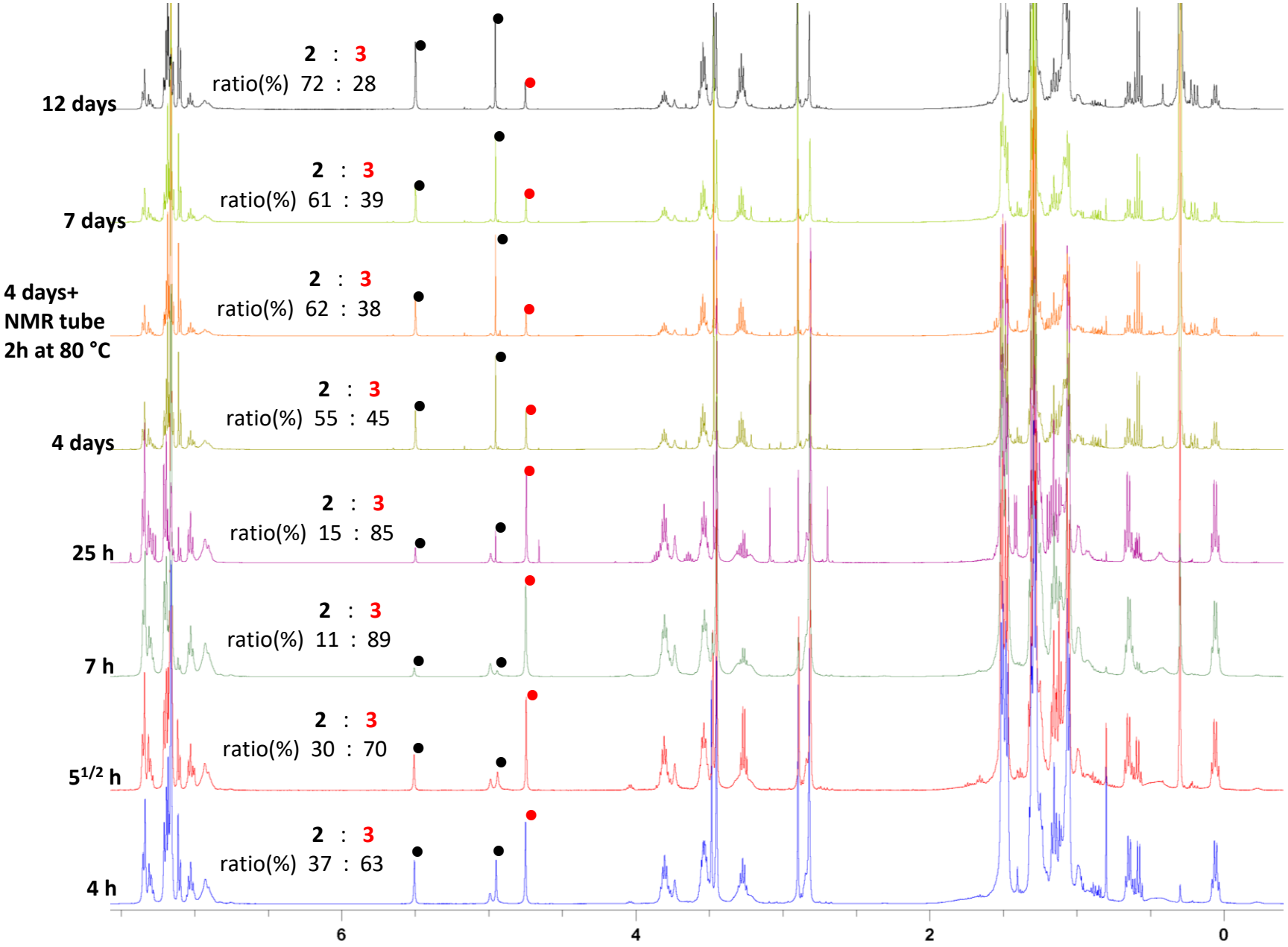

Figure S10. ^{1}H NMR study (**2** to **3** ratio comparison in time) of reaction mixture (Et_2O, -80 °C to RT) of **1** with 2 eq. of Et_2Zn in C_6D_6 at 295 K. Significant NMR signals are marked with dots (black for **2** and red for **3**).

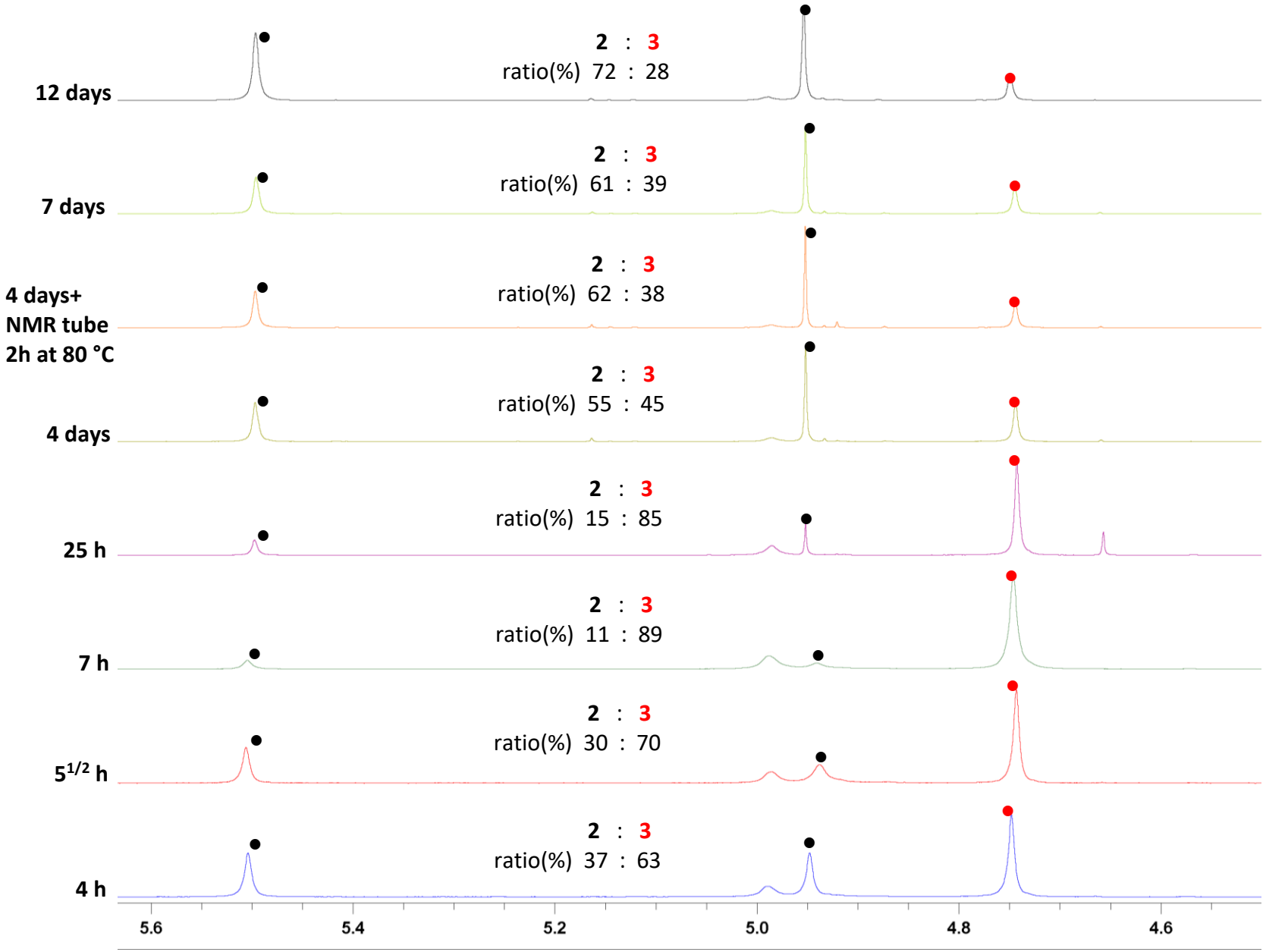

Figure S11. Detail of ^{1}H NMR study (**2** to **3** ratio comparison in time) of reaction mixture (Et_2O, -80 °C to RT) of **1** with 2 eq. of Et_2Zn in C_6D_6 at 295 K. Significant NMR signals are marked with dots (black for **2** and red for **3**).

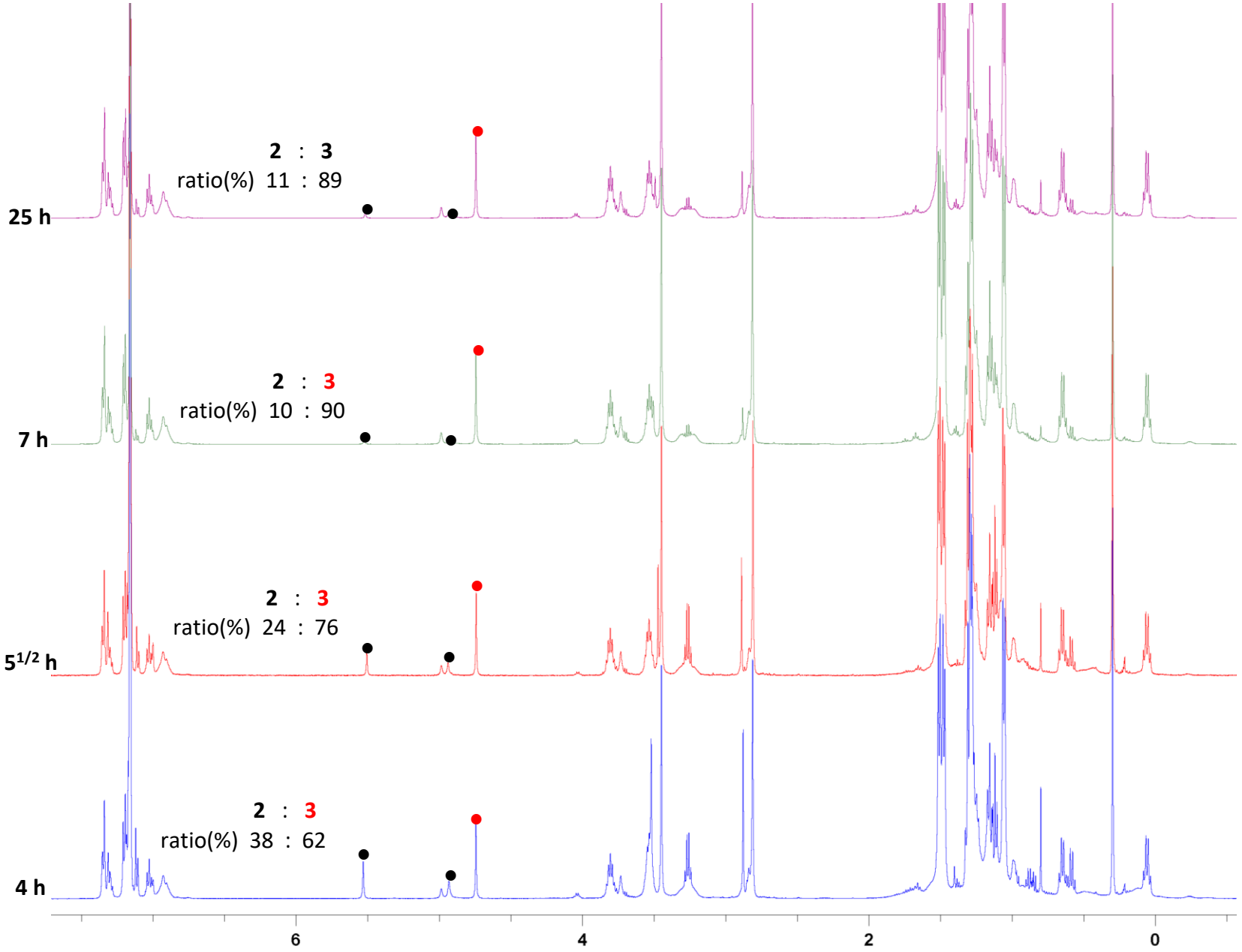

Figure S12. ^{1}H NMR study (**2** to **3** ratio comparison in time) of reaction mixture (Et_2O, -80 °C to RT) of **1** with 6 eq. of Et_2Zn in C_6D_6 at 295 K. Significant NMR signals are marked with dots (black for **2** and red for **3**).

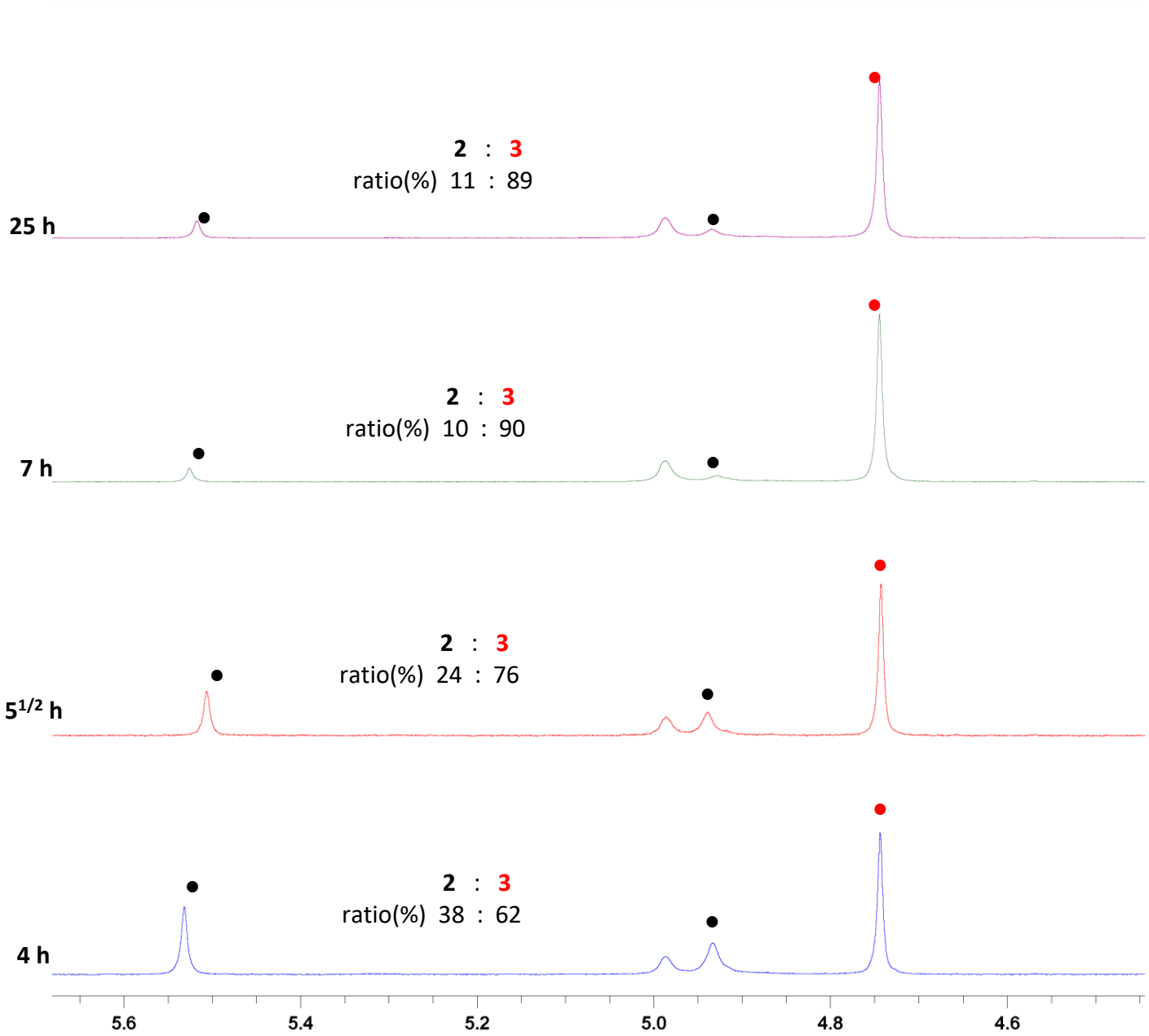

Figure S13. Detail of ^{1}H NMR study (**2** to **3** ratio comparison in time) of reaction mixture (Et_2O, -80 °C to RT) of **1** with 6 eq. of Et_2Zn in C_6D_6 at 295 K. Significant NMR signals are marked with dots (black for **2** and red for **3**).

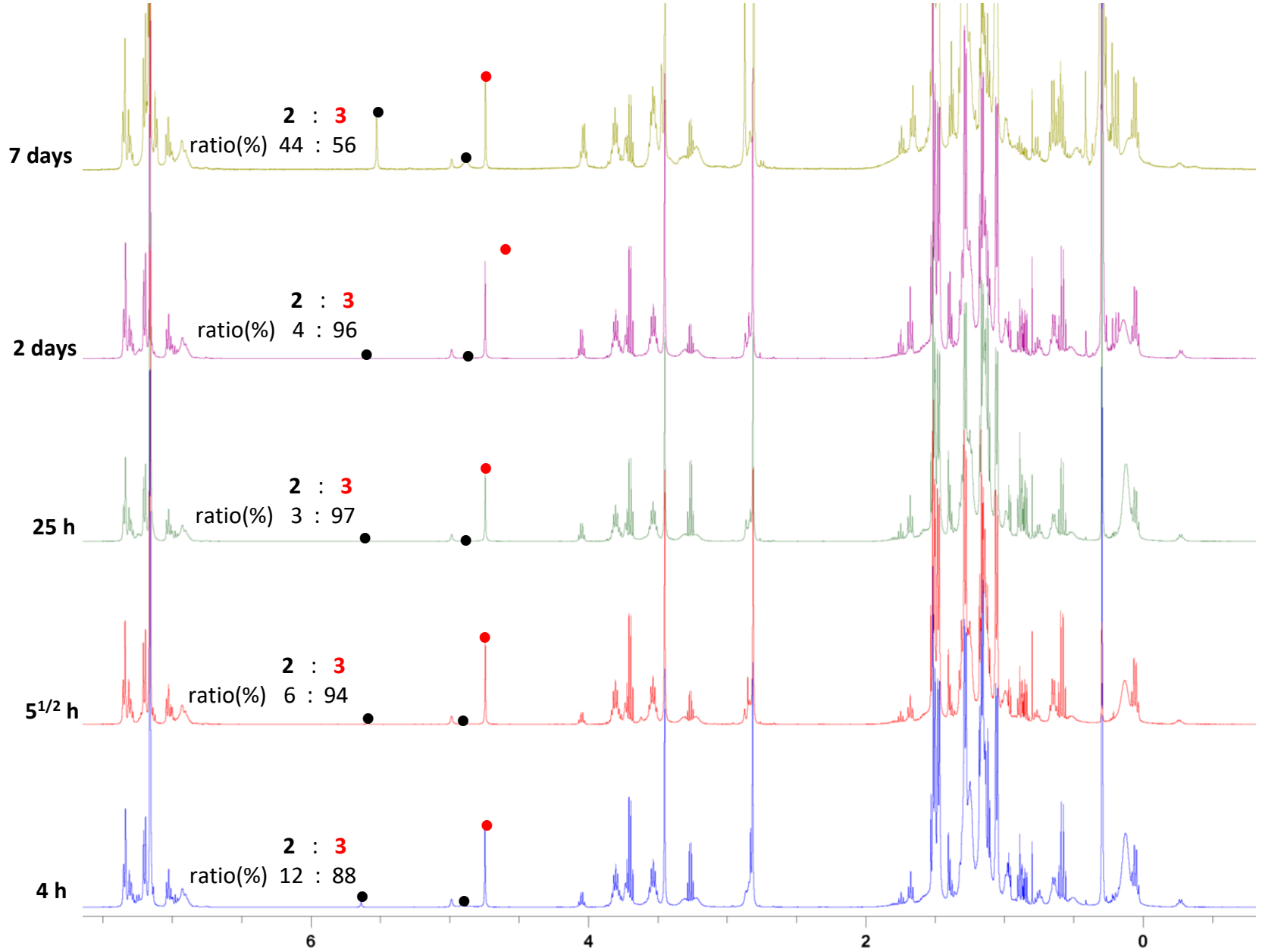

Figure S14. ^{1}H NMR study (**2** to **3** ratio comparison in time) of reaction mixture (Et_2O, -80 °C to RT) of **1** with 20 eq. of Et_2Zn in C_6D_6 at 295 K. Significant NMR signals are marked with dots (black for **2** and red for **3**).

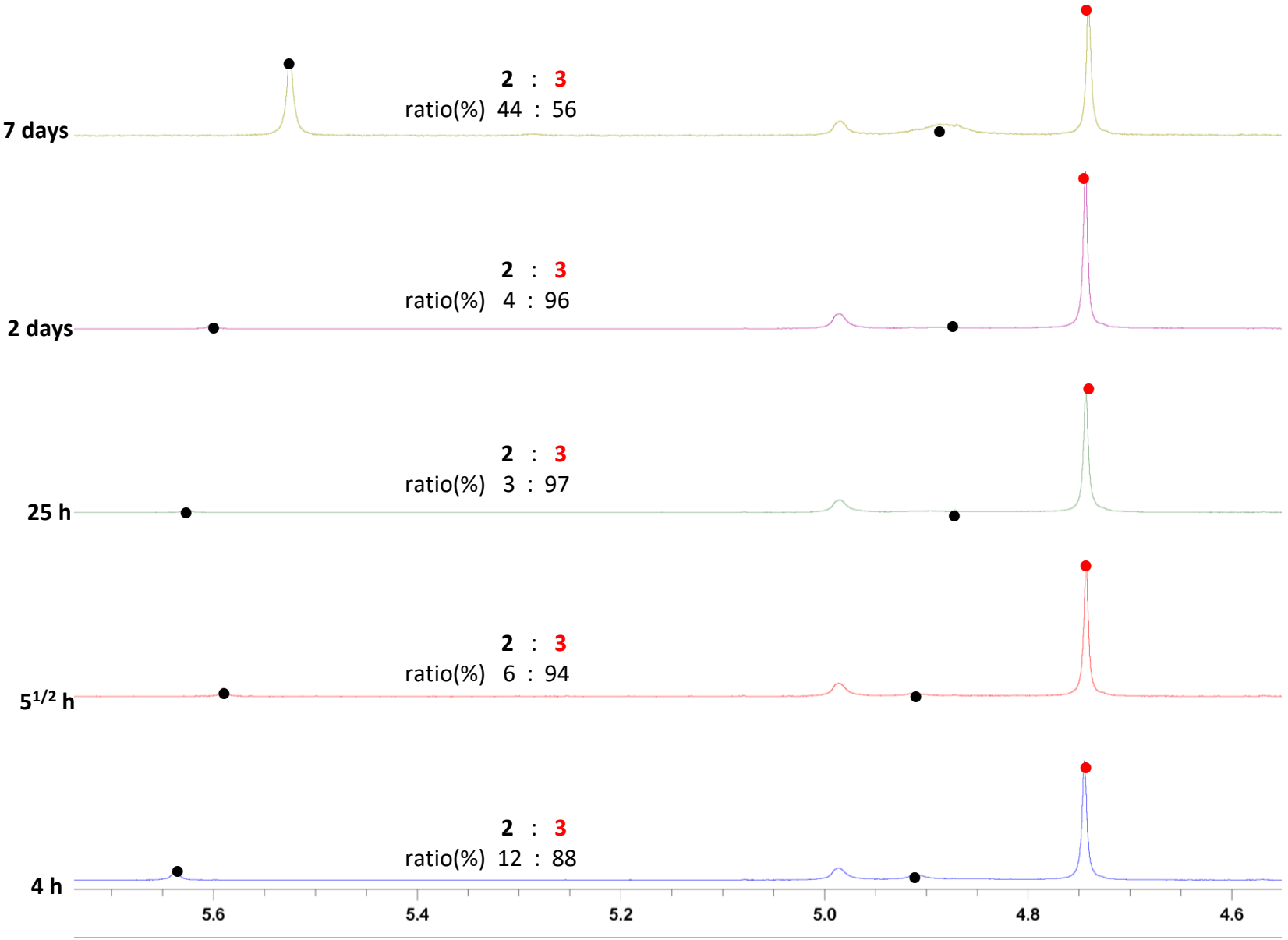

Figure S15. Detail of ^{1}H NMR study (**2** to **3** ratio comparison in time) of reaction mixture (Et_2O, -80 °C to RT) of **1** with 20 eq. of Et_2Zn in C_6D_6 at 295 K. Significant NMR signals are marked with dots (black for **2** and red for **3**).

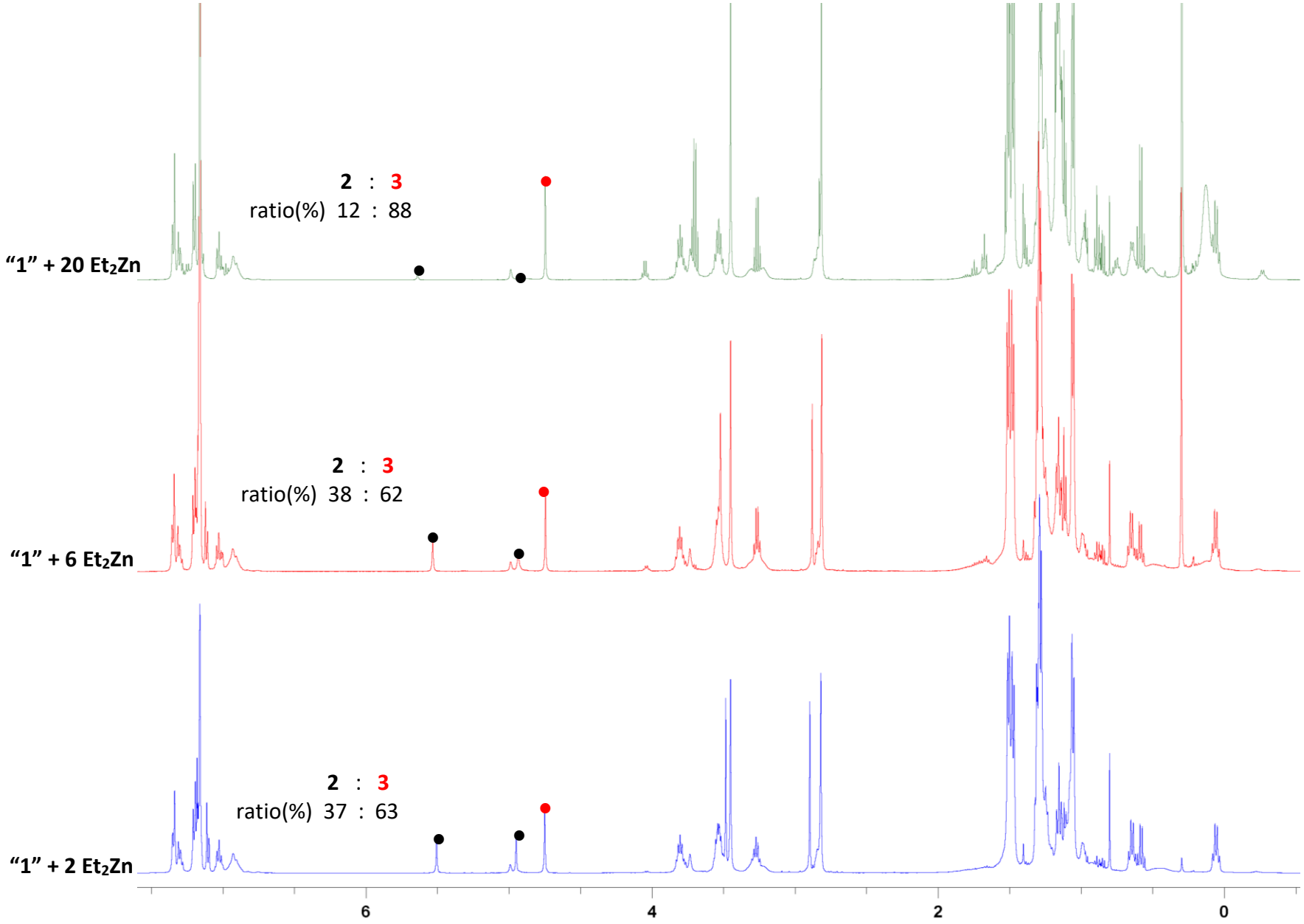

Figure S16. ^{1}H NMR study (**2** to **3** ratio comparison) of reaction mixture (Et_2O, -80 °C to RT) of **1** with 2, 6 or 20 eq. of Et_2Zn after 4 hours in C_6D_6 at 295 K. Significant NMR signals are marked with dots (black for **2** and red for **3**).

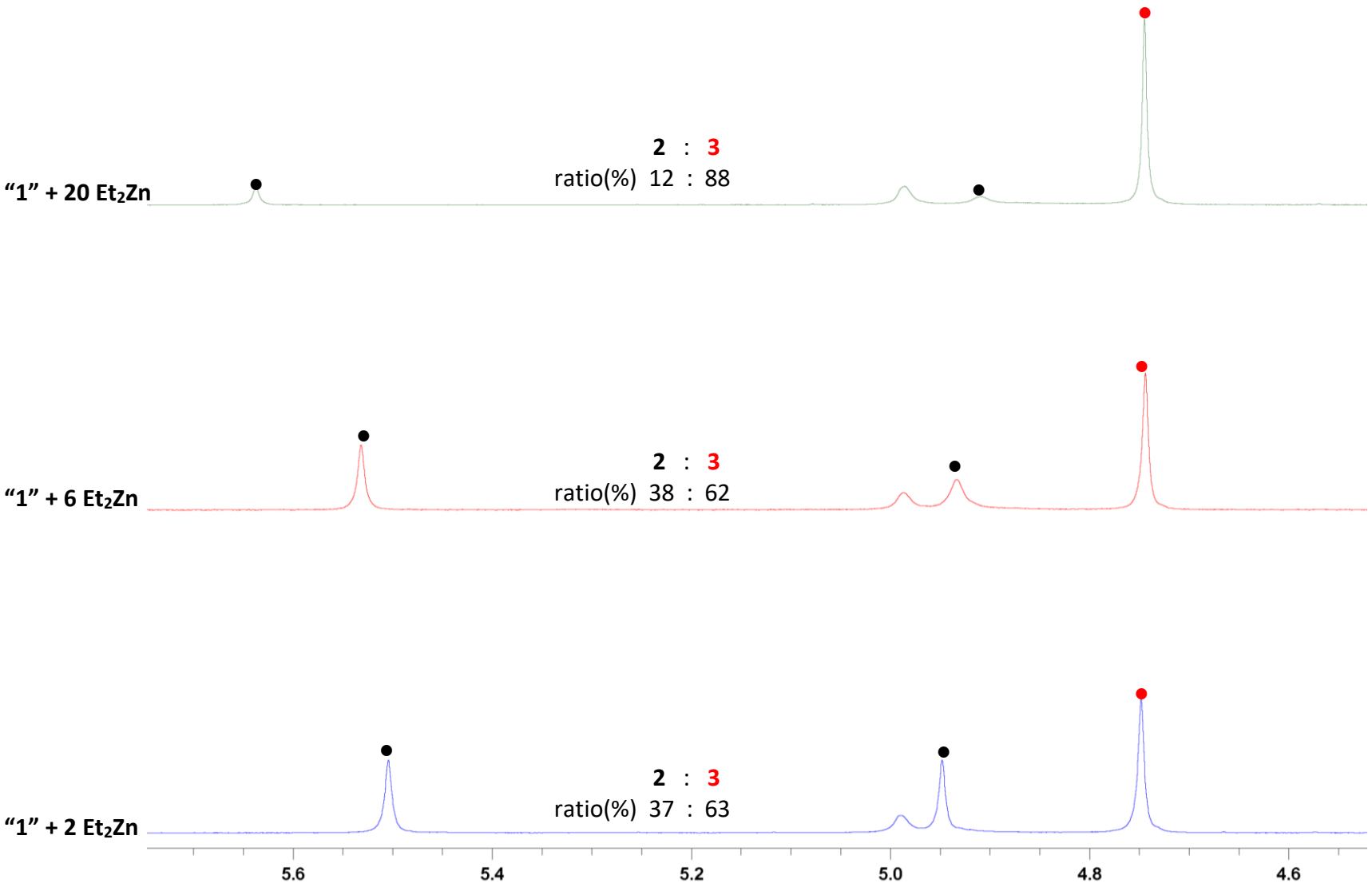

Figure S17. Detail of ^{1}H NMR study (**2** to **3** ratio comparison) of reaction mixture (Et_2O, -80 °C to RT) of **1** with 2, 6 or 20 eq. of Et_2Zn after 4 hours in C_6D_6 at 295 K. Significant NMR signals are marked with dots (black for **2** and red for **3**).

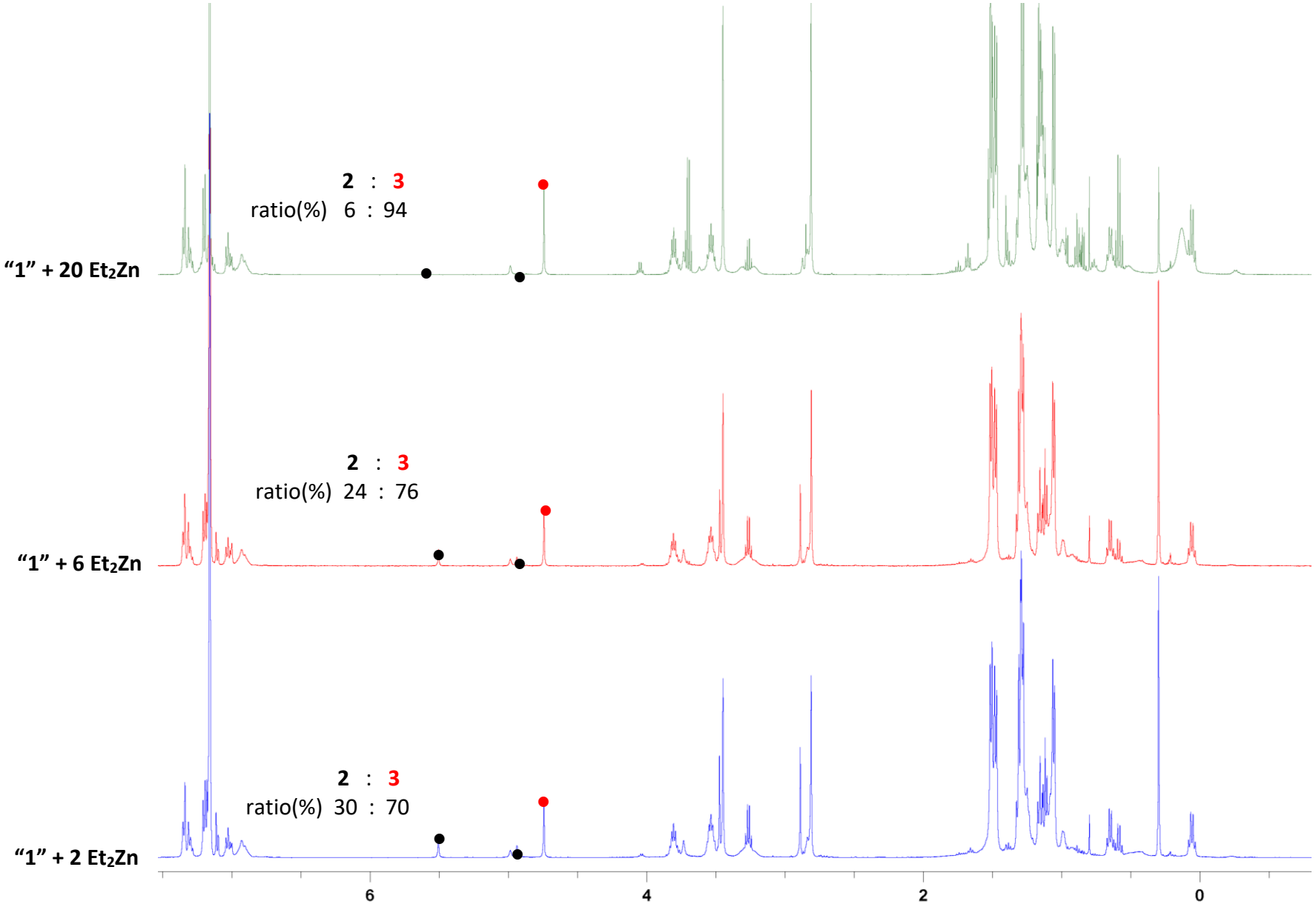

Figure S18. ^{1}H NMR study (**2** to **3** ratio comparison) of reaction mixture (Et_2O, -80 °C to RT) of **1** with 2, 6 or 20 eq. of Et_2Zn after $5^{1/2}$ hours in C_6D_6 at 295 K. Significant NMR signals are marked with dots (black for **2** and red for **3**).

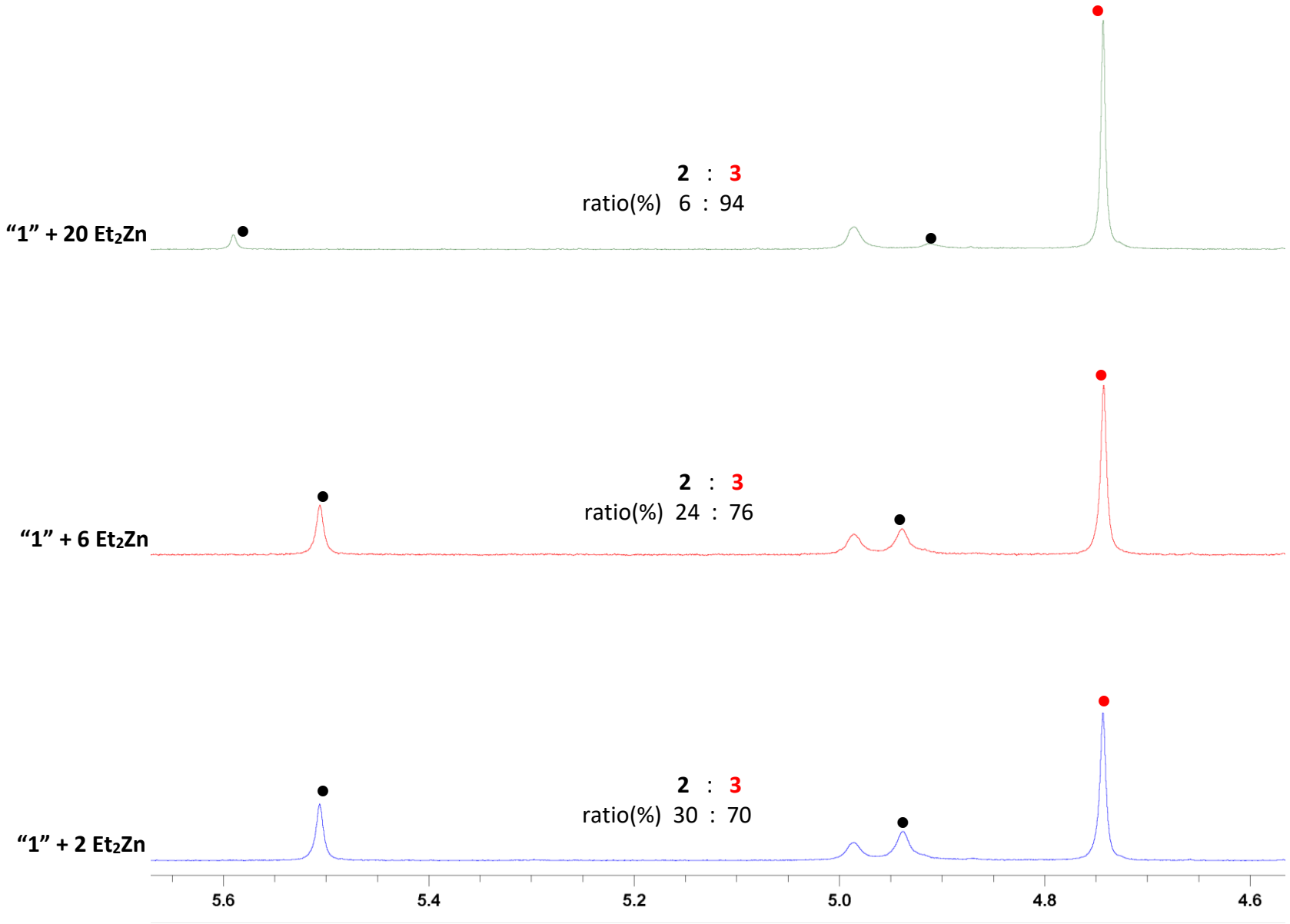

Figure S19. Detail of ^{1}H NMR study (**2** to **3** ratio comparison) of reaction mixture (Et_2O, -80 °C to RT) of **1** with 2, 6 or 20 eq. of Et_2Zn after $5^{1/2}$ hours in C_6D_6 at 295 K. Significant NMR signals are marked with dots (black for **2** and red for **3**).

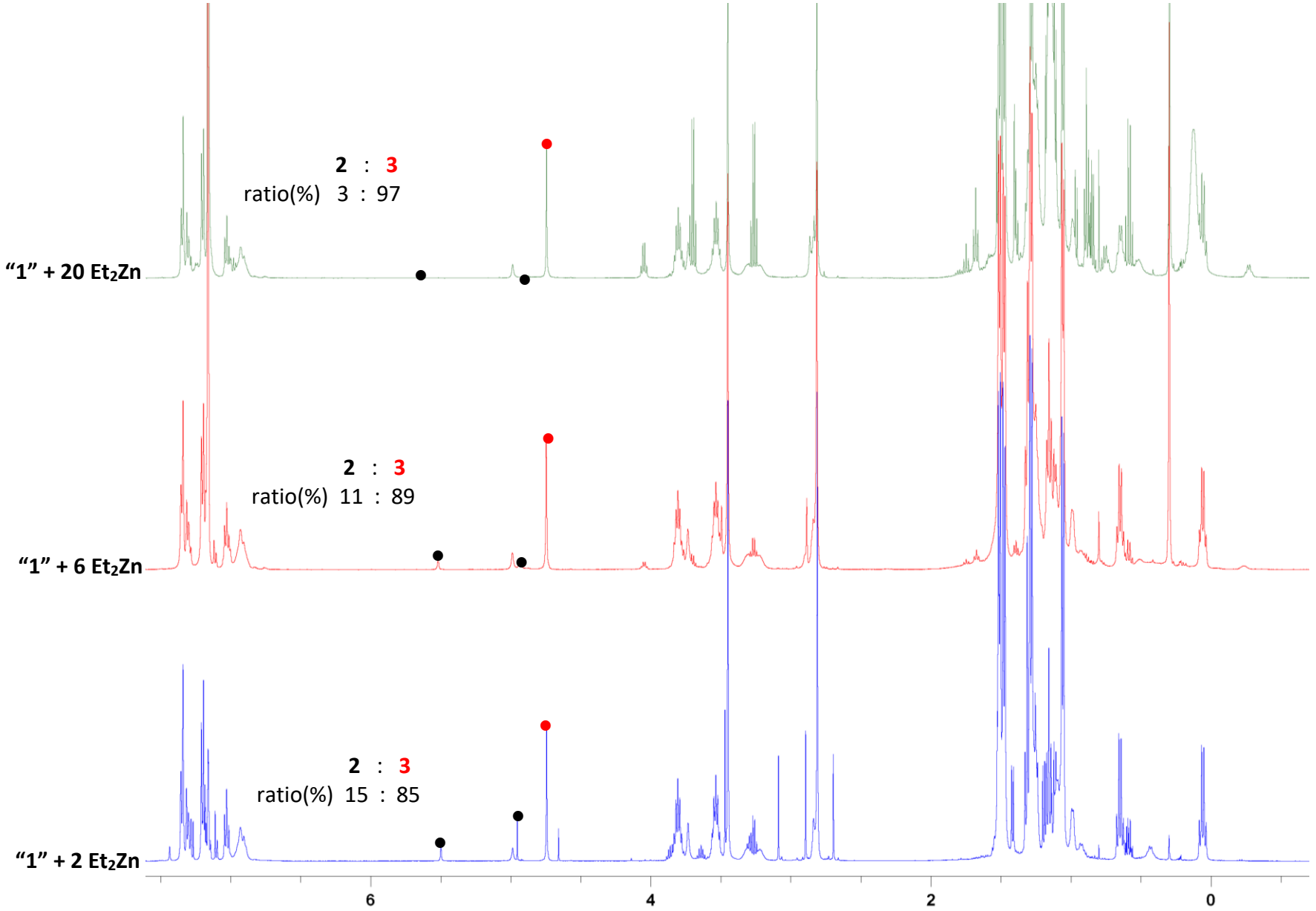

Figure S20. ^{1}H NMR study (**2** to **3** ratio comparison) of reaction mixture (Et_2O, -80 °C to RT) of **1** with 2, 6 or 20 eq. of Et_2Zn after 25 hours in C_6D_6 at 295 K. Significant NMR signals are marked with dots (black for **2** and red for **3**).

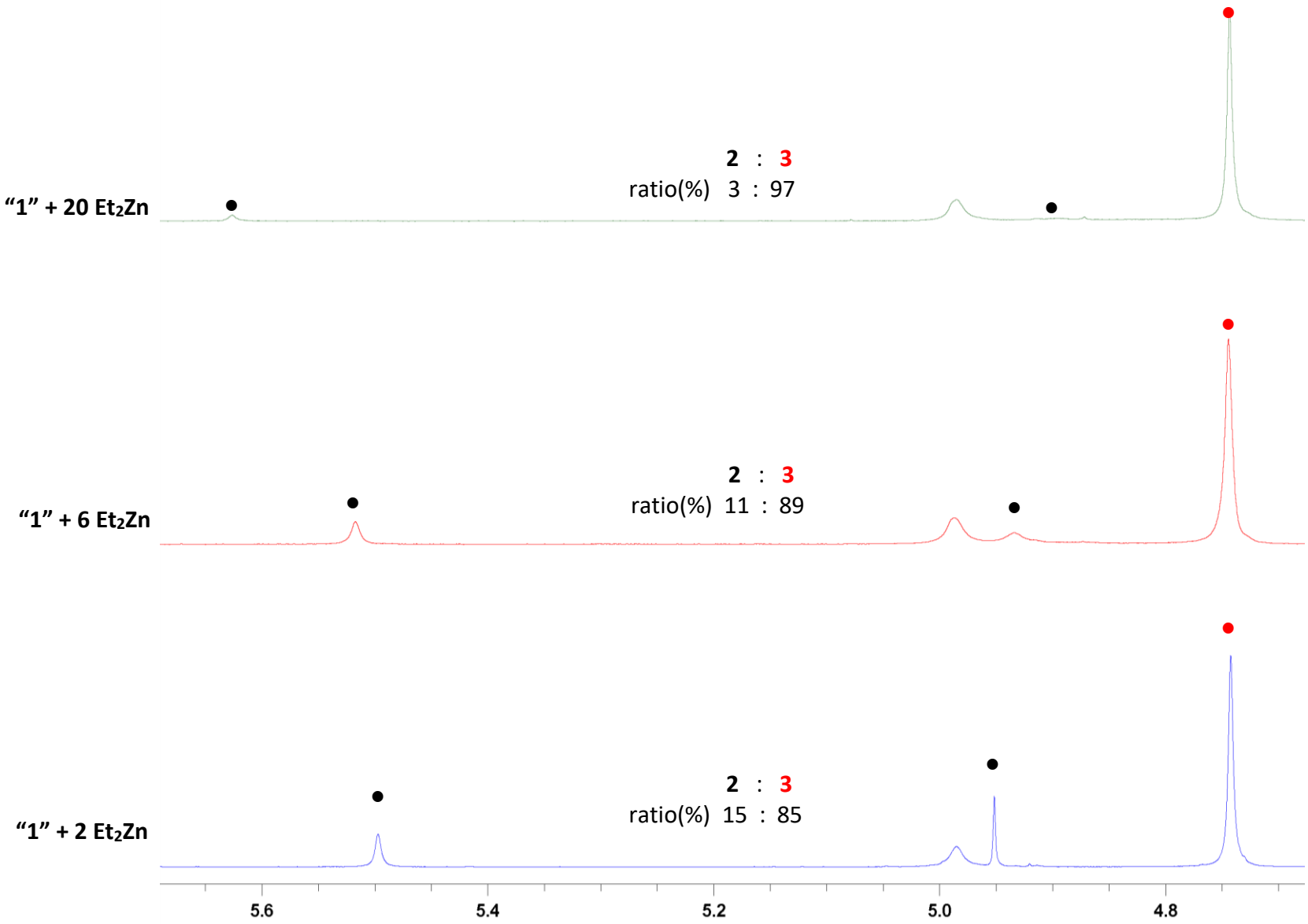

Figure S21. Detail of ^{1}H NMR study (**2** to **3** ratio comparison) of reaction mixture (Et_2O, -80 °C to RT) of **1** with 2, 6 or 20 eq. of Et_2Zn after 25 hours in C_6D_6 at 295 K. Significant NMR signals are marked with dots (black for **2** and red for **3**).

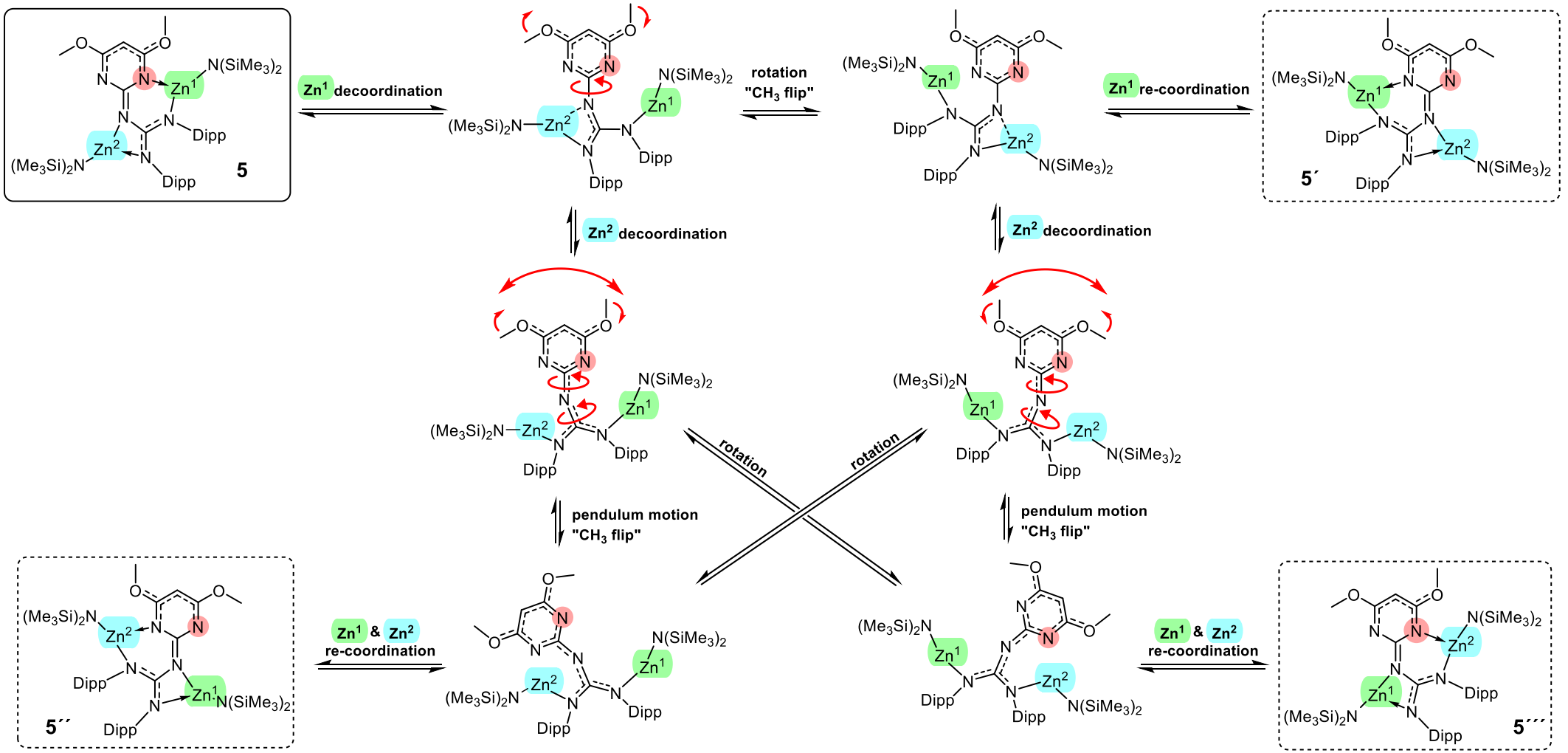

Scheme S2. Detailed view of all plausible transformations of **5** in solution.

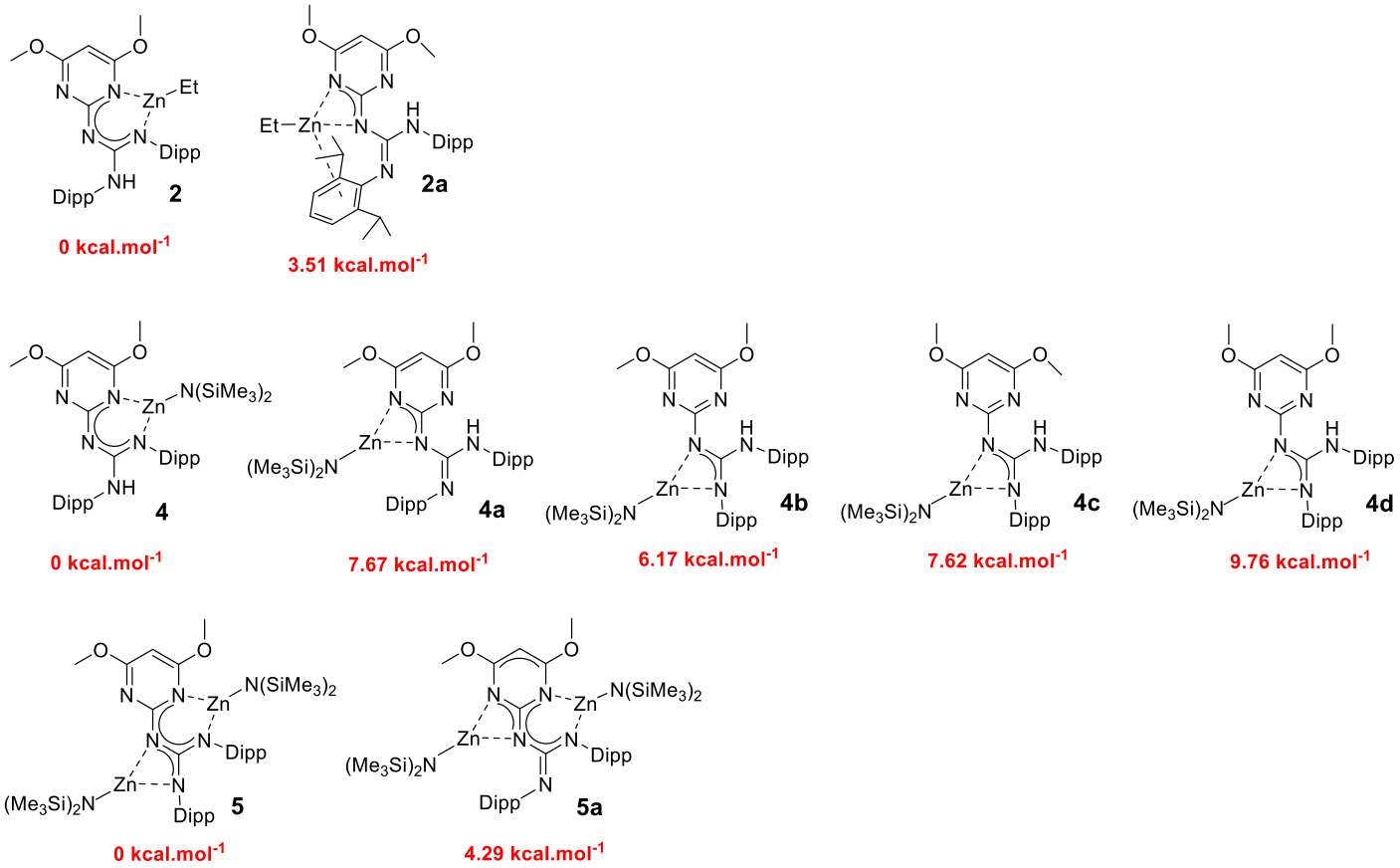

Figure S22. Energetical comparison of solid-state structures of **2**, **4** and **5** with its calculated coodination isomers.

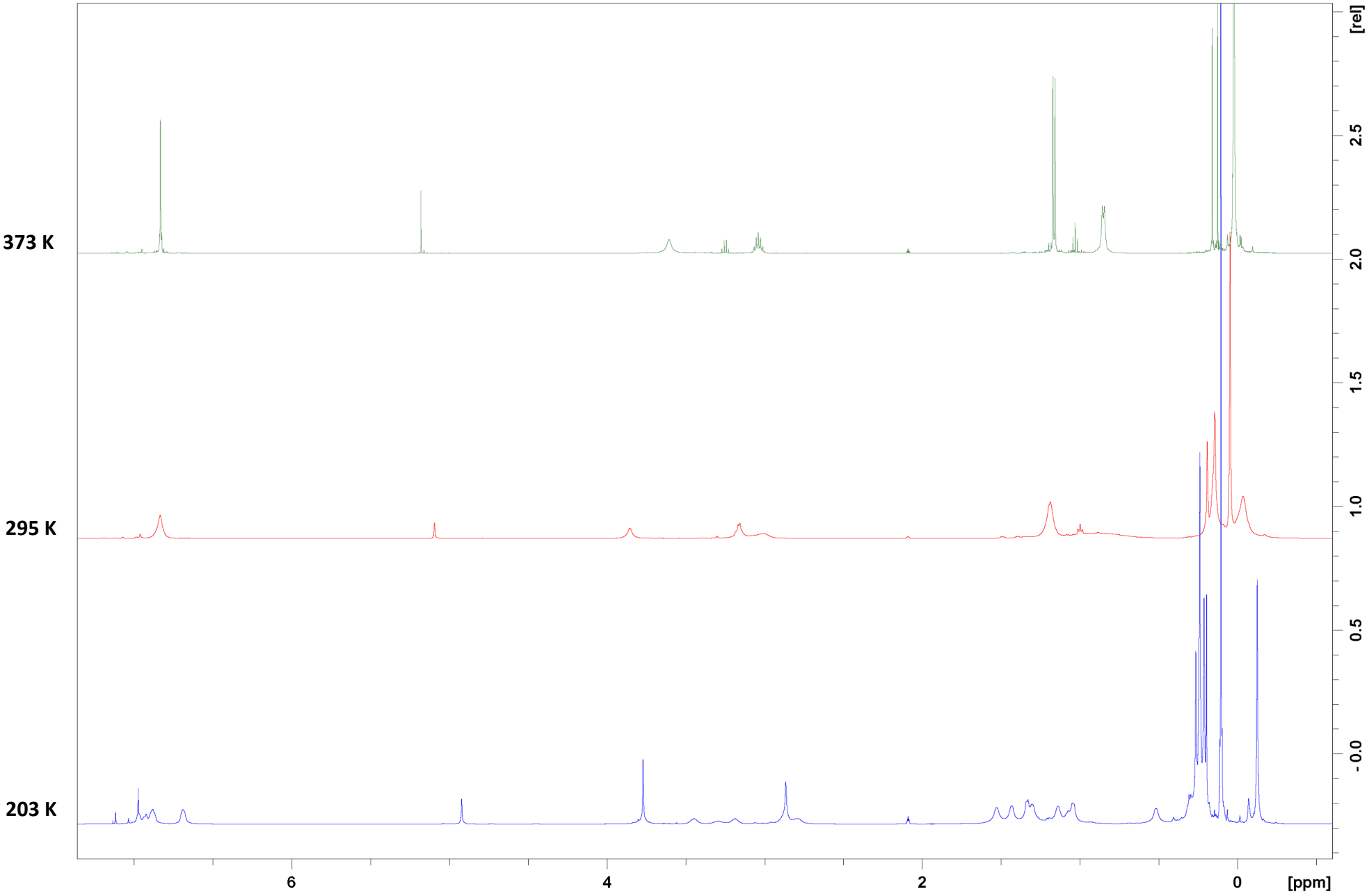

Figure S23. VT ^{1}H NMR spectra of **5** in Tol-d_8 at 203, 295 and 373 K.

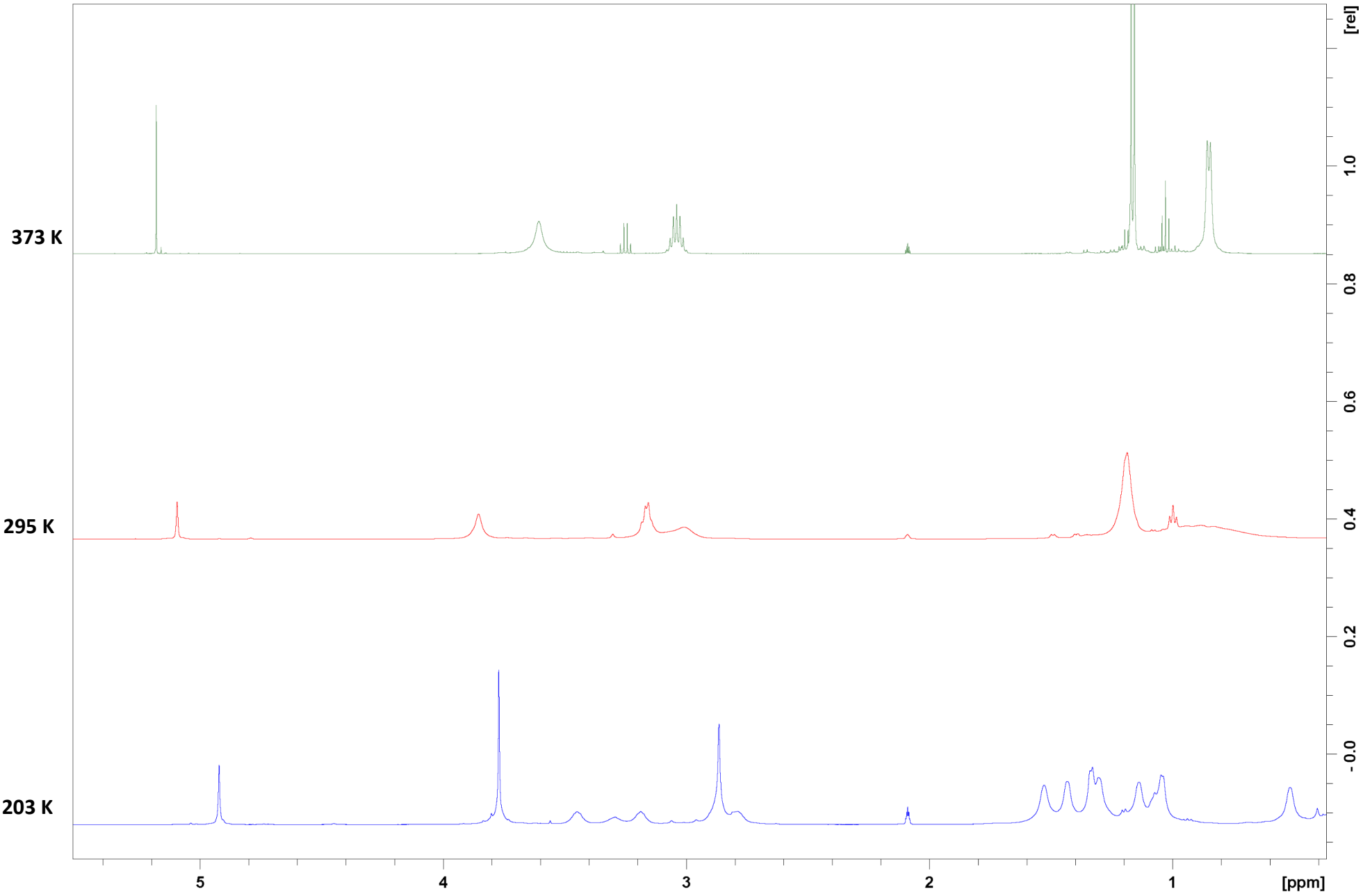

Figure S24. Detail of VT ^{1}H NMR spectra of **5** in Tol-d_8 at 203, 295 and 373 K

Solid State Structures of 2 - 5

The solid state structures of **2** - **5** are discussed in the main text, ORTEP views drawn at 50% probability level are presented here along with all values of interatomic distances and angles.

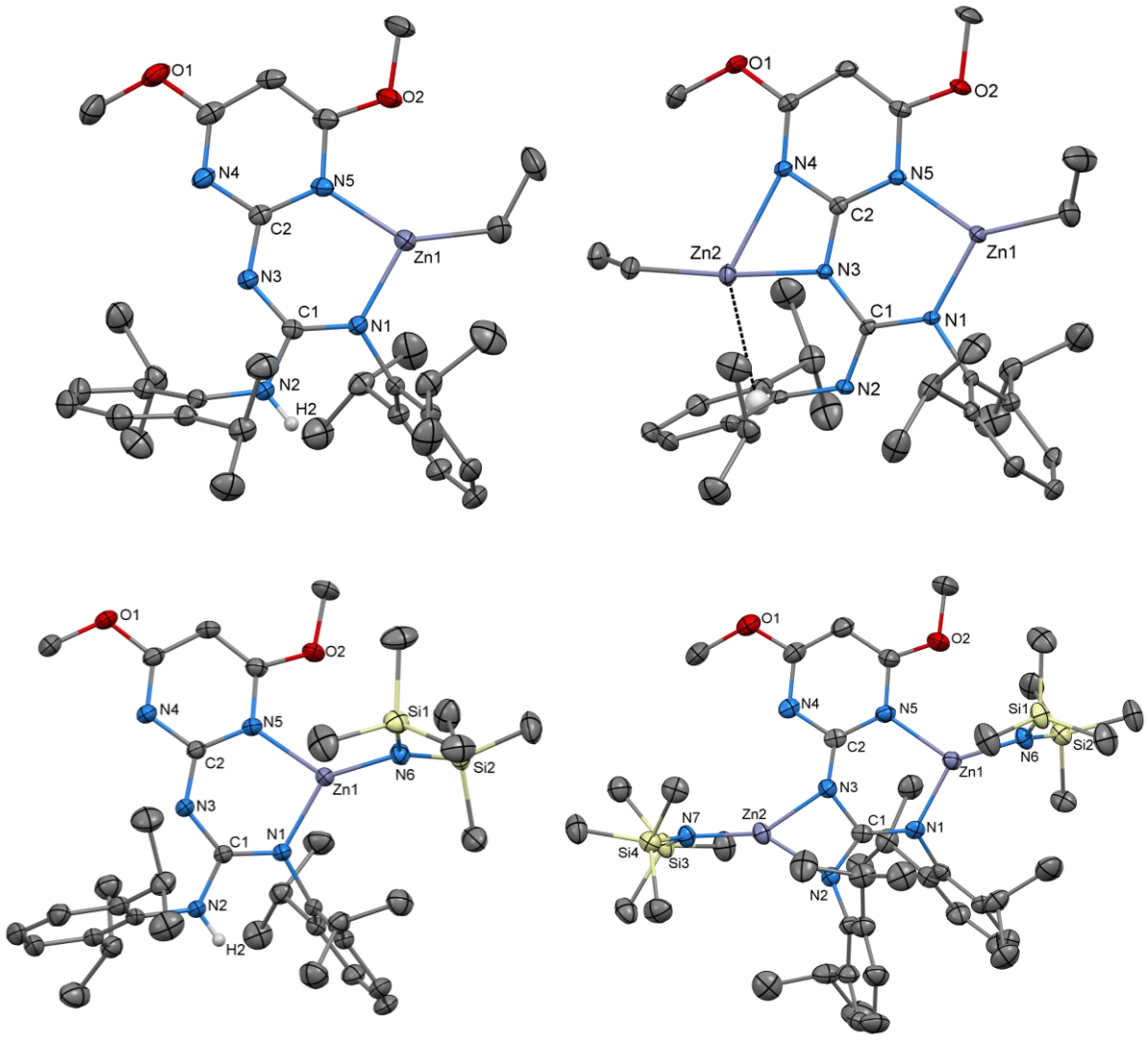

Figure S25. The ORTEP view 50% probability level of molecular structures of **2** (upper left), **3** (lower left), **4** (upper right) and **5** (lower right). Selected bond lengths (Å) and angles (°) for **2**: Zn1–N1 1.9649(15), Zn1–N5 1.9838(15), N1–Zn1–N5 93.02(6), Zn1–C32 1.963(2), C1–N1 1.332(2), C1–N2 1.375(2), C1–N3 1.335(2), C2–N3 1.338(2), C2–N4 1.365(2), C2–N5 1.365(2), C1–N3–C2 126.93(16), C3–N4 1.307(2), C3–C4 1.397(3), C4–C5 1.359(3), C5–N5 1.363(2), C3–O1 1.349(2), C5–O2 1.340(2), N1–N5 2.865(2); for **3**: Zn1–N1 1.9291(17), Zn1–N5 2.0354(17), N1–Zn1–N5 93.59(7), Zn1–C32 1.957(2), Zn2–N3 1.9699(17), Zn2–N4 2.3864(18), N3–Zn2–N4 60.69(6), Zn2–C34 1.948(2), C1–N1 1.356(3), C1–N2 1.301(3), C1–N3 1.410(3), C2–N3 1.345(3), C2–N4 1.371(3), C2–N5 1.345(3), C1–N3–C2 129.73(17), C3–N4 1.318(3), C3–C4 1.395(3), C4–C5 1.369(3), C5–N5 1.361(3), C3–O1 1.331(3), C5–O2 1.330(3), N1–N5 2.891(2); for **4**: Zn1–N1 1.9428(9), Zn1–N5 1.9882(9), N1–Zn1–N5 93.60(4), Zn1–

N6 1.8755(10), C1–N1 1.3386(14), C1–N2 1.3637(14), C1–N3 1.3455(14), C2–N3 1.3314(14), C2–N4 1.3642(14), C2–N5 1.3658(14), C1–N3–C2 126.91(10), N6–Si1 1.7087(10), N6–Si2 1.7114(11), C3–N4 1.3117(15), C3–C4 1.4040(17), C4–C5 1.3665(16), C5–N5 1.3575(14), C3–O1 1.3377(14), C5–O2 1.3410(15), N1–N5 2.866(1); for **5**: Zn1–N1 1.949(8), Zn1–N5 2.015(5), N1–Zn1–N5 96.7(3), Zn1–N6 1.880(8), Zn2–N2 2.018(8), Zn2–N3 1.974(8), N2–Zn2–N3 66.3(3), Zn2–N7 1.863(8), C1–N1 1.320(13), C1–N2 1.337(13), C1–N3 1.417(12), C2–N3 1.272(10), C2–N4 1.360(11), C2–N5 1.3900, C1–N3–C2 132.0(8), N6–Si1 1.699(8), N6–Si2 1.726(9), N7–Si3 1.721(8), N7–Si4 1.700(9), C3–N4 1.3900, C5–N5 1.3900, C3–O1 1.331(13), C5–O2 1.284(10), N1–N5 2.96(1).

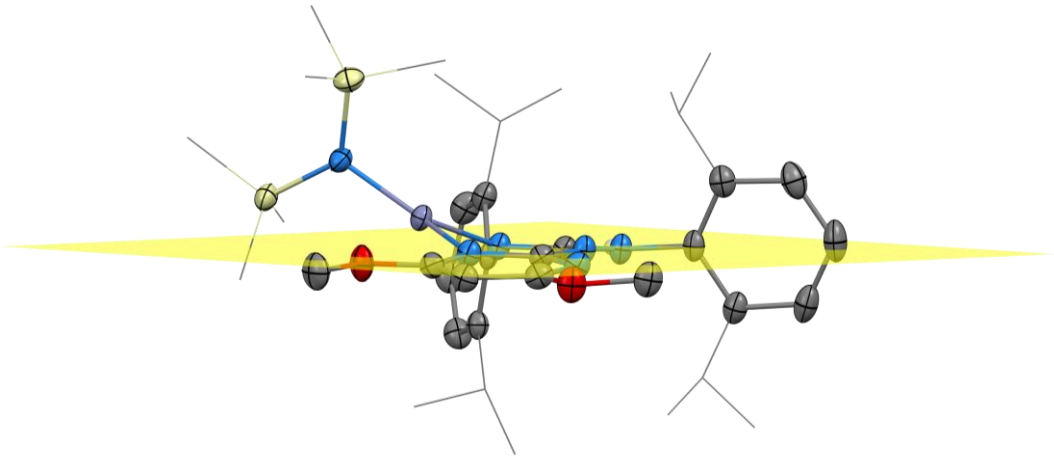

Figure S26. The ORTEP view 50% probability level of molecular structure of **4** – detail of the departure of Zn atom from the ligand's plane.

Attempts of Direct Synthesis of Alkoxyzinc Complexes

Although the polymerization results did not suggest alkoxyzinc complexes have a role of active species, responsible for the polymer activation/propagation, attempts to prepare/isolate alkoxyzinc biguanide were made. The first batch of experiments focused on direct synthetic approach - deprotonation of **1** by zinc methoxide - did not proceed in Et_2O and cyclopentyl(methyl)ether as well. Heating of the reaction mixture, as well as addition of catalytic amount of $NaNH_2$ (basic catalysis), afforded no reaction. Similarly, *in situ* reaction of lithiated biguanide **1** (not separable, not characterized) precursor failed in second step of electrophilic substitution using $Zn(OMe)_2$.

In the second case, **1** mixed with zinc bis(isopropoxide) in toluene under mild conditions did not undergo any reaction, even after heating to 120 °C and to 130 °C in a vacuum-sealed NMR tube in C_6D_6 or Tol-d_8 for couple of hours. On the other hand, temperature over 140 °C led to decomposition (possibly of zinc biguanide species, not observed in the NMR spectra) to a mixture of products

(isopropyl-*N*,*N'*-bis(2,6-diisopropylphenyl)carbamimidate, 2-amino-4,6-dimethoxypyrimidine and *N,N'*-bis(2,6-diisopropyl)carbodiimide) next to unreacted **1**.

Alcoholysis of 2, 4 and 5 and Synthesis, Structure and Properties of 6

Further attempts of preparation of alkoxy substituted zinc biguanide were aimed to substitution reaction - alcoholysis using isopropylalcohol - of ethyl and/or bis(trimethylsilyl)amido group(s) of complexes **2**, **4** and **5** under different conditions (polar aprotic solvent vs. non-polar, room temperature vs. low temperature, catalytic approach, etc.) with the dominant result of protonation of the biguanide ligand. Feasibility of these reactions and the path to alkoxyzinc biguanide(s) was also examined by theoretical calculations, especially the standard free-energy change (ΔG°) of desired reaction.

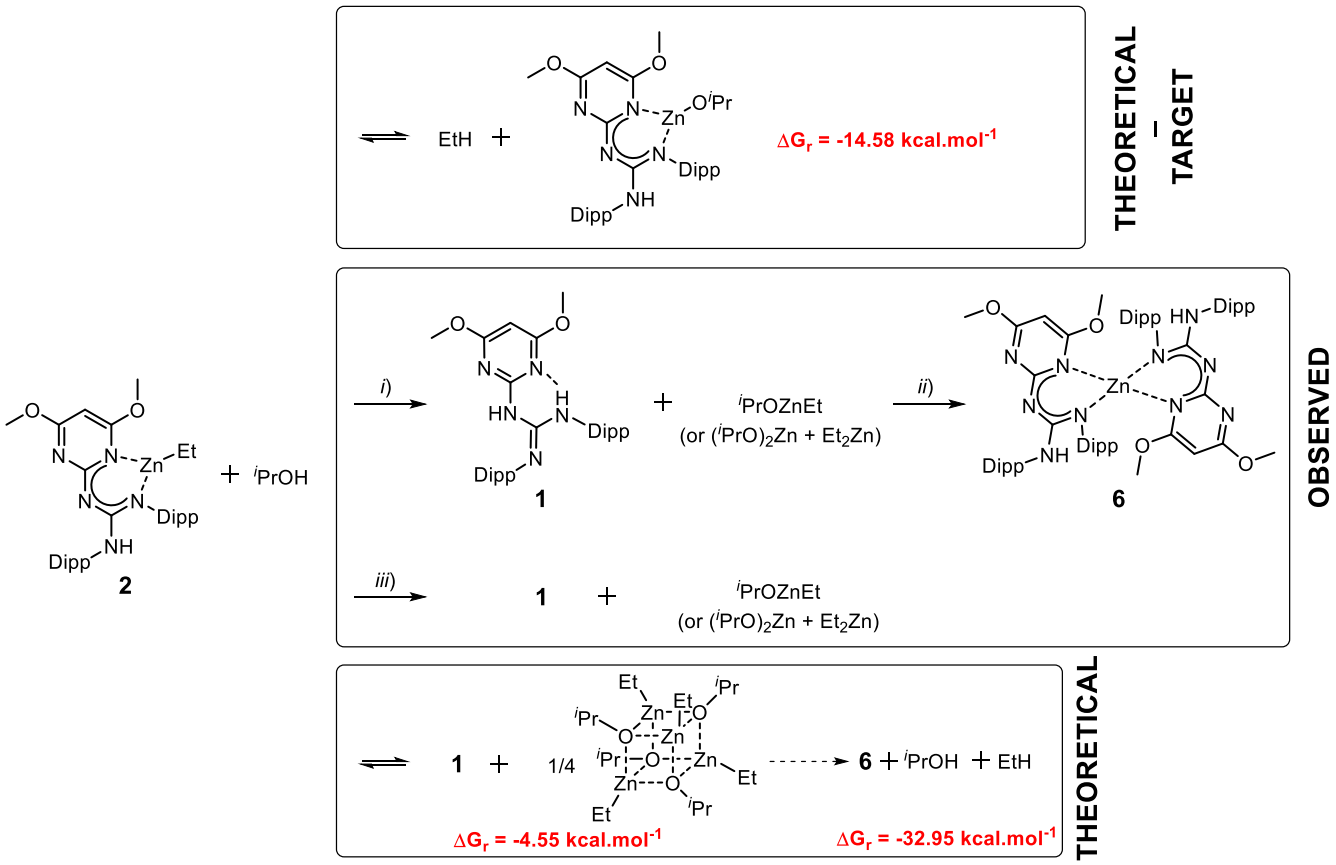

Scheme S3. Theoretical and experimental aspects of alcoholysis of **2** using ^{i}PrOH. *i*) Toluene, RT, 24 h; ii) 80 °C, 8 h, in NMR tube – re-reaction; iii) cat. 10 mol. % of I_2, toluene, -80°C to RT, 24 h.

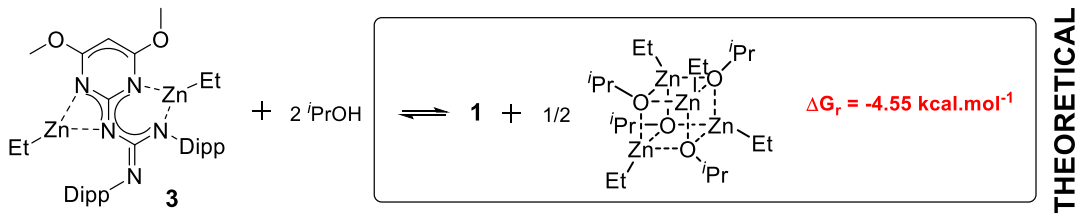

Scheme S4. Theoretical aspect of alcoholysis of **3** using ^{i}PrOH.

In the case of **2** (Scheme 3), the alcoholysis led exclusively to **1** and an alkoxy(alkyl)zinc species even when an attempt to extrude the ethyl group by using a catalytic amount of I_2 was performed. The formed alkoxy(alkyl)zinc species, detected in ^{1}H NMR spectra, reacts with **1** to give new monometallic biguanide, identified by NMR as **6** (see NMR spectra – Figures S28 – S29).

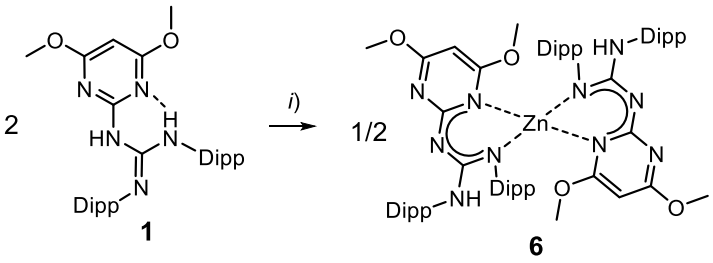

Scheme S5. Synthesis of **6**. *i*) 1/2 Et_2Zn, Et2O, -80 °C to RT, 24 hours.

Therefore, a purposeful direct synthesis of **6** was performed from two equivalents of **1** and diethylzinc (Scheme S5). It shows similar NMR spectra patterns as monometallic complexes **2** and **3** - N*H* resonates at 5.41 ppm in ^{1}H NMR spectra and δ(^{13}C) of Ar_q^{Gua}/Ar_q^{Prm} found at 159.2/161.7, all in THF-d_8).

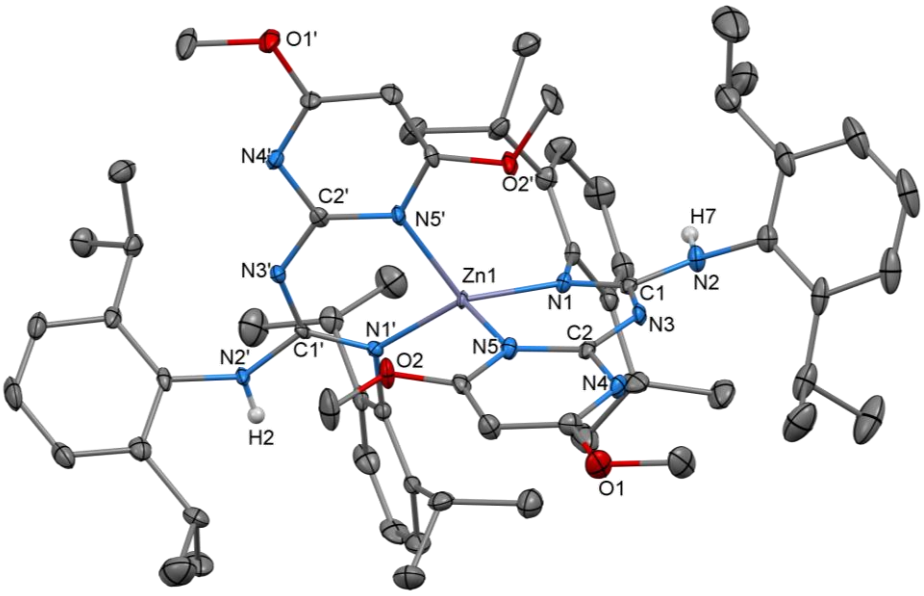

Figure S27. The ORTEP view 50% probability level of molecular structure of **6**. Selected bond lengths (Å) and angles (°): Zn1–N1 1.981(3), Zn1–N1’ 1.975(3), Zn1–N5 2.016(3), Zn1–N5’ 2.020(3), N1–Zn1–N5 94.30(12), N1’–Zn1–N5’ 95.96(12), N1–Zn1–N5’ 124.56(12), N1’–Zn1–N5 121.43(12), N1–Zn1–N1’ 121.13(12), N5–Zn1–N5’ 99.53(12), C1–N1 1.347(4), C1’–N1’ 1.340(4), C1–N2 1.380(5), C1’–N2’ 1.395(4), C1–N3 1.341(5), C1’–N3’ 1.331(4), C2–N3 1.336(5), C2’–N3’ 1.339(5), C2–N4 1.373(5), C2’–N4’ 1.367(4), C2–N5 1.361(4), C2’–N5’ 1.368(4), C1–N3–C2 127.7(3), C1’–N3’–C2’ 128.2(3), N1–N5 2.930(4), N1’–N5’ 2.969(4).

The zinc atom in **6** (Figure S27) in spirocyclic fashion is four-coordinated by nitrogen atoms of six-membered rings which are far from the ideally planar arrangement. One could suggest from similarities of the ligands' high π electron conjugation as discussed for **2**. These irregularities together with a slight elongation of the N1–N5 (2.930(4), resp. N1'–N5' 2.969(4)) and some Zn–N distances (Zn1–N5 2.016(3), Zn1–N5' 2.020(3)), and widening of N1–Zn1–N5 (94.30(12) resp. N1'–Zn1–N5' 95.96(12)) and C1–N3–C2 (127.7(3) resp. C1'–N3'–C2' 128.2(3)) angles are most probably caused only by steric congestion of this highly crowded molecule.

Alcoholysis of **4** (Scheme S6) under similar conditions (in Et_2O) yielded **1** and presumably an oligomer of $(Me_3Si)_2NZnO^iPr$, but, in toluene a mixture of **1** and the before-mentioned new monometallic biguanide **6** was obtained.

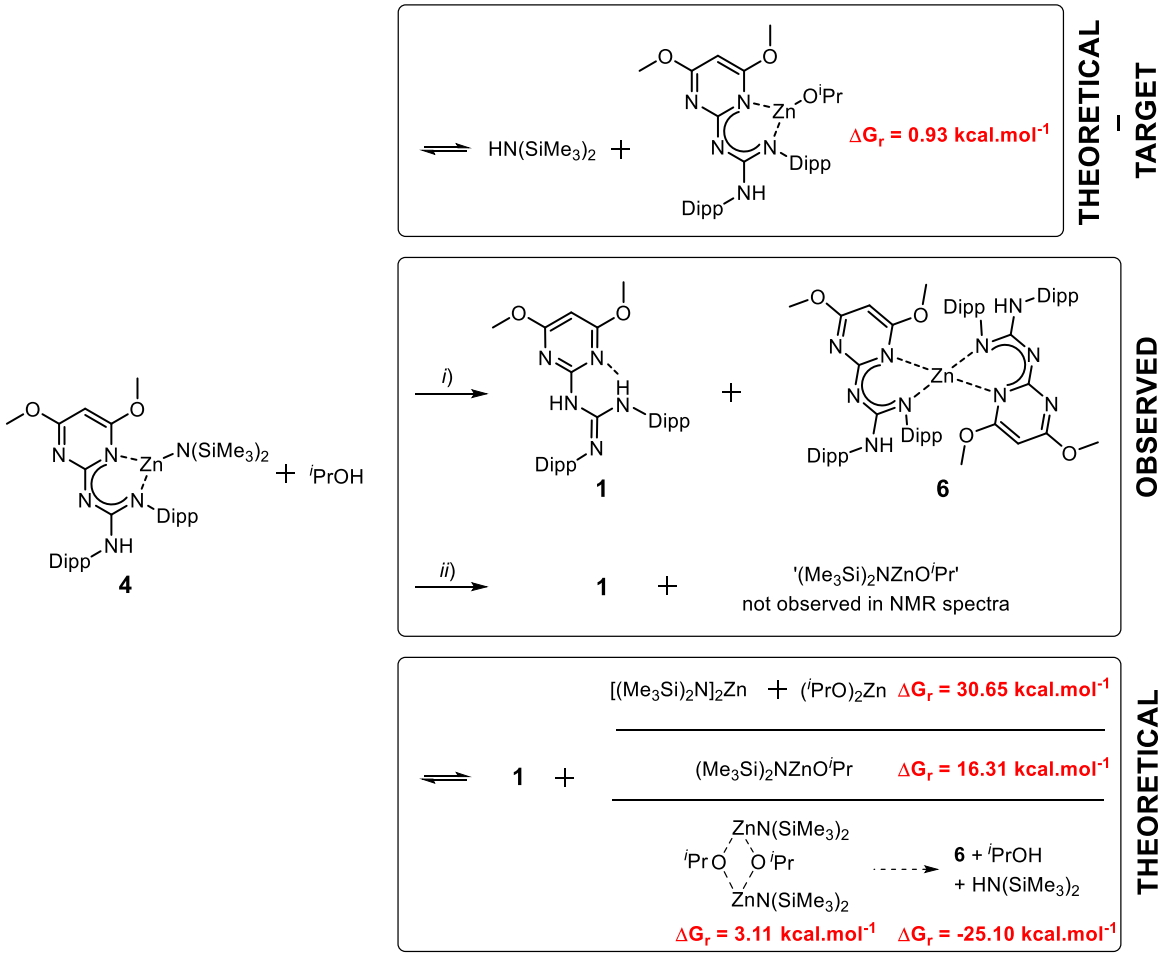

Scheme S6. Theoretical and experimental aspects of alcoholysis of **4** using ^{i}PrOH. *i*) toluene, RT, 24 hours; *ii*) Et_2O, -80°C to RT, 24 hours.

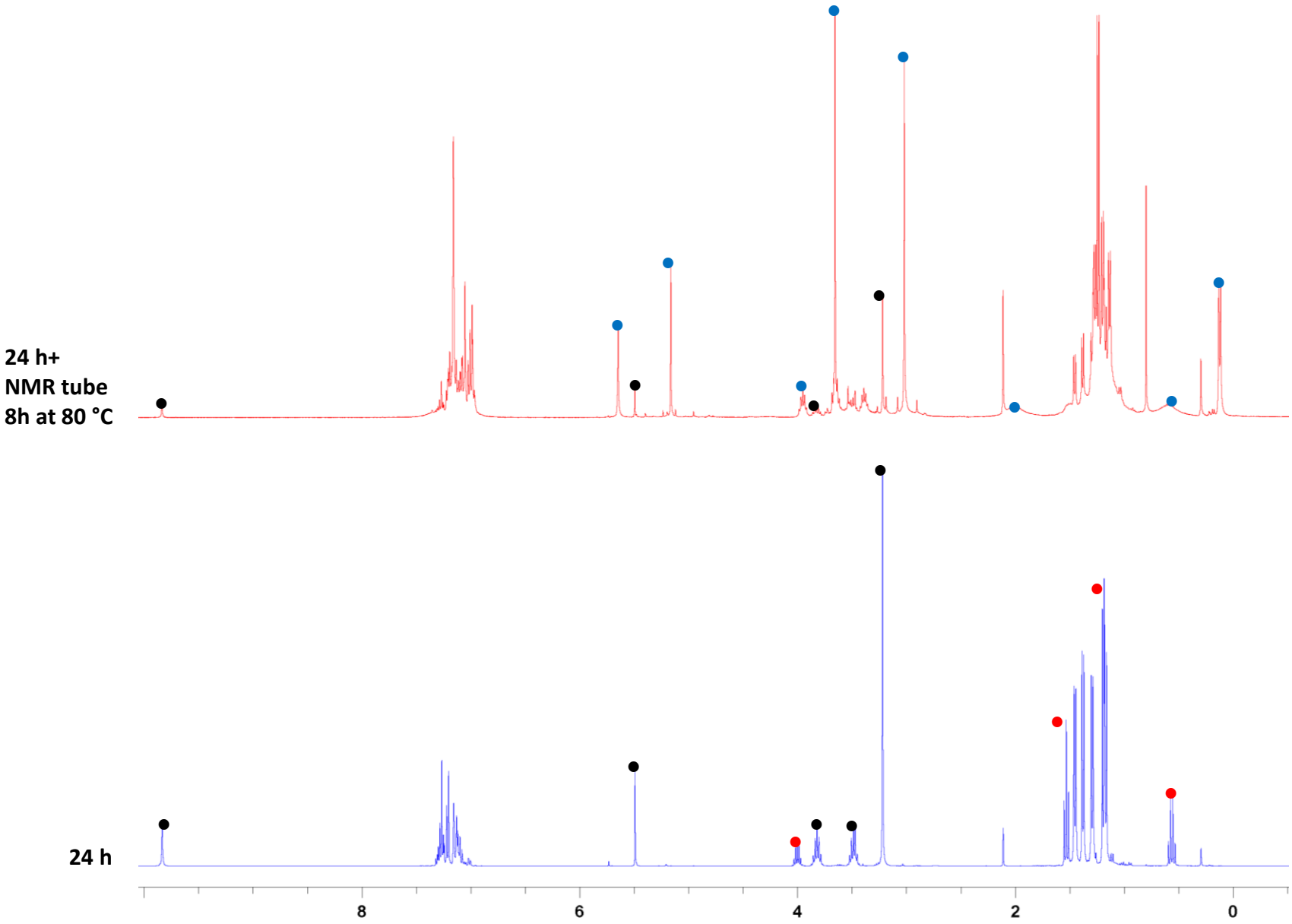

Figure S28. ^{1}H NMR study of the reaction mixture (Tol, RT) of **2** with isopropylalcohol in C_6D_6 at 295 K. Significant NMR signals are marked with dots (black for **1**, red for ^{i}PrOZnEt or equimolar mixture of $(^{i}PrO)_2Zn$ + Et_2Zn and blue for **6**).

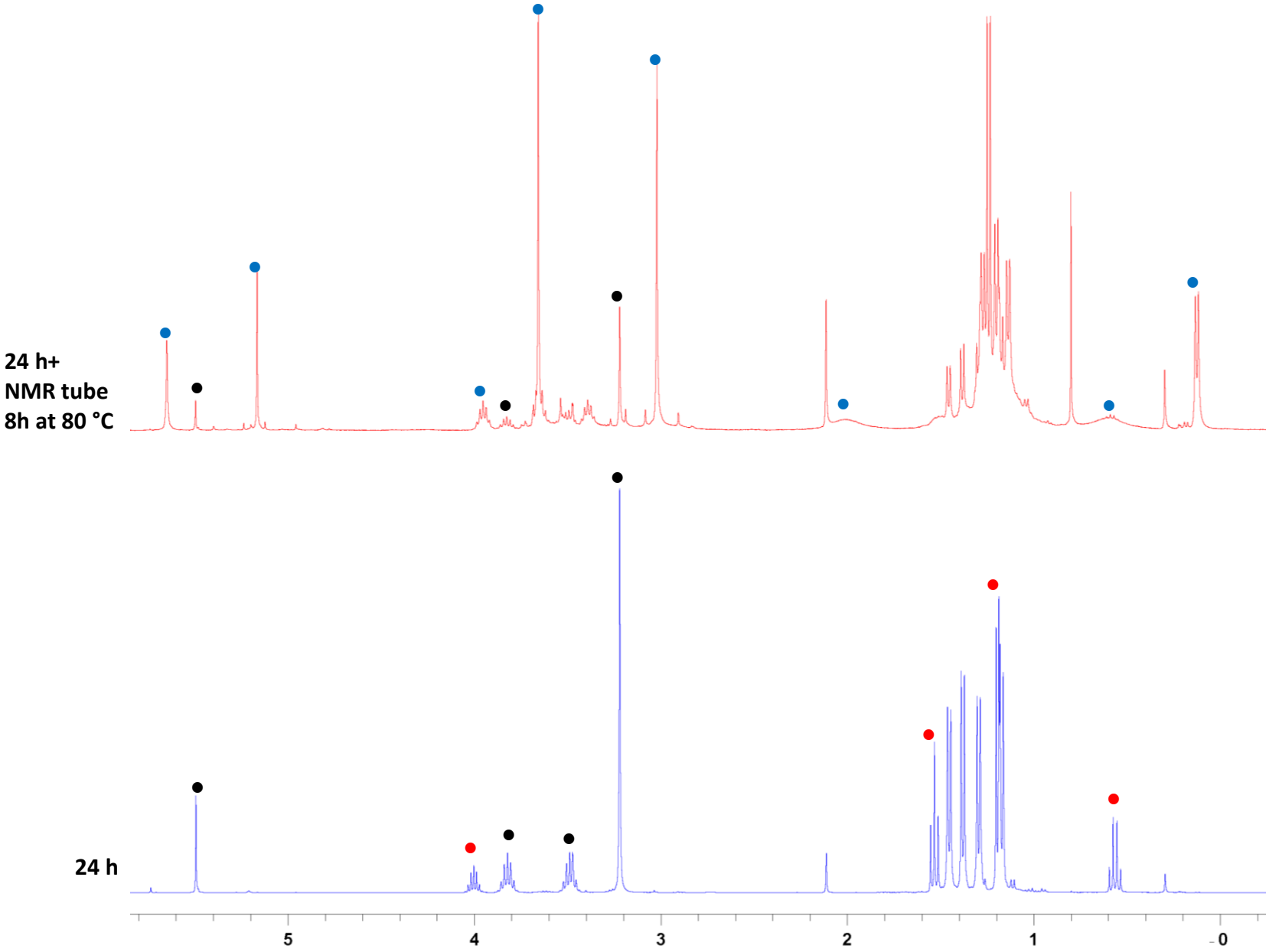

Figure S29. Detail of ^{1}H NMR study of the reaction mixture (Tol, RT) of **2** with isopropylalcohol in C_6D_6 at 295 K. Significant NMR signals are marked with dots (black for **1**, red for ^{i}PrOZnEt or equimolar mixture of $(^{i}PrO)_2Zn$ + Et_2Zn and blue for **6**).

Two equivalents of ^{i}PrOH mixed with **5** (Scheme S7), again, led to the complete decomposition of 5 to **1**. One eq. of ^{i}PrOH, however, led to a mixture, which exhibit complex NMR spectra, lacking the signals of both **1** and **5**. Further attempts to isolate and characterize this compound were unsuccessful.

Calculated isodesmic reactions of **2**, **3**, **4** and **5** with one or two equivalents of ^{i}PrOH, respectively, were examined to yield isopropoxide substituted zinc species and $HN(SiMe_3)_2$ or ethane, on one hand. On the other hand, in the same reaction the formation of complex **6**, identified experimentally, free protoligand **1** and different associates of ^{i}PrOZnEt, $(Me_3Si)_2NZnO^{i}Pr$, Et_2Zn and $(^{i}PrO)_2Zn$ were screened as an alternative. While all the expected protonolytic reactions are slightly endergonic, after the reaction of zinc complexes with isopropylalcohol the formation of **1** and an associate of ^{i}PrOZnEt or $(Me_3Si)_2NZnO^{i}Pr$ in favorable by ~3-19 kcal.mol^{-1} (see Schemes of alcoholysis above). These experiments did not allow us to synthesize isopropoxide zinc biguanides and raise questions about the nature of the active species.

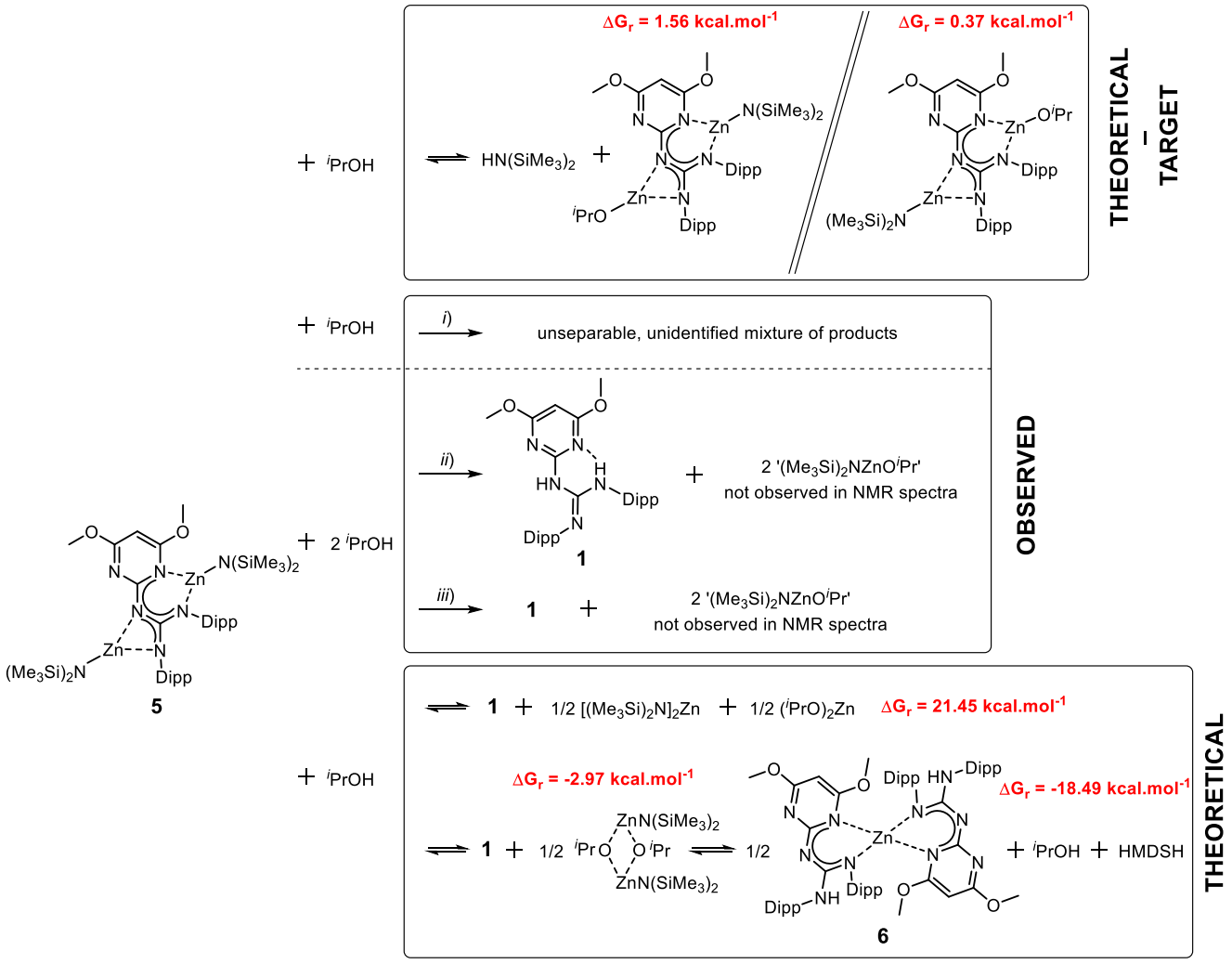

Scheme S7. Theoretical and experimental aspects of alcoholysis of **5** using ^{i}PrOH. *i*) Et_2O, -80°C to RT, 24 hours; *ii*) Et_2O, RT, 24 hours; *iii*) Et_2O, -80°C to RT, 24 hours.

Polymerization Results

Table S2. ROP of *rac*-lactide mediated by complexes **2**, **4**, **5** and **6**[a,b]

Entry	Cat.	[*rac*-LA]: [cat]$_0$: [^{i}PrOH]	Time	Conv (%)[c]	$M_{n,\,theo}$[d]	$M_{n,\,exp}$[f]	$Đ$[f]	P_r[g]
1	**2**	100:1:0	2 h	0	-	-	-	-
2	**2**	100:1:1	2 h	0	-	-	-	-
3	**3**	100:0.5:1	2 h	0	-	-	-	-
4	**4**	100:1:0	2 h	61	8,800[e]	188,000	1.11	n.d.
5	**5**	100:1:0	2 h	32	2,300[e]	54,100	1.66	n.d.
6	**4**	100:1:1	1 min	98	14,100	13,400	1.07	0.63
7	**5**	100:0.5:1	1 min	96	13,800	18,700	1.13	n.d.
8	**5**	100:1:1	1 min	80	11,500	15,800	1.24	n.d.
9	**5**	500:0.5:1	15 min	86	62,000	69,500	1.38	0.72
10	**4**	500:1:1	5 min	98	70,600	57,400	1.21	0.64
11	**4**	1,000:1:1	5 min	94	135,000	116,100	1.08	n.d.
12	**4**	1,000:1:1	3 min	83	119,600	110,700	1.08	0.65
13	**5**	1,000:0.5:1	3 min	43	62,000	60,000	1.40	n.d.
14	**4**	5,000:1:10	30 min	88	63,400	55,900	1.04	n.d.
15	**5**	5,000:0.5:10	20 min	90	64,900	67,100	1.04	n.d.
16	**6**	100:1:1	1 min	10	n.d.	n.d.	n.d.	n.d.
17	$Zn[N(SiMe_3)_2]_2$	100:1:1	2 h	40	5,800	5,500	1.50	n.d.
18	**1**	100:1:1	2 h	0	-	-	-	-
19	**1** + $Zn[N(SiMe_3)_2]_2$	1,000:1:1	3 min	14	20,200	45,800	1.95	n.d.

[a] All reactions have been at least duplicated. Polymerization conditions: [*rac*-LA]$_0$ = 1.5 M, DCM, 25 °C. [b] Reactions performed with a batch of recrystallized and sublimed LA. [c] Monomer conversion calculated from ^{1}H NMR spectra. [d] Calculated using $M_{n,\,theo}$ = [*rac*-LA]$_0$/[^{i}PrOH]$_0$ × M_{LA} × conversion. [e] Calculated using $M_{n,\,theo}$ = [*rac*-LA]$_0$/[Zn]$_0$ × M_{LA} × conversion. [f] Measured by GPC in THF (45°C) using PS standards and corrected by applying the appropriate correcting factor (0.58). [g] Determined from the methine region of the selectively homodecoupled 1D-^{1}H NMR spectrum.

As the homoleptic complex **6** is suspected to be formed under catalytic conditions, we performed the ROP of *rac*-LA in the presence of **6**. The results showed that it was active, but much less than **4** and **5**, producing PLA with only 10% conversion after 1 minute at room temperature and with a 1 mol% catalyst loading (Table S2, entry 16).

One should highlight that the combination of $Zn[N(SiMe_3)_2]_2$ and alcohol has been previously described as effective catalyst for the ROP of cyclic esters.[5] We therefore carried out ROP tests using either $Zn[N(SiMe_3)_2]_2$/^{i}PrOH (1:1), biguanide **1**/^{i}PrOH (1:1) or a mixture of **1**, $Zn[N(SiMe_3)_2]_2$ and ^{i}PrOH in a 1:1:1 ratio (Table S2, entries 17–19). All these combinations failed to match the performance of complexes **4** and **5**, both in terms of activity and polymerization control, suggesting that the biguanide-Zn and Zn-biguanide-Zn entities are preserved under catalytic conditions and 'responsible' for the catalytic activity.

Polymerization – representative ^{1}H NMR Spectra

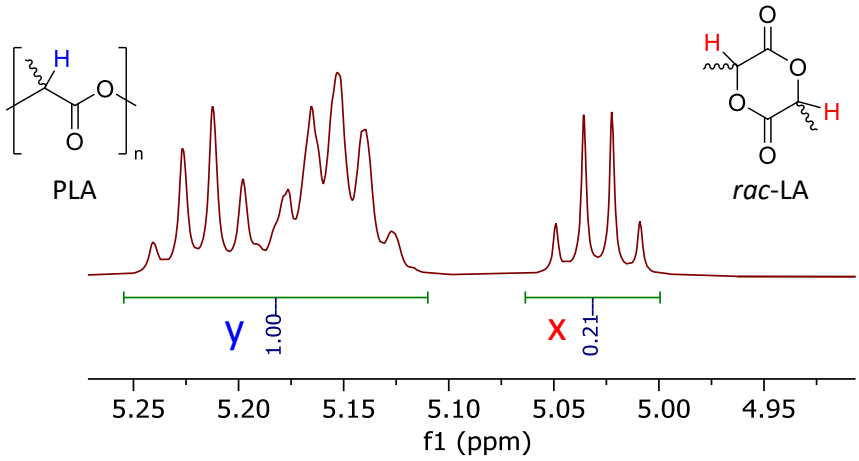

Figure S30. ^{1}H NMR spectrum in $CDCl_3$ of the methine region of a crude PLA produced using **4** in DCM at 25 °C ([*rac*-LA:**4**:^{i}PrOH] = 1000:1:1, 3 min) aiming to determine PLA conversion = [y/(x+y)] × 100% (Table S2, entry 12).

5. Yuan, Y.; Jing, X.; Xiao, H.; Chen, X.; Huang, Y. Zinc-based catalyst for the ring-opening polymerization of cyclic esters. *J. Appl. Polym. Sci.* **2011**, *121*, 2378–2385. DOI: 10.1002/app.33956.

Table S3. Bernouillan equations of probability obtained for the different tetrads present in PLA obtained with *rac*-LA.

Tetrad	Bernouillian Probability
mmm	$P_m^2 + P_rP_m/2$
mmr	$P_rP_m/2$
rmm	$P_rP_m/2$
rmr	$P_r^2/2$
mrm	$P_r^2 + P_rP_m/2$

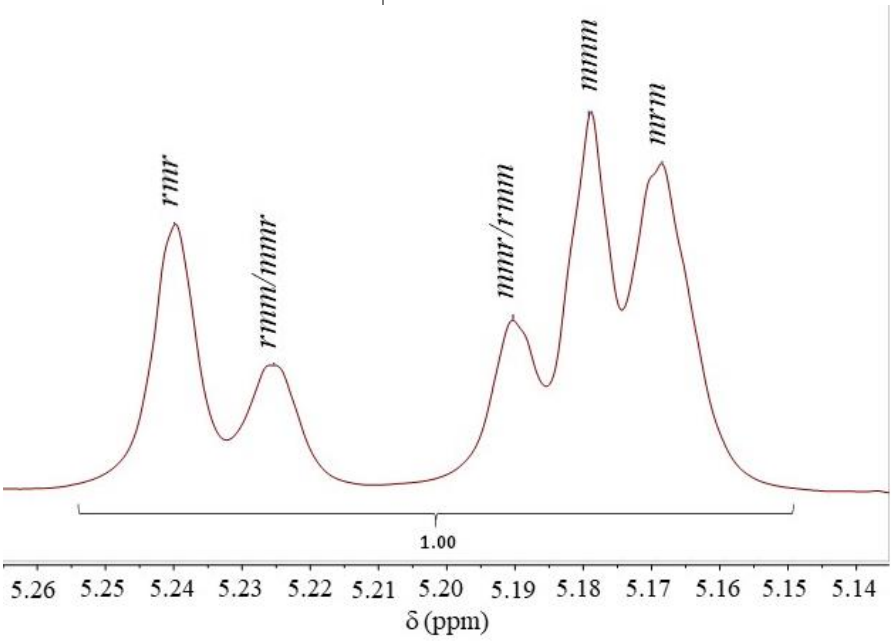

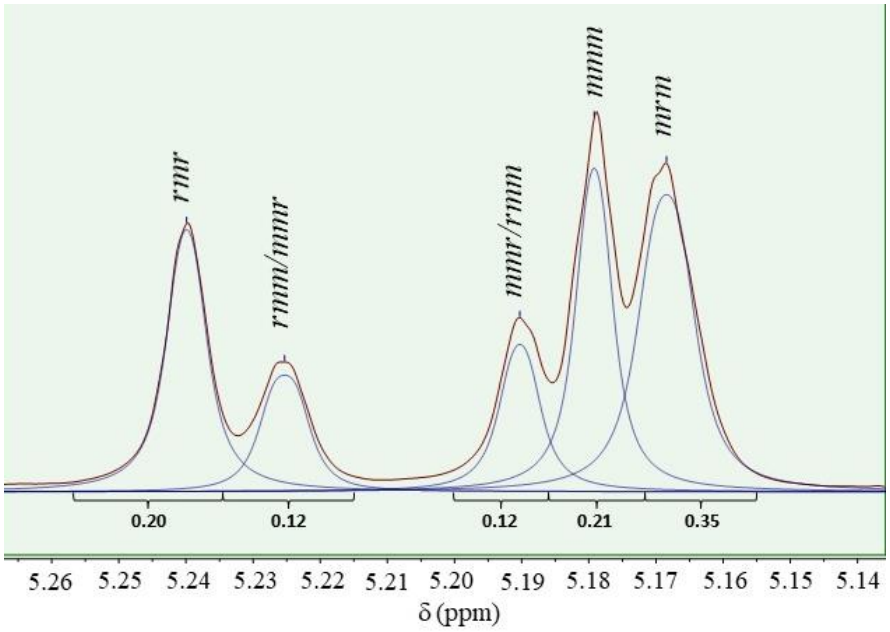

Figure S31. Top: Homonuclear decoupled ^{1}H NMR spectrum in $CDCl_3$ of the methine region of PLA prepared from *rac*-lactide with **4** in DCM at 25 °C ([*rac*-LA:**4**:^{i}PrOH] = 1000:1:1, 3 min). Bottom: Deconvoluted spectrum with the integrations of each peak (P_r = 0.65, Table S2, entry 12).

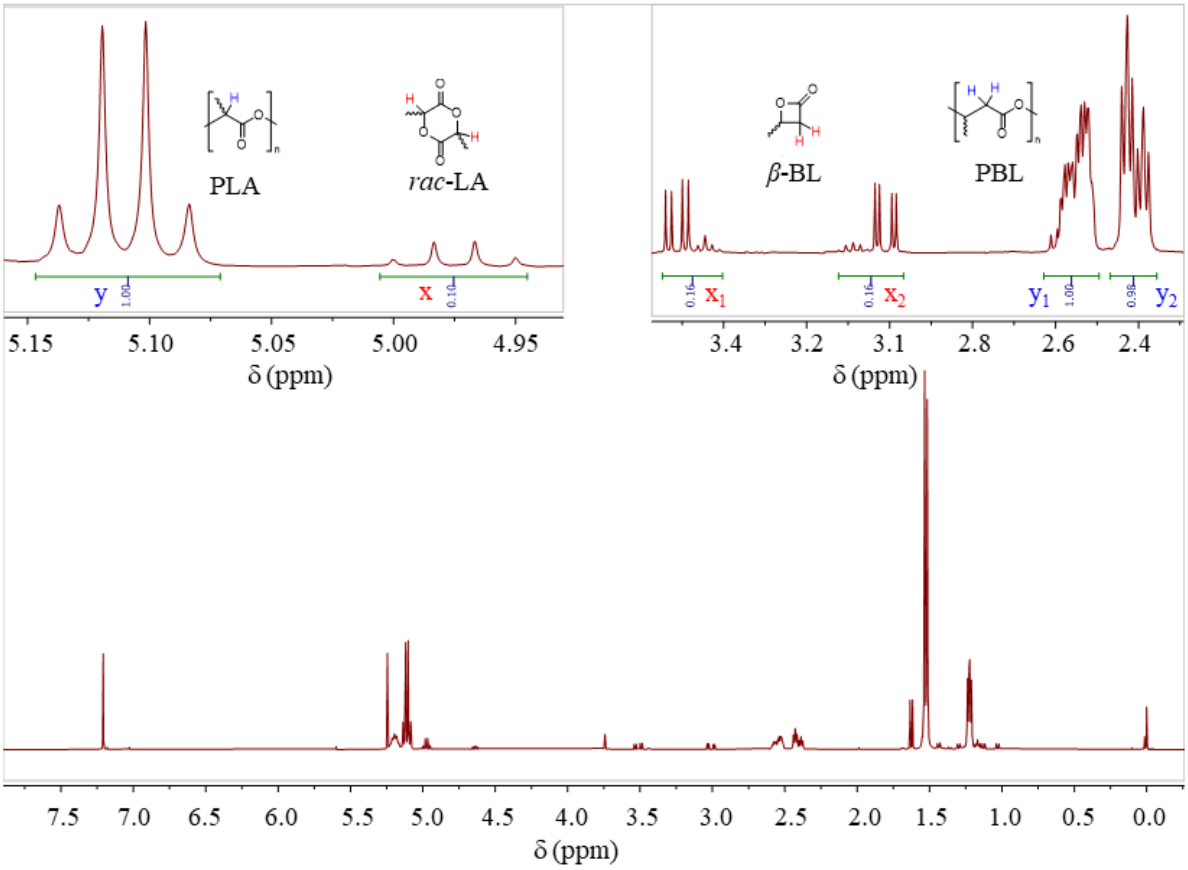

Figure S32. ^{1}H NMR spectrum of crude PLLA-*b*-PHB in $CDCl_3$ produced using **4** in DCM at 45°C aiming to determine PLA conversion = [y/(x+y)] × 100% and PHB conversion = [(y_1'+y_2')/(x_1'+x_2'+ y_1'+y_2')] × 100% (see Table S2 in Main text, entry 3). The copolymer composition showed a PLLA/PHB ratio of 50/50.

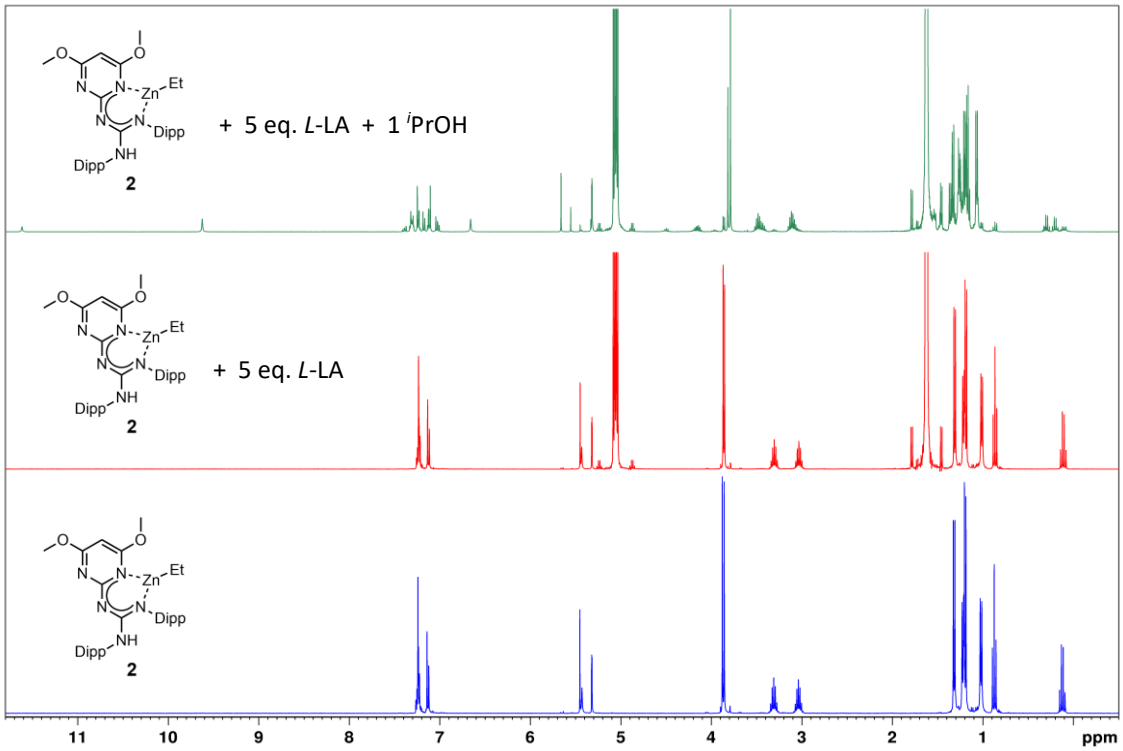

Figure S33. Top: ^{1}H NMR spectrum of complex **2** in CD_2Cl_2 at 25 °C, Middle: ^{1}H NMR spectrum of complex **2** with 5 eq. of *L*-LA in in CD_2Cl_2 at 25 °C. Bottom: ^{1}H NMR spectrum of complex **2** with 5 eq. of *L*-LA and 1 equiv. of ^{i}PrOH in CD_2Cl_2 at 25 °C (10 min after addition of ^{i}PrOH).

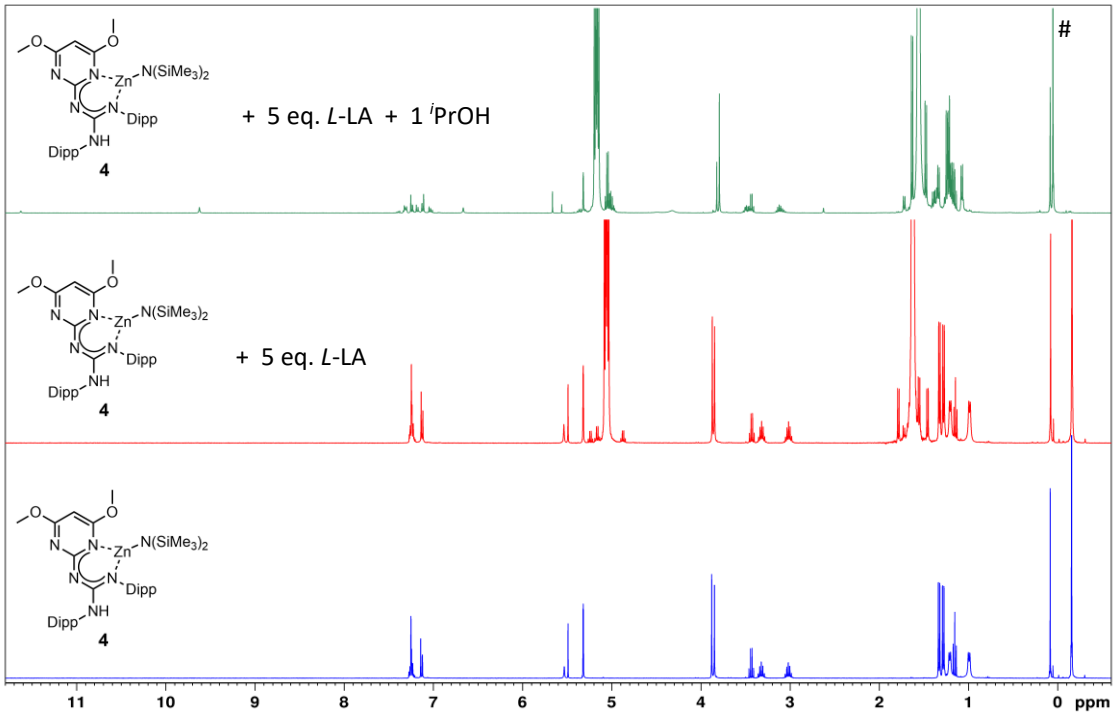

Figure S34. Top: ^{1}H NMR spectrum of complex **4** in CD_2Cl_2 at 25 °C, Middle: ^{1}H NMR spectrum of complex **4** with 5 eq. of *L*-LA in in CD_2Cl_2 at 25 °C. Bottom: ^{1}H NMR spectrum of complex **4** with 5 equiv. of *L*-LA and 1 eq. of ^{i}PrOH in CD_2Cl_2 at 25 °C (10 min after addition ^{i}PrOH). The signal of bis(trimethylsilyl)amine is marked with #.

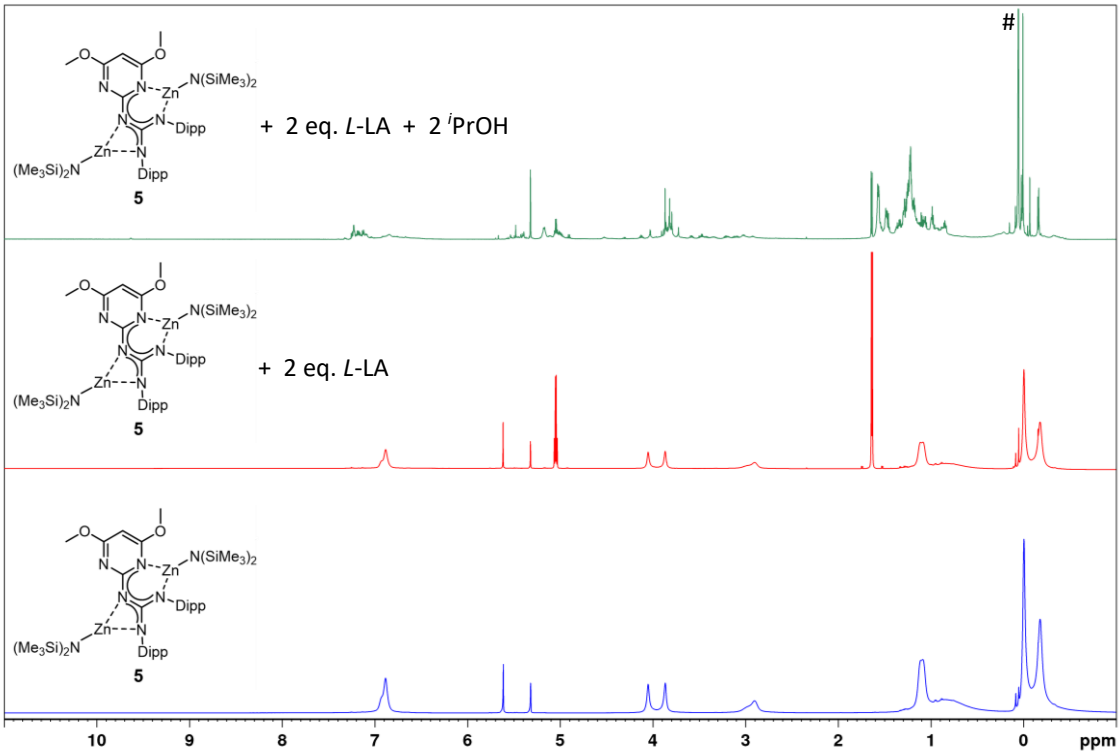

Figure S35. Top: ^{1}H NMR spectrum of complex **5** in CD_2Cl_2 at 25 °C, Middle: ^{1}H NMR spectrum of complex **5** with 2 eq. of *L*-LA in in CD_2Cl_2 at 25 °C. Bottom: ^{1}H NMR spectrum of complex **5** with 2 equiv. of *L*-LA and 2 eq. of ^{i}PrOH in CD_2Cl_2 at 25 °C (10 min after addition ^{i}PrOH). The signal of bis(trimethylsilyl)amine is marked with #.

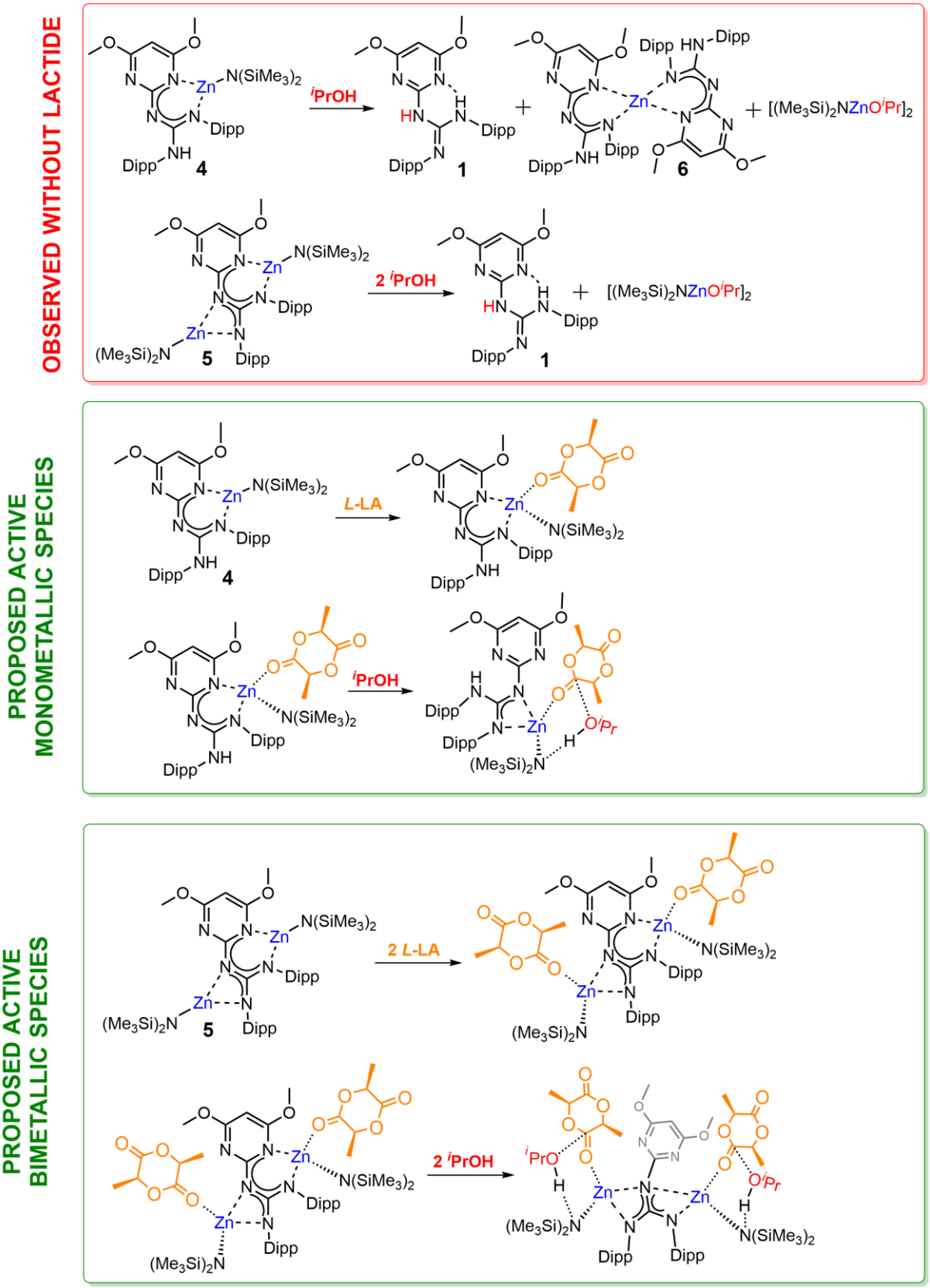

Figure S36. Top - behavior of complexes **4** and **5** in the presence of an initiator, observed in NMR spectra of stoichiometric reactions and supported by DFT calculations. Middle and bottom – working hypothesis of proposed active species originating from complexes **4** and **5**.

Diffusion ordered NMR spectroscopy (DOSY)

DOSY NMR analysis was used to differentiate copolymer chains from a mixture of homopolymers by showing the presence of a single diffusion coefficient or distinct diffusion coefficients. In addition, the average molar mass of the (co)polymers produced was determined on the basis of DOSY NMR calibration experiments and showed good agreement with the GPC data.[6] For samples of standard LA, BL, LA+BL, PLA, PHB, PLA+PHB, PHB-*b*-PLLA and PHB-*b*-PLLA-*b*-PDLA, NMR tubes were prepared from 1.0 mg of monomer(s) or (co)polymer(s) and 1 ml of $CDCl_3$. Control experiments were carried out to ensure that there was no entanglement of the PLA and PHB homopolymer chains, or at least that this did not affect the diffusion coefficient (see Fig. S38a-S38g).

Table S4. Diffusion coefficients determined via DOSY for PLA standard in $CDCl_3$.

Entry	M_n (g/mol)[a]	$Đ$[a]	D ($m^2.s^{-1}$)
1[b]	144	-	$1.61 \cdot 10^{-9}$
2	4,200	1.07	$2.02 \cdot 10^{-10}$
3	14,200	1.15	$1.01 \cdot 10^{-10}$
4	22,100	1.15	$7.5 \cdot 10^{-11}$
5	39,700	1.11	$5.4 \cdot 10^{-11}$
6	58,600	1.15	$4.22 \cdot 10^{-11}$
7	116,100	1.08	$3.05 \cdot 10^{-11}$

[a]Measured by GPC in THF (45°C) using PS standards and corrected by applying the appropriate correcting factor (0.58). [b]Lactide used as standard

6. Voorter, P.; McKay, A.; Dai, J.; Paravagna, O.; Cameron, N. R.; Junkers, T. Solvent-Independent Molecular Weight Determination of Polymers Based on a Truly Universal Calibration. *Angew. Chem. Int. Ed.* **2022**, *6*, e202114536. DOI: 10.1002/anie.202114536.

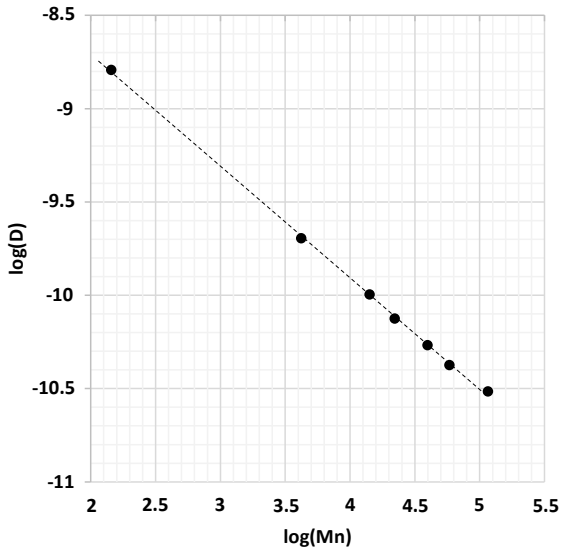

Figure S37. Plot of log(*D*) versus log(Mn) giving the DOSY calibration curve using PLA standard. Coefficient of correlation R^2 = 0.9993.

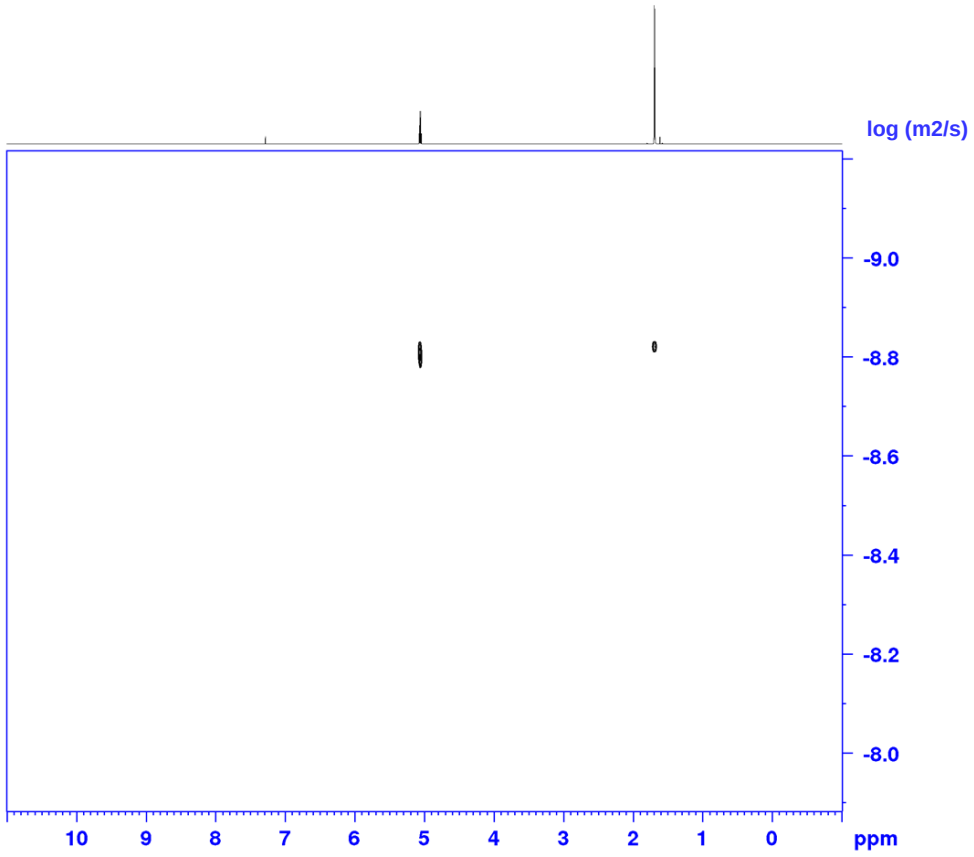

Figure S1a. DOSY NMR spectrum of *L*-LA in $CDCl_3$.

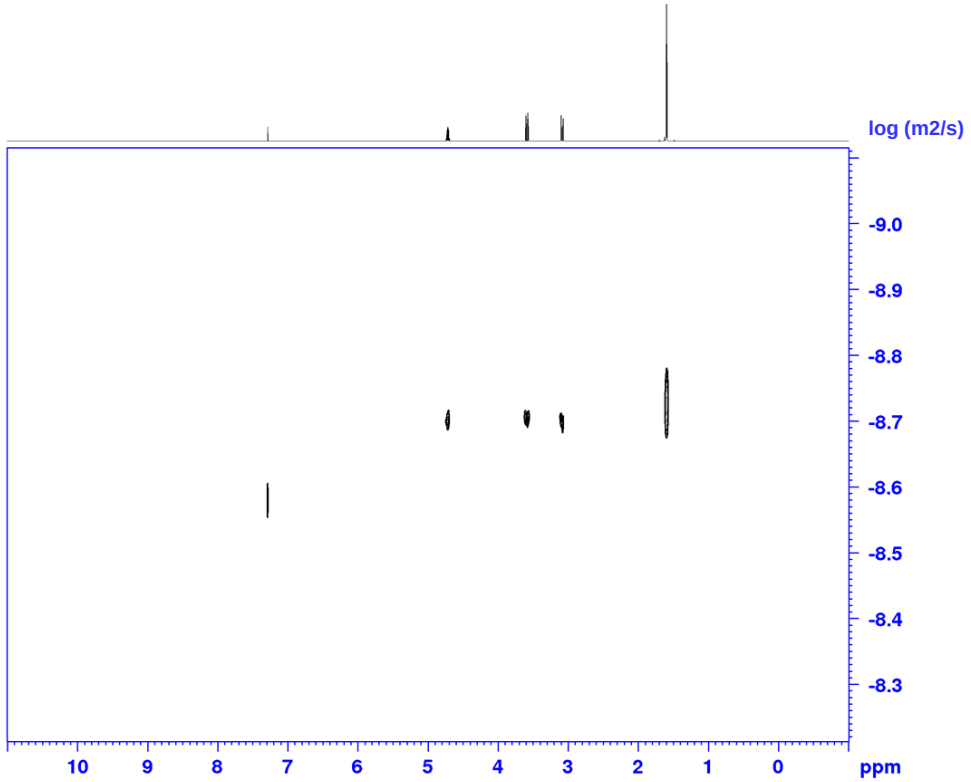

Figure S2b. DOSY NMR spectrum of *rac*-BL in $CDCl_3$.

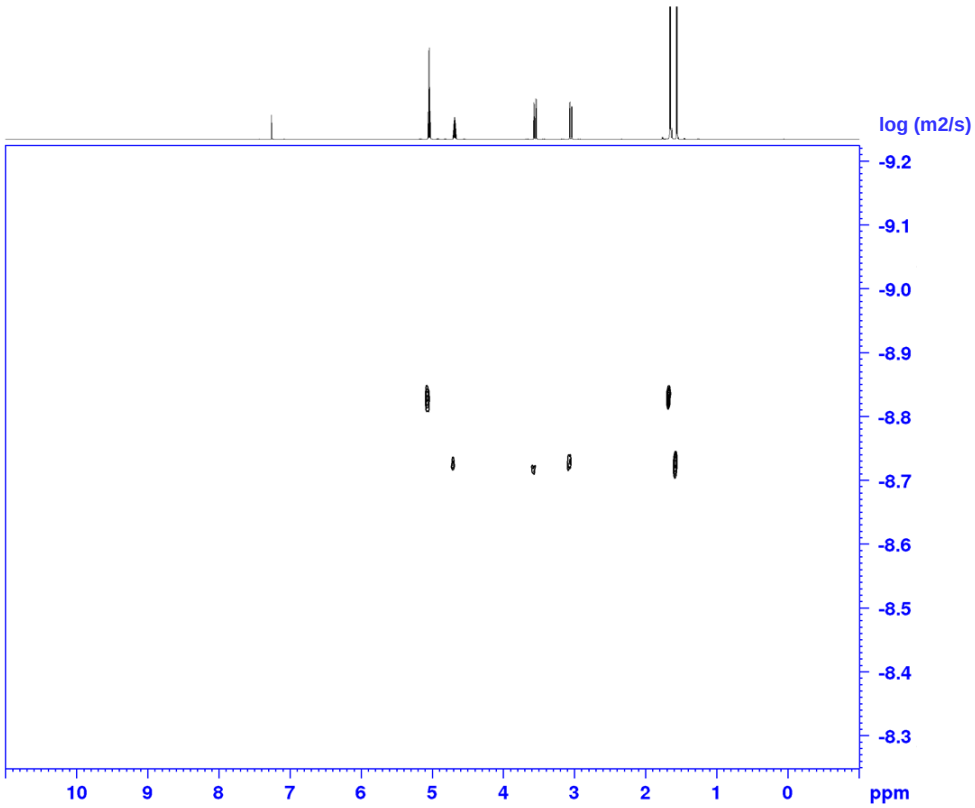

Figure S3c. DOSY NMR spectrum of a mixture of *L*-LA and *rac*-BL in $CDCl_3$.

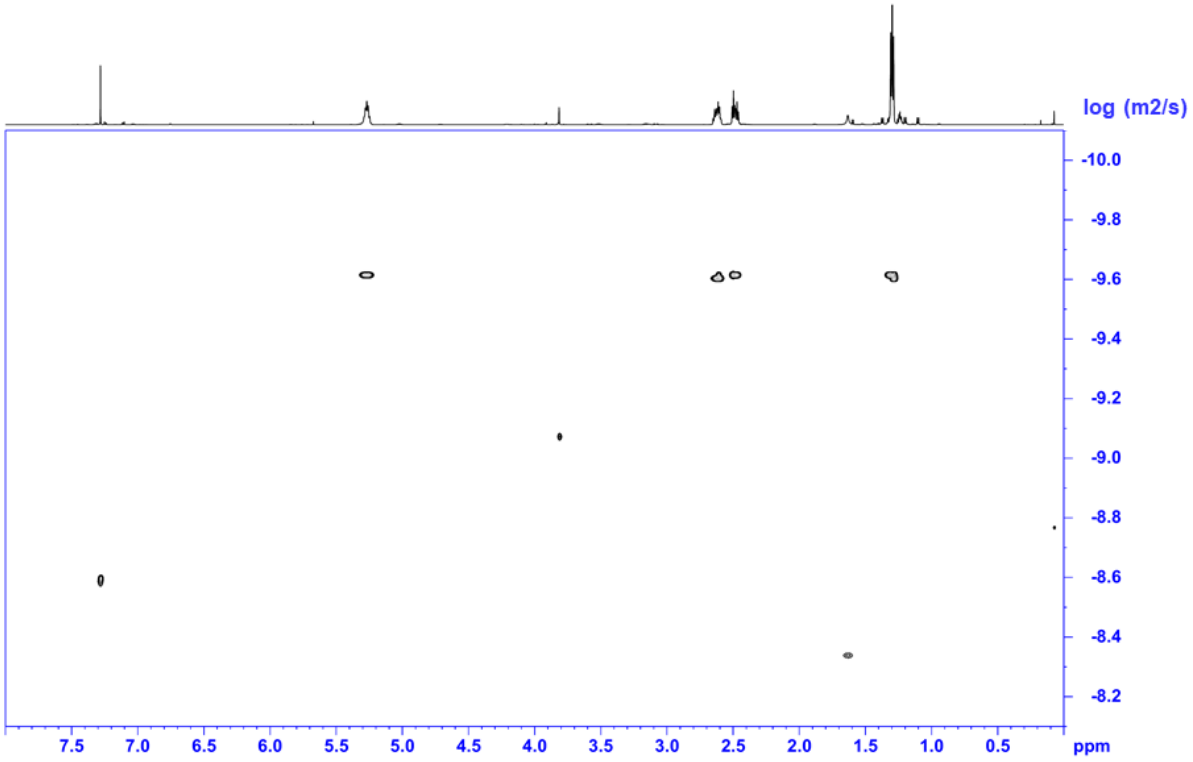

Figure S4d. DOSY NMR spectrum of PHB in $CDCl_3$ (Table S5, entry 1).

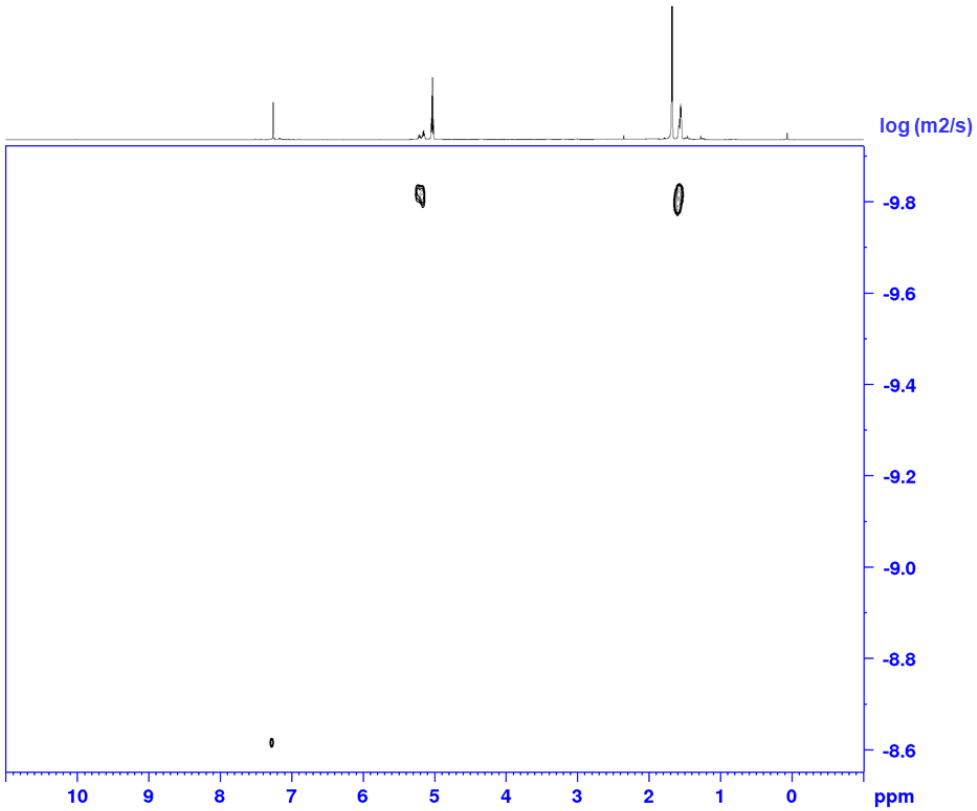

Figure S5e. DOSY NMR spectrum of PLA in $CDCl_3$ ($M_{n,\,GPC}$ = 5,576; $Đ$ =1.17).

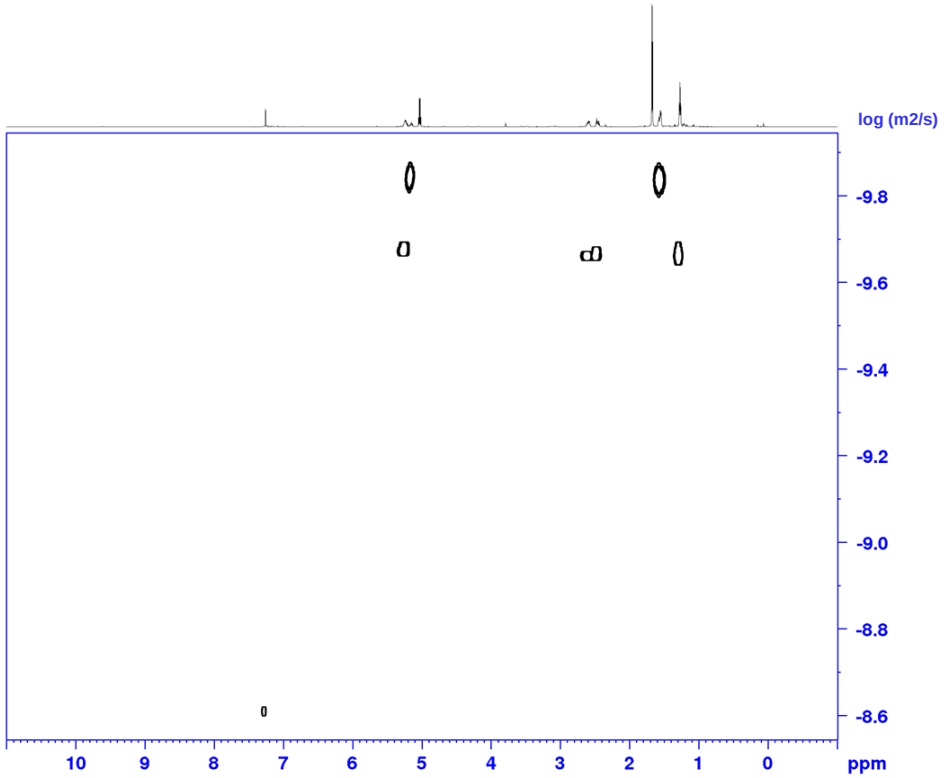

Figure S6f. DOSY NMR spectrum of a mixture of PLA ($M_{n,\,GPC}$ = 5,576; $Đ$ =1.17).and PHB ($M_{n,\,GPC}$ = 2,964; $Đ$ = 1.08) in $CDCl_3$

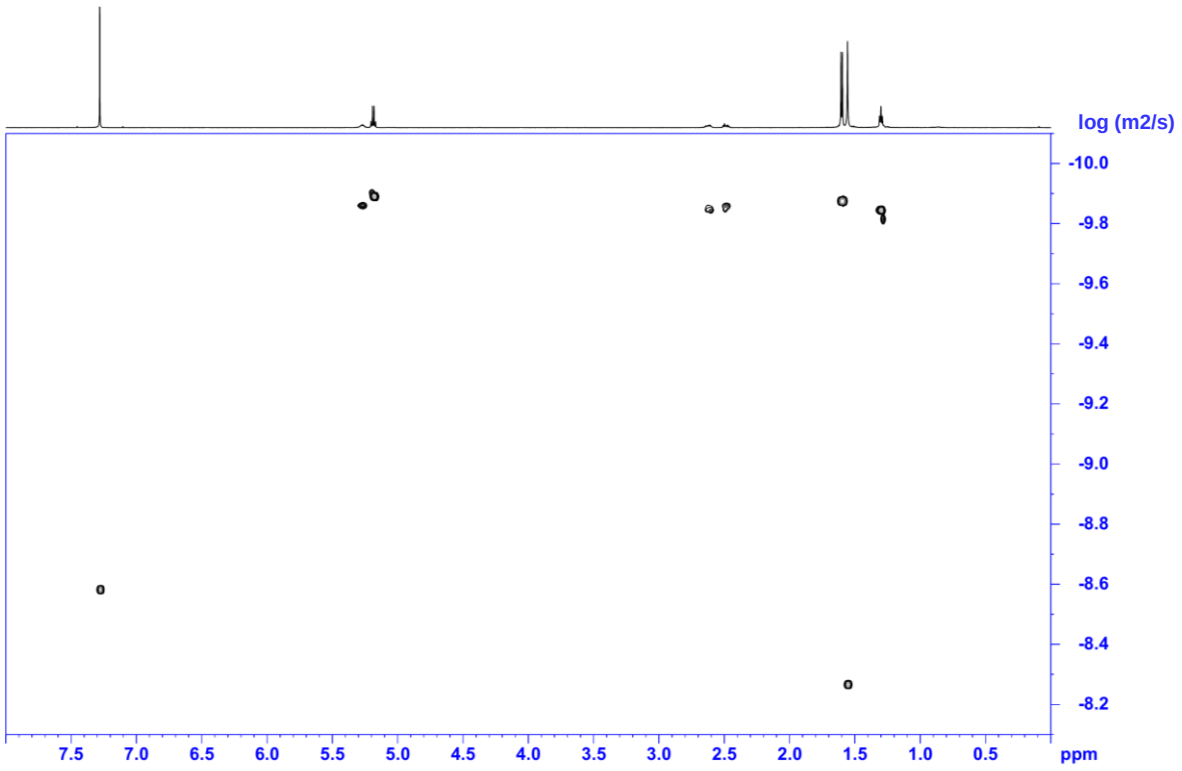

Figure S7g. DOSY NMR spectrum of PHB-*b*-PLLA in $CDCl_3$ (Table S5, entry 2).

Table S5. Approximation of the molecular weight number by DOSY NMR in $CDCl_3$ of PHB (entry 1) and PHB-*b*-PLLA (entry 2) using the DOSY calibration curve.

Entry	*Ratio* (*rac*-BL:L-LA:Cat:^{i}PrOH)	*Conv. BL* (%)	*Conv. LA* (%)	$M_{n,\ theo}$ (g.mol^{-1})[c]	$M_{n\ DOSY}$ (g.mol^{-1})	*D* ($m^2.s^{-1}$) -
1[a]	[50:0:1:1]	93	-	4,000	3,500	$2.34.10^{-10}$
2[b]	[50:50:1:1]	90	90	10,400	10,300	$1.22.10^{-10}$

[a] *Polymerization conditions: [rac-BL]$_0$ = 1.5 M, DCM, 45 °C, 3 h.* [b] *Table 2 in article, entry 5.* [c] *Calculated using* $M_{n,\ theo} = [rac\text{-}LA]_0/[^{i}PrOH]_0 \times M_{LA} \times Conv._{LA} + [rac\text{-}BL]_0/[^{i}PrOH]_0 \times M_{BL} \times Conv._{BL}$ *(g.mol^{-1}).*

Representative GPC Spectra

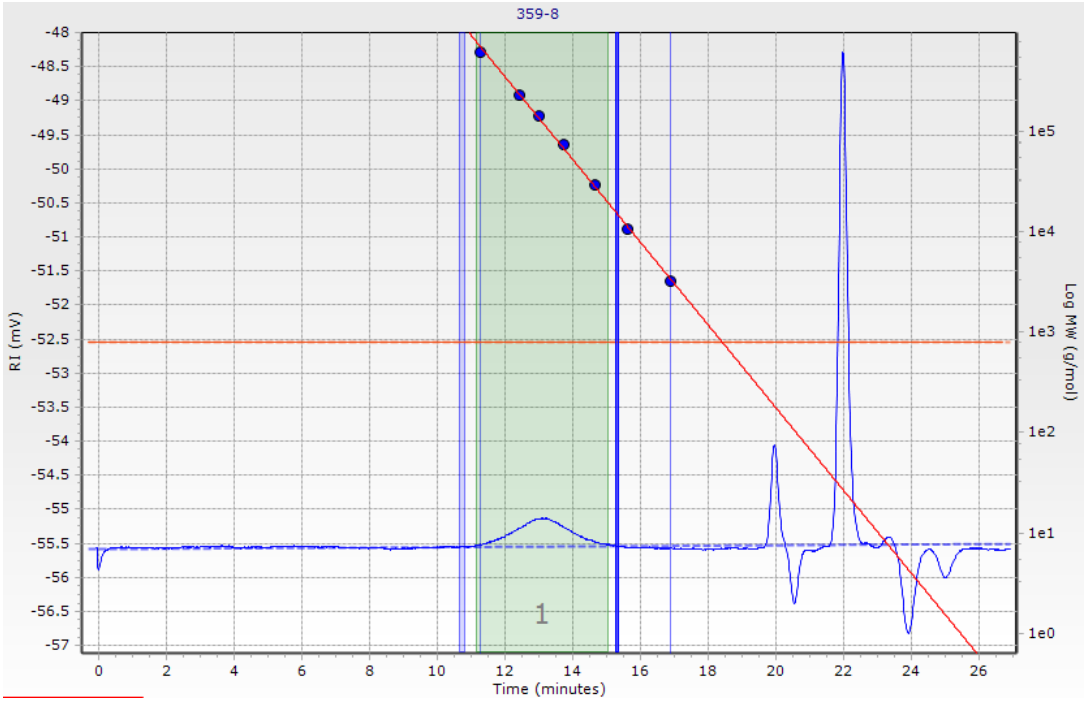

Figure S39. GPC spectrum of crude PLA produced using **5** in DCM at 25°C ([*rac*-LA:**5**:^{i}PrOH] = 100:1:0, 2 h) (see Table 1 in article, entry 2).

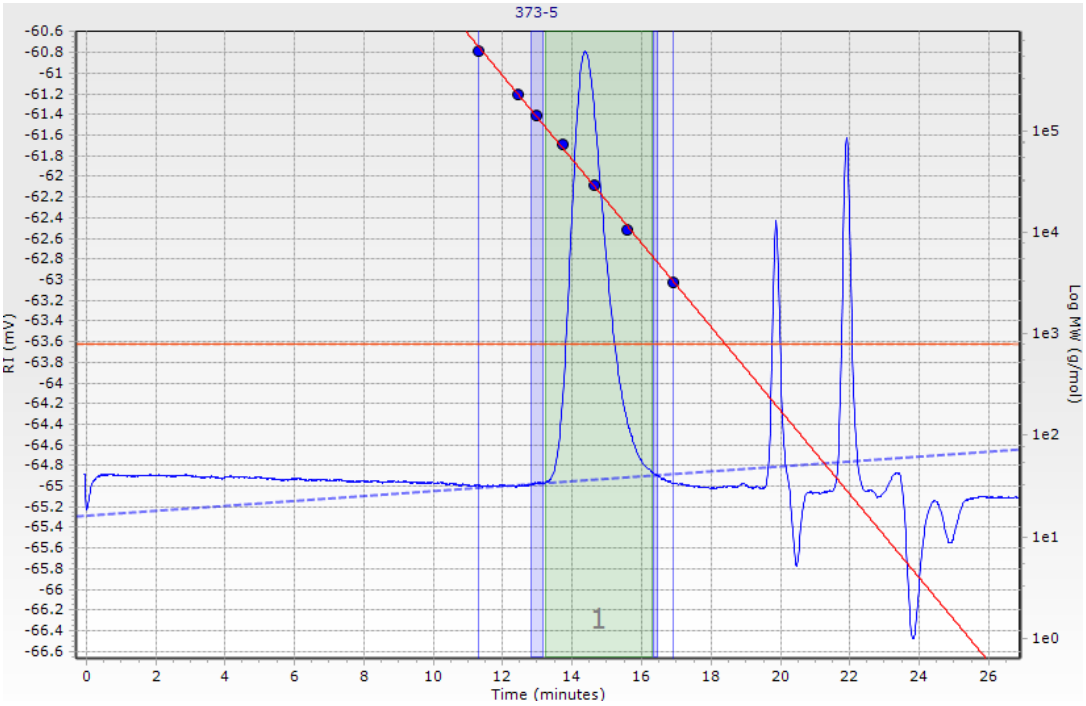

Figure S40. GPC spectrum of crude PLA produced using **5** in DCM at 25°C ([*rac*-LA:**5**:^{i}PrOH] = 100:1:1, 1 min) (see Table 1 in article, entry 5).

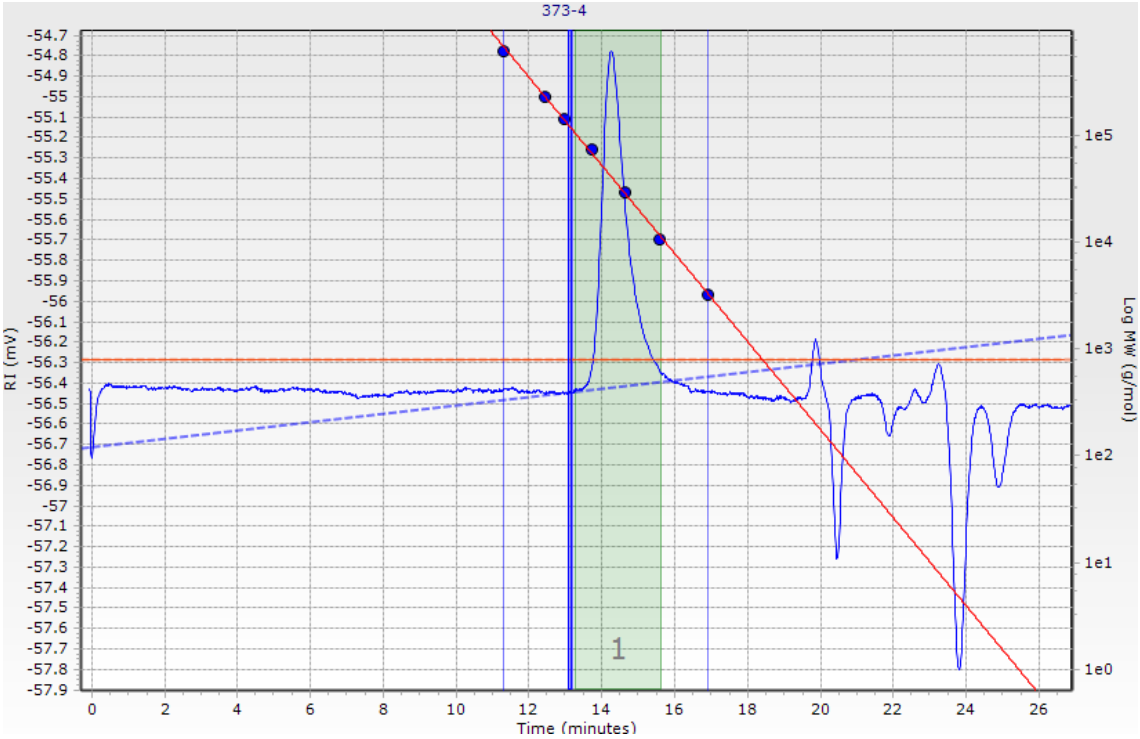

Figure S41. GPC spectrum of crude PLA produced using **5** in DCM at 25°C ([*rac*-LA:**5**:^{i}PrOH] = 100:0.5:1, 1 min) (see Table 1 in article, entry 4).

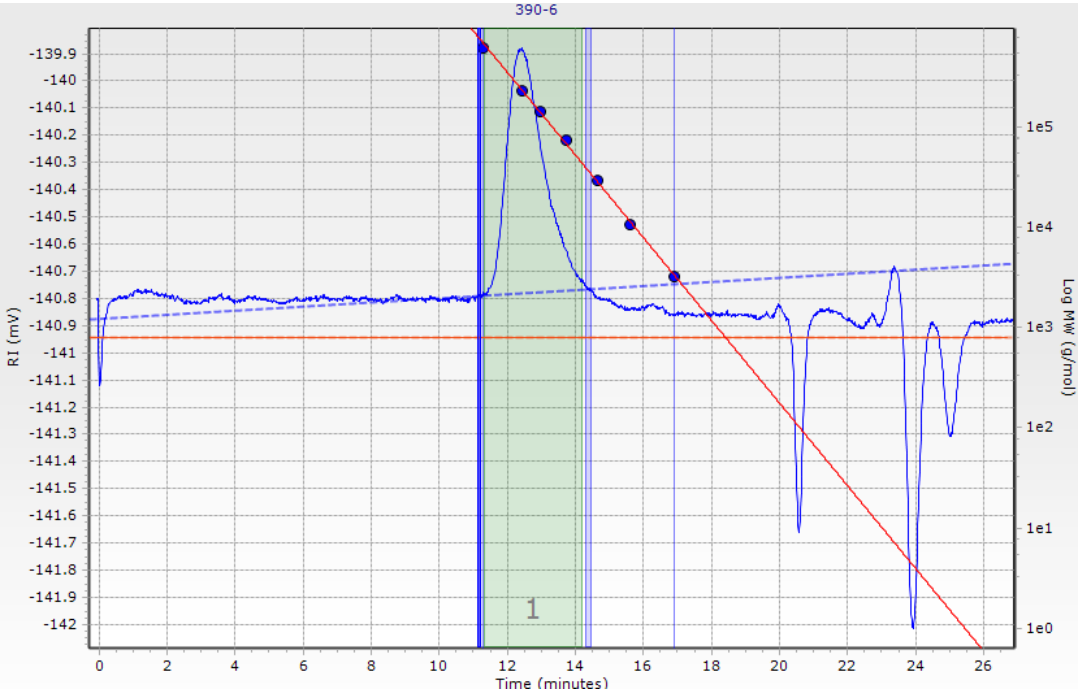

Figure S42. GPC spectrum of crude PLA produced using **5** in DCM at 25°C ([*rac*-LA:**5**:^{i}PrOH] = 500:0.5:1, 1 min) (see Table 1 in article, entry 6).

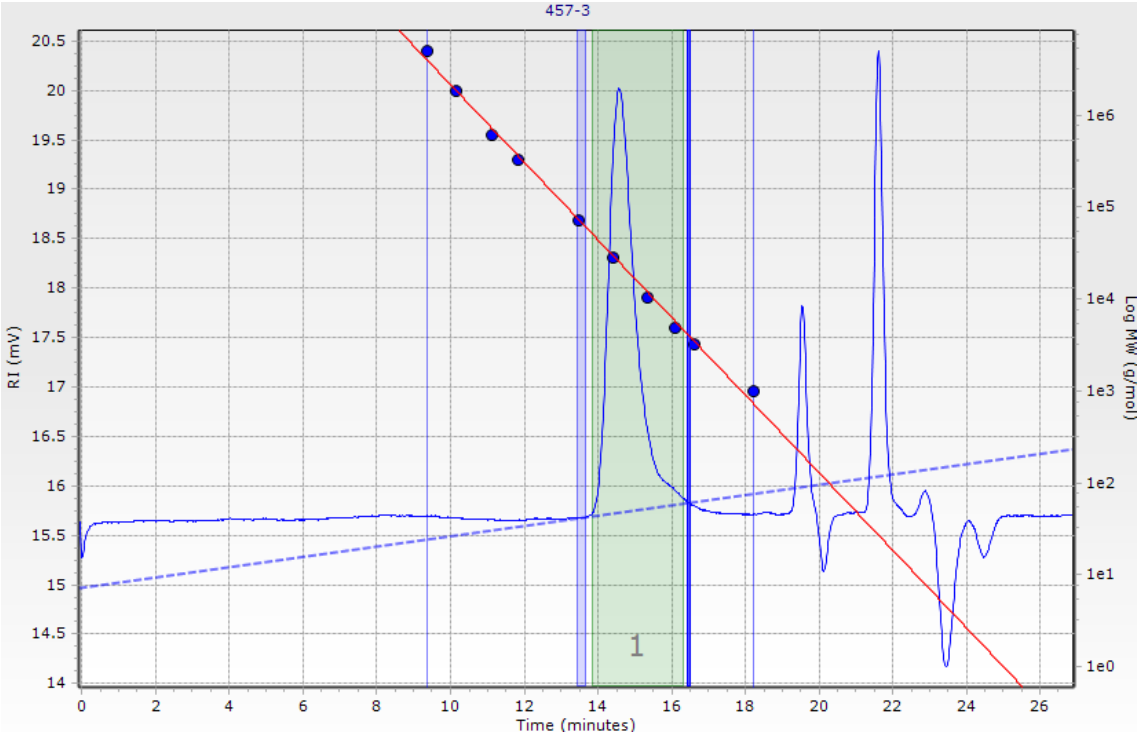

Figure S43. GPC spectrum of crude PHB-*b*-PLLA produced using **4** in DCM at 45°C/25°C ([*rac*-BL:*L*-LA:**4**:^{i}PrOH] = 50:50:1:1, 3 h/1 min) (see Table 2 in article, entry 5).

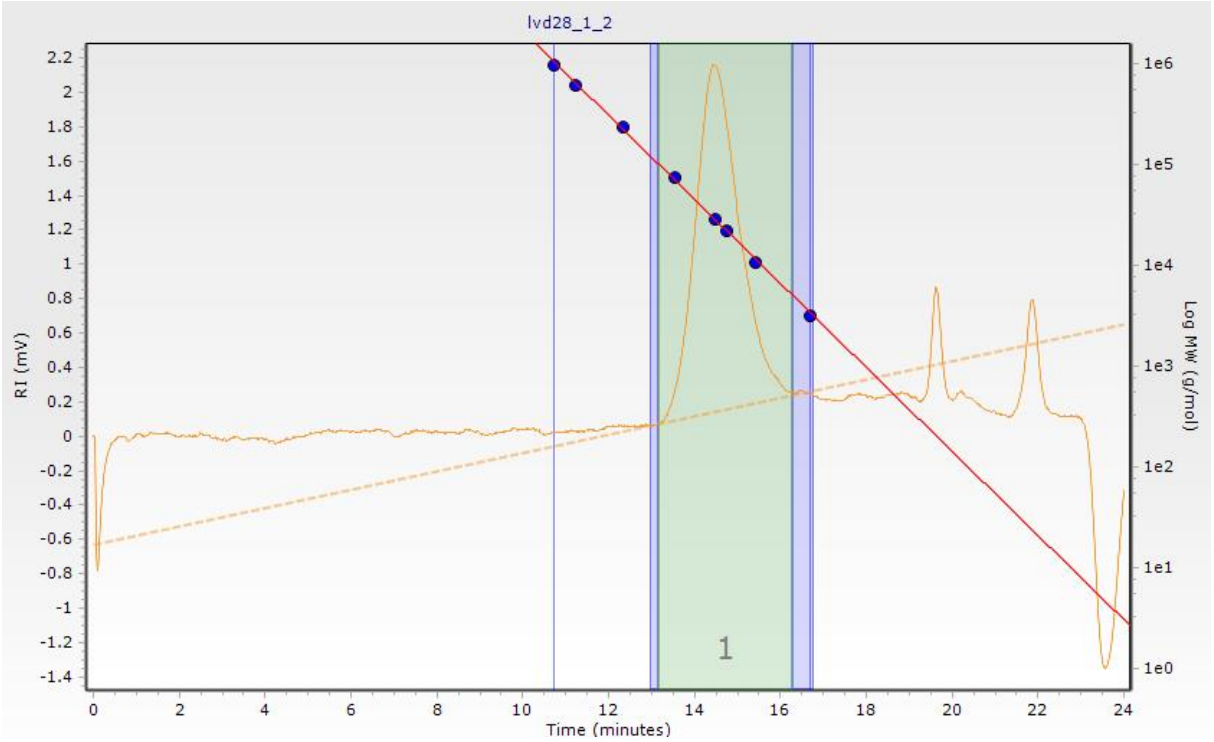

Figure S44. GPC spectrum of crude PLA-*b*-PHB-*b*-PLA produced using **4** in DCM at 20°C/45°C/20°C ([*rac*-LA:*rac*-BL:*rac*-LA:**5**:^{i}PrOH] = 50:50:50:1:1, 2 min/5 h/30 min) (see Table 2 in article, entry 7).

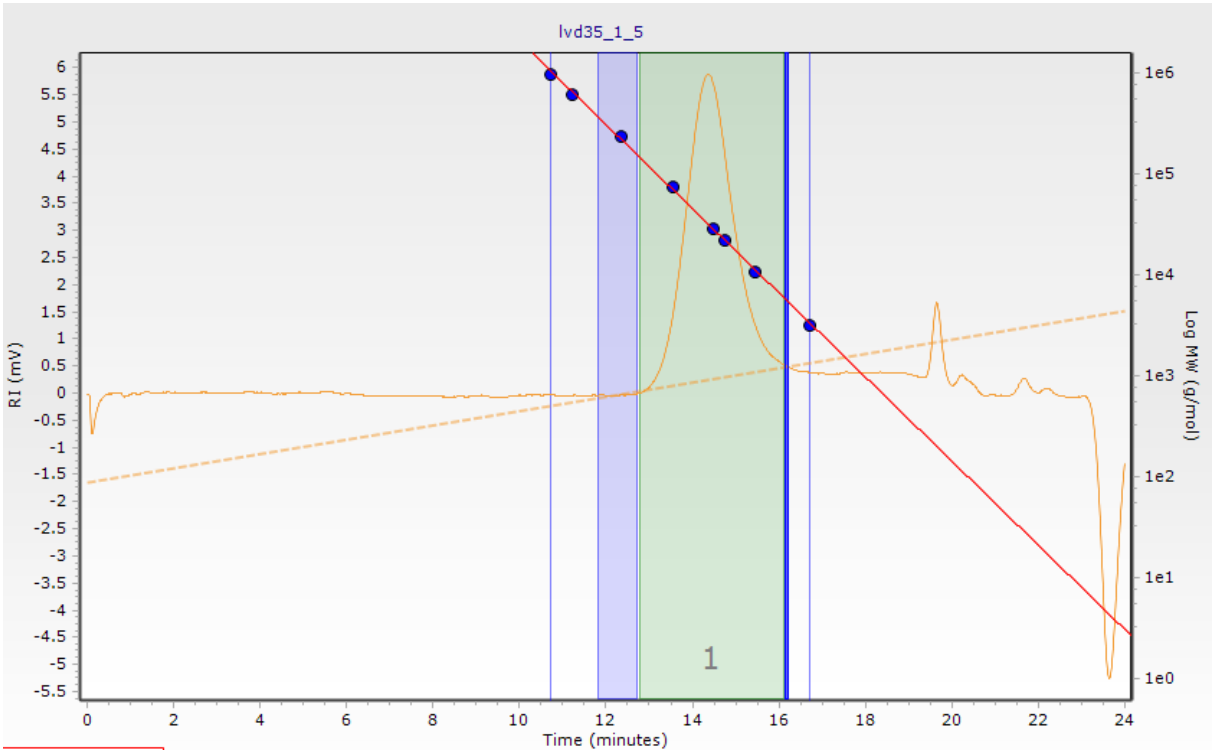

Figure S45. GPC spectrum of crude PLA-*b*-PHB-*b*-PLA produced using **5** in DCM at 20°C/45°C/20°C ([*rac*-LA:*rac*-BL:*rac*-LA:**5**:^{i}PrOH] = 50:50:50:0.5:1, 2 min/40 h/6 h) (see Table 2 in article, entry 8).

Kinetic Studies

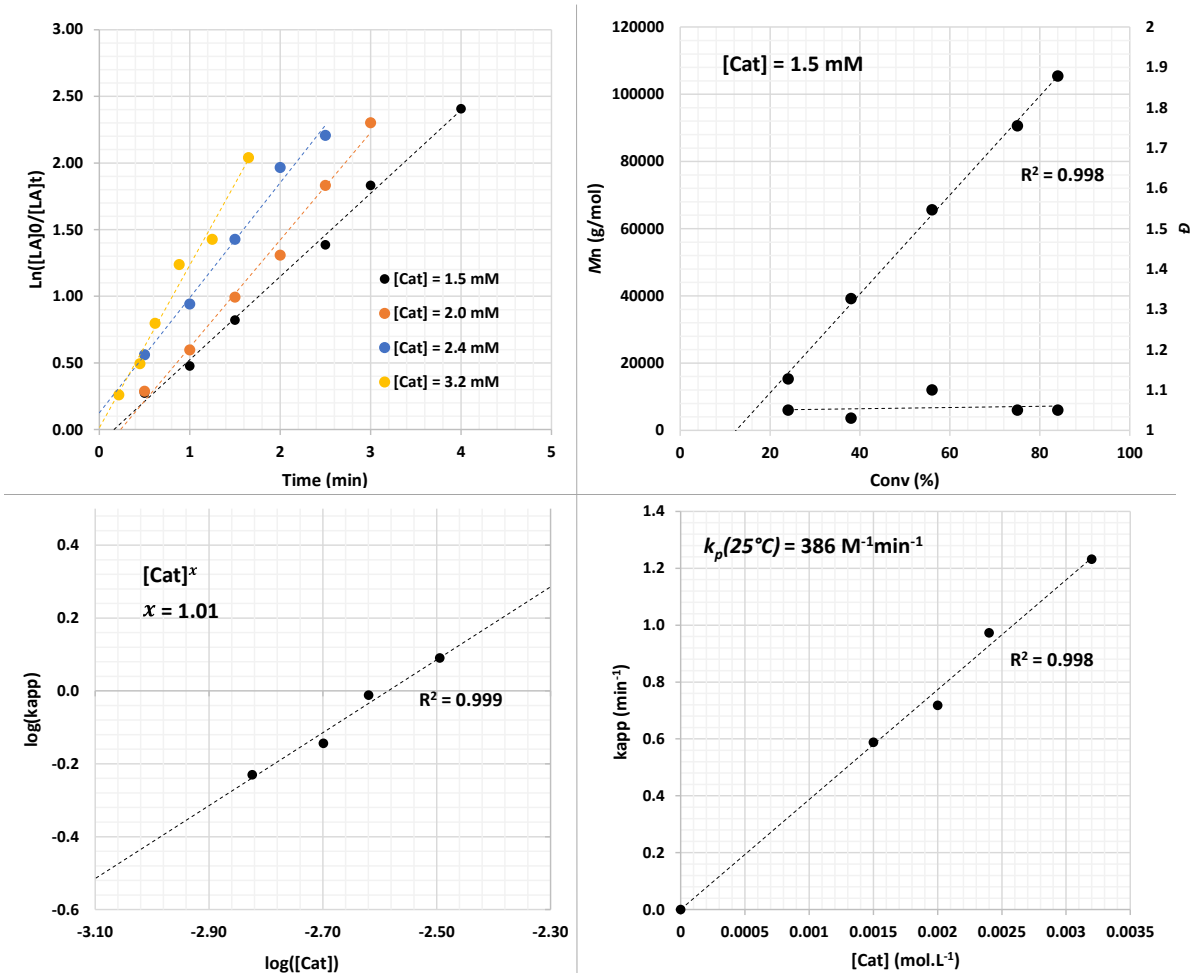

Figure S46a. Top left: First-order semi-logarithmic plot for the polymerization of *rac*-LA at 25°C in CH_2Cl_2 using **4** at different concentrations with ^{i}PrOH as co-initiator. Top right: M_n and $Đ$ against conversion associated using **4** (1.5mM) and ^{i}PrOH (1 equiv.). Bottom left: logarithmic plot of log k_{app} *vs* log $[\mathbf{4}]_0$. Bottom right: plot of k_{app} as a function of $[\mathbf{4}]_0$.

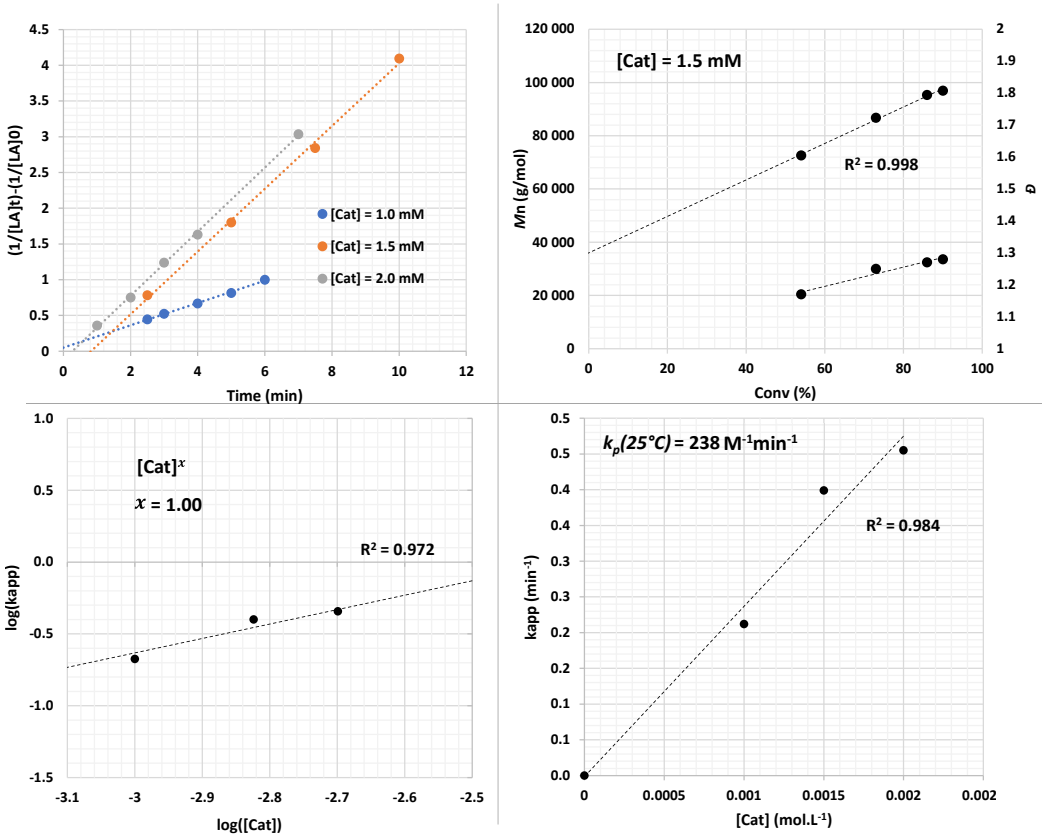

Figure S46b. Top left: Second-order plot for the polymerization of *rac*-LA at 25 °C in CH_2Cl_2 using **5** at different concentrations with ^{i}PrOH as co-initiator. Top right: M_n and *Đ* against conversion associated using **5** (1.5 mM) and ^{i}PrOH ([LA]$_0$:[**5**]$_0$:[^{i}PrOH]$_0$ = 500:0.5:1). Bottom left: plot of log k_{app} as a function of log [**5**]$_0$. Bottom right: plot of k_{app} *vs* [**5**]$_0$.

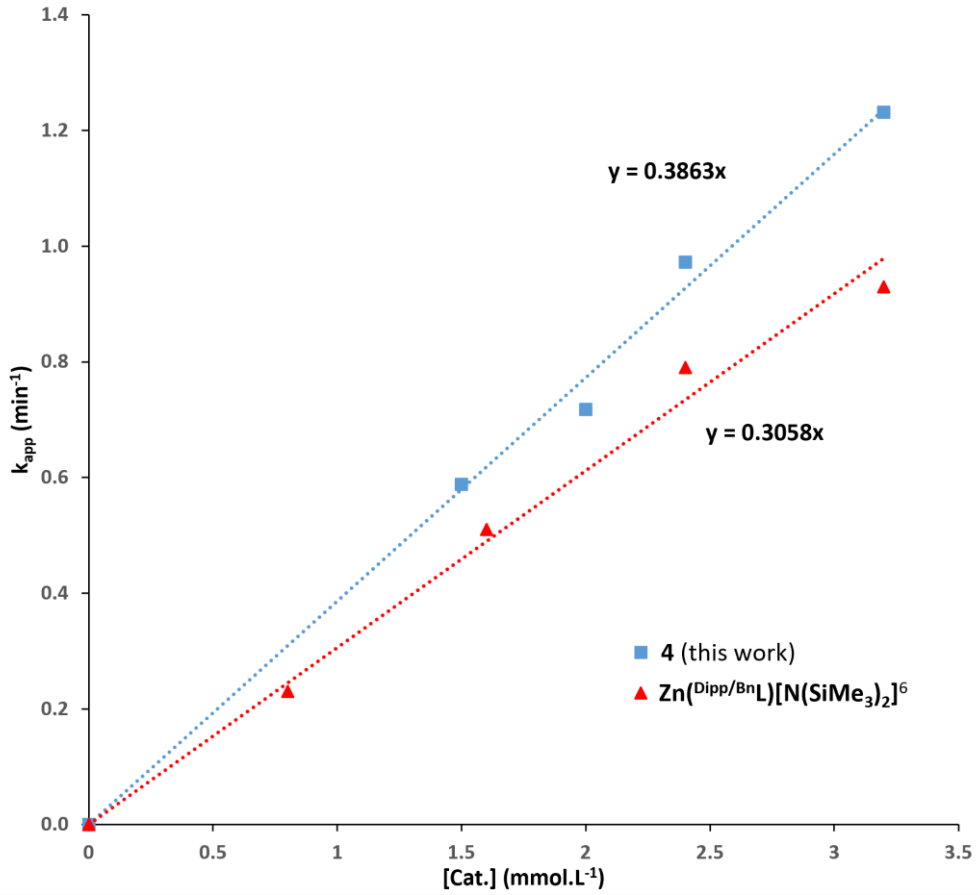

Figure S46c. Values of k_p(25 °C) calculated for catalyst **4** compared to **Zn($^{Dipp/Bn}$L)[N(SiMe$_3$)$_2$]**, reported by Robinson,[7] plotted against catalyst concentration in polymerization of *rac*-LA.

Table S6. Table of k_{app} determined at various [Zn] concentrations at 25°C using **4** with ^{i}PrOH in 1:1 ratio

Entry	[4] (mM)	k_{app} (min^{-1})	Δk_{app} (min^{-1})
1	1.5	0.59	0.04
2	2.0	0.72	0.07
3	2.4	0.97	0.07
4	3.2	1.23	0.10

Table S7. Table of k_{app} determined at various [Zn] concentrations at 25°C using **5** with ^{i}PrOH in 0.5:1 ratio

Entry	[5] (mM)	k_{app} (min^{-1})	Δk_{app} (min^{-1})
1	1.0	0.42	0.06
2	1.5	0.66	0.04

7. Chellali, J. E. ; Alverson, A. K.; Robinson, J. R. Zinc Aryl/Alkyl β-diketiminates: Balancing Accessibility and Stability for High-Activity Ring-Opening Polymerization of *rac*-Lactide. *ACS Catal.* **2022**, *12*, 5585–5594. DOI: 10.1021/acscatal.2c00858.

MALDI-TOF Spectra of PLA samples

These analyses were performed to determine the linear or cyclic nature of the PLA chains as well as the end-chain group. The presence or absence of peaks between the majority peaks can be used to assess the degree of transesterification.

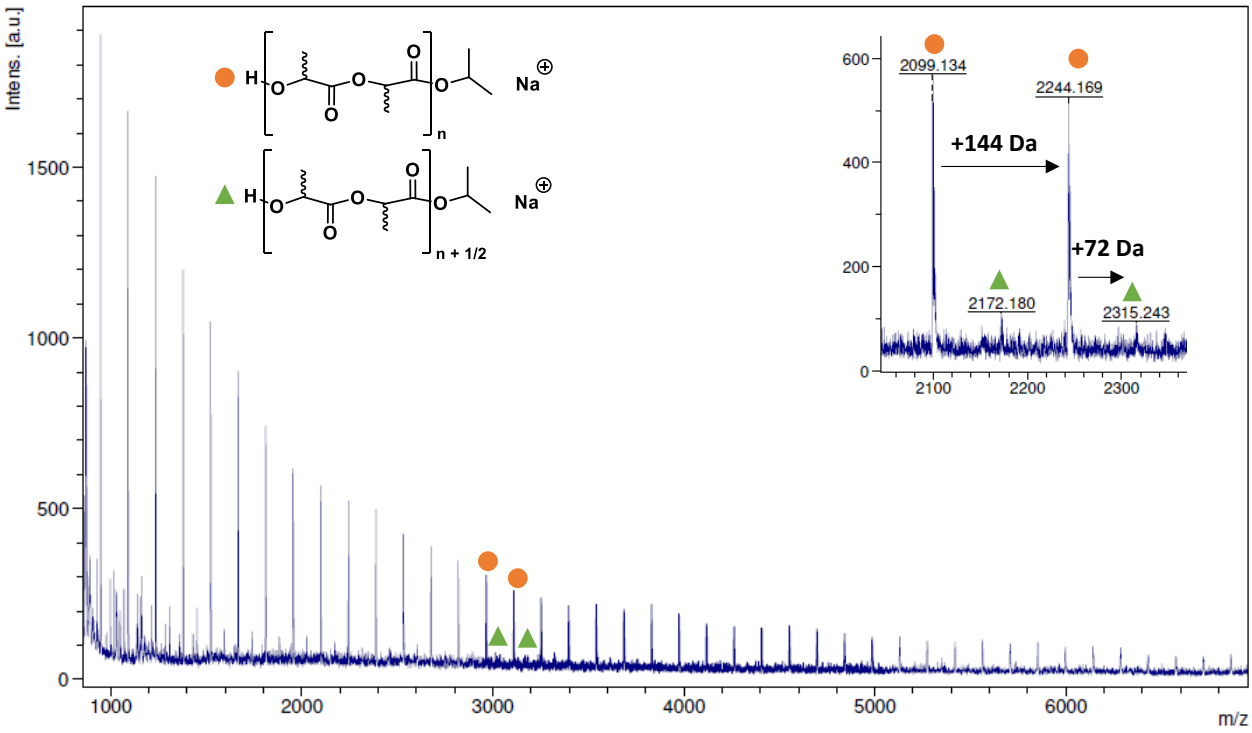

Figure S47. MALDI-TOF spectrum of PLA produced using **5** with ^{i}PrOH as co-initiator (25°C, 1 min, 25:1:1). Magnified versions are provided to assist in identifying the repeat unit.

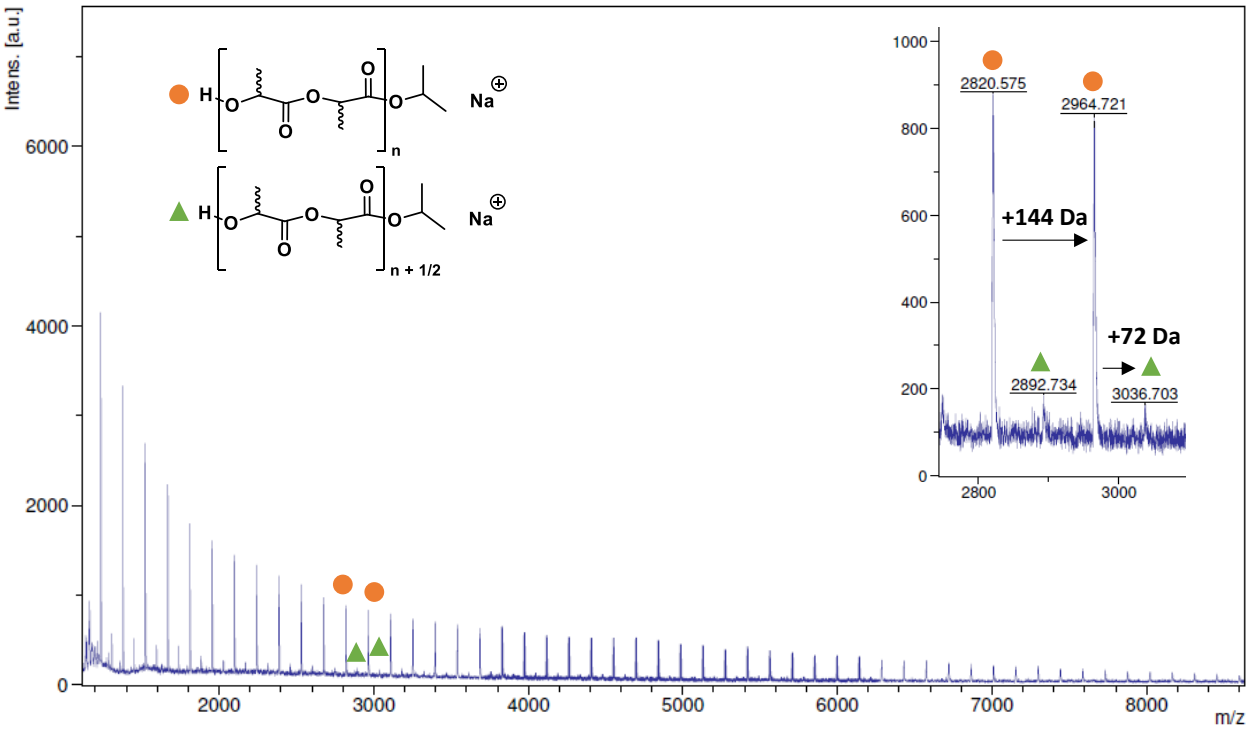

Figure S48. MALDI-TOF spectrum of PLA produced using **5** with ^{i}PrOH as co-initiator (25°C, 1 min, 25:0.5:1). Magnified versions are provided to assist in identifying the repeat unit.

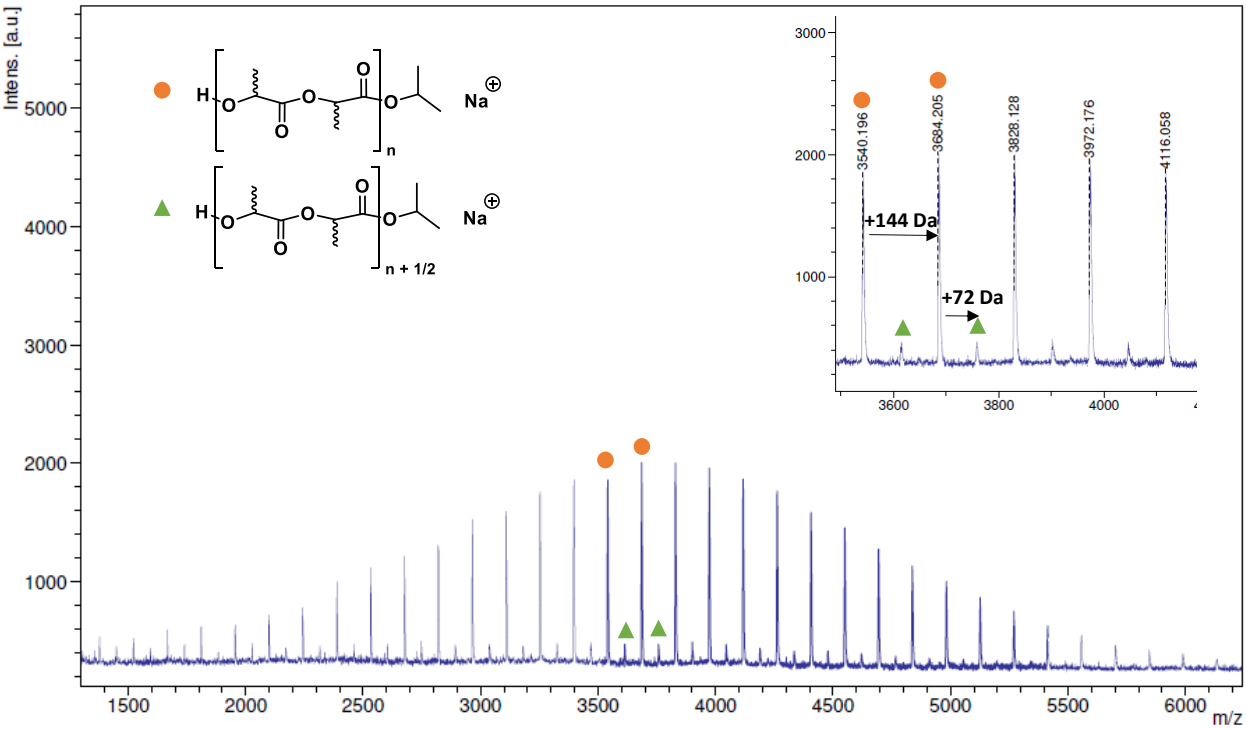

Figure S49. MALDI-TOF spectrum of PLA produced using **4** with ^{i}PrOH as co-initiator (25°C, 1 min, 300:1:10). Magnified versions are provided to assist in identifying the repeat unit.

General Methods, Preparation and Characterization of Compounds

All solvents and chemical reagents were purchased from commercial sources, and used without further purification. Some synthetic procedures were performed using the standard Schlenk techniques under an inert argon atmosphere (99.999%) (inert gas was passed through the oxygen/moisture trap Supelco before entering the vacuum/inert line) and solvents were dried with the help of solvent purification system PureSolv MD 7 supplied by Innovative Technology, Inc., degassed and then stored under argon atmosphere over a potassium or sodium mirror, if needed. Single crystals suitable for X-ray analyses were obtained from corresponding saturated solutions of products in organic solvent(s) cooled to 7 or -30 °C or by slow evaporation at room temperature. Deuterated solvents for NMR spectroscopy were distilled, degassed, and stored over a K or Na-mirror under an argon atmosphere.

Elemental analyses (C, H, N,) were performed on an automatic microanalyzer Flash 2000 Organic elemental analyzer (**1**) or Thermo Scientific - Flash*Smart* CHNS/O analyser (**2**, **4**, **5**).

Mass spectra of PLA samples were acquired on a time-of-flight mass spectrometer (MALDI-ToF-Microflex LRF, Bruker Daltonics). An external quadratic multi-point calibration was carried out before each measurement using polyethylene glycol (PEG) mixed in THF with dithranol (DIT). Analysis was performed with DIT as matrix (10 mg/mL) and sodium trifluoroacetate (10 mg/mL) as an additive. The polymer (10 mg/mL), the matrix and the additive were mixed in a volumetric ratio of 1/1/0.5 in THF. All the analyses were performed in positive reflectron mode.

For GPC analysis, the number-average, weight-average masses (M_n and M_w respectively) and molar distribution (M_w/M_n) of the polyester samples were determined by size exclusion chromatography at 45°C with the Agilent 1260 Infinity system equipped with Varian 390-LC refractometer detector. Tetrahydrofuran (THF) was used as the eluent and the flow rate was set up at 1.0 mL/min. A 5 µm pre-column and two aligned Polypore 5 µm (7.5 × 300 mm) were used. Calibration was performed using polystyrene standards (900-1,000,000 g/mol) and raw values of M_n were thus obtained.

NMR spectra were recorded from solutions of appropriate compounds in deuterated solvent(s) on a Bruker Avance 500 spectrometer (equipped with a Z-gradient 5 mm Prodigy™ cryoprobe) at frequencies for ^{1}H (500.13 MHz) or $^{13}C\{^{1}H\}$ (125.76 MHz) or a Bruker UltraShield™ 400 spectrometer at frequencies for ^{1}H (400.13 MHz), $^{13}C\{^{1}H\}$ (100.62 MHz) at 295 K or in some cases at various temperatures. Low-temperature NMR experiments of Zn complex **5** were performed on a Bruker Avance II spectrometer with a triple resonance broad-band probe (5 mm TBO BB-1H/19F/D Z-GRD) operating at 499.9 MHz for ^{1}H and 125.7 MHz for ^{13}C. Solutions were obtained by dissolving approximately 40 mg of each compound in approximately 0.6 mL of deuterated solvents. Values of ^{1}H

chemical shifts were referenced to residual signals of benzene ($\delta(^1H)$ = 7.16), tetrahydrofuran ($\delta(^1H)$ = 1.73) or toluene ($\delta(^1H)$ = 2.09). Values of ^{13}C chemical shifts were calibrated to signals of benzene ($\delta(^{13}C)$ = 128.4), tetrahydrofuran ($\delta(^{13}C)$ = 67.6), or toluene ($\delta(^{13}C)$ = 20.4). All ^{13}C NMR spectra were measured using a standard proton-decoupled experiment and CH/CH_3 vs. C_q/CH_2 were sometimes differentiated with the APT method's help[8]. NMR signal assignment was supported by $^1H,^1H$-COSY, $^1H,^1H$-NOESY, $^1H,^{13}C$-HSQC or $^1H,^{13}C$-HMBC 2D spectra. The DOSY spectra were recorded on a Bruker Avance III HD 600 spectrometer equipped with an ATMA BBOF 5mm Cryoprobe with a z-axis gradient coil operating at 600.13 MHz (^1H). The maximum gradient strength was 65.8 G/cm. The DOSY spectra were acquired in 5 mm NMR tubes and all the experiments were performed at 25°C and without sample spinning to avoid convection. All DOSY experiments were performed using standard Bruker pulse sequence - *dstebpgp3s* - a double stimulated echo sequence with bipolar gradient pulses and three spoil gradients with convection compensation. The diffusion time was 0.1 s (D). The duration of the magnetic field pulse gradients was adjusted for each polymer in a range of 500–2000 ms (d/2). The delay for gradient recovery was 0.2 ms and the eddy current delay 5 ms. For each DOSY-NMR experiment, a series of 16 spectra on 32 K data points were collected. The pulse gradients were incremented from 2% to 98% of the maximum gradient strength in a linear ramp with a total experiment time of 23 min. The temperature was set and controlled at 295 K. with an air flow of 400 L/h in order to avoid any temperature fluctuations due to sample heating during the magnetic field pulse gradients. After Fourier transformation and baseline correction, the diffusion dimension was processed with the Topspin 3.6.1 software and Dynamic Center 2.4.4. Stokes-Einstein equation: $D = b'M^{-v}$ (b', v = constant) is used to determine molecular molar mass of polymers via the diffusion coefficient.[6]

8. Patt, S.; Shoolery, J. N. Attached proton test for carbon-13 NMR. *J. Magn. Reson.* **1982**, *46*, 535–539. DOI : 10.1016/0022-2364(82)90105-6.

Preparation and Characterization of **1**

To a colorless solution of 2-amino-4,6-dimethoxypyrimidine (5.000 g; 32.23 mmol) in THF (400 mL) cooled to -60 C, a 1.6 M solution of *n*BuLi in hexane (20.10 mL; 32.23 mmol) was added. The reaction mixture was allowed to warm to room temperature and stirred for 24 hours. The resulting lithium (4,6-dimethoxypyrimidin-2-yl)azanide was not isolated and used *in situ* as is. After that, the reaction mixture was cooled to -60 °C and a solution of *N,N'*-bis(2,6-diisopropyl)carbodiimide (11.680 g; 32.23 mmol) in THF (80 mL) was added. The reaction mixture was allowed to warm to room temperature and stirred for 24 hours. The resulting corresponding lithium biguanide-like precursor (also not isolated and used as is) was quenched *in situ* by the addition of wet THF prepared as a solution of H_2O (0.58 mL; 32.23 mmol) in THF (20 mL). A small amount of white solid (some Li salts) was precipitated. The reaction mixture was stirred for further 24 hours and filtered. Subsequently, all solvents were evaporated under vacuum, and a crude product of **1** was extracted with Et_2O (300 mL). After, all volatiles were evaporated under vacuum to give 15.843 g (95 %) of white crystalline **1**. Single crystals suitable for *sc*XRD analyses were obtained by free evaporation of a saturated solution of **1** in Et_2O. Mp 172.5–173.5 °C. Anl_{calcd}: C 71.92, H 8.37, N 13.53; found: C 72.15, H 8.67, N 13.52.

NMR spectra of **1** show the presence of two isomers at THF-d_8 and C_6D_6. For measurement in THF-d_8 at 295 K, the major one is *ca* 89 mol %, and the second minor *ca* 11 mol %. In contrast, the amount of the minor increases with decreasing temperature (and *vice versa*) to ratio 66:34 at 213 K. Chemical shift values of **1** in THF-d_8 at 328 K, 313 K, 295 K, 273 K, 253 K, 233 K and 213 K (see Figure S2–S5) differ for major and minor tautomer in all VT ^{1}H NMR spectra. Signals of the second (minor) tautomer in THF-d_8 and C_6D_6 were not assigned (are marked by dots in NMR spectra – see Figure S41–S47). **NMR spectra in C_6D_6 at 295 K for major** -^{1}H NMR (C_6D_6, 400.13 MHz, 295 K) δ: 9.84 (s, 1H, N*H*^{Dipp}); 7.33–7.23 (m, 3H, Ar*H*^{Dipp}); 7.21 (d, $^3J_{H,H}$ = 7.6 Hz, 2H, Ar*H*^{Dipp}); 7.13 (s, 1H, N*H*^{Prm}); 7.10 (t, $^3J_{H,H}$ = 7.7 Hz, 1H, Ar*H*^{Dipp}); 5.49 (s, 1H, Ar*H*^{Prm}); 3.82 (m, $^3J_{H,H}$ = 6.8 Hz, 2H, C*H*^{Dipp}); 3.49 (m, $^3J_{H,H}$ = 6.9 Hz, 2H, C*H*^{Dipp}); 3.23 (s, 6H, OC*H*$_3$); 1.45 (d, $^3J_{H,H}$ = 6.9 Hz, 6H, C*H*$_3^{Dipp}$); 1.38 (d, $^3J_{H,H}$ = 6.9 Hz, 6H, C*H*$_3^{Dipp}$); 1.30 (d, $^3J_{H,H}$ = 6.8 Hz, 6H, C*H*$_3^{Dipp}$); 1.17 (d, $^3J_{H,H}$ = 6.9 Hz, 6H, C*H*$_3^{Dipp}$). ^{13}C NMR (C_6D_6, 100.58 MHz, 295 K) δ: 172.3 (Ar_q^{Prm}-OCH_3); 158.1 (Ar_q^{Prm}); 148.1 (Ar_q^{Dipp}); 143.6 (Ar_q^{Gua}); 143.3 (Ar_q^{Dipp}); 141.6 (Ar_q^{Dipp}); 134.2 (Ar_q^{Dipp}); 128.6 (ArH^{Dipp}); 124.3 (2x ArH^{Dipp}); 123.9 (ArH^{Dipp}); 83.9 (ArH^{Prm}); 54.1 (O*C*H$_3$); 29.6 (*C*H^{Dipp}); 28.7 (*C*H^{Dipp}); 26.3 (*C*H$_3^{Dipp}$); 24.8 (*C*H$_3^{Dipp}$); 24.4 (*C*H$_3^{Dipp}$); 23.2 (*C*H$_3^{Dipp}$). **NMR spectra in THF-*d*$_8$ at 295 K for major** -^{1}H NMR (THF-d_8, 500.13 MHz, 295 K) δ: 9.66 (s, 1H, N*H*^{Dipp}); 7.26–7.18 (m, 3H, Ar*H*^{Dipp}); 7.07 (d, $^3J_{H,H}$ = 7.6 Hz, 2H, Ar*H*^{Dipp}); 6.95 (t, $^3J_{H,H}$ = 7.6 Hz, 1H, Ar*H*^{Dipp}); 6.75 (s, 1H, N*H*^{Prm}); 5.72 (s, 1H, Ar*H*^{Prm}); 3.79 (s, 6H, OC*H*$_3$); 3.55 (m, $^3J_{H,H}$ = 6.9 Hz, 2H, C*H*^{Dipp}); 3.16 (m, $^3J_{H,H}$ = 6.9 Hz, 2H, C*H*^{Dipp}); 1.34 (d, $^3J_{H,H}$ = 6.9 Hz, 6H, C*H*$_3^{Dipp}$); 1.22 (d, $^3J_{H,H}$ = 6.9 Hz, 6H, C*H*$_3^{Dipp}$); 1.19 (d, $^3J_{H,H}$ = 6.9 Hz, 6H, C*H*$_3^{Dipp}$); 1.05 (d, $^3J_{H,H}$ = 6.9 Hz, 6H, C*H*$_3^{Dipp}$). ^{13}C NMR (THF-d_8, 125.76 MHz, 295 K) δ: 173.0 (Ar_q^{Prm}-OCH_3); 158.4 (Ar_q^{Prm}); 148.3 (Ar_q^{Dipp});

143.7 (Ar_q^{Gua}); 143.5 (Ar_q^{Dipp}); 141.6 (Ar_q^{Dipp}); 134.5 (Ar_q^{Dipp}); 128.4 (ArH^{Dipp}); 124.1 (ArH^{Dipp}); 123.9 (ArH^{Dipp}); 123.8 (ArH^{Dipp}); 83.7 (ArH^{Prm}); 54.8 (OCH_3); 29.7 (CH^{Dipp}); 28.8 (CH^{Dipp}); 26.2 (CH_3^{Dipp}); 24.7 (CH_3^{Dipp}); 24.3 (CH_3^{Dipp}); 23.2 (CH_3^{Dipp}).

Preparation and Characterization of **2**

To a suspension of **1** (1.000 g; 1.93 mmol) in hexane (40 mL) cooled to -80 °C, a 1.0 M solution of Et_2Zn in hexane (1.93 mL; 1.93 mmol) was added and the reaction mixture became homogeneous immediately. Then it was allowed to warm to room temperature and stirred for 24 hours with gradual precipitation of white solid. The resulting white precipitate of **2** was filtered and all volatiles were evaporated under vacuum to give 1.015 g (86 %) of the pure white powder of **2**. Single crystals suitable for *sc*XRD analyses were obtained from a saturated solution of **2** in Et_2O at 4 °C. AnI_{calcd}: C 64.86, H 7.75, N 11.46; found: C 63.56, H 7.55, N 11.34.

^{1}H NMR (C_6D_6, 500.13 MHz, 295 K) δ: 7.20-7.17 (m, 3H, ArH^{Dipp}); 7.16–7.14 (m, 1H, ArH^{Dipp}); 7.11-7.09 (m, 2H, ArH^{Dipp}); 5.50 (s, 1H, NH^{Dipp}); 5.00 (s, 1H, ArH^{Prm}); 3.54 (m, $^3J_{H,H}$ = 6.8 Hz, 2H, CH^{Dipp}); 3.47 (s, 3H, OCH_3); 3.28 (m, $^3J_{H,H}$ = 6.9 Hz, 2H, CH^{Dipp}); 2.90 (s, 3H, OCH_3); 1.50 (d, $^3J_{H,H}$ = 5.8 Hz, 6H, CH_3^{Dipp}); 1.32-1.27 (m, 15H, 2 x CH_3^{Dipp} and CH_3^{Et}); 1.08 (d, $^3J_{H,H}$ = 6.2 Hz, 6H, CH_3^{Dipp}); 0.58 (q, $^3J_{H,H}$ = 8.1 Hz, 2H, CH_2^{Et}). ^{13}C NMR (C_6D_6, 100 MHz, 295 K) δ: 173.1 (Ar_q^{Prm}-OCH_3); 170.3 (Ar_q^{Prm}-OCH_3); 161.9 (Ar_q^{Prm}); 158.6 (Ar_q^{Gua}); 146.7 (Ar_q^{Dipp}); 144.5 (Ar_q^{Dipp}); 141.8 (Ar_q^{Dipp}); 134.6 (Ar_q^{Dipp}); 127.8 (ArH^{Dipp}); 127.2 (ArH^{Dipp}); 124.9 (ArH^{Dipp}); 123.7 (ArH^{Dipp}); 76.8 (ArH^{Prm}); 55.0 (OCH_3); 54.1 (OCH_3); 29.5 (CH^{Dipp}); 28.9 (CH^{Dipp}); 25.6 (CH_3^{Dipp}); 24.6 (2x CH_3^{Dipp}); 23.8 (CH_3^{Dipp}); 12.6 (CH_3^{Et}); 1.6 (CH_2^{Et}). ^{1}H NMR (THF-d_8, 500.13 MHz, 295 K) δ: 7.20 (d, $^3J_{H,H}$ = 7.5 Hz, 2H, ArH^{Dipp}); 7.12 (t, $^3J_{H,H}$ = 7.5 Hz, 1H, ArH^{Dipp}); 7.20 (t, $^3J_{H,H}$ = 7.5 Hz, 1H, ArH^{Dipp}); 7.02 (d, $^3J_{H,H}$ = 7.5 Hz, 2H, ArH^{Dipp}); 5.67 (s, 1H, NH^{Dipp}); 5.44 (s, 1H, ArH^{Prm}); 3.81 (s, 3H, OCH_3); 3.70 (s, 3H, OCH_3); 3.45 (m, $^3J_{H,H}$ = 6.8 Hz, 2H, CH^{Dipp}); 3.20 (m, $^3J_{H,H}$ = 6.8 Hz, 2H, CH^{Dipp}); 1.32 (d, $^3J_{H,H}$ = 7.0 Hz, 6H, CH_3^{Dipp}); 1.22 (br s, 6H, CH_3^{Dipp}); 1.21 (d, $^3J_{H,H}$ = 6.7 Hz, 6H, CH_3^{Dipp}); 1.02 (br s, 6H, CH_3^{Dipp}); 0.84 (t, $^3J_{H,H}$ = 8.1 Hz, 3H, CH_3^{Et}); -0.40 (q, $^3J_{H,H}$ = 8.1 Hz, 2H, CH_2^{Et}) ppm. ^{13}C NMR (THF-d_8, 125.76 MHz, 295 K) δ: 173.2 (Ar_q^{Prm}-OCH_3); 171.4 (Ar_q^{Prm}-OCH_3); 162.6 (Ar_q^{Prm}); 158.8 (Ar_q^{Gua}); 147.2 (Ar_q^{Dipp}); 144.9 (Ar_q^{Dipp}); 143.4 (Ar_q^{Dipp}); 136.0 (Ar_q^{Dipp}); 127.2 (ArH^{Dipp}); 126.4 (ArH^{Dipp}); 124.7 (ArH^{Dipp}); 123.4 (ArH^{Dipp}); 76.1 (ArH^{Prm}); 55.8 (OCH_3); 53.7 (OCH_3); 29.4 (CH^{Dipp}); 29.0 (CH^{Dipp}); 25.6 (CH_3^{Dipp}); 24.6 (2x CH_3^{Dipp}); 24.4 (CH_3^{Dipp}); 13.0 (CH_3^{Et}); 0.4 (CH_2^{Et}) ppm.

Preparation and Characterization of **3**

To a colorless solution of **1** (1.005 g; 1.94 mmol) in Et_2O (40 mL) cooled to -80 °C, a 1.0 M solution of Et_2Zn in hexane (3.88 mL; 3.88 mmol) was added. The reaction mixture was allowed to warm to room

temperature (*ca* 3 hours) and stirred for 4 hours with gradual precipitation of white solid. The resulting white precipitate of **3** was filtered and all volatiles were evaporated under vacuum to give 1.149 g (84 %) of white crystalline **3** in *ca* 95+ % of purity (based on ^{1}H NMR spectrum). Single crystals suitable for *sc*XRD analyses were obtained from a saturated solution of **3** in Et_2O at 4 °C.

^{1}H NMR (C_6D_6, 500.13 MHz, 295 K) δ: 7.35 (d, $^{3}J_{H,H}$ = 7.5 Hz, 2H, Ar*H*^{Dipp}); 7.30 (t, $^{3}J_{H,H}$ = 7.5 Hz, 1H, Ar*H*^{Dipp}); 7.20 (d, $^{3}J_{H,H}$ = 7.7 Hz, 2H, Ar*H*^{Dipp}); 7.03 (t, $^{3}J_{H,H}$ = 7.6 Hz, 1H, Ar*H*^{Dipp}); 4.74 (s, 1H, Ar*H*^{Prm}); 3.80 (m, $^{3}J_{H,H}$ = 6.9 Hz, 2H, C*H*^{Dipp}); 3.53 (m, $^{3}J_{H,H}$ = 6.8 Hz, 2H, C*H*^{Dipp}); 3.45 (s, 3H, OC*H*$_3$); 2.81 (s, 3H, OC*H*$_3$); 1.51 (d, $^{3}J_{H,H}$ = 6.8 Hz, 6H, C*H*$_3^{Dipp}$); 1.48 (d, $^{3}J_{H,H}$ = 6.9 Hz, 6H, C*H*$_3^{Dipp}$); 1.31 (t, $^{3}J_{H,H}$ = 8.1 Hz, 3H, C*H*$_3^{Et}$); 1.28 (d, $^{3}J_{H,H}$ = 7.2 Hz, 6H, C*H*$_3^{Dipp}$); 1.16 (t, $^{3}J_{H,H}$ = 8.1 Hz, 3H, C*H*$_3^{Et}$); 1.06 (d, $^{3}J_{H,H}$ = 6.9 Hz, 6H, C*H*$_3^{Dipp}$), 0.65 (q, $^{3}J_{H,H}$ = 8.1 Hz, 2H, C*H*$_2^{Et}$); 0.06 (q, $^{3}J_{H,H}$ = 8.2 Hz, 2H, C*H*$_2^{Et}$). ^{13}C NMR (C_6D_6, 125.76 MHz, 295 K) δ: 172.2 (Ar$_q^{Prm}$-OCH$_3$); 171.3 (Ar$_q^{Prm}$-OCH$_3$); 162.4 (Ar$_q^{Prm}$); 152.6 (Ar$_q^{Gua}$); 146.2 (Ar$_q^{Dipp}$); 145.9 (Ar$_q^{Dipp}$); 144.5 (Ar$_q^{Dipp}$); 142.2 (Ar$_q^{Dipp}$); 126.9 (ArH^{Dipp}); 125.3 (ArH^{Dipp}); 124.3 (ArH^{Dipp}); 123.7 (ArH^{Dipp}); 77.2 (ArH^{Prm}); 55.5 (O*C*H$_3$); 54.7 (O*C*H$_3$); 29.0 (*C*H^{Dipp}); 28.4 (*C*H^{Dipp}); 26.3 (*C*H$_3^{Dipp}$); 25.4 (*C*H$_3^{Dipp}$); 24.3 (2x *C*H$_3^{Dipp}$); 13.0 (*C*H$_3^{Et}$); 12.6 (*C*H$_3^{Et}$); 1.8 (*C*H$_2^{Et}$); -1.3 (*C*H$_2^{Et}$). ^{1}H NMR (THF-d_8, 500.13 MHz, 295 K) δ: 6.87-6.66 (m, 6H, Ar*H*^{Dipp}); 5.54 (s, 1H, Ar*H*^{Prm}); 3.91 (br s, 3H, OC*H*$_3$); 3.82 (s, 3H, OC*H*$_3$); 3.25–3.06 (m, 4H, 2 x C*H*^{Dipp}); 1.17 (br s, 3H, C*H*$_3^{Et}$); 1.04 (not completely split doublet, $^{3}J_{H,H}$ = 4.3 Hz, 6H, C*H*$_3^{Dipp}$); 1.00 (not completely split doublet, $^{3}J_{H,H}$ = 3.8 Hz, 6H, C*H*$_3^{Dipp}$); 0.93 (d, $^{3}J_{H,H}$ = 6.3 Hz, 6H, C*H*$_3^{Dipp}$); 0.87 (br s, 6H, C*H*$_3^{Dipp}$); 0.67 (t, $^{3}J_{H,H}$ = 7.0 Hz, 3H, C*H*$_3^{Et}$); 0.24 (br s, 2H, C*H*$_2^{Et}$); -0.24 (br s, 2H, C*H*$_2^{Et}$). ^{13}C NMR (THF-d_8, 125.76 MHz, 295 K) δ: 173.3 (Ar$_q^{Prm}$-OCH$_3$); 172.0 (Ar$_q^{Prm}$-OCH$_3$); 165.0 (br s, Ar$_q^{Prm}$); 160.3 (br s, Ar$_q^{Gua}$); 146.2 (br s, Ar$_q^{Dipp}$); 144.9 (br s, Ar$_q^{Dipp}$); 143.7 (br s, Ar$_q^{Dipp}$); 143.5 (br s, Ar$_q^{Dipp}$); 124.2 (ArH^{Dipp}); 123.5 (ArH^{Dipp}); 123.4 (br s, ArH^{Dipp}); 123.2 (br s, ArH^{Dipp}); 76.3 (ArH^{Prm}); 56.0 (O*C*H$_3$); 54.1 (br s, O*C*H$_3$); 28.9 (2x *C*H^{Dipp}); 26.6 (br s, *C*H$_3^{Dipp}$); 25.9 (br s, *C*H$_3^{Dipp}$); 23.8 (br s, *C*H$_3^{Dipp}$); 22.5 (br s, *C*H$_3^{Dipp}$); 13.4 (*C*H$_3^{Et}$); 12.7 (*C*H$_3^{Et}$); 1.7 (br s, *C*H$_2^{Et}$); -0.4 (br s, *C*H$_2^{Et}$).

Preparation and Characterization of **4**

To a colorless solution of **1** (1.176 g; 2.27 mmol) in Et_2O (40 mL) cooled to -80 °C, a colorless solution of Zn[N(SiMe$_3$)$_2$]$_2$ (0.92 mL; 2.27 mmol) in Et_2O (20 mL) was added. The reaction mixture was allowed to warm to room temperature and stirred for 24 hours with gradual precipitation of a white solid of **4**. After that, all solvents were evaporated under vacuum to give 1.687 g (>99 %) of the pure white powder of **4**. Single crystals suitable for *sc*XRD analyses were obtained from a saturated solution of **4** in Et_2O at 4 °C. AnI_{calcd}: C 59.85, H 8.15, N 11.32; found: C 60.07, H 8.40, N 11.34.

^{1}H NMR (C_6D_6, 500.13 MHz, 295 K) δ: 7.20–7.15 (m, 3H, Ar*H*^{Dipp}); 7.15–7.11 (m, 1H, Ar*H*^{Dipp}); 7.08 (d, $^{3}J_{H,H}$ = 7.6 Hz, 2H, Ar*H*^{Dipp}); 5.62 (s, 1H, N*H*^{Dipp}); 5.03 (s, 1H, Ar*H*^{Prm}); 3.59 (m, $^{3}J_{H,H}$ = 7.0 Hz, 2H, C*H*^{Dipp}); 3.40 (s, 3H, OC*H*$_3$); 3.23 (m, $^{3}J_{H,H}$ = 6.8 Hz, 2H, C*H*^{Dipp}); 3.06 (s, 3H, OC*H*$_3$); 1.48 (d, $^{3}J_{H,H}$ = 6.8 Hz,

6H, CH_3^{Dipp}); 1.45 (br s, 6H, CH_3^{Dipp}); 1.28 (d, $^3J_{H,H}$ = 6.9 Hz, 6H, CH_3^{Dipp}); 1.06 (br s, 6H, CH_3^{Dipp}); 0.14 (s, 18H, N(Si(CH_3)$_3$)$_2$). ^{13}C NMR (C_6D_6, 125.76 MHz, 295 K) δ: 173.6 (Ar_q^{Prm}-OCH_3); 169.8 (Ar_q^{Prm}-OCH_3); 162.4 (Ar_q^{Prm}); 159.8 (Ar_q^{Gua}); 146.7 (Ar_q^{Dipp}); 144.8 (Ar_q^{Dipp}); 140.8 (Ar_q^{Dipp}); 134.2 (Ar_q^{Dipp}); 128.0 (ArH^{Dipp}); 127.5 (ArH^{Dipp}); 125.3 (ArH^{Dipp}); 123.8 (ArH^{Dipp}); 77.6 (ArH^{Prm}); 54.9 (OCH_3); 54.2 (OCH_3); 29.4 (CH^{Dipp}); 29.0 (CH^{Dipp}); 26.3 (CH_3^{Dipp}); 24.7 (CH_3^{Dipp}); 24.5 (2x CH_3^{Dipp}); 5.5 (N(Si(CH_3)$_3$)$_2$).

Preparation and Characterization of **5**

To a colorless solution of **1** (0.522 g; 1.01 mmol) in Et_2O (30 mL) cooled to -80 °C, a colorless solution of Zn[N($SiMe_3$)$_2$]$_2$ (0.81 mL; 2.02 mmol) in Et_2O (30 mL) was added. The reaction mixture was allowed to warm to room temperature and stirred for 7 days. After that, all solvents were evaporated under vacuum with a yield of 0.883 g (>99 %) of white crystalline **5**. Single crystals suitable for *sc*XRD analyses were obtained from a saturated solution of **5** in hexane at -30 °C. Anl_{calcd}: C 53.40, H 8.02, N 10.14; found: C 53.80, H 8.14, N 10.39.

^{1}H NMR (C_6D_6, 500.13 MHz, 295 K) δ: 6.93 (br s, 6H, ArH^{Dipp}); 5.10 (s, 1H, ArH^{Prm}); 3.88 (br s, 3H, OCH_3); 3.12 (br s, 4h, CH^{Dipp}); 3.05 (br s, 3H, OCH_3); 1.30 (br s, 12H, CH_3^{Dipp}); 1.00 (br s, 6H, CH_3^{Dipp}); 0.90 (br s, 6H, CH_3^{Dipp}); 0.27 (br s, 18H, N((SiCH_3)$_3$)$_2$); 0.08 (br s, 18H, N((SiCH_3)$_3$)$_2$). ^{1}H NMR (Tol-d_8, 500.13 MHz, 295 K) δ: 6.83 (br s, 6H, ArH^{Dipp}); 5.10 (s, 1H, ArH^{Prm}); 3.86 (br s, 3H, OCH_3); 3.19-2.90 (m, 7H, CH^{Dipp} and OCH_3); 1.19 (br s, 12H, CH_3^{Dipp}); 0.88 (br s, 12H, CH_3^{Dipp}); 0.15 (br s, 18H, N((SiCH_3)$_3$)$_2$); -0.03 (br s, 18H, N((SiCH_3)$_3$)$_2$).^{1}H NMR (Tol-d_8, 499.9 MHz, 373 K) δ: 6.85-6.81 (m, 6H, ArH^{Dipp}); 5.18 (s, 1H, ArH^{Prm}); 3.61 (br s, 6H, OCH_3); 3.04 (m, $^3J_{H,H}$ = 6.8 Hz, 4H, CH^{Dipp}); 1.16 (d, $^3J_{H,H}$ = 6.8 Hz, 12H, CH_3^{Dipp}); 0.85 (d, $^3J_{H,H}$ = 6.4 Hz, 12H, CH_3^{Dipp}); 0.02 (s, 36H, N((SiCH_3)$_3$)$_2$). ^{13}C NMR (Tol-d_8, 125.7 MHz, 373 K) δ: 172.3 (br s, Ar_q^{Prm}-OCH_3); 165.6 (Ar_q^{Gua}); 160.6 (Ar_q^{Prm}); 143.8 (2x Ar_q^{Dipp}); 142.1 (Ar_q^{Dipp}); 125.8 (ArH^{Dipp}); 124.0 (2x ArH^{Dipp}); 78.5 (ArH^{Prm}); 54.9 (OCH_3); 28.8 (CH^{Dipp}); 26.9 (CH_3^{Dipp}); 22.9 (CH_3^{Dipp}); 5.3 (N((SiCH_3)$_3$)$_2$). ^{1}H NMR (Tol-d_8, 499.9 MHz, 203 K) δ: 6.98–6.85 (m, 4H, ArH^{Dipp}); 6.69 (br s, 2H, ArH^{Dipp}); 4.92 (s, 1H, ArH^{Prm}); 3.77 (s, 3H, OCH_3); 3.45 (br s, 1H, CH^{Dipp}); 3.19 (br s, 1H, CH^{Dipp}); 2.89 (br s, 1H, CH^{Dipp}); 2.87 (s, 3H, OCH_3); 2.79 (br s, 1H, CH^{Dipp}); 1.53 (br s, 3H, CH_3^{Dipp}); 1.43 (br s, 3H, CH_3^{Dipp}); 1.34 (br s, 3H, CH_3^{Dipp}); 1.31 (br s, 3H, CH_3^{Dipp}); 1.14 (br s, 3H, CH_3^{Dipp}); 1.04 (br s, 3H, CH_3^{Dipp}); 0.52 (br s, 3H, CH_3^{Dipp}); 0.29 (br s, 3H, CH_3^{Dipp}); 0.24 (s, 18H, N(Si(CH_3)$_3$)$_2$); 0.11 (s, 18H, N(Si(CH_3)$_3$)$_2$). ^{13}C NMR (Tol-d_8, 125.7 MHz, 203 K) δ: 172.7 (Ar_q^{Prm}-OCH_3); 169.5 (Ar_q^{Prm}-OCH_3); 164.9 (Ar_q^{Gua}); 159.3 (Ar_q^{Prm}); 143.7 (Ar_q^{Dipp}); 142.8 (Ar_q^{Dipp}); 142.1 (Ar_q^{Dipp}); 141.4 (Ar_q^{Dipp}); 141.3 (Ar_q^{Dipp}); 140.9 (Ar_q^{Dipp}); 125.6 (ArH^{Dipp}); 124.8 (ArH^{Dipp}); 124.3 (ArH^{Dipp}); 123.2 (2x ArH^{Dipp}); 122.8 (ArH^{Dipp}); 77.9 (ArH^{Prm}); 54.7 (OCH_3); 54.1 (OCH_3); 29.0 (CH^{Dipp}); 28.5 (CH^{Dipp}); 28.1 (CH^{Dipp}); 27.9 (CH^{Dipp}); 27.1 (CH_3^{Dipp}); 26.9 (CH_3^{Dipp}); 26.8 (CH_3^{Dipp}); 25.9 (CH_3^{Dipp}); 24.4 (CH_3^{Dipp}); 22.0 (CH_3^{Dipp}); 21.9 (CH_3^{Dipp}); 21.5 (CH_3^{Dipp}); 5.1 (N(Si(CH_3)$_3$)$_2$); 2.5 (N(Si(CH_3)$_3$)$_2$).

Preparation and Characterization of **6**

To a colorless solution of **1** (1.000 g; 1.93 mmol) in Et_2O (40 mL) cooled to -80 °C, a 1.0 M solution of Et_2Zn in hexane (0.97 mL; 0.97 mmol) was added. The reaction mixture was allowed to warm to room temperature and stirred for 24 hours with gradual precipitation of white solid. The resulting white precipitate of **6** was filtered and all volatiles were evaporated under vacuum to give 0.761 g (82 %) of white crystalline **6**. Single crystals suitable for *sc*XRD analyses were obtained from a saturated solution of **6** in Et_2O at 4 °C.

^{1}H NMR (THF-d_8, 500.13 MHz, 295 K) δ: 7.18 (dd, $^3J_{H,H}$ = 7.7 Hz, $^4J_{H,H}$ = 1.5 Hz, 2H, Ar*H*^{Dipp}); 7.06–7.01 (m, 6H, Ar*H*^{Dipp}); 6.99 (br s, 2H, Ar*H*^{Dipp}); 6.96 (dd, $^3J_{H,H}$ = 7.7 Hz, $^4J_{H,H}$ = 1.6 Hz, 2H, Ar*H*^{Dipp}); 5.41 (br s, 2H, N*H*^{Dipp}); 5.40 (s, 2H, Ar*H*^{Prm}); 3.92 (m, $^3J_{H,H}$ = 6.7 Hz, 2H, C*H*^{Dipp}); 3.72 (s, 6H, OC*H*$_3$); 3.49 (s, 6H, OC*H*$_3$); 3.32–3.07 (m, 4H, 2 x C*H*^{Dipp}); 2.94 (br s, 2H, C*H*^{Dipp}); 1.60 (br s, 6H, C*H*$_3^{Dipp}$); 1.27 (d, $^3J_{H,H}$ = 6.9 Hz, 6H, C*H*$_3^{Dipp}$); 1.15–1.05 (m, 18H, 3 x C*H*$_3^{Dipp}$); 1.00 (d, $^3J_{H,H}$ = 6.7 Hz, 6H, C*H*$_3^{Dipp}$); 0.51 (br s, 6H, C*H*$_3^{Dipp}$); -0.07 (d, $^3J_{H,H}$ = 6.7 Hz, 6H, C*H*$_3^{Dipp}$). ^{13}C NMR (THF-d_8, 125.76 MHz, 295 K) δ: 173.1 (Ar$_q^{Prm}$-OCH$_3$); 170.8 (Ar$_q^{Prm}$-OCH$_3$); 161.7 (Ar$_q^{Prm}$); 159.2 (Ar$_q^{Gua}$); 147.4 (Ar$_q^{Dipp}$); 145.4 (Ar$_q^{Dipp}$); 142.8 (Ar$_q^{Dipp}$); 136.0 (Ar$_q^{Dipp}$); 126.9 (ArH^{Dipp}); 126.6 (ArH^{Dipp}); 126.0 (ArH^{Dipp}); 125.6 (ArH^{Dipp}); 122.9 (br s, 2x ArH^{Dipp}); 77.0 (ArH^{Prm}); 56.1 (OCH$_3$); 53.7 (OCH$_3$); 29.5 (br s, 2x *C*H^{Dipp}); 29.2 (*C*H^{Dipp}); 27.5 (br s, incld: *C*H^{Dipp} + *C*H$_3^{Dipp}$); 25.7 (*C*H$_3^{Dipp}$); 25.1 (*C*H$_3^{Dipp}$); 23.6 (*C*H$_3^{Dipp}$); rest of the signals corresponding to 2x Ar$_q^{Dipp}$ and 4x *C*H$_3^{Dipp}$ carbon atoms from the one of Dipp substituent were not observed due to its dynamic behavior.

X-ray Crystallography

The X-ray data for colorless crystals of all complexes were obtained at 150K using Oxford Cryostream low-temperature device with a Bruker D8-Venture diffractometer equipped with Mo (Mo/K$_\alpha$ radiation; λ = 0.71073 Å) microfocus X-ray (IμS) source, Photon CMOS detector and Oxford Cryosystems cooling device was used for data collection. Obtained data were treated by XT-version 2014/5 and SHELXL-2017/1 software implemented in APEX3 v2016.9-0 (Bruker AXS) system.[9] $R_{int} = \sum | F_o^2 - F_{o,mean}^2 | / \sum F_o^2$, $S = [\sum(w(F_o^2 - F_c^2)^2)/(N_{diffrs} - N_{params})]^{½}$ for all data, $R(F) = \sum | | F_o | - | F_c | | / \sum | F_o |$ for observed data, $wR(F^2) = [\sum(w(F_o^2 - F_c^2)^2)/(\sum w(F_o^2)^2)]^{½}$ for all data. Crystallographic data for all structural analysis have been deposited with the Cambridge Crystallographic Data Centre, CCDC nos. 2120578, 2377227–2377231. Copies of this information may be obtained free of charge from The Director, CCDC, 12 Union Road, Cambridge CB2 1EY, UK (fax: +44-1223-336033; e-mail: deposit@ccdc.cam.ac.uk or www: http://www.ccdc.cam.ac.uk).

9. Sheldrick, G.M. SHELXT – Integrated space-group and crystal-structure determination. *Acta Cryst.* **2015,** *A71,* 3-8. DOI: 10.1107/S2053273314026370.

The frames for all complexes were integrated with the Bruker SAINT software package using a narrow-frame algorithm. Data were corrected for absorption effects using the Multi-Scan method (SADABS). The structures were solved and refined using the Bruker SHELXTL Software Package.

Hydrogen atoms were mostly localized on a difference Fourier map, however, to ensure uniformity of treatment of crystal, most of the hydrogen atoms were recalculated into idealized positions (riding model) and assigned temperature factors Hiso(H) = 1.2 Ueq (pivot atom) or of 1.5Ueq (methyl). H atoms in methyl, methylene, methine moieties and C-H in aromatic rings were placed with C-H distances of 0.96, 0.97, 0.98 and 0.93Å. Hydrogen atoms in NH groups were added freely according the maxima on the difference Fourier map. Complex **5** crystallizes in chiral space group as a twin. In **6**, four disordered *n*-hexane molecules were masked by SQUEEZE[10] program.

10. Spek, A. L. PLATON SQUEEZE: a tool for the calculation of the disordered solvent contribution to the calculated structure factors. *Acta Cryst.* **2015**, *C71*, 9-18. DOI: 10.1107/s2053229614024929.

Table S8. Crystal data and structure refinement for **1**.

Crystal data	
Chemical formula	$C_{31}H_{43}N_5O_2$
M_r	517.70
Crystal system, space group	Monoclinic, $P2_1/n$
Temperature (K)	150
a, b, c (Å)	10.4903(11), 15.321(2), 18.8955(19)
β (°)	102.118(4)
V (Å^3)	2969.2(6)
Z	4
Radiation type	Mo$K\alpha$
μ (mm^{-1})	0.07
Crystal size (mm)	0.42 × 0.34 × 0.27
Data collection	
Diffractometer	Bruker D8 - Venture
Absorption correction	Multi-scan *SADABS2016*/2 - Bruker AXS area detector scaling and absorption correction
T_{min}, T_{max}	0.561, 0.746
No. of measured, independent and observed [$I > 2\sigma(I)$] reflections	58426, 5221, 3635
R_{int}	0.118
$(\sin\theta/\lambda)_{max}$ (Å^{-1})	0.595
Refinement	
$R[F^2 > 2\sigma(F^2)]$, $wR(F^2)$, S	0.052, 0.119, 1.00
No. of reflections	5221
No. of parameters	361
No. of restraints	288
H-atom treatment	H atoms treated by a mixture of indep. and constrained refinement
$\Delta\rho_{max}$, $\Delta\rho_{min}$ (e Å^{-3})	0.25, −0.23

Computer programs: Bruker Instrument Service vV6.2.3, *APEX3* v2016.5-0 (Bruker AXS), *SAINT* V8.37A (Bruker AXS Inc., 2015), XT, VERSION 2014/5, *SHELXL2016*/6 (Sheldrick, 2016), *PLATON* (Spek, 2009).

Hydrogen-bond geometry (Å, °)

D—H···*A*	*D*—H	H···*A*	*D*···*A*	*D*—H···*A*
N1—H2···N5	0.87(2)	2.00(2)	2.710(2)	138.4(18)

Table S9. Crystal data and structure refinement for **2**.

Crystal data	
Chemical formula	$C_{33}H_{47}N_5O_2Zn$
M_r	611.12
Crystal system, space group	Triclinic, *P*-1
Temperature (K)	150
a, *b*, *c* (Å)	9.4794(5), 11.6231(6), 15.9856(8)
α, β, γ (°)	83.476(2), 73.337(2), 75.825(2)
V (Å^3)	1634.17(15)
Z	2
Radiation type	Mo*K*α
μ (mm^{-1})	0.79
Crystal size (mm)	0.51 × 0.27 × 0.22
Data collection	
Diffractometer	Bruker D8 - Venture
Absorption correction	Multi-scan *SADABS2016*/2 - Bruker AXS area detector scaling and absorption correction
T_{min}, T_{max}	0.635, 0.746
No. of measured, independent and observed [$I > 2\sigma(I)$] reflections	32122, 7508, 6204
R_{int}	0.047
$(\sin \theta/\lambda)_{max}$ (Å^{-1})	0.651
Refinement	
$R[F^2 > 2\sigma(F^2)]$, $wR(F^2)$, *S*	0.038, 0.083, 1.07
No. of reflections	7508
No. of parameters	386
No. of restraints	317
H-atom treatment	H atoms treated by a mixture of independent and constrained refinement
$\Delta\rho_{max}$, $\Delta\rho_{min}$ (e Å^{-3})	0.37, −0.74

Computer programs: Bruker Instrument Service vV6.2.3, *APEX3* v2016.5-0 (Bruker AXS), *SAINT* V8.37A (Bruker AXS Inc., 2015), XT, VERSION 2014/5, *SHELXL2016*/6 (Sheldrick, 2016), *PLATON* (Spek, 2009).

Table S10. Crystal data and structure refinement for **3**.

Crystal data	
Chemical formula	$C_{35}H_{51}N_5O_2Zn_2$
M_r	704.54
Crystal system, space group	Monoclinic, $P2_1/n$
Temperature (K)	150
a, b, c (Å)	10.7166(3), 23.0090(8), 14.2279(5)
β (°)	94.049(1)
V (Å^3)	3499.5(2)
Z	4
Radiation type	Mo$K\alpha$
μ (mm^{-1})	1.41
Crystal size (mm)	0.56 × 0.06 × 0.05
Data collection	
Diffractometer	Bruker D8 - Venture
Absorption correction	Multi-scan *SADABS2016*/2 - Bruker AXS area detector scaling and absorption correction
T_{min}, T_{max}	0.599, 0.746
No. of measured, independent and observed [$I > 2\sigma(I)$] reflections	108323, 8054, 6284
R_{int}	0.110
$(\sin \theta/\lambda)_{max}$ (Å^{-1})	0.651
Refinement	
$R[F^2 > 2\sigma(F^2)]$, $wR(F^2)$, S	0.039, 0.073, 1.06
No. of reflections	8054
No. of parameters	409
No. of restraints	339
H-atom treatment	H-atom parameters constrained
$\Delta\rho_{max}$, $\Delta\rho_{min}$ (e Å^{-3})	0.38, −0.40

Computer programs: Bruker Instrument Service vV6.2.3, *APEX3* v2016.5-0 (Bruker AXS), *SAINT* V8.37A (Bruker AXS Inc., 2015), XT, VERSION 2014/5, *SHELXL2016*/6 (Sheldrick, 2016), *PLATON* (Spek, 2009).

Table S11. Crystal data and structure refinement for **4**.

Crystal data	
Chemical formula	$C_{37}H_{60}N_6O_2Si_2Zn$
M_r	742.46
Crystal system, space group	Triclinic, *P*-1
Temperature (K)	150
a, *b*, *c* (Å)	10.9611(3), 14.0370(3), 14.3646(3)
α, β, γ (°)	102.626(1), 104.747(1), 93.733(1)
V (Å^3)	2068.52(8)
Z	2
Radiation type	Mo*K*α
μ (mm^{-1})	0.69
Crystal size (mm)	0.59 × 0.46 × 0.39
Data collection	
Diffractometer	Bruker D8 - Venture
Absorption correction	Multi-scan *SADABS2016*/2 - Bruker AXS area detector scaling and absorption correction Reference: Krause, L., Herbst-Irmer, R., Sheldrick G.M. & Stalke D., J. Appl. Cryst. 48 (2015) 3-10.
T_{min}, T_{max}	0.770, 1.000
No. of measured, independent and observed [$I > 2\sigma(I)$] reflections	95355, 10265, 9404
R_{int}	0.045
$(\sin \theta/\lambda)_{max}$ (Å^{-1})	0.667
Refinement	
$R[F^2 > 2\sigma(F^2)]$, $wR(F^2)$, *S*	0.027, 0.073, 1.03
No. of reflections	10265
No. of parameters	452
No. of restraints	384
H-atom treatment	H atoms treated by a mixture of independent and constrained refinement
$\Delta\rho_{max}$, $\Delta\rho_{min}$ (e Å^{-3})	0.36, −0.38

Computer programs: Bruker Instrument Service vV6.2.3, *APEX4* v2022.10-0 (Bruker AXS), *SAINT* V8.37A (Bruker AXS Inc., 2015), XT, VERSION 2014/5, *SHELXL2016*/6 (Sheldrick, 2016), *PLATON* (Spek, 2009).

Table S12. Crystal data and structure refinement for **5**.

Crystal data	
Chemical formula	$C_{43}H_{77}N_7O_2Si_4Zn_2$
M_r	967.21
Crystal system, space group	Orthorhombic, $P2_12_12_1$
Temperature (K)	150
a, *b*, *c* (Å)	13.2208(12), 13.4940(11), 29.513(2)
V (Å^3)	5265.1(8)
Z	4
Radiation type	Mo*K*α
μ (mm^{-1})	1.04
Crystal size (mm)	0.24 × 0.18 × 0.13
Data collection	
Diffractometer	Bruker D8 - Venture
Absorption correction	Multi-scan *SADABS2016*/2 - Bruker AXS area detector scaling and absorption correction Reference: Krause, L., Herbst-Irmer, R., Sheldrick G.M. & Stalke D., J. Appl. Cryst. 48 (2015) 3-10.
T_{min}, T_{max}	0.560, 0.746
No. of measured, independent and observed [$I > 2\sigma(I)$] reflections	46992, 10853, 10138
R_{int}	0.069
$(\sin\theta/\lambda)_{max}$ (Å^{-1})	0.628
Refinement	
$R[F^2 > 2\sigma(F^2)]$, $wR(F^2)$, *S*	0.069, 0.218, 1.08
No. of reflections	10853
No. of parameters	553
No. of restraints	468
H-atom treatment	H-atom parameters constrained
	$w = 1/[\sigma^2(F_o^2) + (0.1359P)^2 + 64.8811P]$ where $P = (F_o^2 + 2F_c^2)/3$
$\Delta\rho_{max}$, $\Delta\rho_{min}$ (e Å^{-3})	1.63, −0.78
Absolute structure	Flack x determined using 4222 quotients [(I+)-(I-)]/[(I+)+(I-)] (Parsons, Flack and Wagner, Acta Cryst. B69 (2013) 249-259).
Absolute str. param.	0.084(5)

Computer programs: Bruker Instrument Service vV6.2.3, *APEX4* v2022.10-0 (Bruker AXS), *SAINT* V8.37A (Bruker AXS Inc., 2015), XT, VERSION 2014/5, *SHELXL2016*/6 (Sheldrick, 2016), *PLATON* (Spek, 2009).

Table S13. Crystal data and structure refinement for **6**.

Crystal data	
Chemical formula	$C_{62}H_{84}N_{10}O_4Zn·0.5(C_6H_{14})$
M_r	1141.84
Crystal system, space group	Monoclinic, *C*2/*c*
Temperature (K)	150
a, *b*, *c* (Å)	22.3877(7), 24.1084(10), 23.7970(9)
β (°)	105.299(1)
V (Å^3)	12388.8(8)
Z	8
Radiation type	Mo*K*α
μ (mm^{-1})	0.45
Crystal size (mm)	0.51 × 0.20 × 0.17
Data collection	
Diffractometer	Bruker D8 - Venture
Absorption correction	Multi-scan *SADABS2016*/2 - Bruker AXS area detector scaling and absorption correction
T_{min}, T_{max}	0.625, 0.746
No. of measured, independent and observed [$I > 2\sigma(I)$] reflections	94495, 14200, 11884
R_{int}	0.095
$(\sin\theta/\lambda)_{max}$ (Å^{-1})	0.650
Refinement	
$R[F^2 > 2\sigma(F^2)]$, $wR(F^2)$, S	0.091, 0.171, 1.20
No. of reflections	14200
No. of parameters	722
No. of restraints	648
H-atom treatment	H atoms treated by a mixture of independent and constrained refinement $w = 1/[\sigma^2(F_o^2) + (0.0265P)^2 + 104.2132P]$ where $P = (F_o^2 + 2F_c^2)/3$
$\Delta\rho_{max}$, $\Delta\rho_{min}$ (e Å^{-3})	0.68, −1.09

Computer programs: Bruker Instrument Service vV6.2.3, *APEX3* v2016.5-0 (Bruker AXS), *SAINT* V8.37A (Bruker AXS Inc., 2015), XT, VERSION 2014/5, *SHELXL2016*/6 (Sheldrick, 2016), *PLATON* (Spek, 2009).

Computational Data

All the calculations were performed with the Gaussian 16 program.[11] The geometries of all compounds and their selected isomers as well as by products and starting materials were fully optimized at B3LYP/6-311+G(d,p), level of theory[12, 13] without any structure simplifications. The structure of complexes obtained by X-ray diffraction were mostly used as the input structures. The conductor-like polarizable continuum model (CPCM)[14] was employed for the solvation effects (THF, benzene). The empirical dispersion correction D3 was applied for all structures.[15] All the structures are minima on the potential energy surface, as confirmed by the frequency calculations at the same level of theory and transition states by only one imaginary frequency. The topological analysis of the theoretical function ρ(*r*) was performed using the AIMAll program package.[16] Within the framework of Atoms in Molecules theory, the atomic charges in all compounds together with bond, ring and cluster critical points were calculated, the interaction energies within the critical points were calculated according to Espinosa's equation.[2] The total enthalpies and Gibbs free energies were calculated at T = 298.15 K. The NMR parameters were calculated by GIAO method.[17] Appropriate Cartesian coordinates for all computed structures are given in separate files. The visualization of the transition state in a 'pendulum'-like equilibrium is attached as gif file.

11. Gaussian 16, Revision A.03, Frisch, M. J.; Trucks, G. W.; Schlegel, H. B.; Scuseria, G. E.; Robb, M. A.; Cheeseman, J. R.; Scalmani, G.; Barone, V.; Petersson, G. A.; Nakatsuji, H.; Li, X.; Caricato, M.; Marenich, A. V.; Bloino, J.; Janesko, B. G.; Gomperts, R.; Mennucci, B.; Hratchian, H. P.; Ortiz, J. V.; Izmaylov, A. F.; Sonnenberg, J. L.; Williams-Young, D.; Ding, F.; Lipparini, F.; Egidi, F.; Goings, J.; Peng, B.; Petrone, A.; Henderson, T.; Ranasinghe, D.; Zakrzewski, V. G.; Gao, J.; Rega, N.; Zheng, G.; Liang, W.; Hada, M.; Ehara, M.; Toyota, K.; Fukuda, R.; Hasegawa, J.; Ishida, M.; Nakajima, T.; Honda, Y.; Kitao, O.; Nakai, H.; Vreven, T.; Throssell, K.; Montgomery, J. A., Jr.; Peralta, J. E.; Ogliaro, F.; Bearpark, M. J.; Heyd, J. J.; Brothers, E. N.; Kudin, K. N.; Staroverov, V. N.; Keith, T. A.; Kobayashi, R.; Normand, J.; Raghavachari, K.; Rendell, A. P.; Burant, J. C.; Iyengar, S. S.; Tomasi, J.; Cossi, M.; Millam, J. M.; Klene, M.; Adamo, C.; Cammi, R.; Ochterski, J. W.; Martin, R. L.; Morokuma, K.; Farkas, O.; Foresman, J. B.; Fox, D. J. Gaussian, Inc., Wallingford CT, 2016.
12. Becke, A. D. Density-functional thermochemistry. III. The role of exact Exchange. *J. Chem. Phys*. **1993**, *98*, 5648−5652. DOI: 10.1063/1.464913.
13. Dunning, T. H. Jr. Gaussian basis sets for use in correlated molecular calculations. I. The atoms boron through neon and hydrogen. *J. Chem. Phys.* **1989**, *90*, 1007−1023. DOI : 10.1063/1.456153.
14. Tomasi, J.; Mennucci, B.; Cammi, R. Quantum mechanical continuum solvation models. *Chem. Rev*. **2005**, *105*, 2999−3093. DOI: 10.1021/cr9904009.
15. Grimme, S.; Antony, J.; Ehrlich, S.; Krieg, H. A. Consistent and accurate *ab initio* parametrization of density functional dispersion correction (DFT-D) for the 94 elements H-Pu. *J. Chem. Phys.* **2010**, *132*, 154104–154119. DOI: 10.1063/1.3382344.
16. AIMAll, Version 19.10.12 Keith, T. A. TK Gristmill Software, Overland Park KS, USA, 2019.
17. Wolinski, K.; Hilton, J. F.; Pulay, P. Efficient Implementation of the Gauge-Independent Atomic Orbital Method for NMR Chemical Shift Calculations. *J. Am. Chem. Soc.* **1990**, *112*, 8251–8260. DOI : 10.1021/ja00179a005.

Typical PLA synthesis procedure in solution

Under argon atmosphere, to a solution of *rac*-lactide (288.3 mg; 100 eq.; 2.00 mmol) in the chosen solvent (1.3 mL; $[LA]_0$ = 1.50 M), 1 eq. of catalyst and 1 eq. of co-initiator ^{i}PrOH (1.53 µL; 0.02 mmol) were added. The vial was crimped and let under stirring at the desired temperature. The reaction vial was opened to air in order to quench the reaction. The conversion was determined by ^{1}H NMR spectroscopy and the molar mass and dispersity by Gel Permeation Chromatography (GPC). The provided PLA can be washed with methanol in order to remove the residual monomer and catalyst.

Typical PHB synthesis procedure in solution

Under argon atmosphere, to a solution of *rac*-β-butyrolactone (0.1 mL; 100 eq.; 1.23 mmol) in the chosen solvent (0.8 mL; $[BL]_0$ = 1.50 M), 1 eq. of catalyst and 1 eq. of co-initiator - ^{i}PrOH (0.94 µL; 0.01 mmol) were added. The vial was crimped and let under stirring at the desired temperature. The reaction vial was opened to air in order to quench the reaction. The conversion was determined by ^{1}H NMR spectroscopy and the molar mass and dispersity by GPC.

Typical PHB-*b*-PLLA synthesis procedure in solution

Under argon atmosphere, to a solution of *rac*-β-butyrolactone (0.1 mL; 50 eq.; 1.23 mmol) in DCM (0.8 mL; $[BL]_0$ = 1.50 M), 1 eq. of catalyst and 1 eq. of co-initiator ^{i}PrOH (1.88 µL; 0.02 mmol) were added. The vial was crimped and let under stirring at 45 °C for 3 hours. After, a solution of *L*-lactide (177.3 mg; 50 eq.; 1.23 mmol) in DCM (0.8 mL; $[LA]_0$ = 0.75 M) was added to the reaction. The vial was closed and let under stirring at 25 °C for 1 minute. The reaction vial was opened to air in order to quench the reaction. The conversion was determined by ^{1}H NMR spectroscopy and the molar mass and dispersity by GPC and DOSY NMR analysis.

Typical PLLA- *b*-PHB synthesis procedure in solution

Under argon atmosphere, to a solution of *L*-lactide (177.3 mg; 50 eq.; 1.23 mmol) in DCM (0.8 mL; $[LA]_0$ = 1.50 M), 1 eq. of catalyst and 1 eq. of co-initiator ^{i}PrOH (1.88 µL; 0.02 mmol) were added. The vial was closed and let under stirring at 25 °C for 1 minute. After, a solution of *rac*-β-butyrolactone (0.1 mL; 50 eq.; 1.23 mmol) in DCM (0.8 mL; $[BL]_0$ = 0.75 M) was added to the reaction. The vial was crimped and let under stirring at 45 °C for the desired time. The reaction vial was opened to air in order to quench the reaction. The conversion was determined by ^{1}H NMR spectroscopy and the molar mass and dispersity by GPC and DOSY NMR analysis.

Typical PHB- *b*-PLLA- *b*-PDLA synthesis procedure in solution

Under argon atmosphere, to a solution of *rac*-β-butyrolactone (81.5 µL; 50 eq.; 1.00 mmol) in DCM (1.0 mL; $[BL]_0$ = 1.00 M), 1 eq. of catalyst and 1 eq. of co-initiator ^{i}PrOH (0.76 µL; 0.01 mmol) were added. The vial was crimped and let under stirring at 45 °C for 3.5 hours. After, a solution of *L*-lactide (144.1 mg; 50 eq.; 1.00 mmol) in DCM (1.0 mL; $[LA]_0$ = 0.50 M) was added to the reaction. The vial was closed and let under stirring at 25 °C for 15 minutes. After, a solution of *D*-lactide (144.1 mg; 50 eq.; 1.00 mmol) in DCM (1.0 mL; $[LA]_0$ = 0.33 M) was added to the reaction. The vial was closed and let under stirring at 25 °C for 25 minutes. The reaction vial was opened to air in order to quench the reaction. The conversion was determined by ^{1}H NMR spectroscopy and the molar mass by DOSY NMR analysis.

Typical PLA- *b*-PHB- *b*-PLA synthesis procedure in solution

Under argon atmosphere, to a solution of *rac*-lactide (144.1 mg; 50 eq.; 1.00 mmol) in DCM (1.0 mL; $[LA]_0$ = 1.00 M), 1 or 0.5 eq. of catalyst and 1 eq. of co-initiator ^{i}PrOH (0.76 µL; 0.01 mmol) were added. The vial was crimped and let under stirring at 25 °C for 2 minutes. After, a solution of rac-β-butyrolactone (81.5 µL; 50 eq.; 1.00 mmol) in DCM (1.0 mL; $[BL]_0$ = 0.50 M) was added to the reaction. The vial was crimped and let under stirring at 45 °C for the desired time. After, a solution of *rac*-lactide (144.1 mg; 50 eq.; 1.00 mmol) in DCM (1.0 mL; $[LA]_0$ = 0.33 M) was added to the reaction. The vial was closed and let under stirring at 25 °C for the desired time. The reaction vial was opened to air in order to quench the reaction. The conversion was determined by ^{1}H NMR spectroscopy and the molar mass and dispersity by GPC and DOSY NMR analysis.

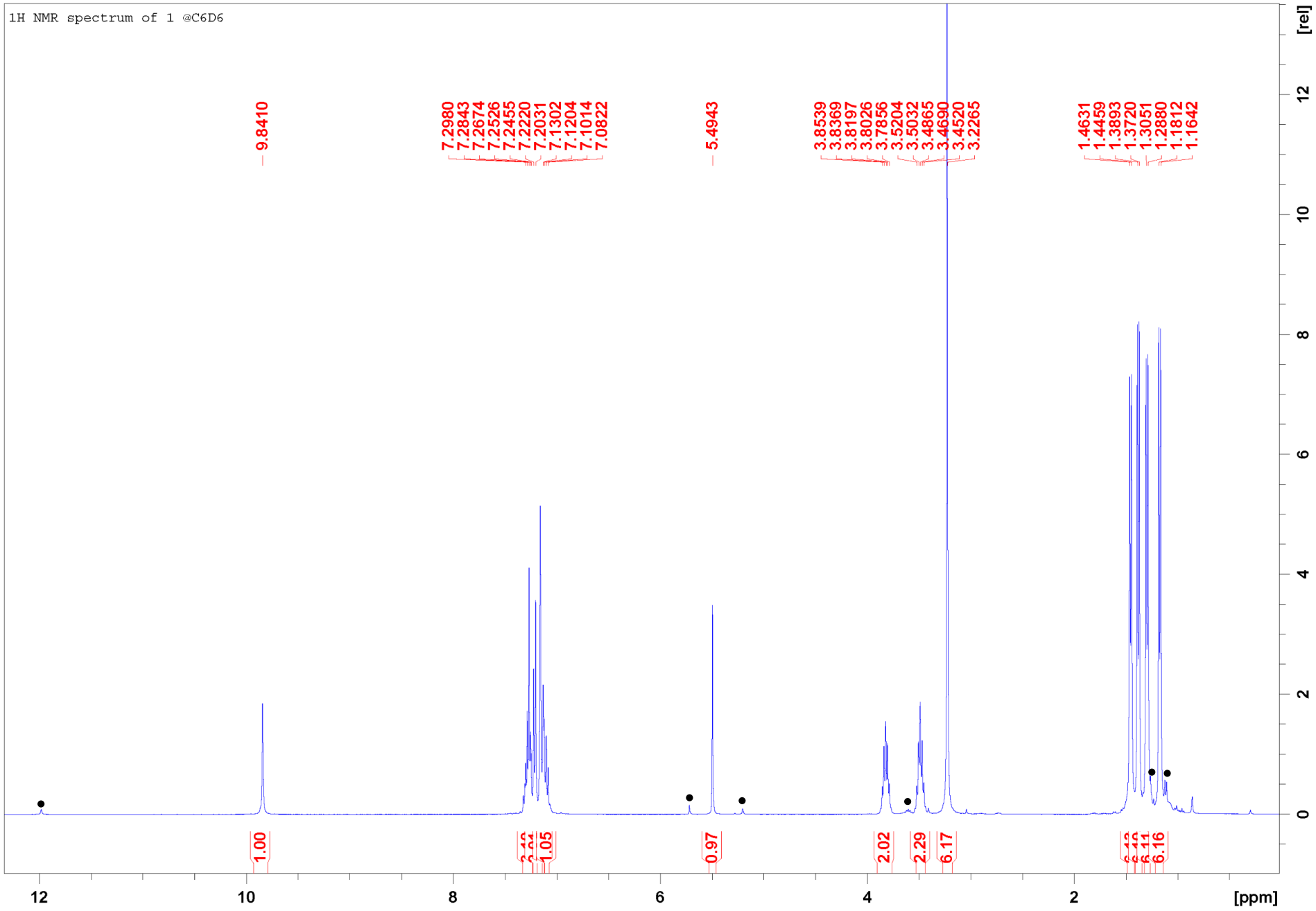

Figure S50. ^{1}H NMR spectrum of **1** in C_6D_6 at 295 K. Signals of the minor form are marked with black dots.

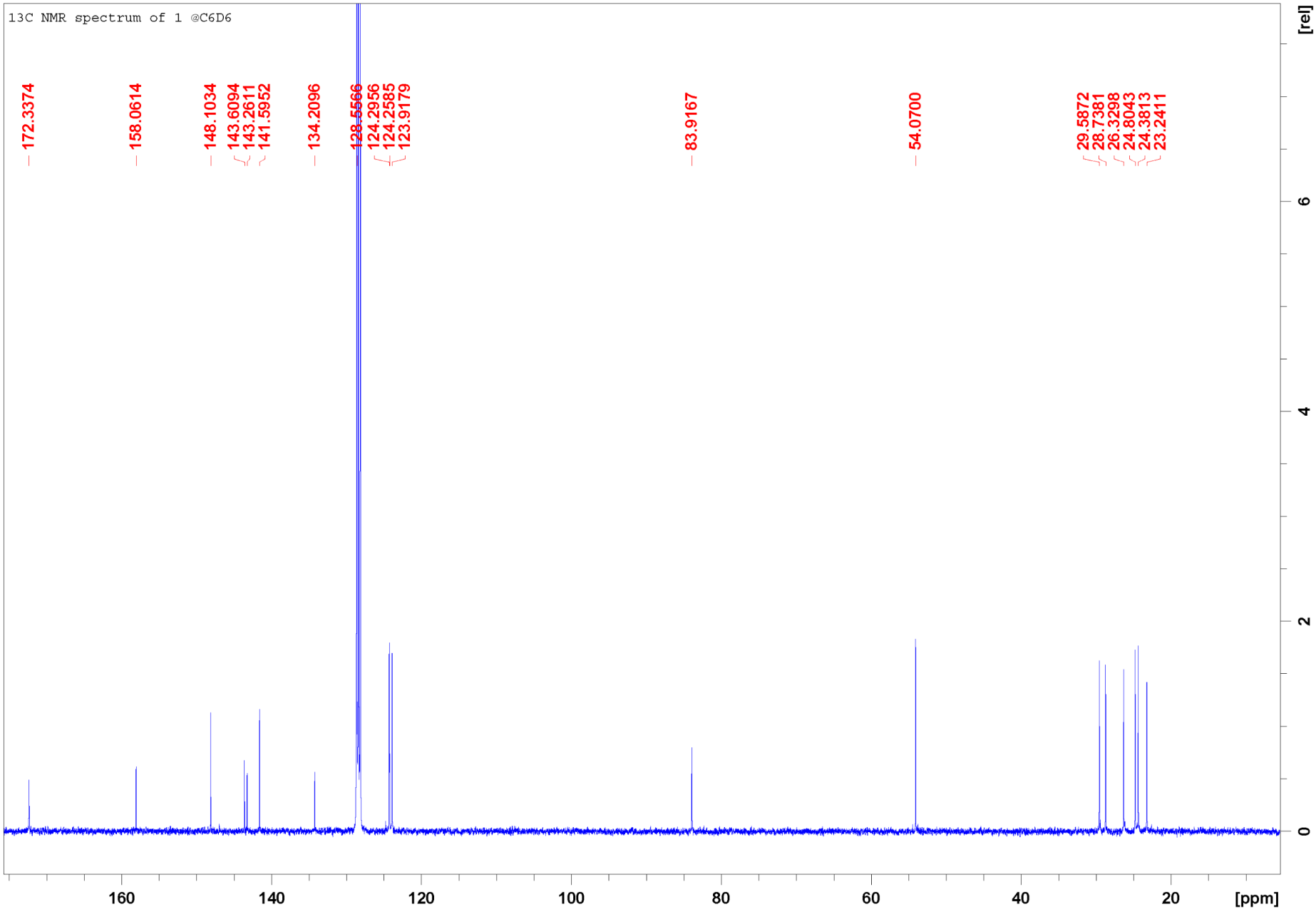

Figure S51. ^{13}C NMR spectrum of **1** in C_6D_6, 295 K.

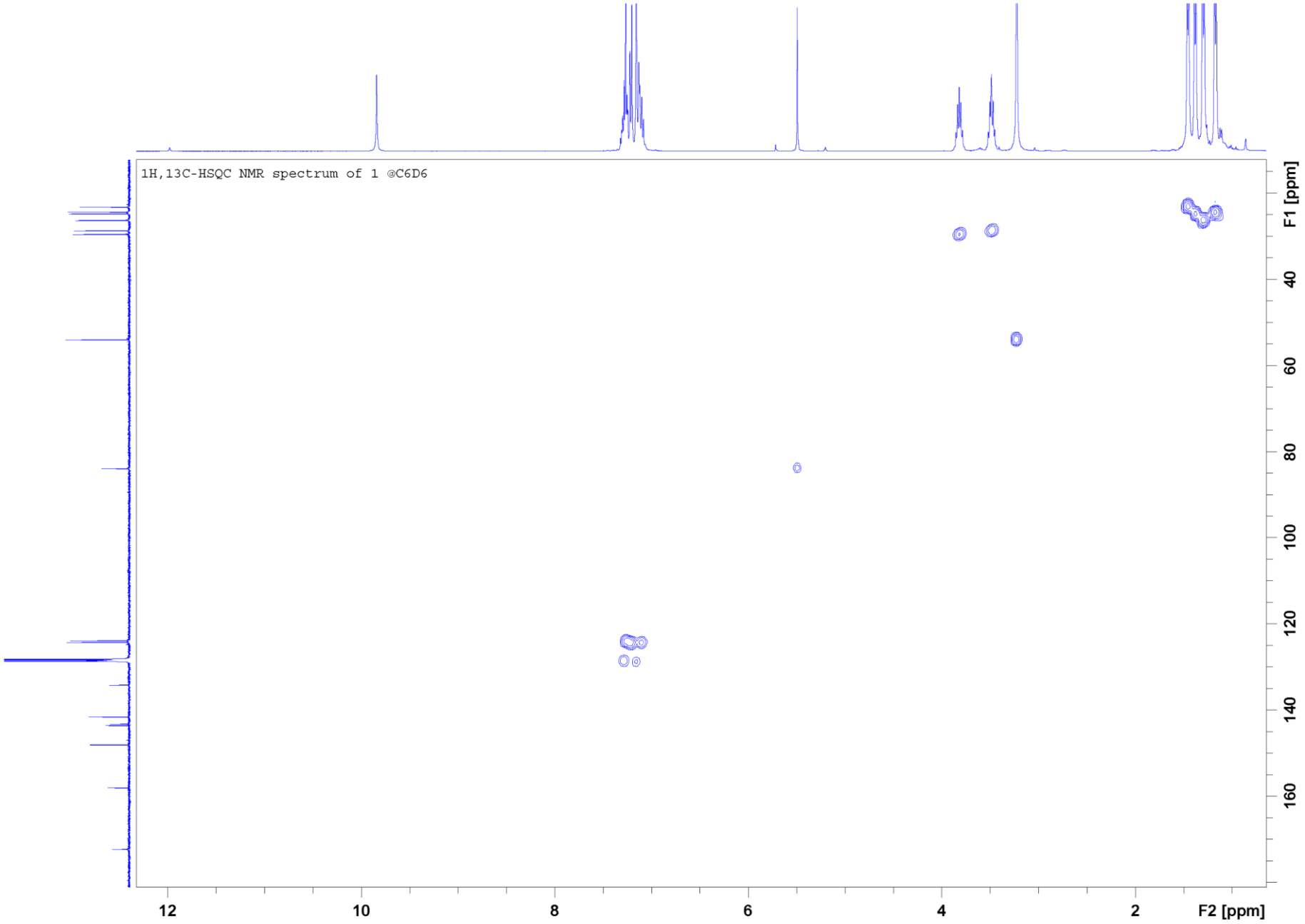

Figure S52. $^{1}H,^{13}C$-HSQC NMR spectrum of **1** in C_6D_6, 295 K.

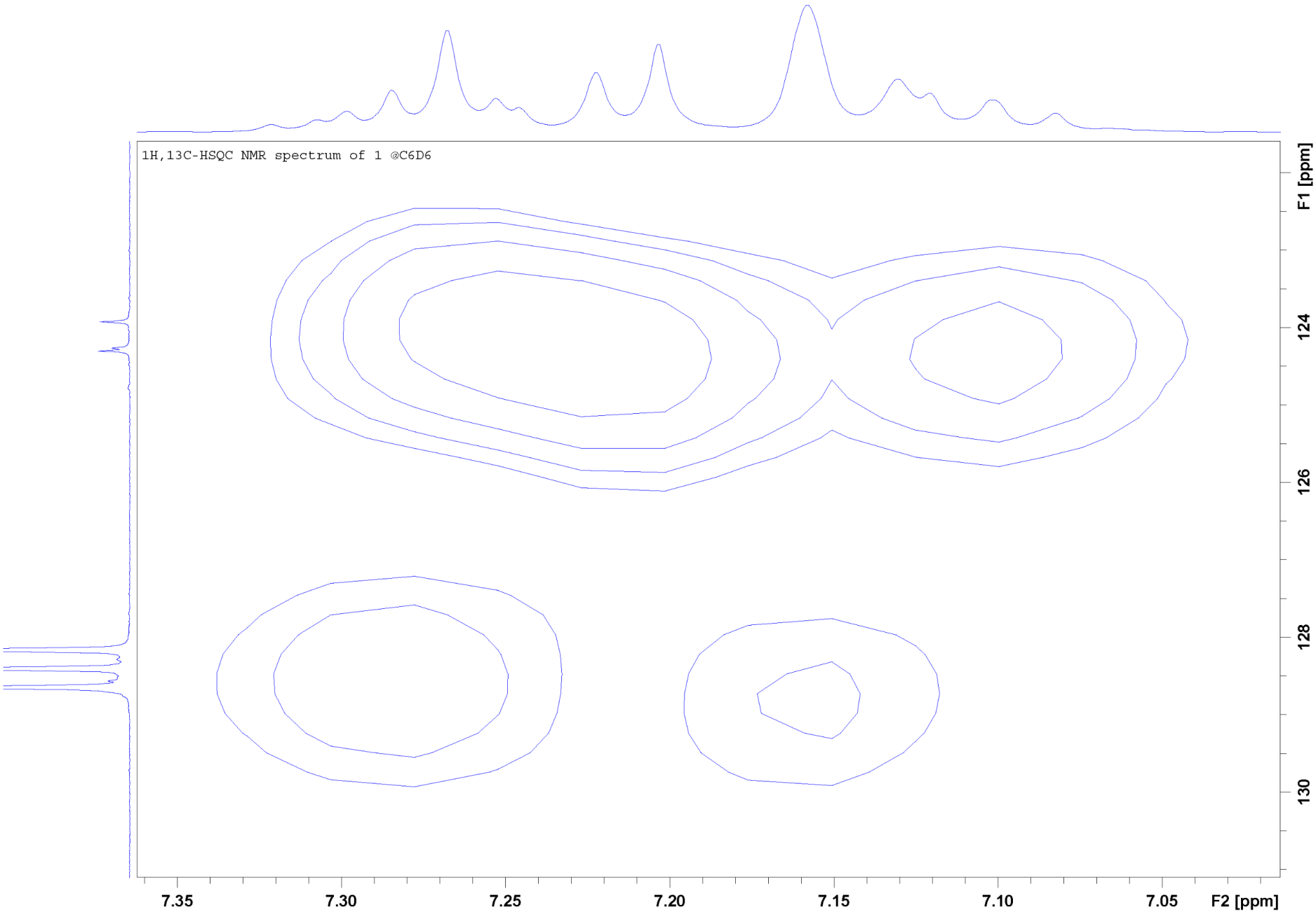

Figure S53. Detail of ^{1}H,^{13}C-HSQC NMR spectrum of **1** in C_6D_6, 295 K.

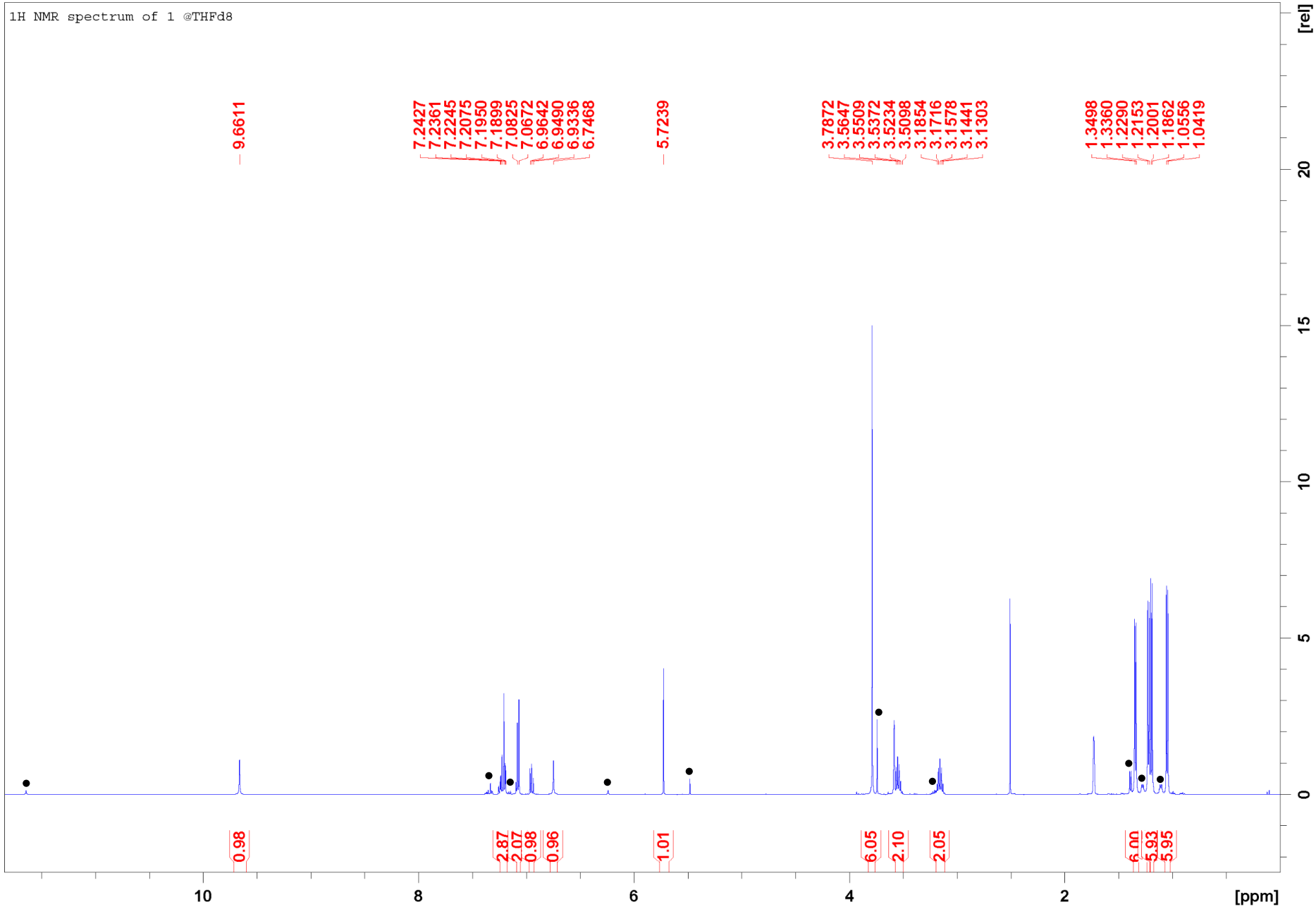

Figure S54. ^{1}H NMR spectrum of **1** in THF-d_8, 295 K. Signals of the minor form are marked with black dots.

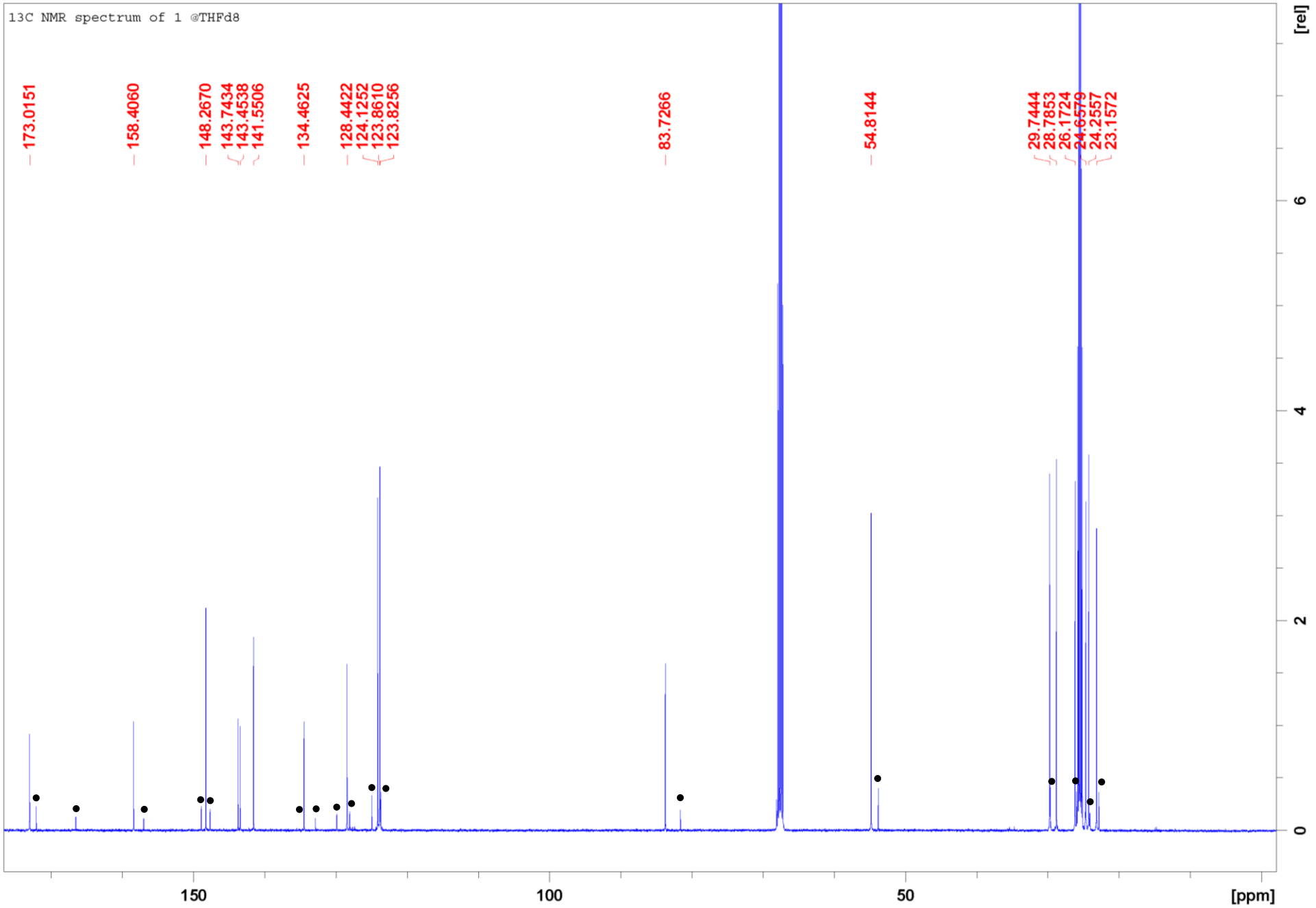

Figure S55. ^{13}C NMR spectrum of **1** in THF-d_8, 295 K. Signals of the minor form are marked with black dots.

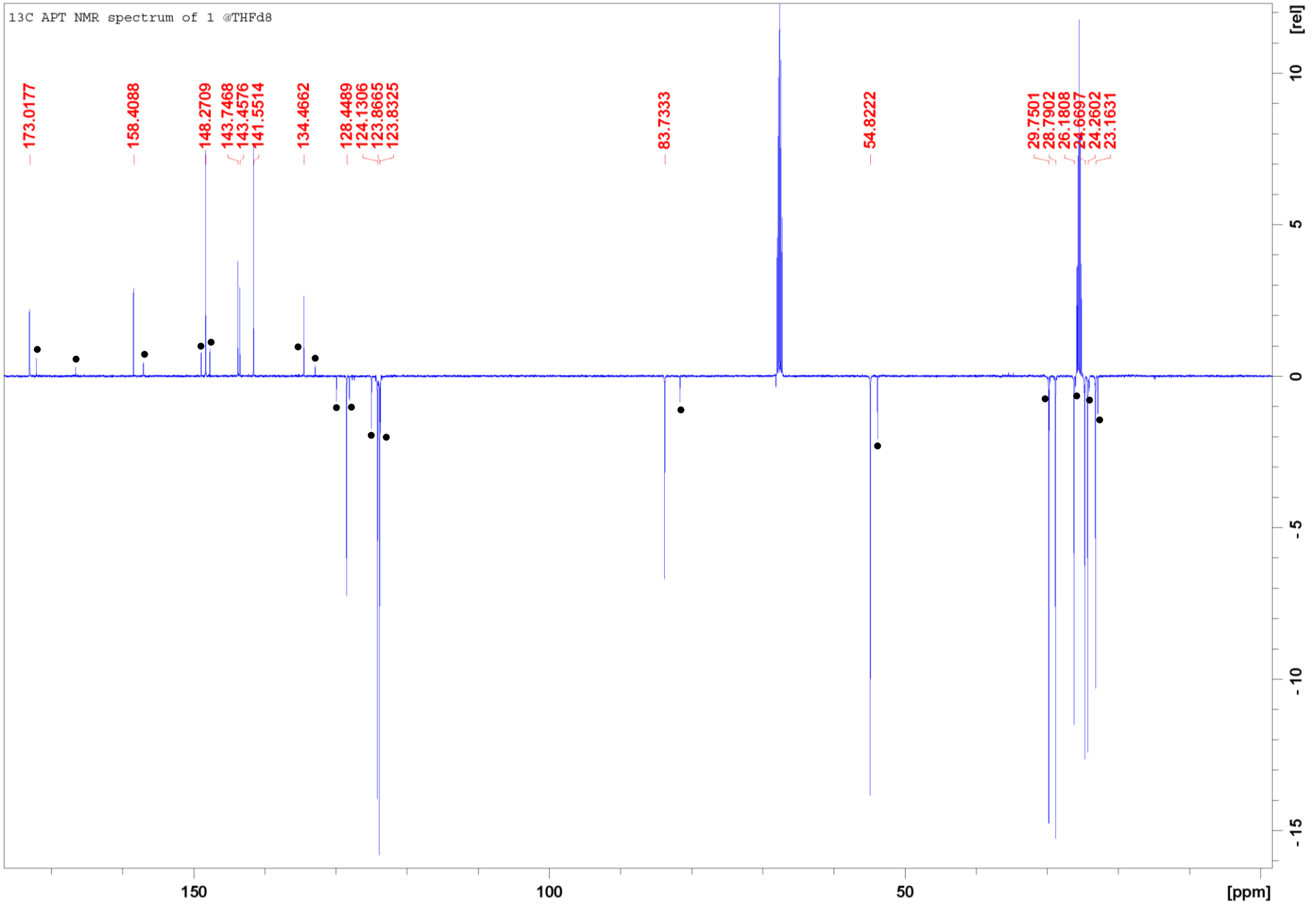

Figure S56. ^{13}C APT NMR spectrum of **1** in THF-d_8, 295 K. Signals of the minor form are marked with black dots.

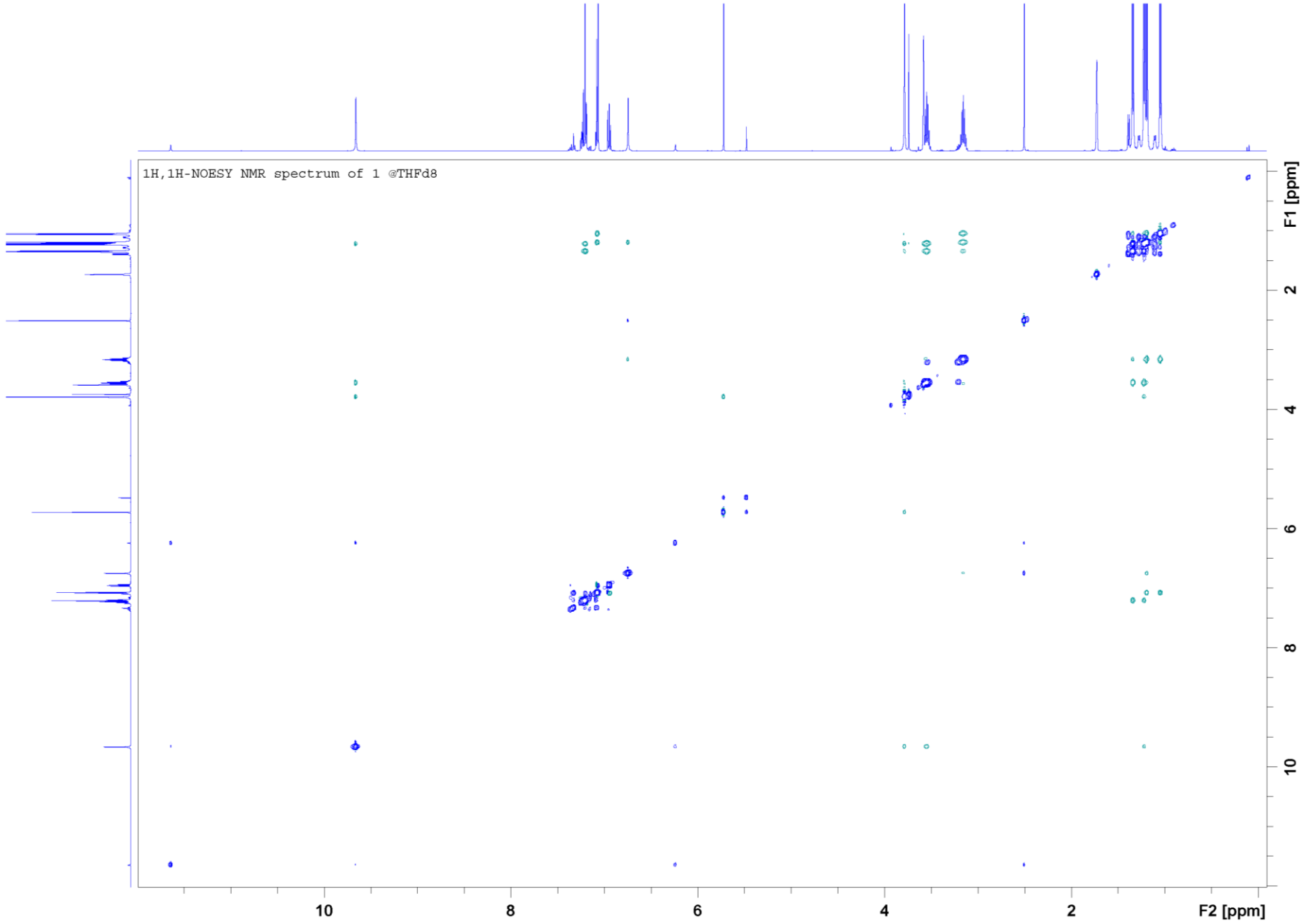

Figure S57. $^{1}H,^{1}H$-NOESY NMR spectrum of **1** in THF-d_8, 295 K.

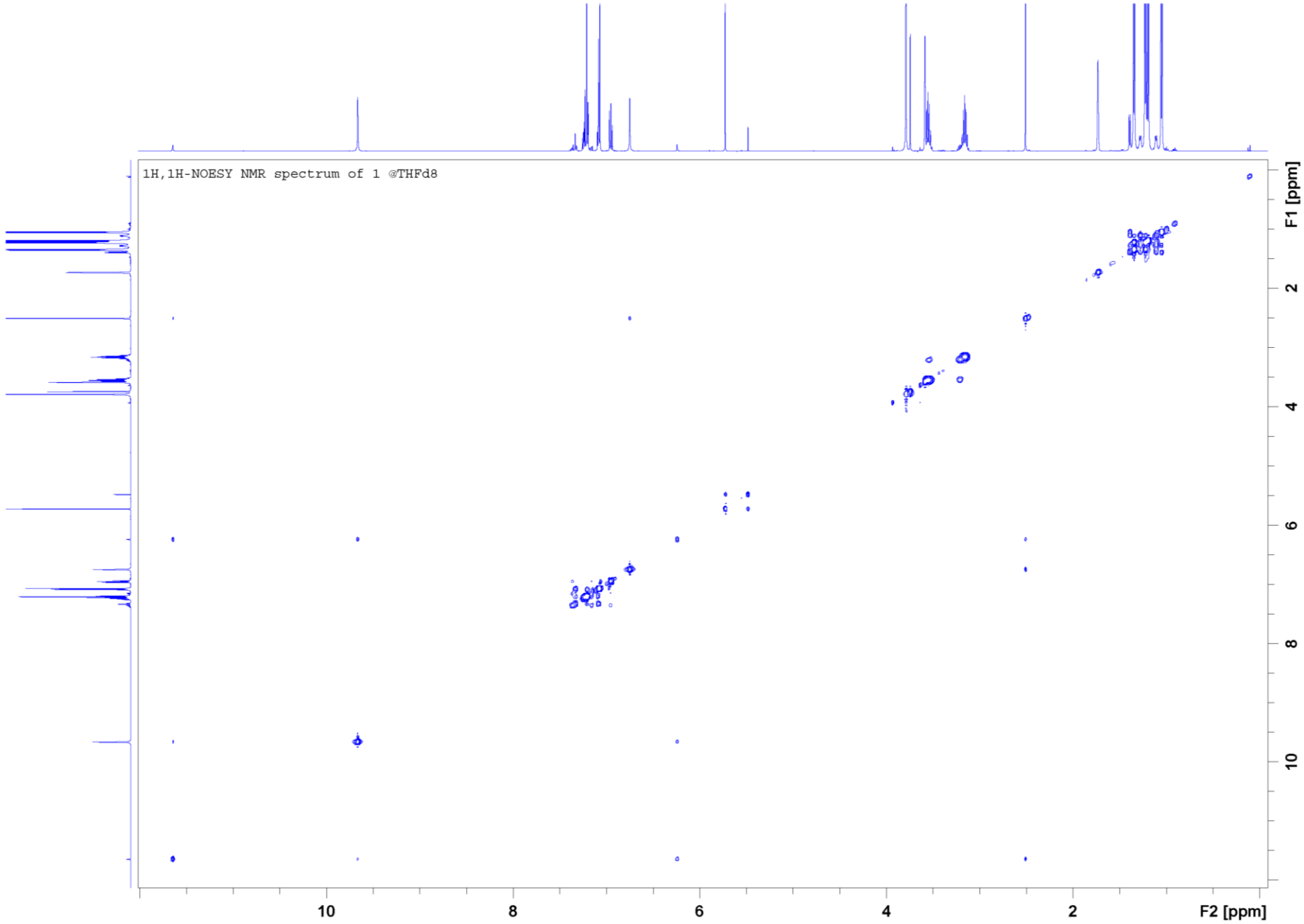

Figure S58. $^{1}H,^{1}H$-NOESY NMR spectrum of **1** in THF-d_8, 295 K. Only peaks of the same phase as the diagonal peaks are displayed (chemical exchange).

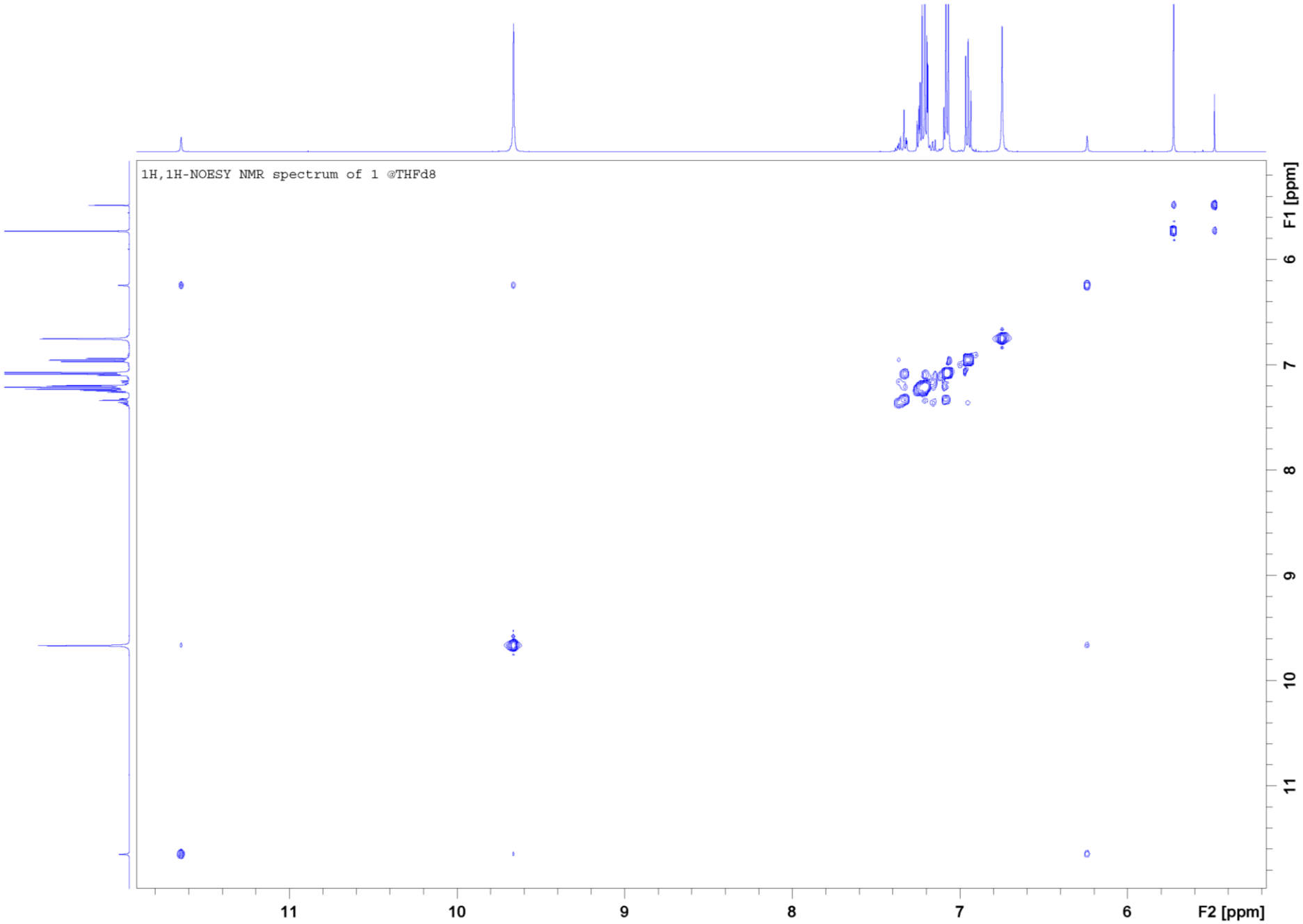

Figure S59. Detail of ^{1}H,^{1}H-NOESY NMR spectrum of **1** in THF-d_8, 295 K. Only peaks of the same phase as the diagonal peaks are displayed (chemical exchange).

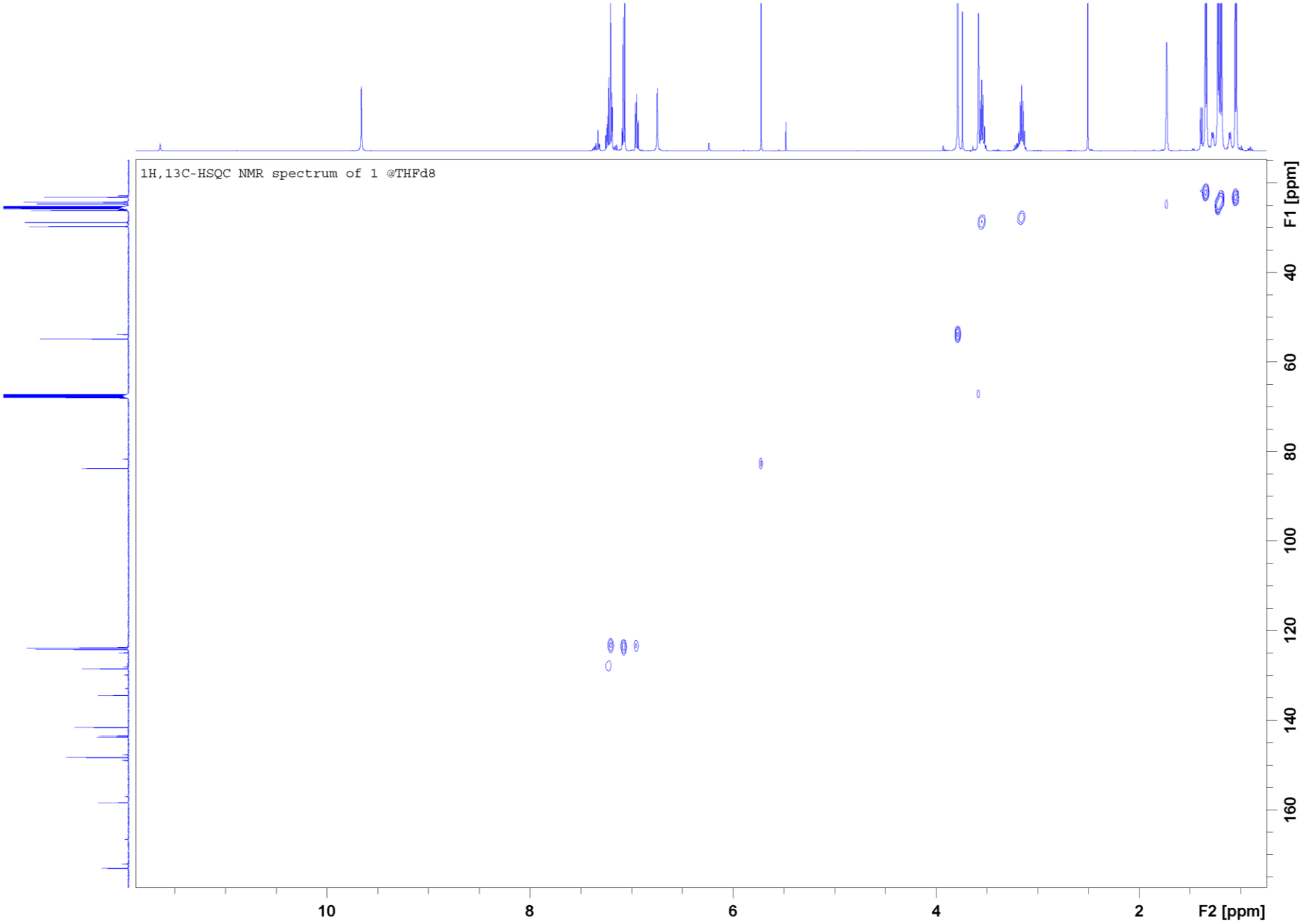

Figure S60. $^{1}H,^{13}C$-HSQC NMR spectrum of **1** in THF-d_8, 295 K.

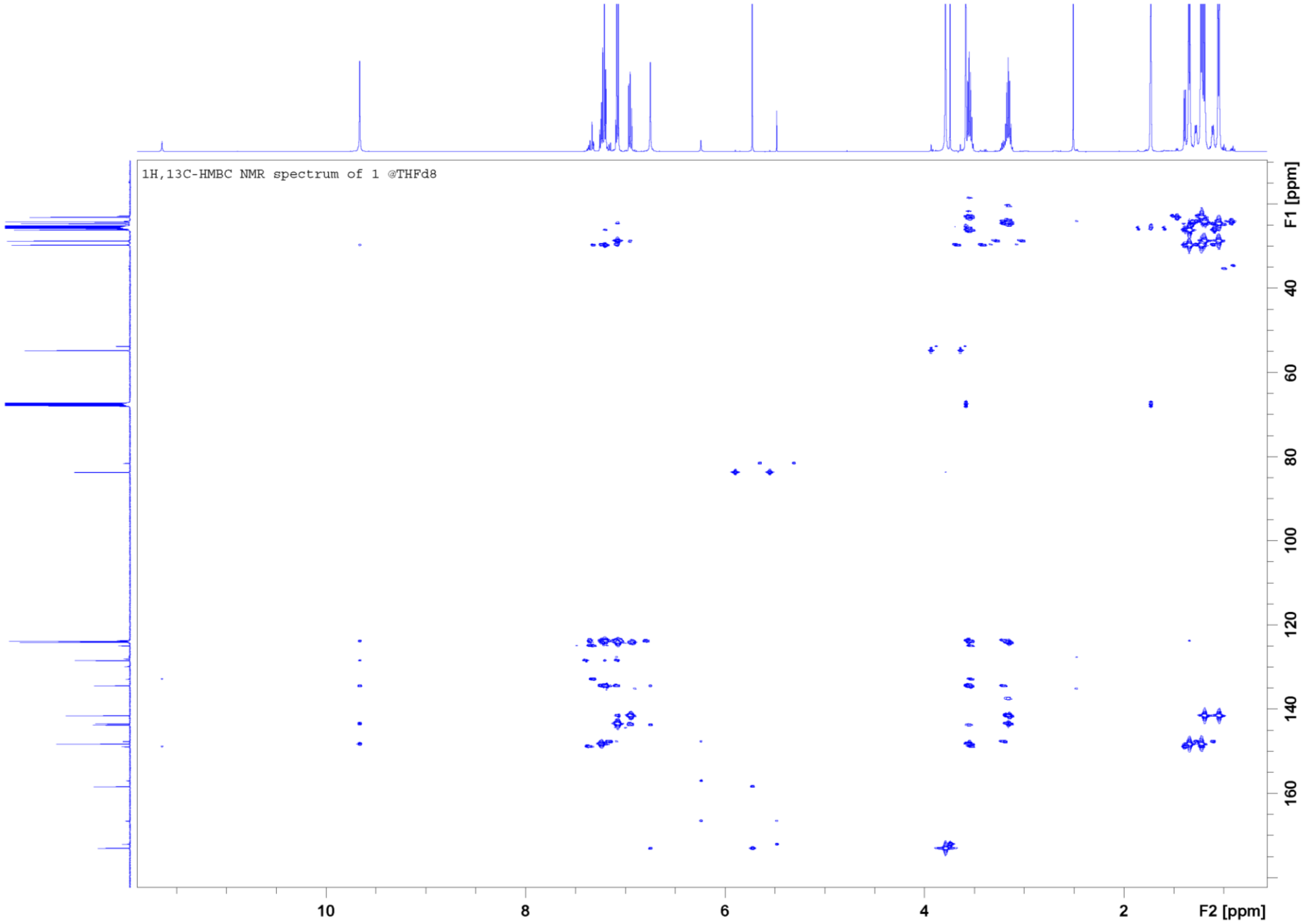

Figure S61. $^{1}H,^{13}C$-HMBC NMR spectrum of **1** in THF-d_8, 295 K.

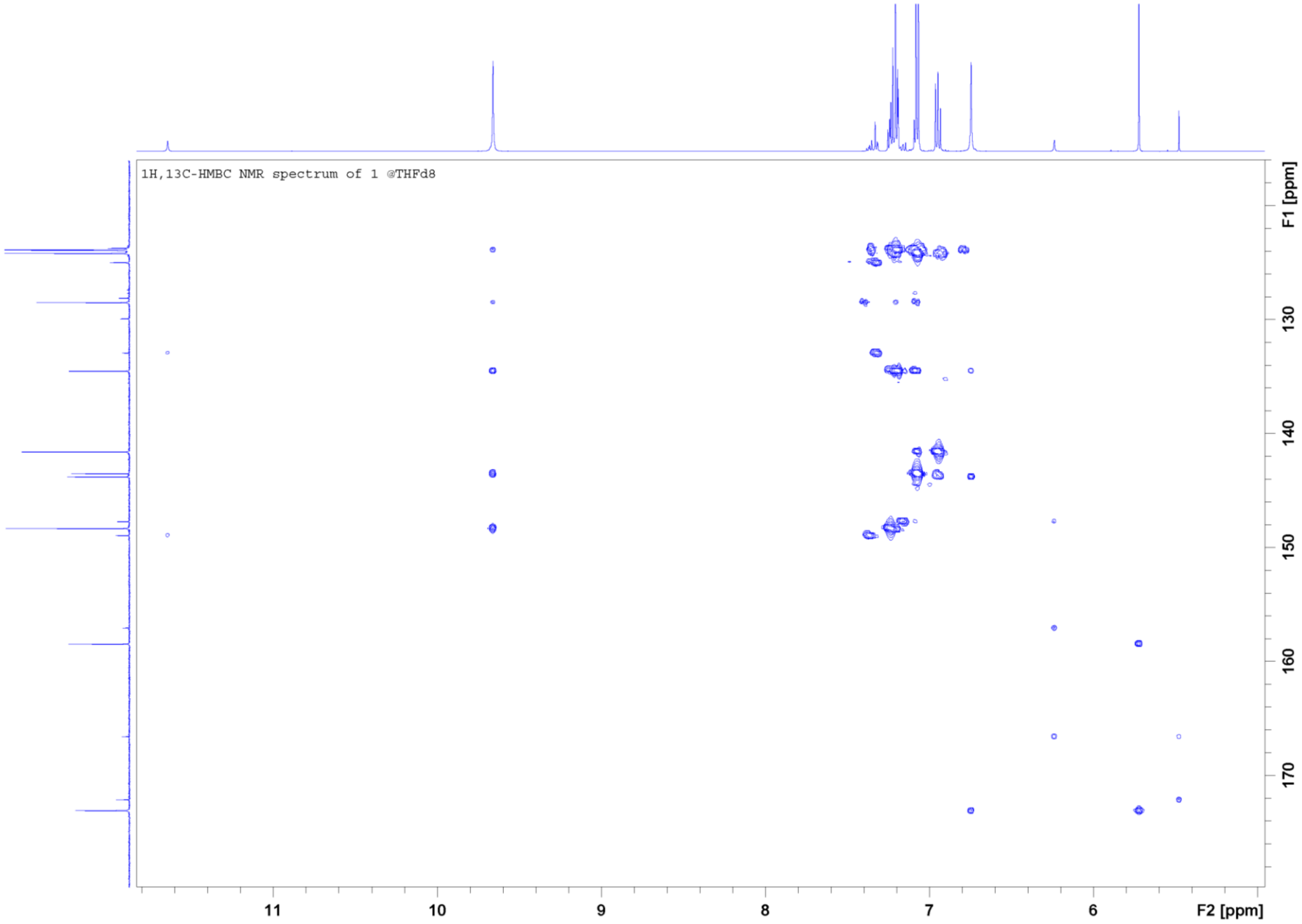

Figure S62. Detail of $^{1}H,^{13}C$-HMBC NMR spectrum of **1** in THF-d_8, 295 K.

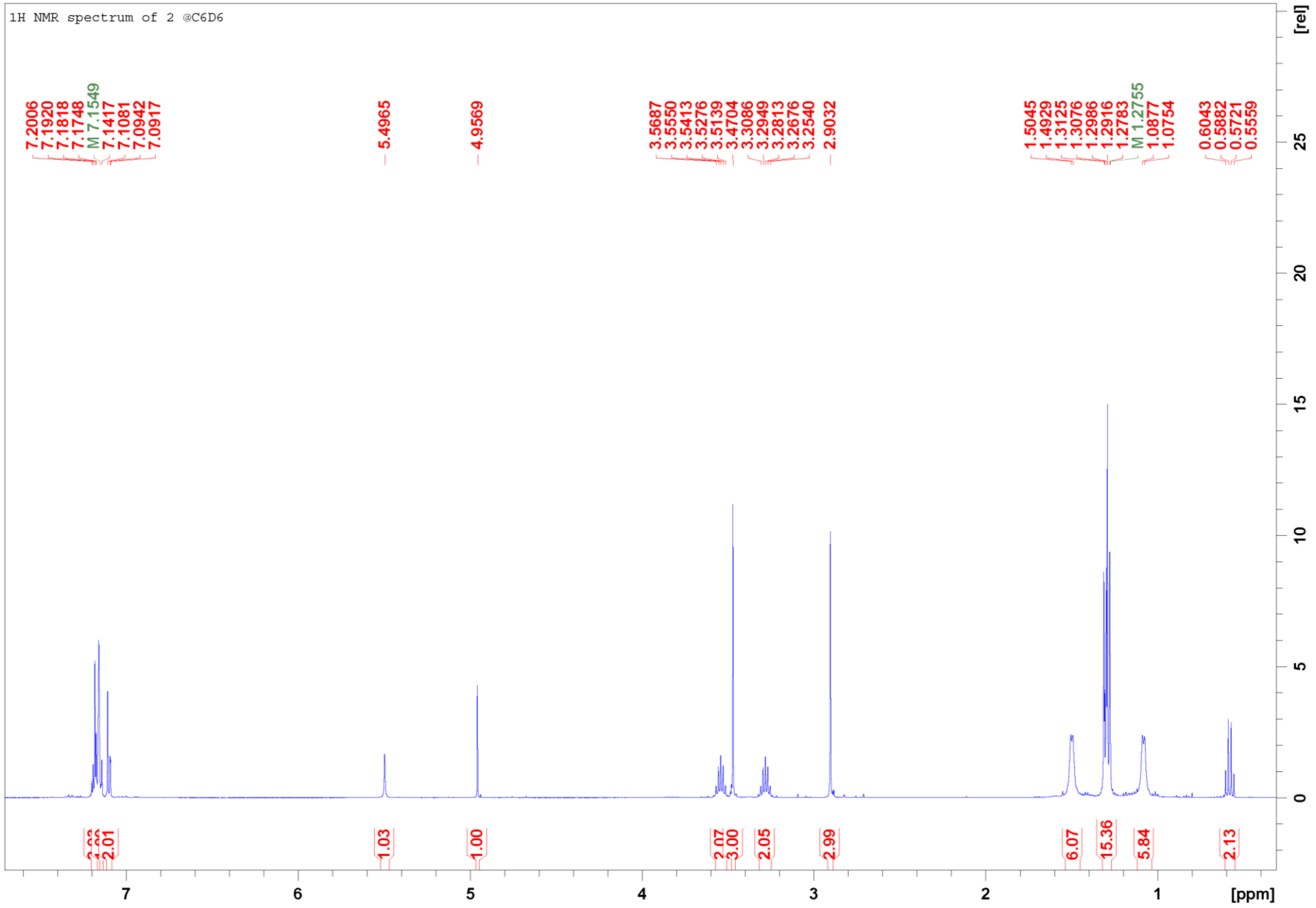

Figure S63. ^{1}H NMR spectrum of **2** in C_6D_6, 295 K.

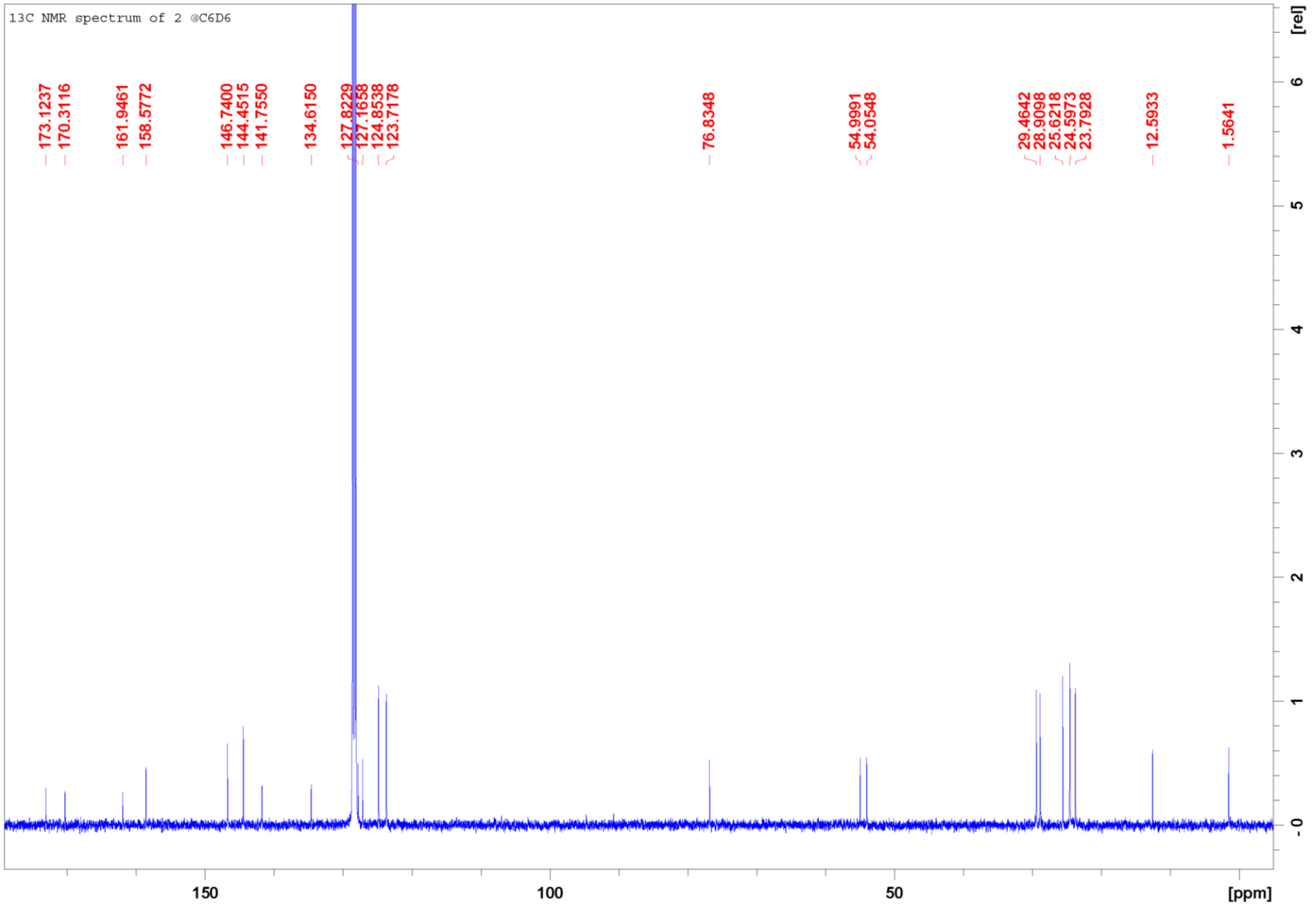

Figure S64. ^{13}C NMR spectrum of **2** in C_6D_6, 295 K.

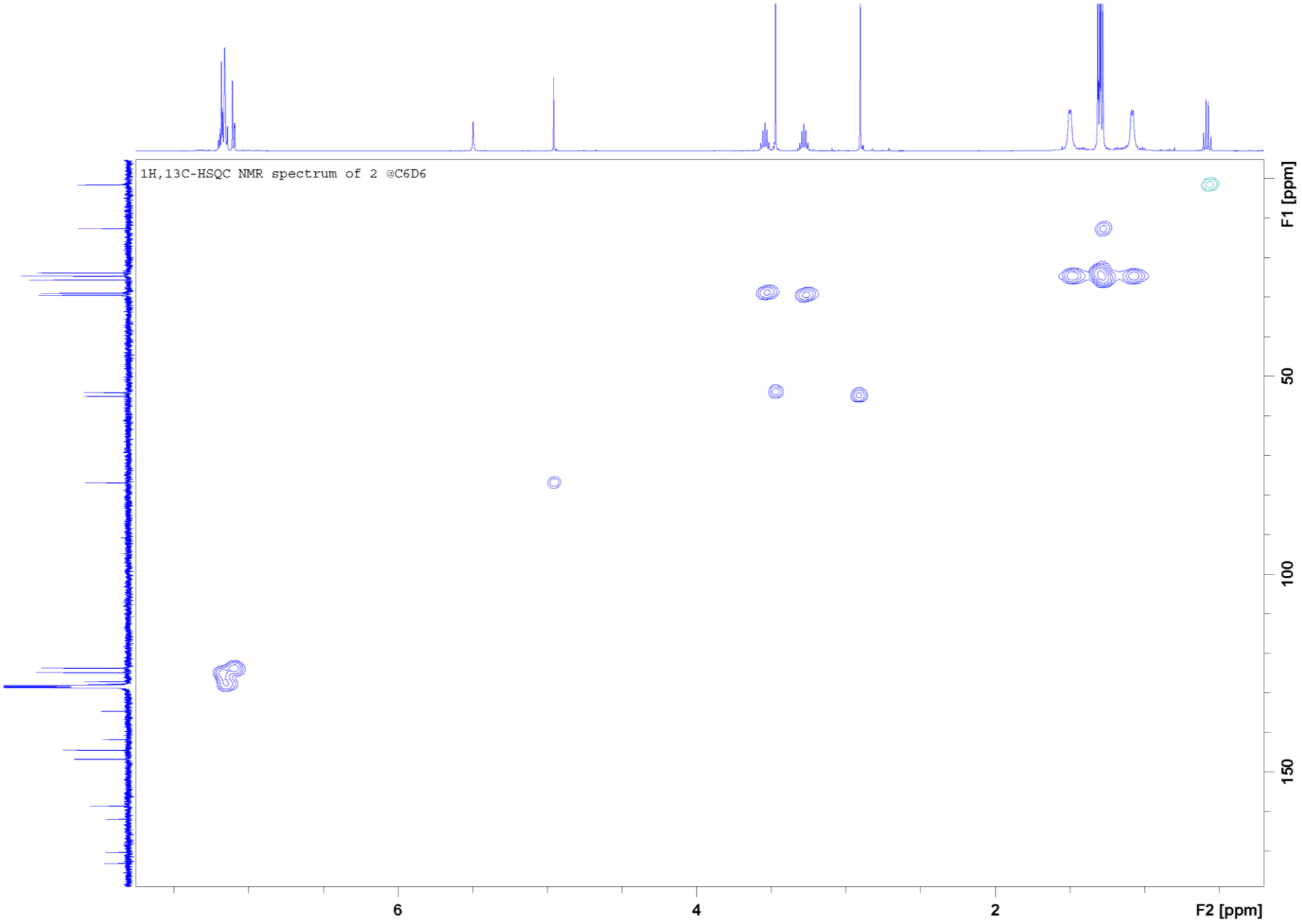

Figure S65. $^{1}H,^{13}C$-HSQC NMR spectrum of **2** in C_6D_6, 295 K.

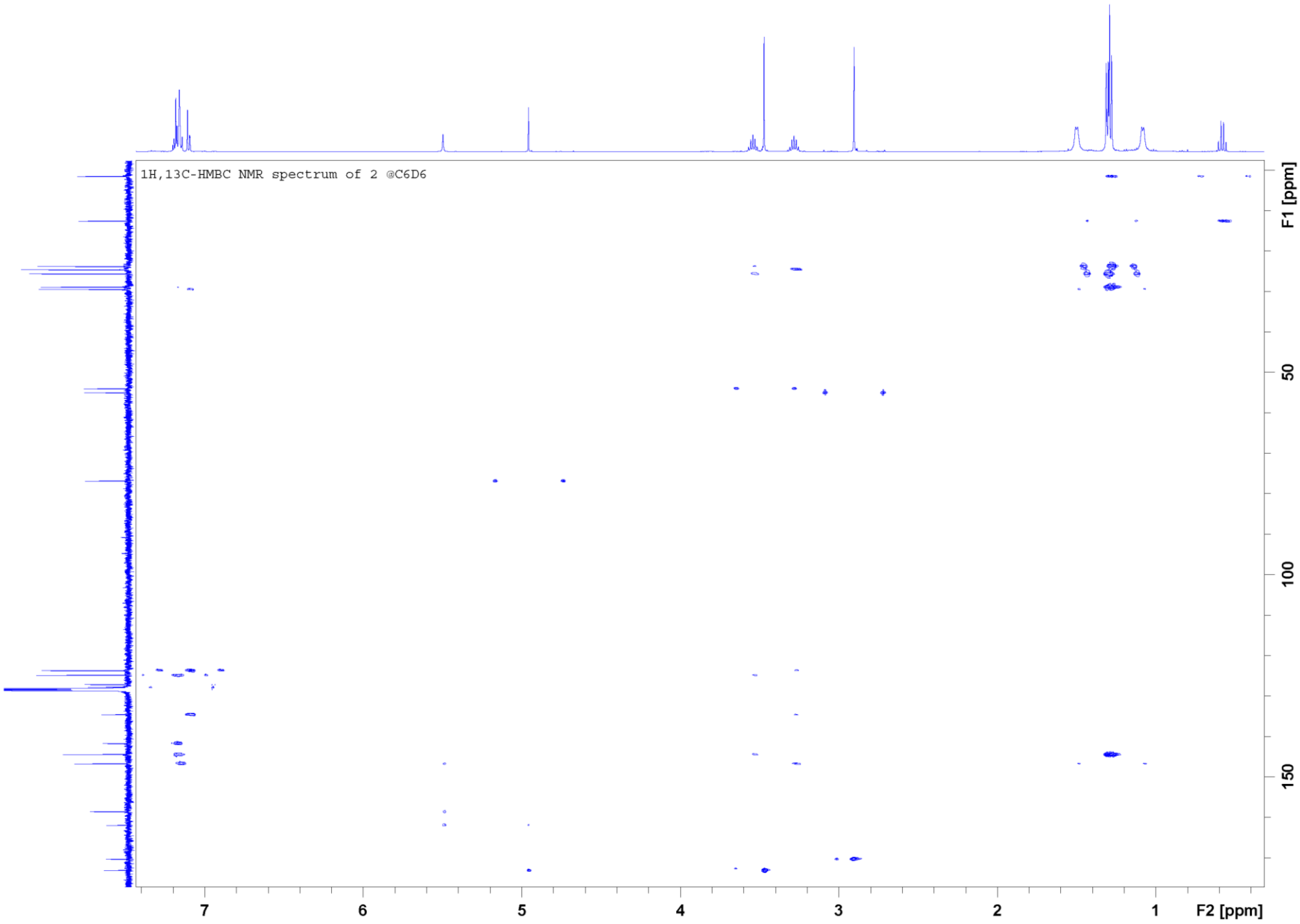

Figure S66. $^{1}H,^{13}C$-HMBC NMR spectrum of **2** in C_6D_6, 295 K.

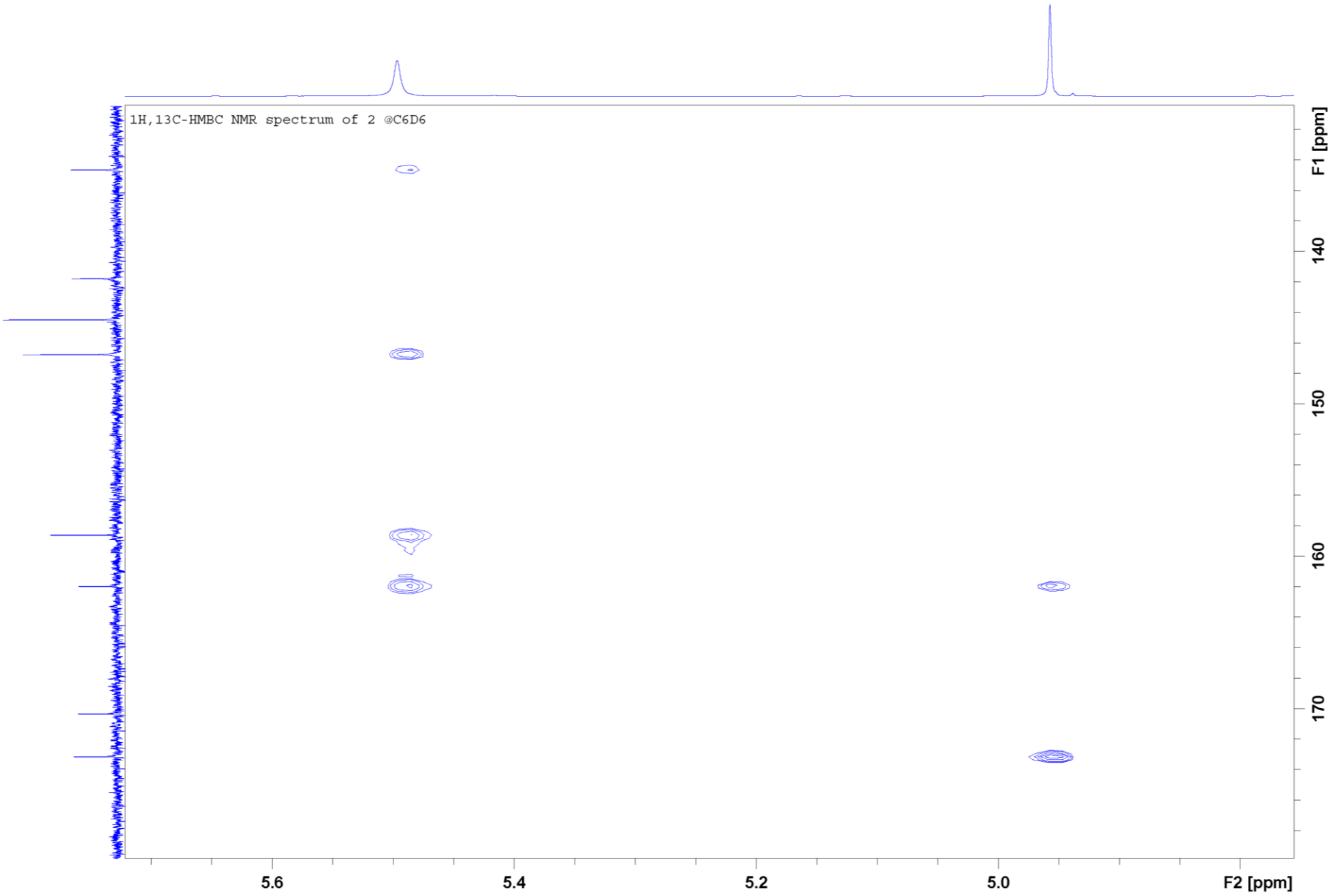

Figure S67. Detail of $^{1}H,^{13}C$-HMBC NMR spectrum of **2** in C_6D_6, 295 K.

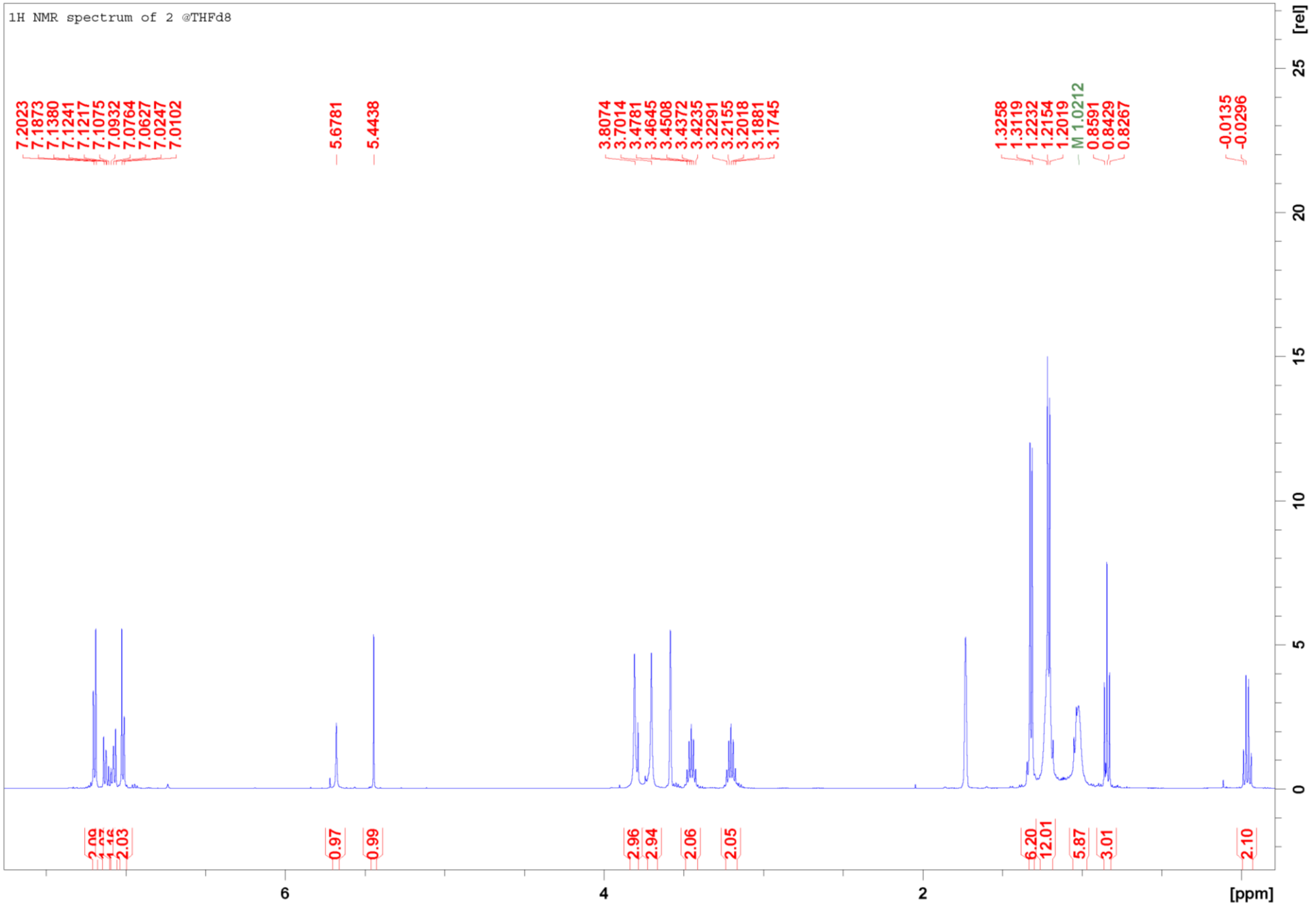

Figure S68. ^{1}H NMR spectrum of **2** in THF-d_8, 295 K.

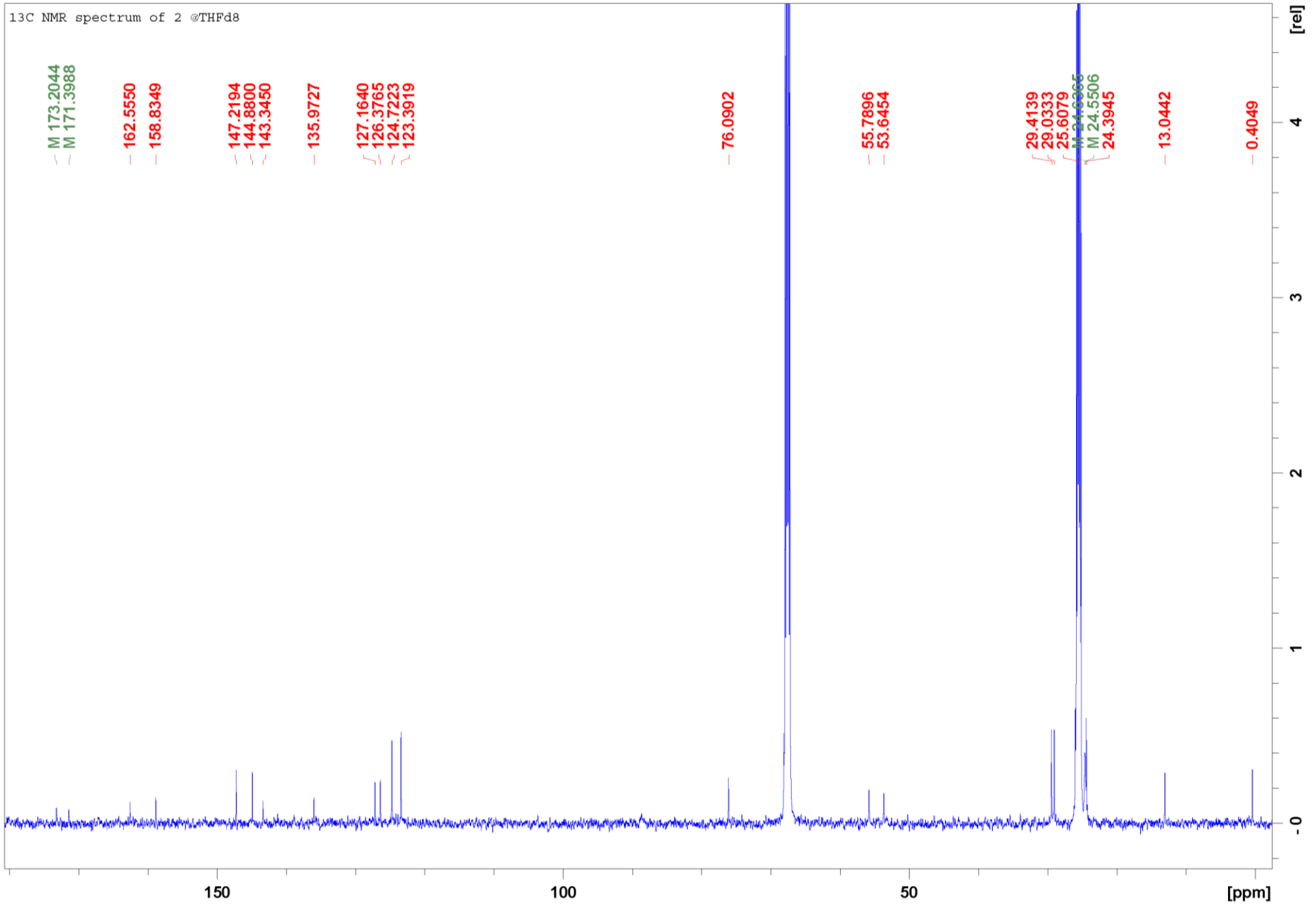

Figure S69. ^{13}C NMR spectrum of **2** in THF-d_8, 295 K.

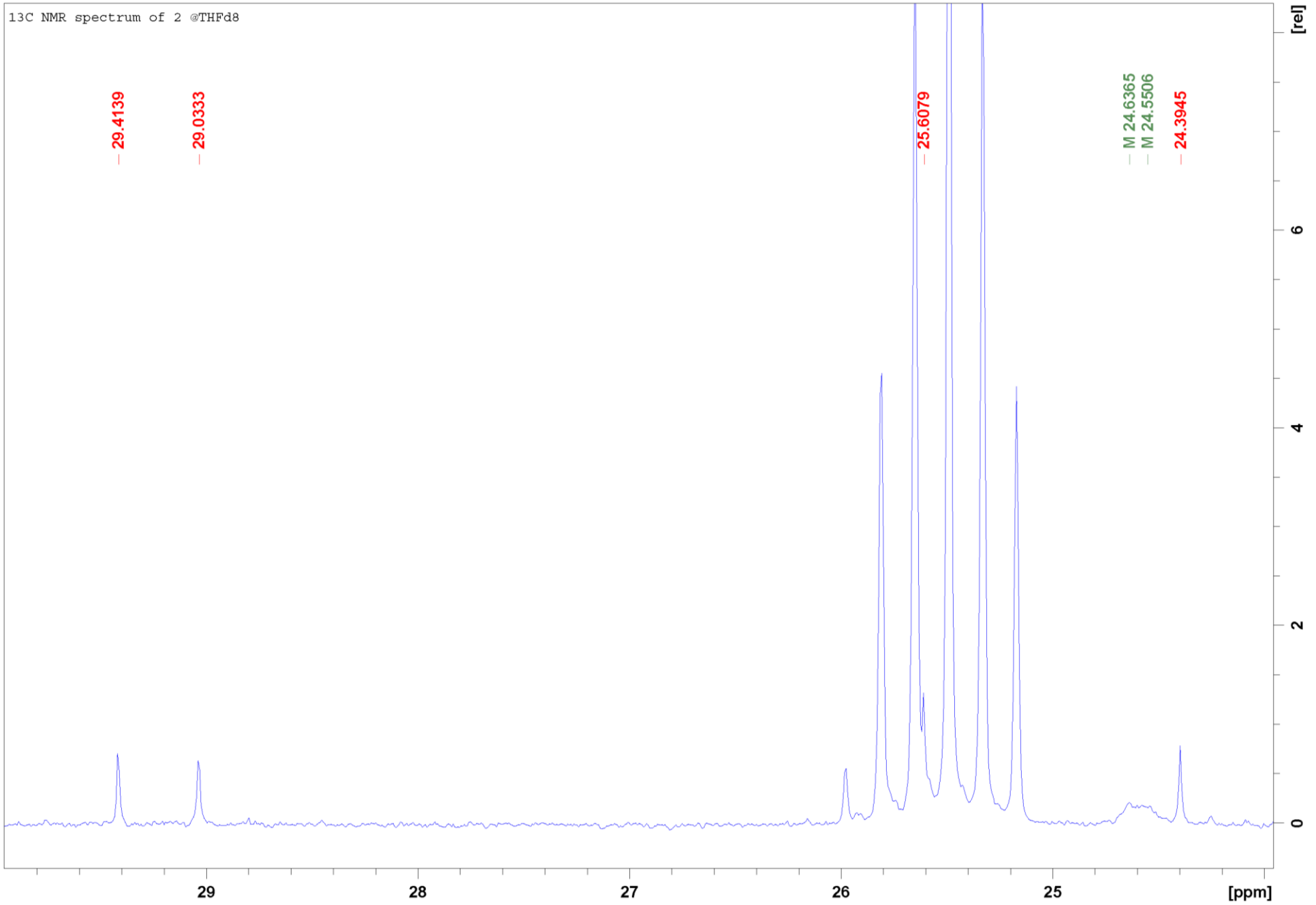

Figure S70. Detail of ^{13}C NMR spectrum of **2** in THF-d_8, 295 K.

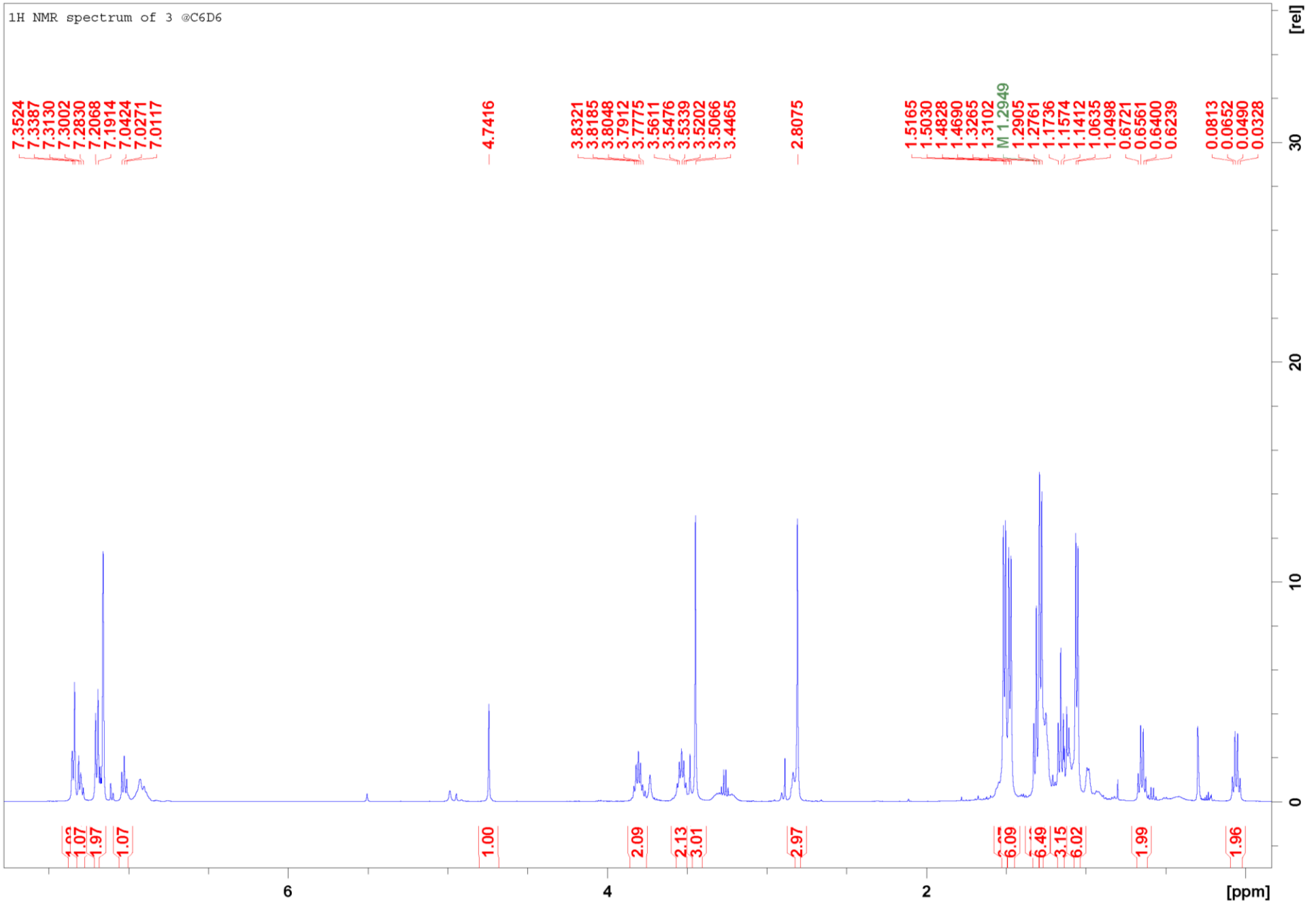

Figure S71. ^{1}H NMR spectrum of **3** in C_6D_6, 295 K.

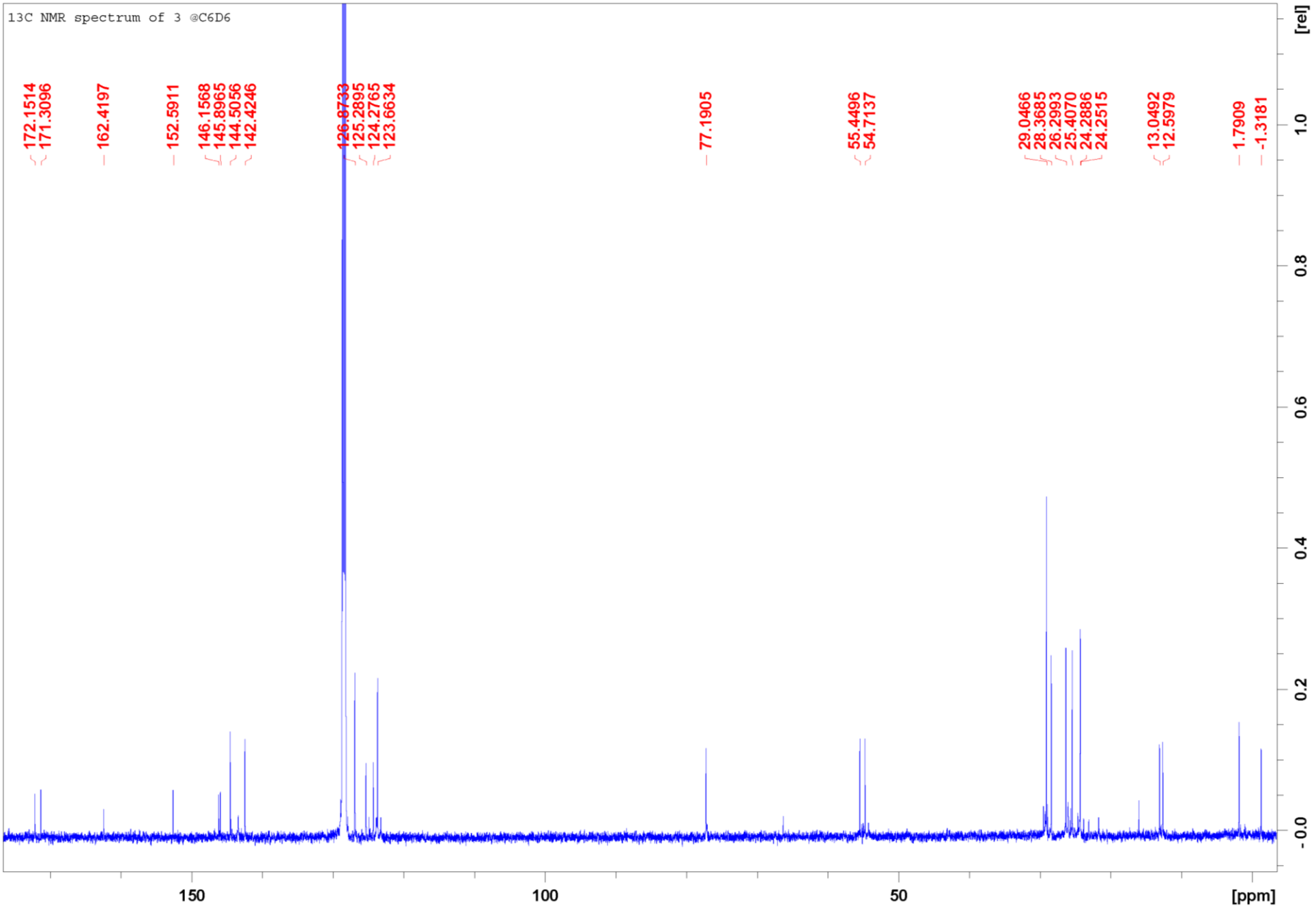

Figure S72. ^{13}C NMR spectrum of **3** in C_6D_6, 295 K.

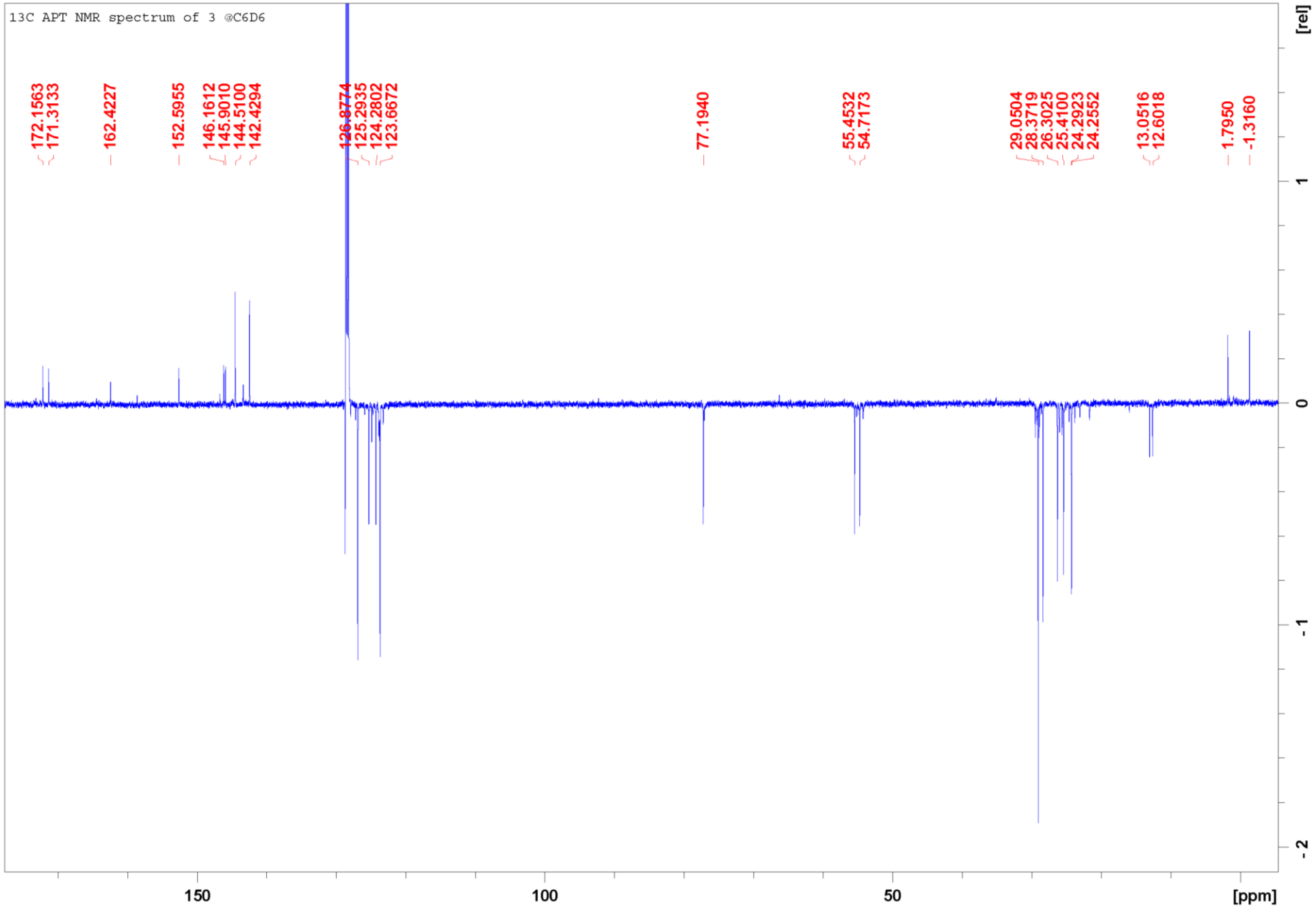

Figure S73. ^{13}C APT NMR spectrum of **3** in C_6D_6, 295 K.

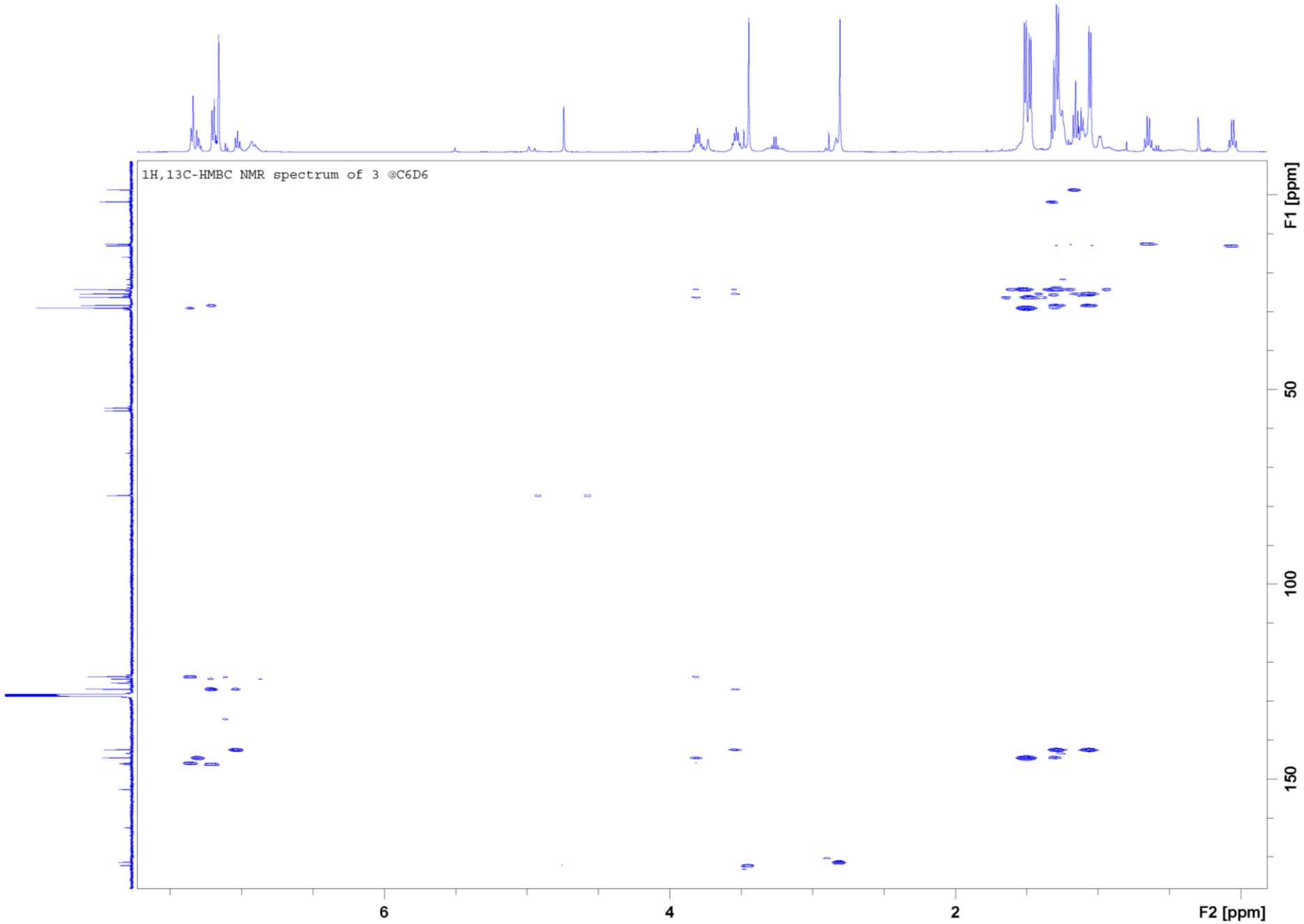

Figure S74. $^{1}H,^{13}C$-HMBC NMR spectrum of **3** in C_6D_6, 295 K.

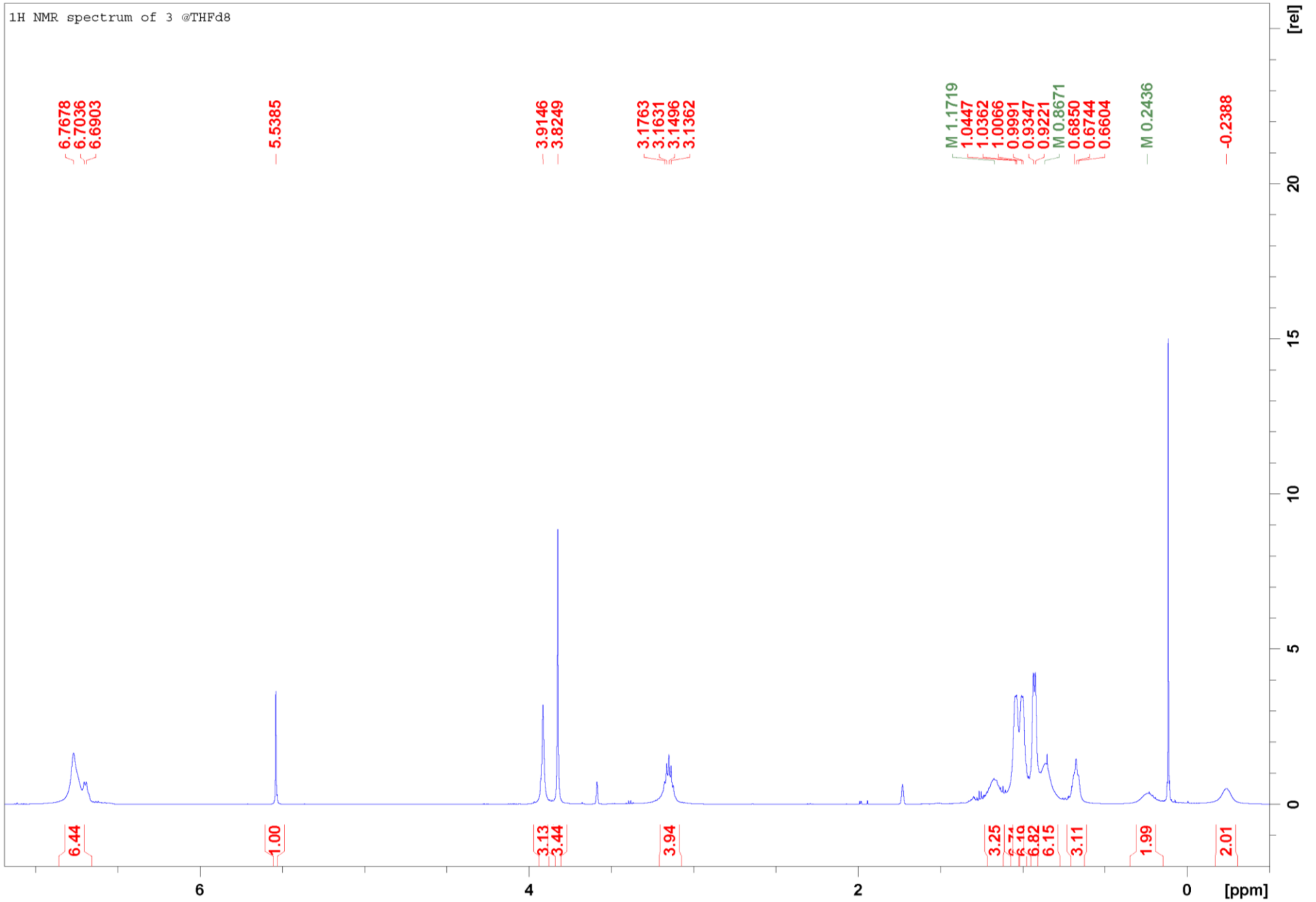

Figure S75. ^{1}H NMR spectrum of **3** in THF-d_8, 295 K.

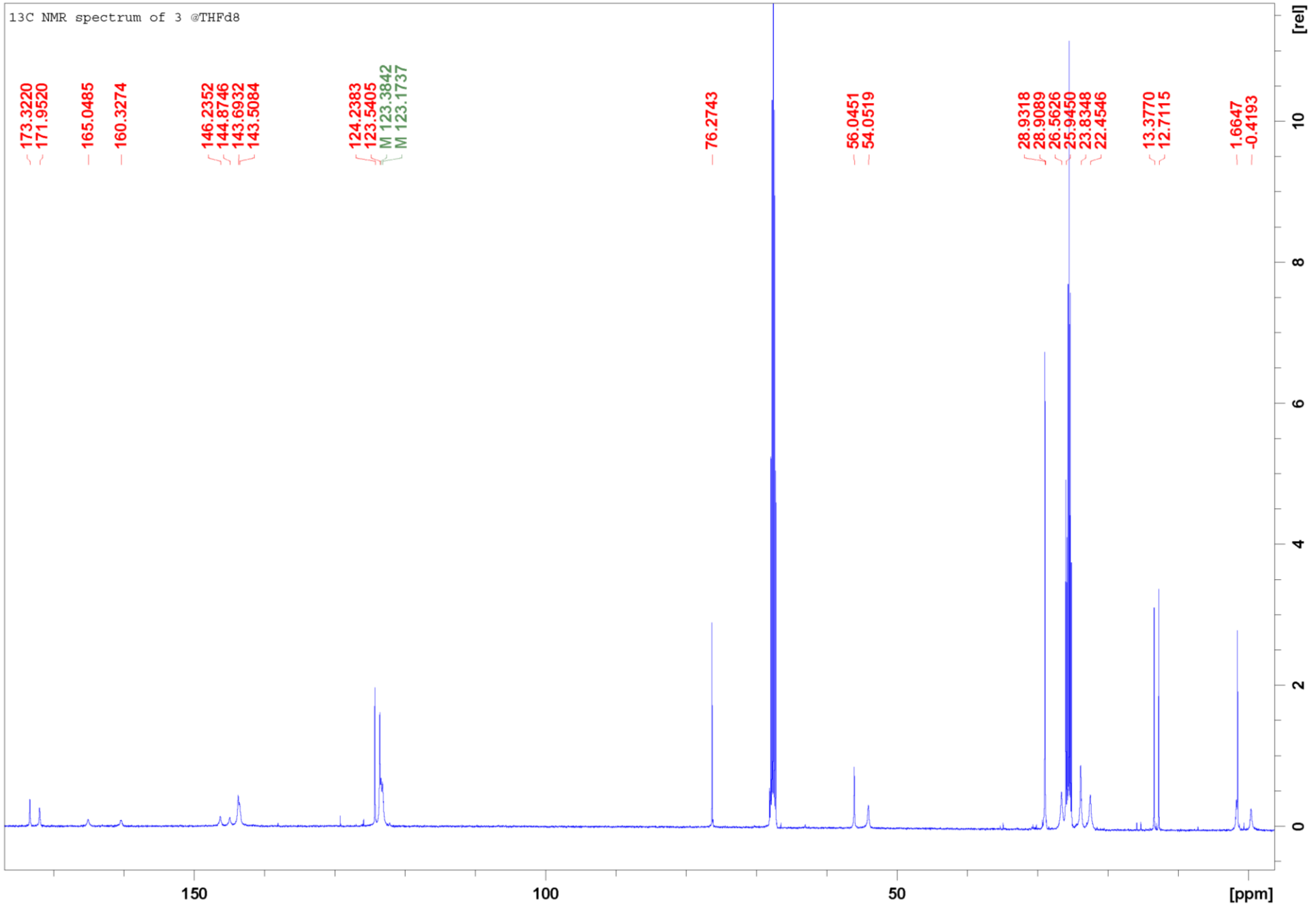

Figure S76. ^{13}C NMR spectrum of **3** in THF-d_8, 295 K.

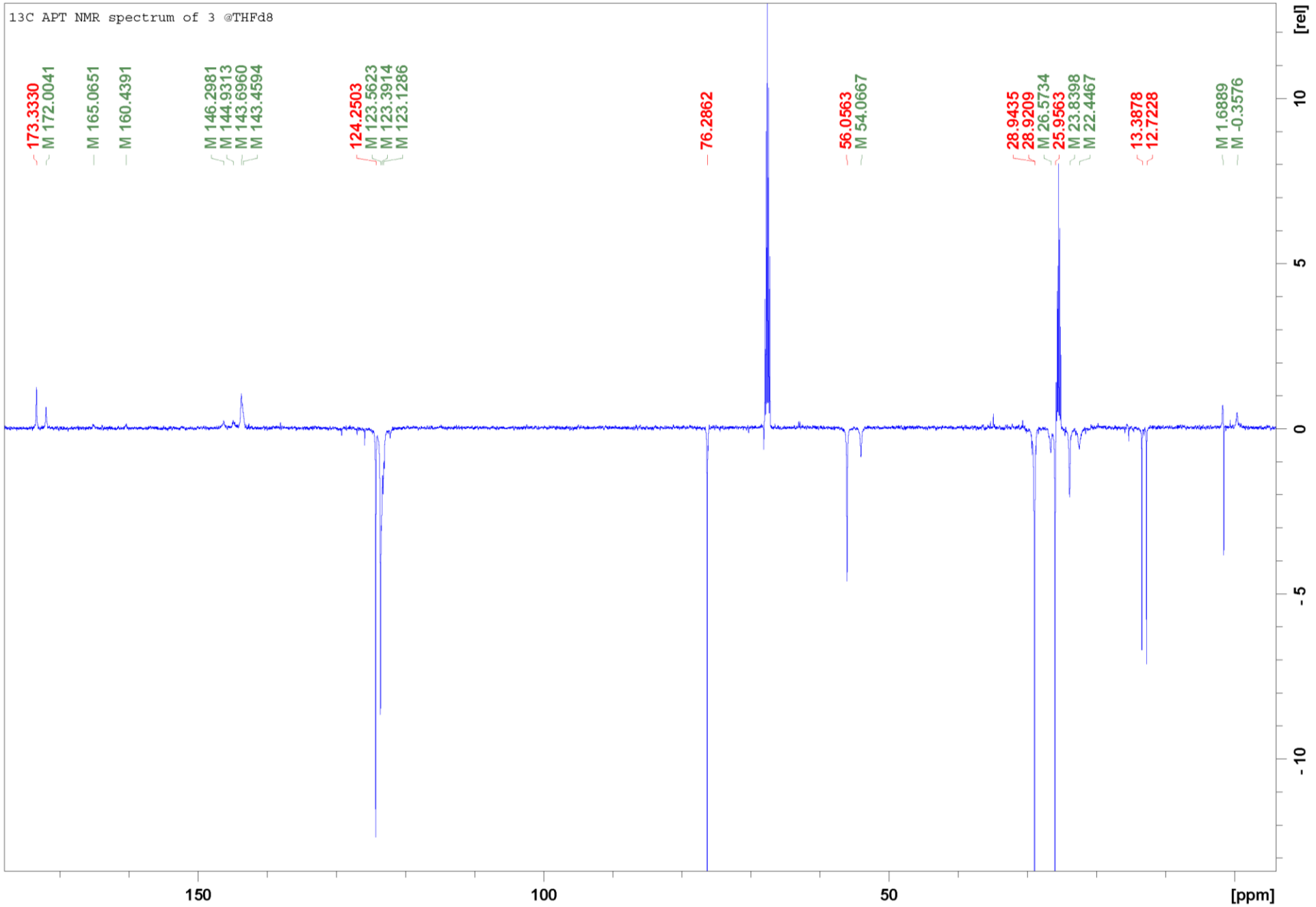

Figure S77. ^{13}C APT NMR spectrum of **3** in THF-d_8, 295 K.

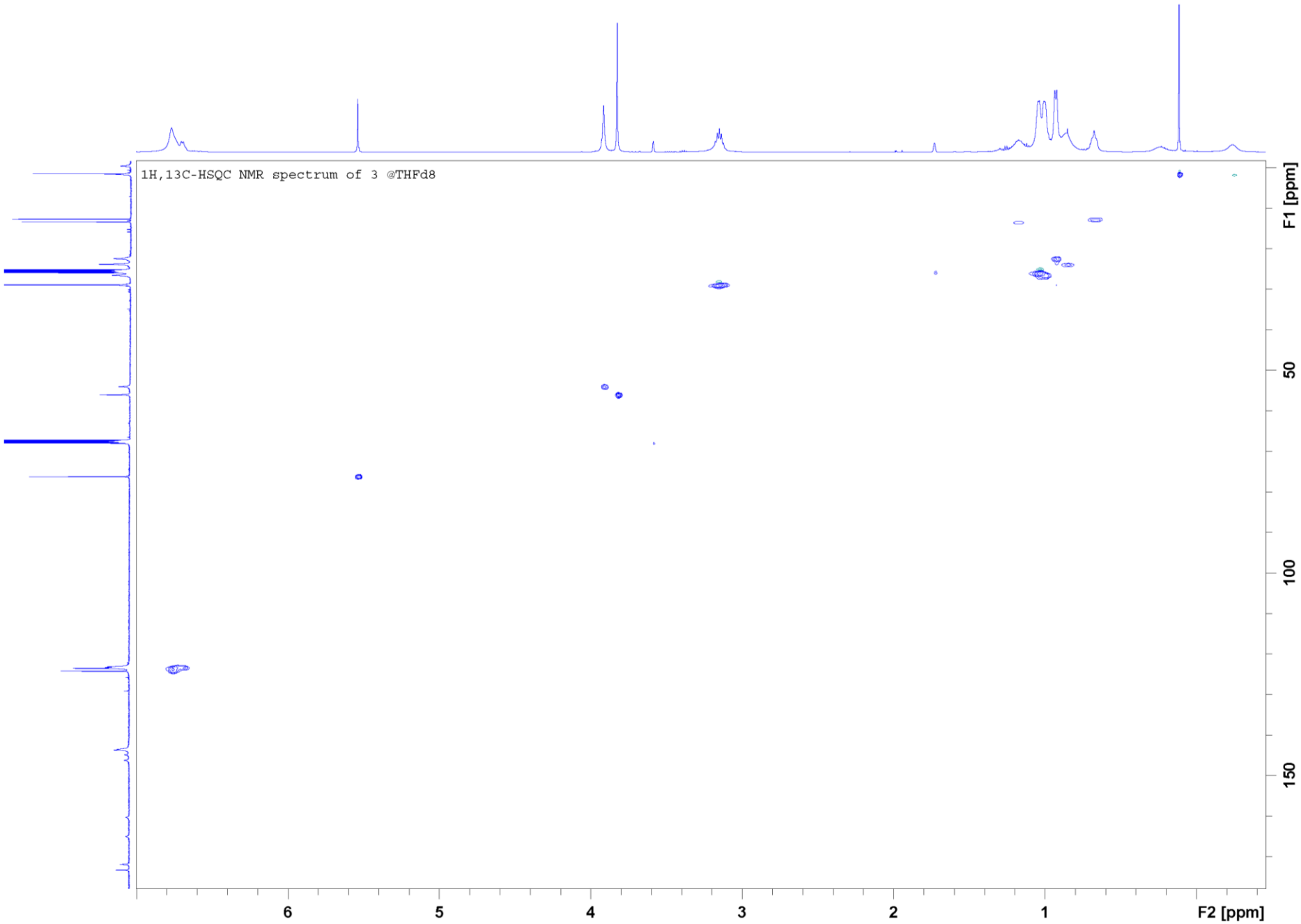

Figure S78. $^{1}H,^{13}C$-HSQC NMR spectrum of **3** in THF-d_8, 295 K.

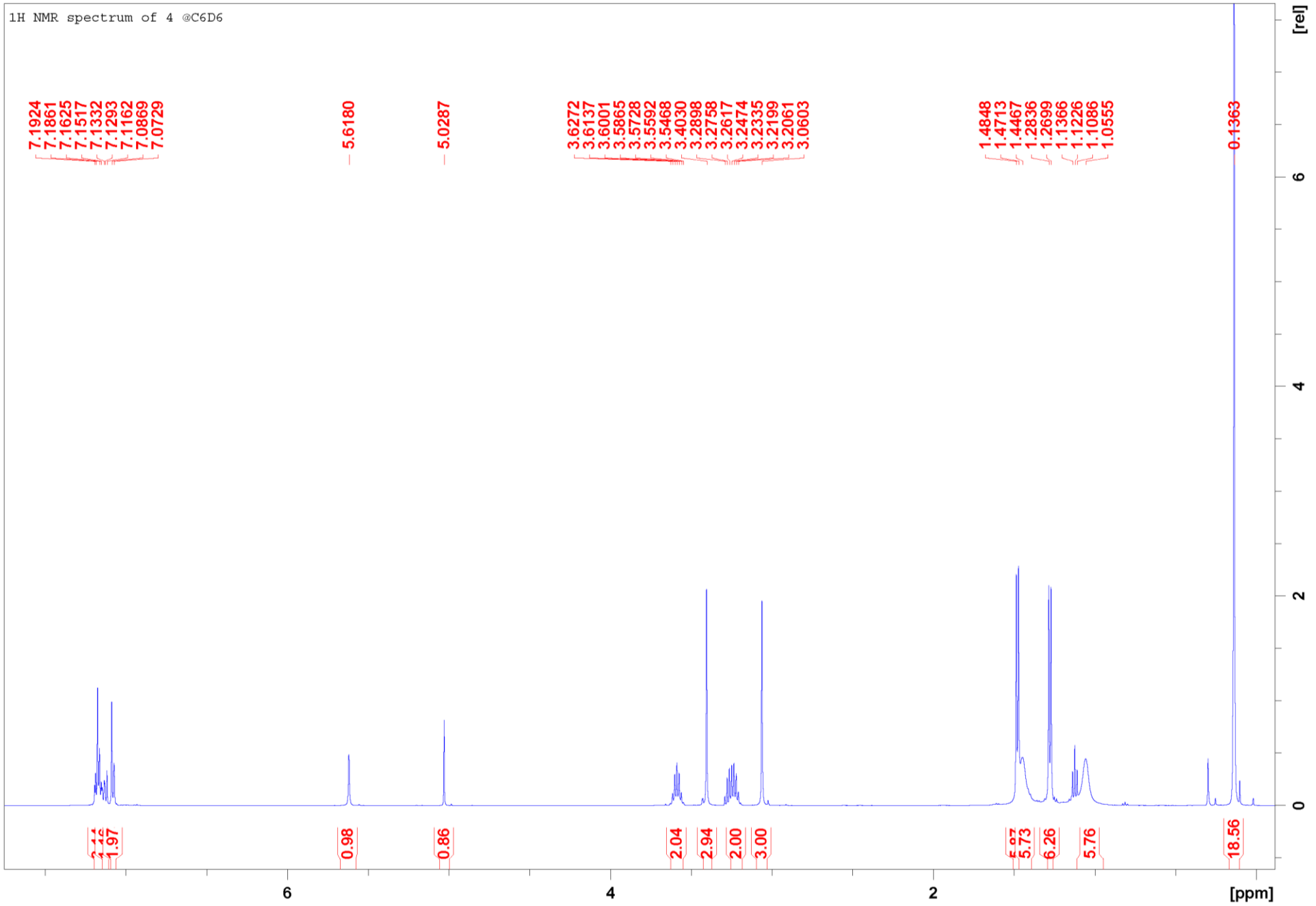

Figure S79. ^{1}H NMR spectrum of **4** in C_6D_6, 295 K.

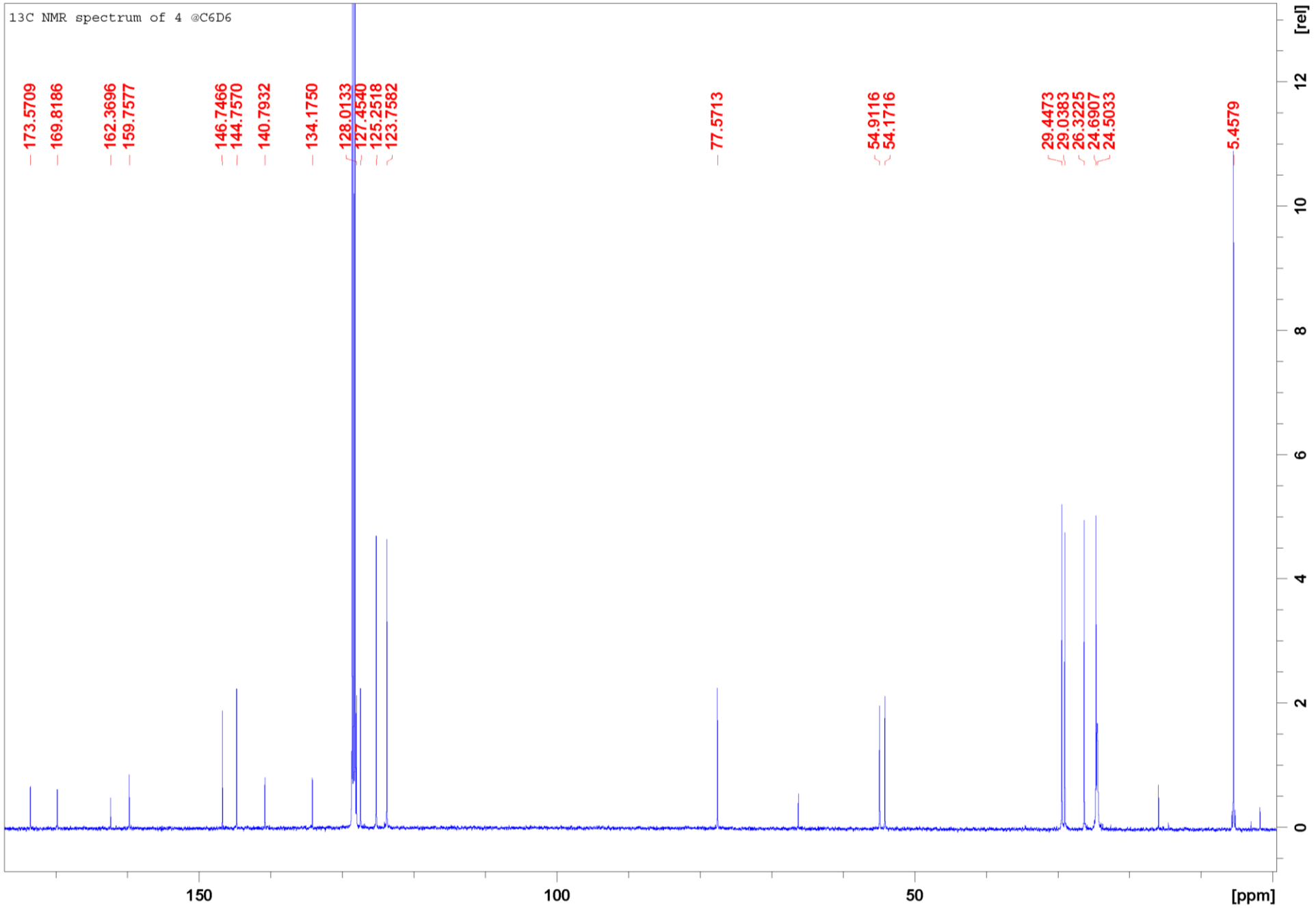

Figure S80. ^{13}C NMR spectrum of **4** in C_6D_6, 295 K.

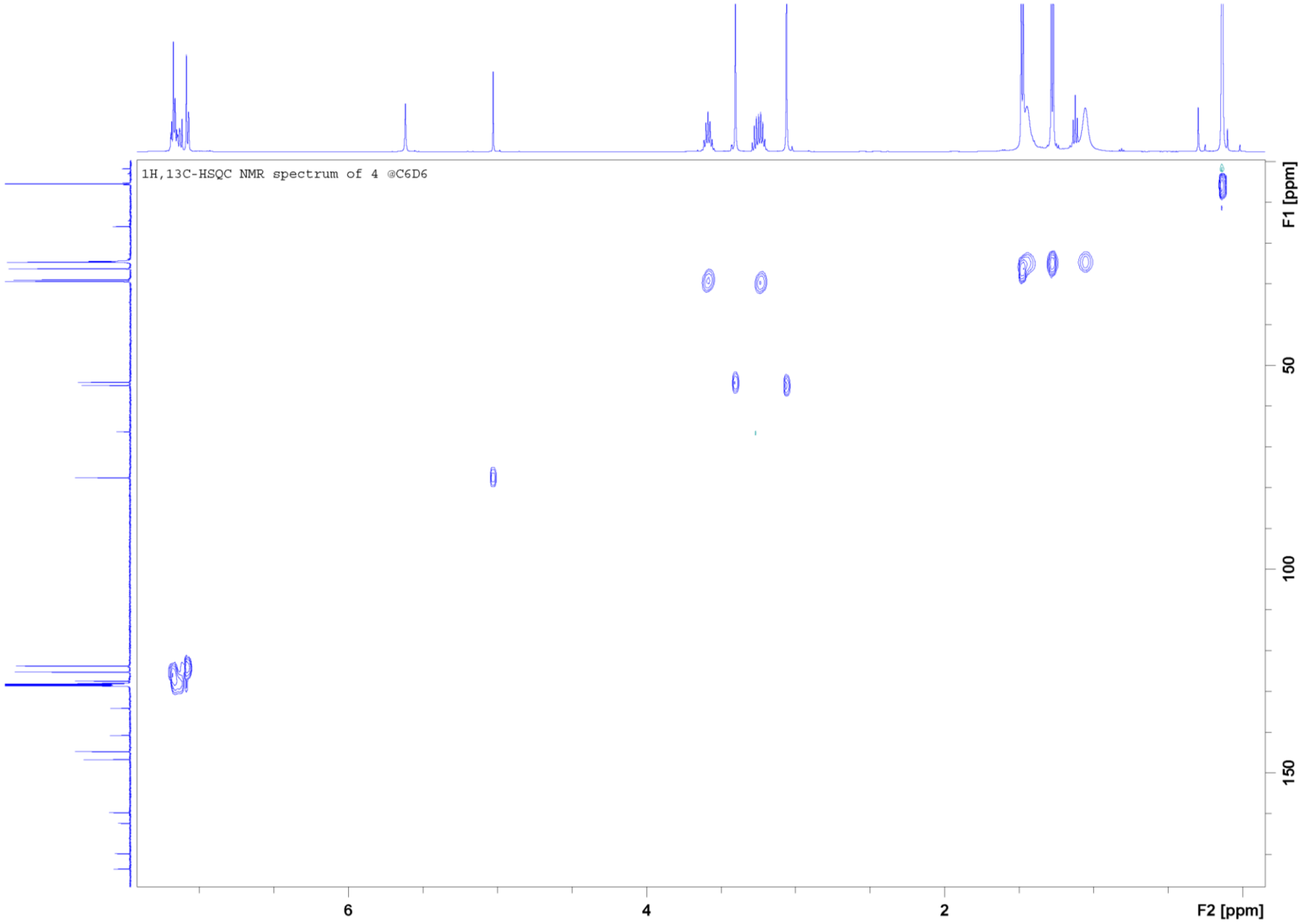

Figure S81. $^{1}H,^{13}C$-HSQC NMR spectrum of **4** in C_6D_6, 295 K.

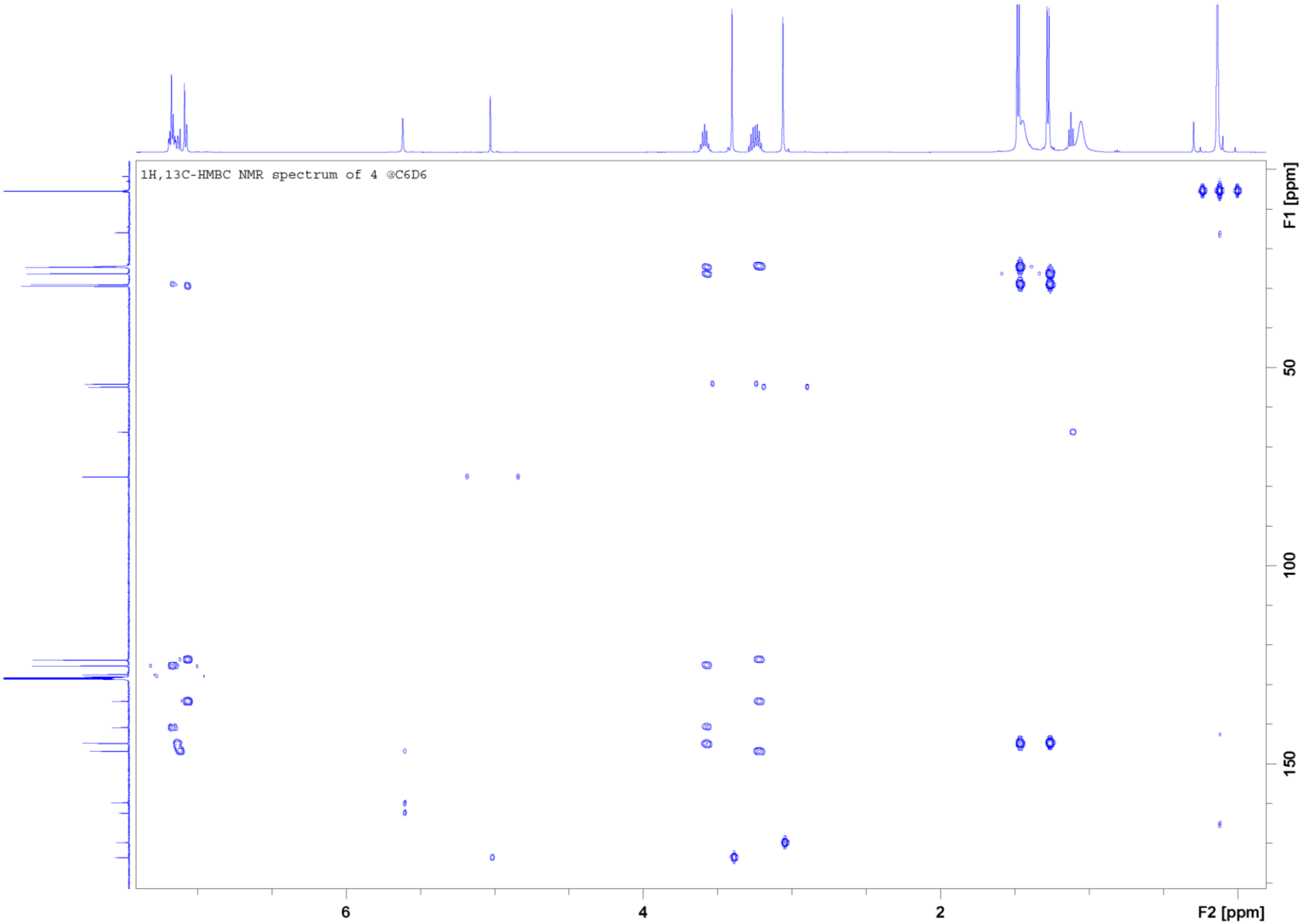

Figure S82. $^{1}H,^{13}C$-HMBC NMR spectrum of **4** in C_6D_6, 295 K.

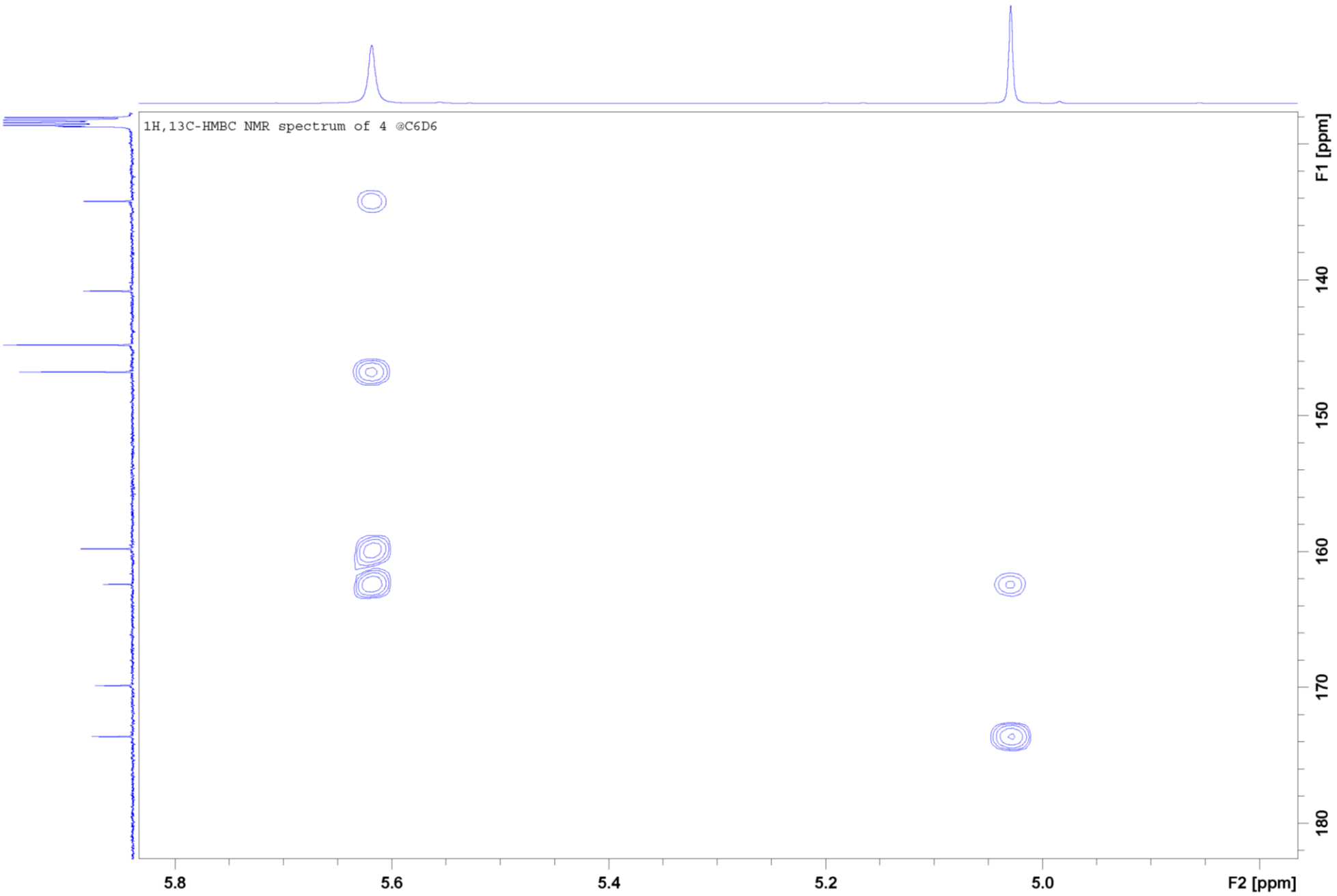

Figure S83. Detail of $^{1}H,^{13}C$-HMBC NMR spectrum of **4** in C_6D_6, 295 K.

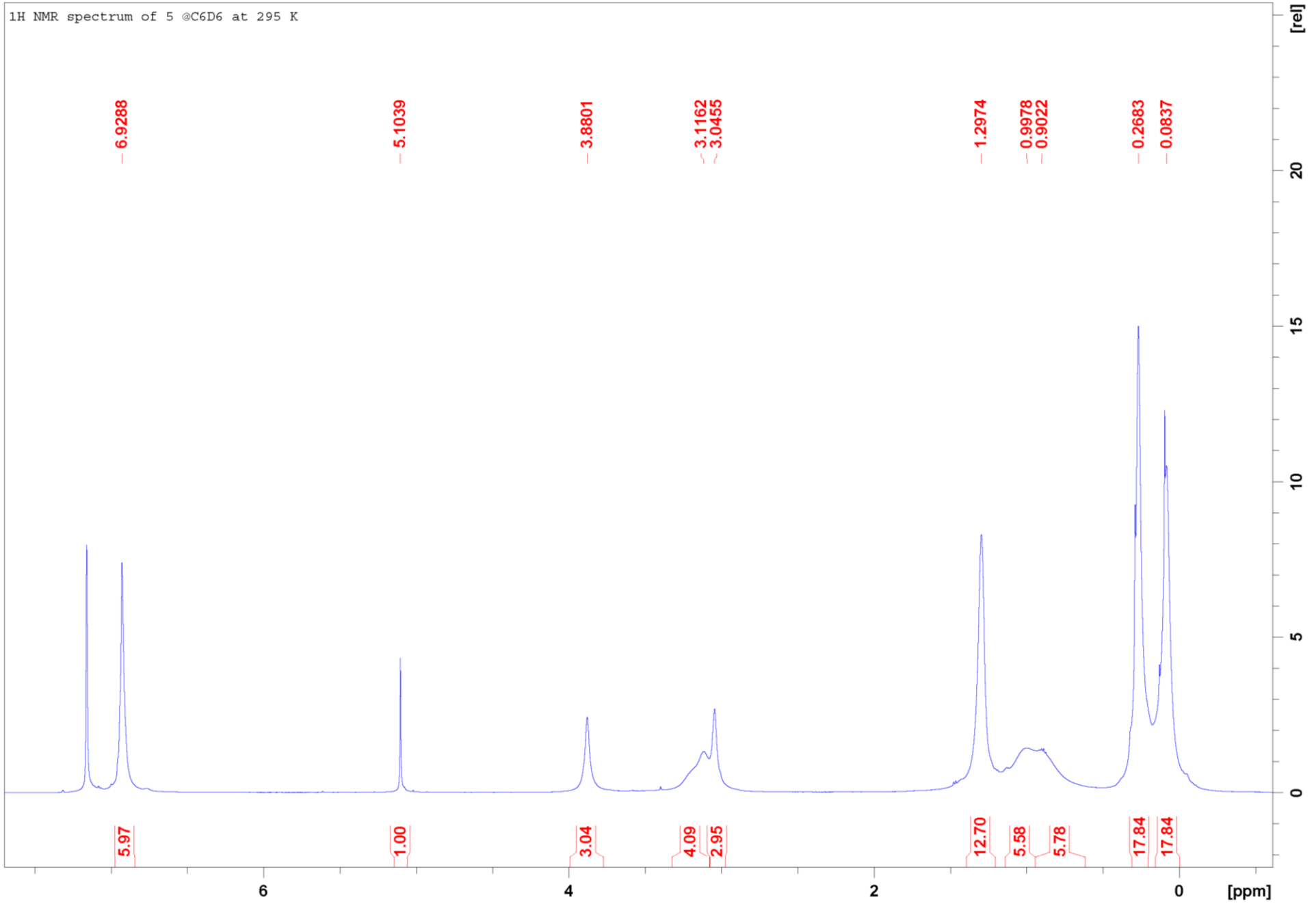

Figure S84. ^{1}H NMR spectrum of **5** in C_6D_6, 295 K.

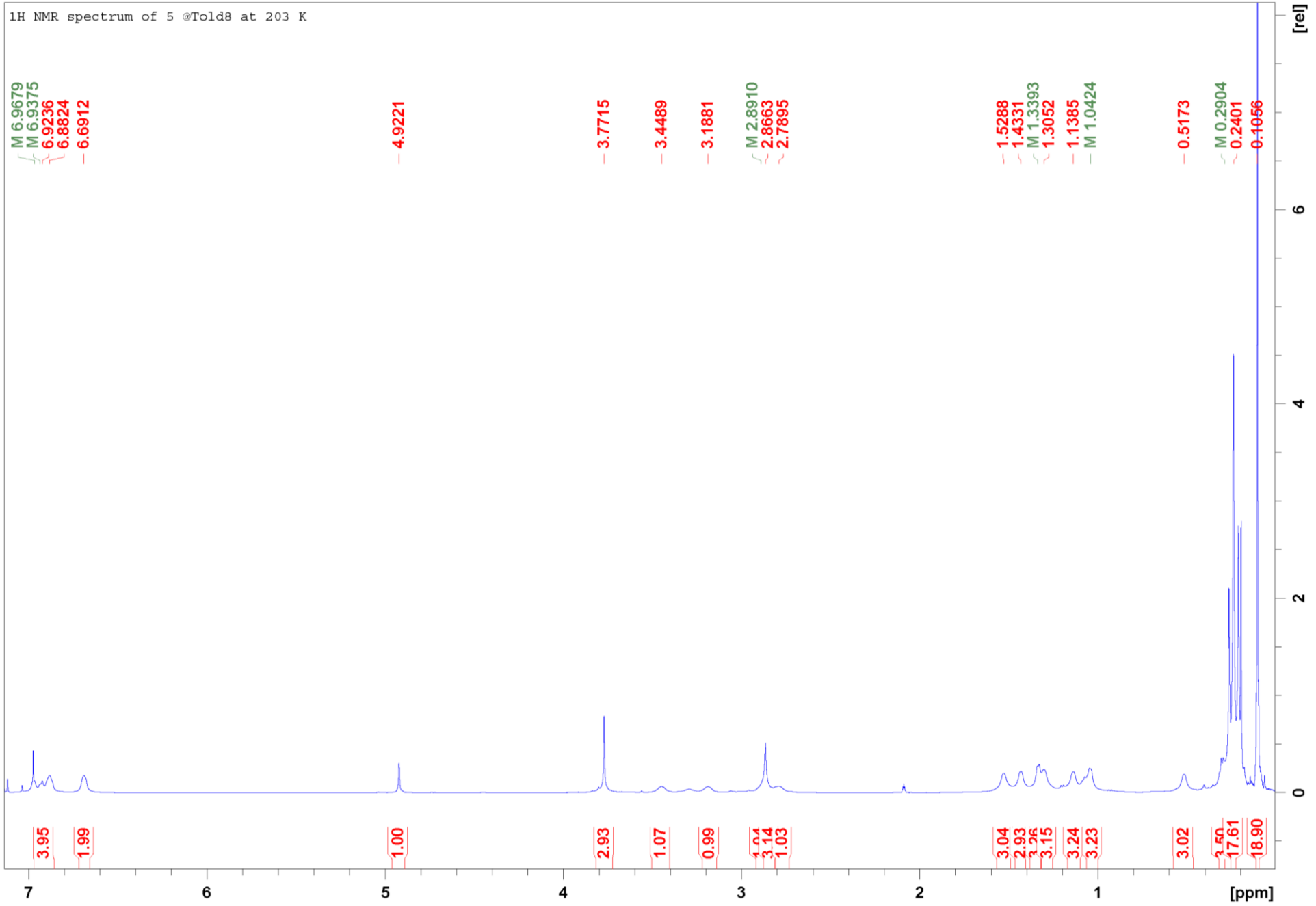

Figure S85. ^{1}H NMR spectrum of **5** in Tol-d_8, 203 K.

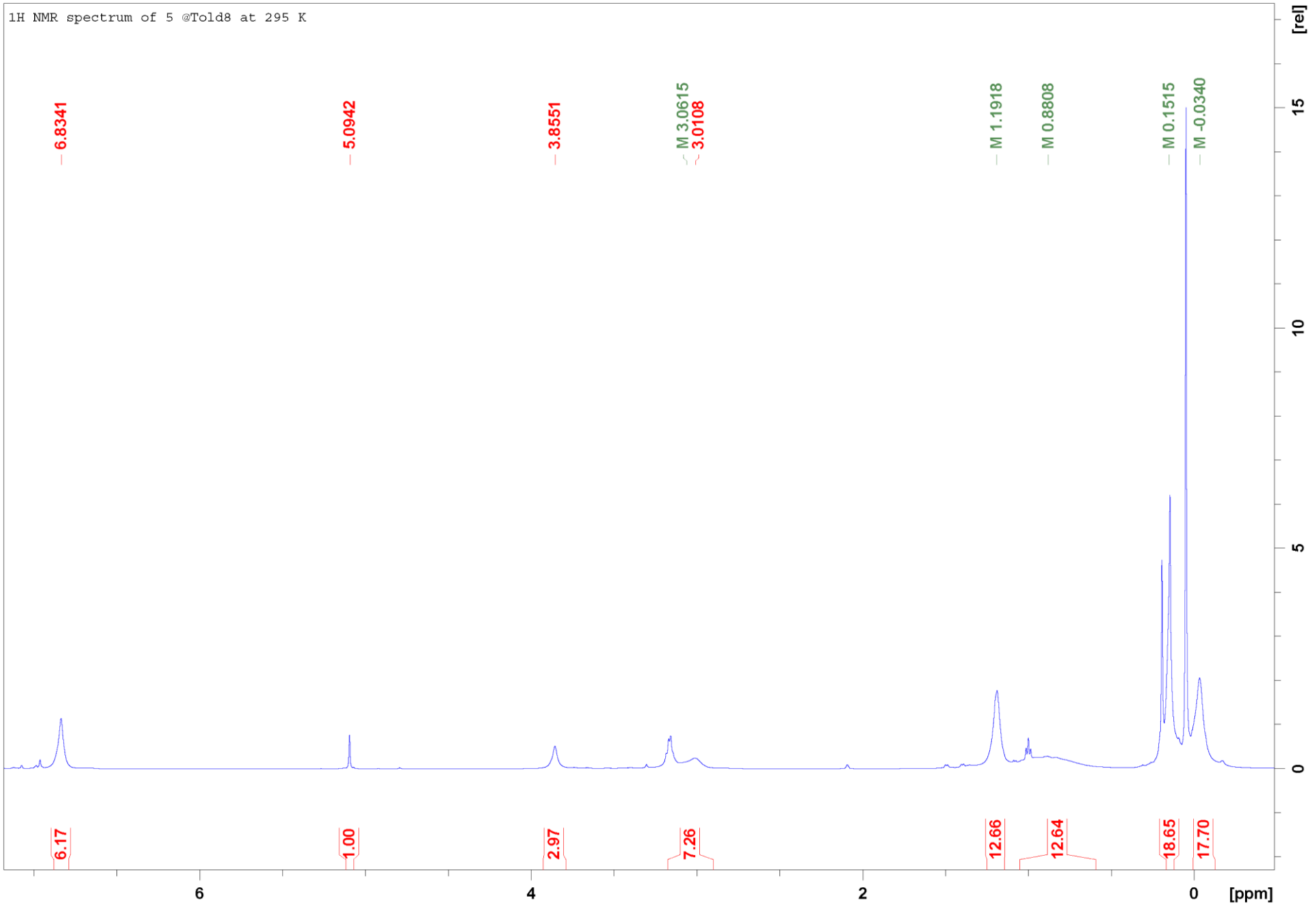

Figure S86. ^{1}H NMR spectrum of **5** in Tol-d_8, 295 K.

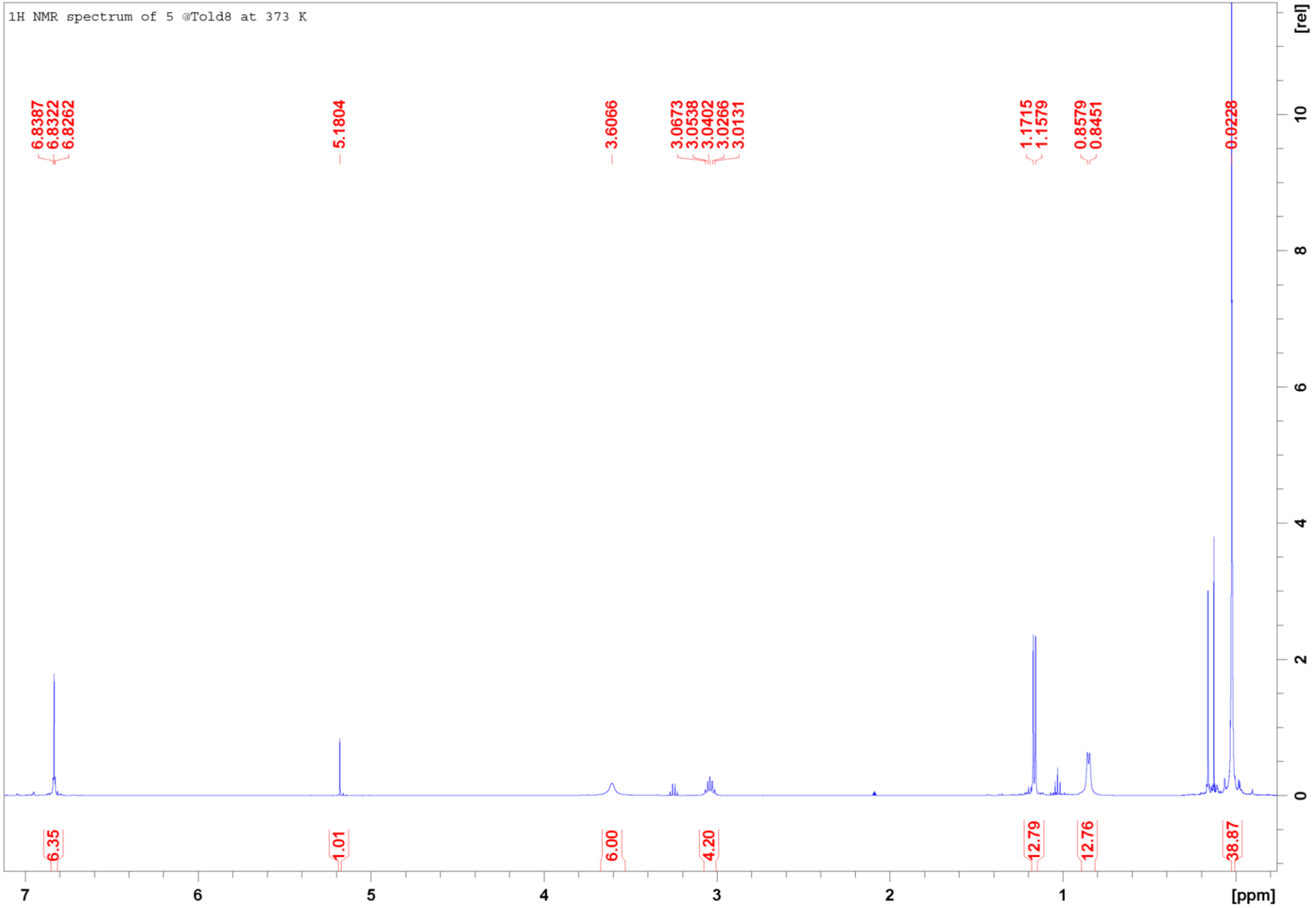

Figure S87. ^{1}H NMR spectrum of **5** in Tol-d_8, 373 K.

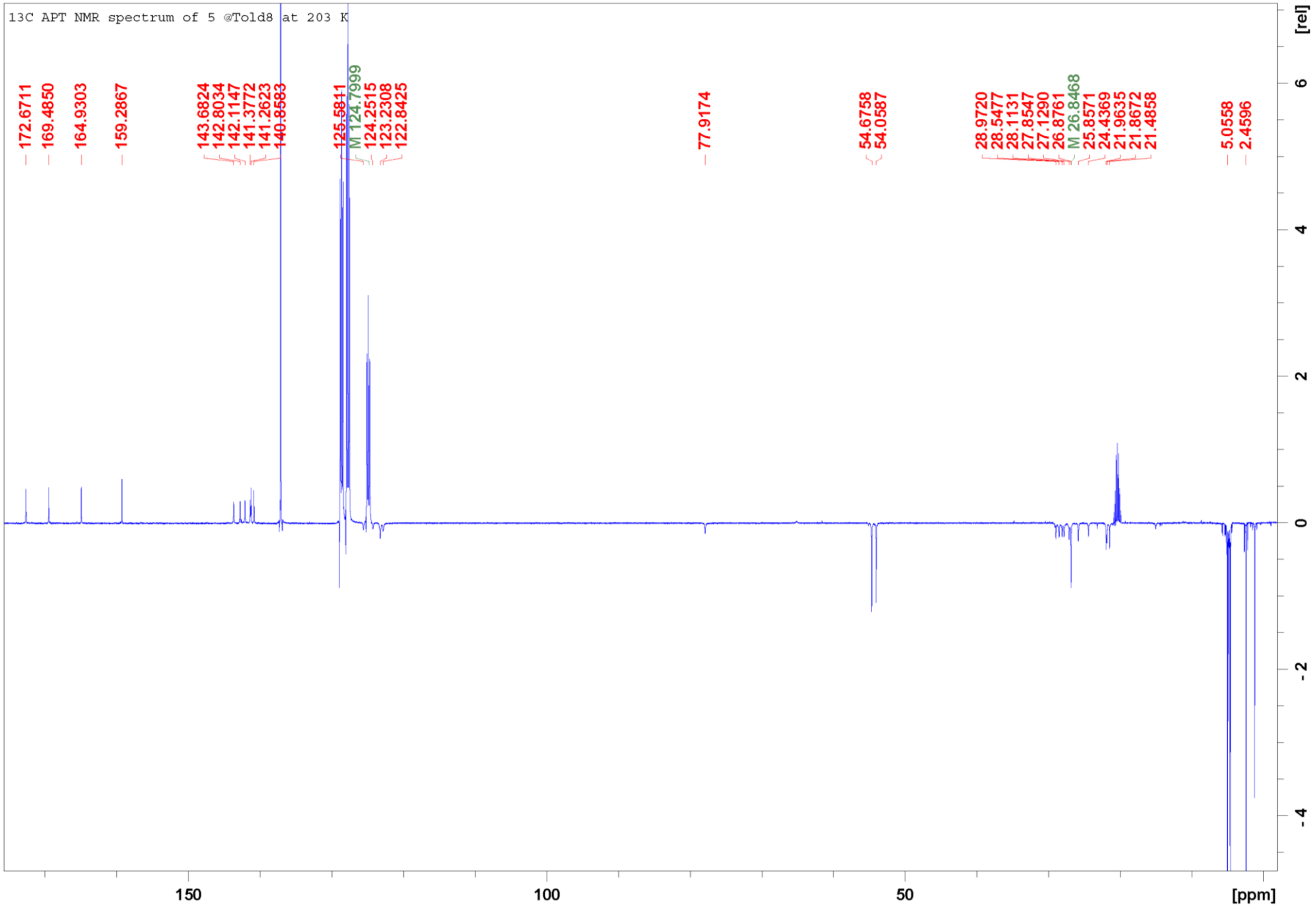

Figure S88. ^{13}C APT NMR spectrum of **5** in Tol-d_8, 203 K.

Figure S89. Detail of ^{13}C APT NMR spectrum of **5** in Tol-d_8, 203 K.

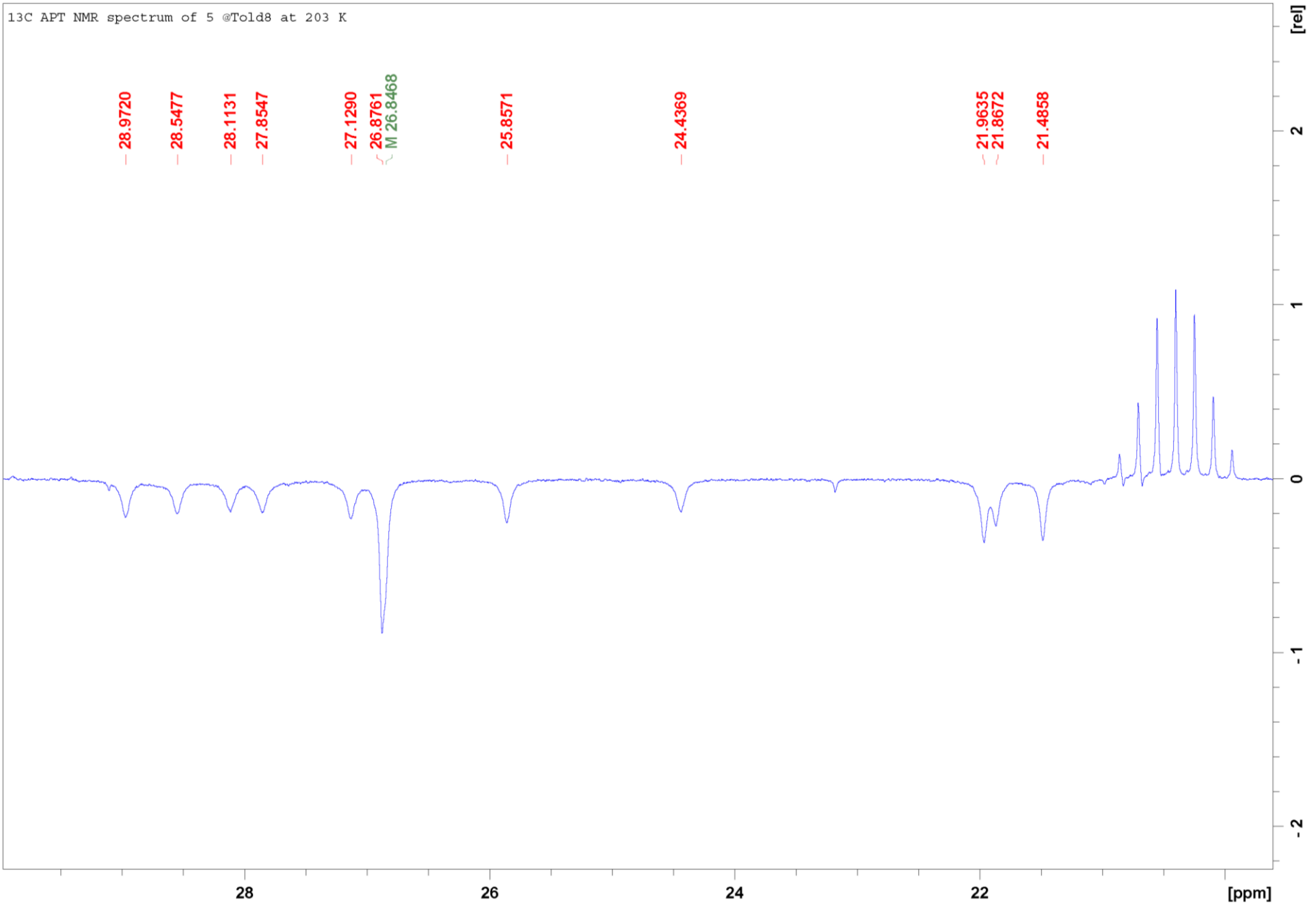

Figure S90. Detail of ^{13}C APT NMR spectrum of **5** in Tol-d_8, 203 K.

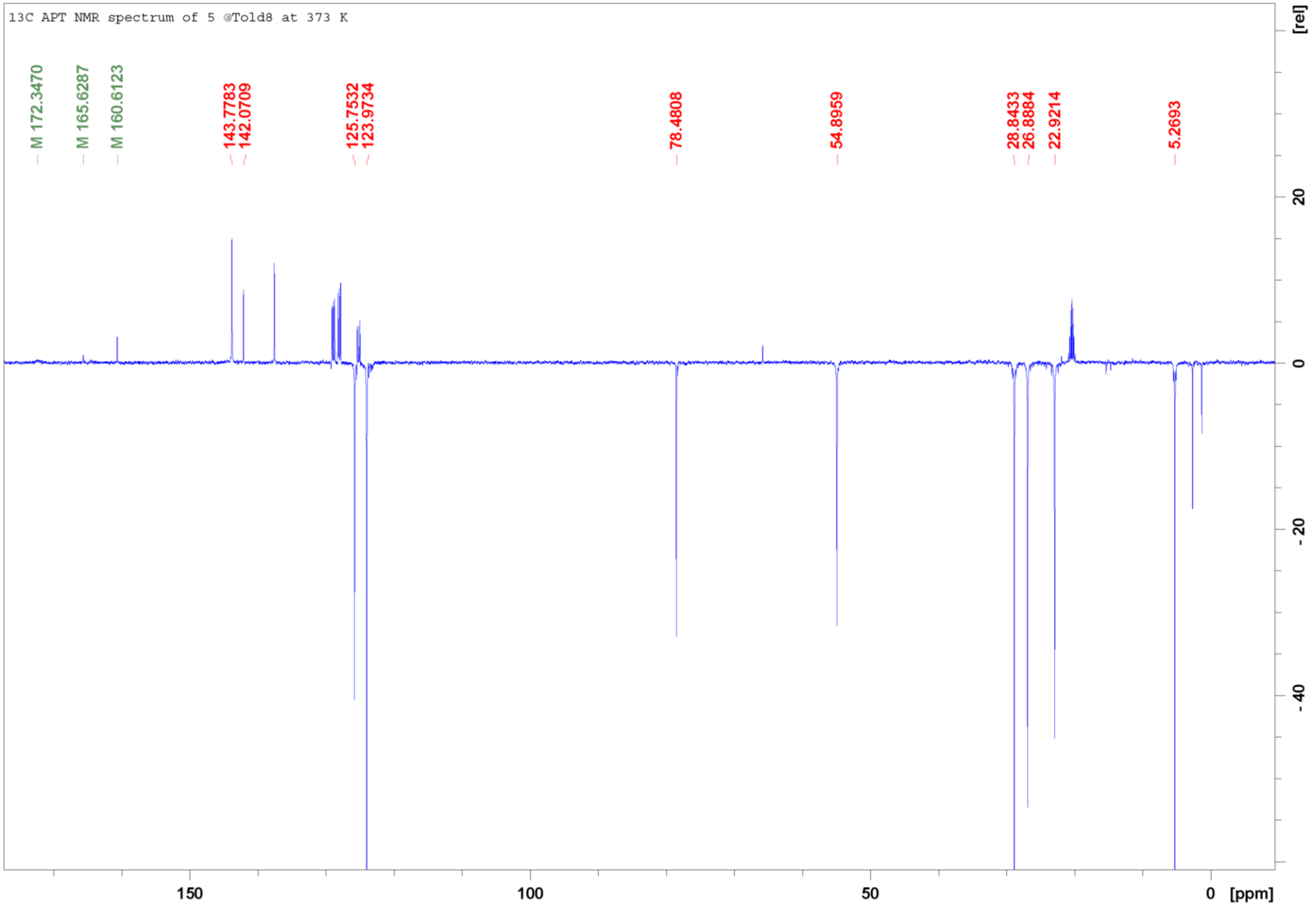

Figure S91. ^{13}C APT NMR spectrum of **5** in Tol-d_8, 373 K.

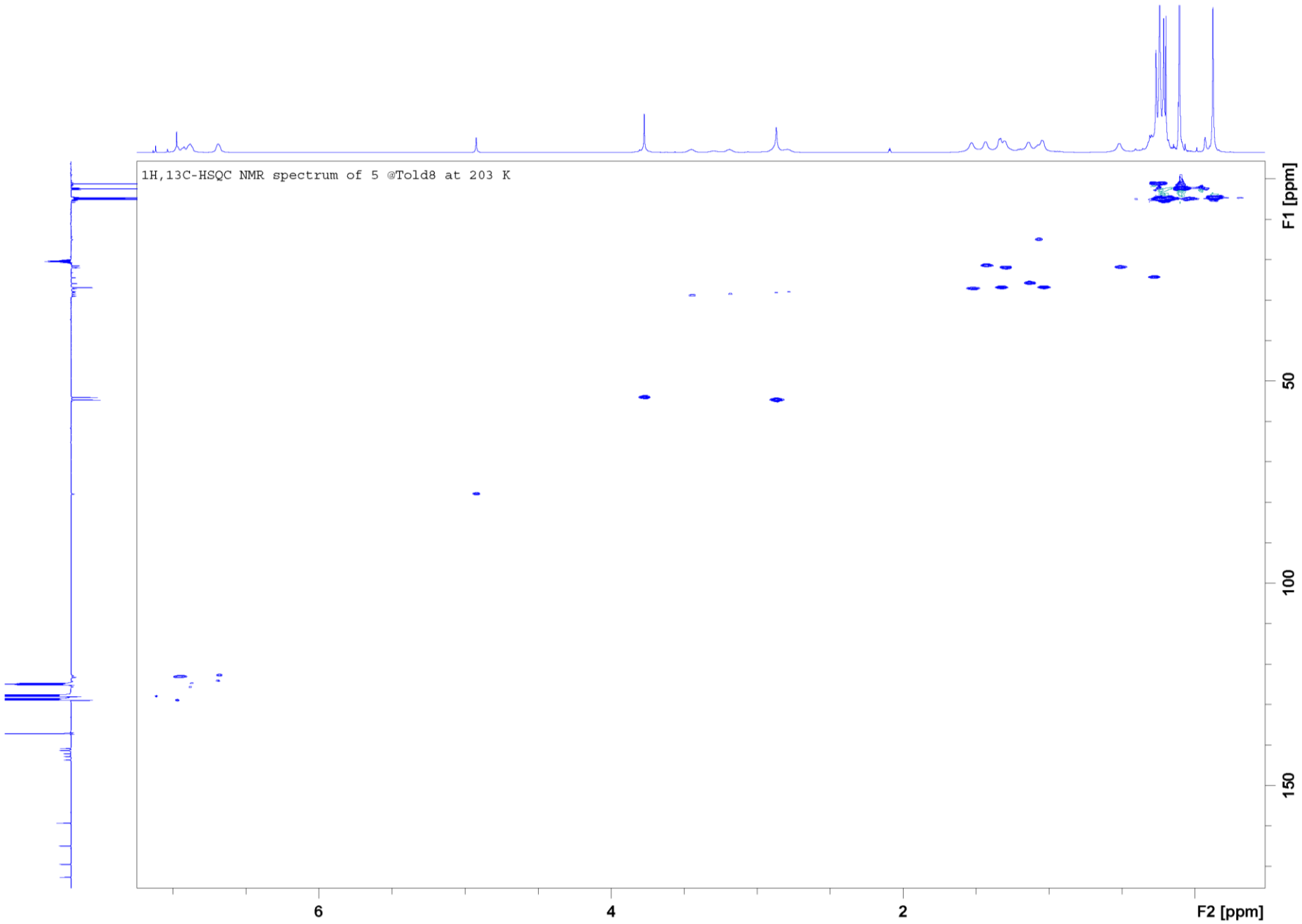

Figure S92. $^{1}H,^{13}C$-HSQC NMR spectrum of **5** in Tol-d_8, 203 K.

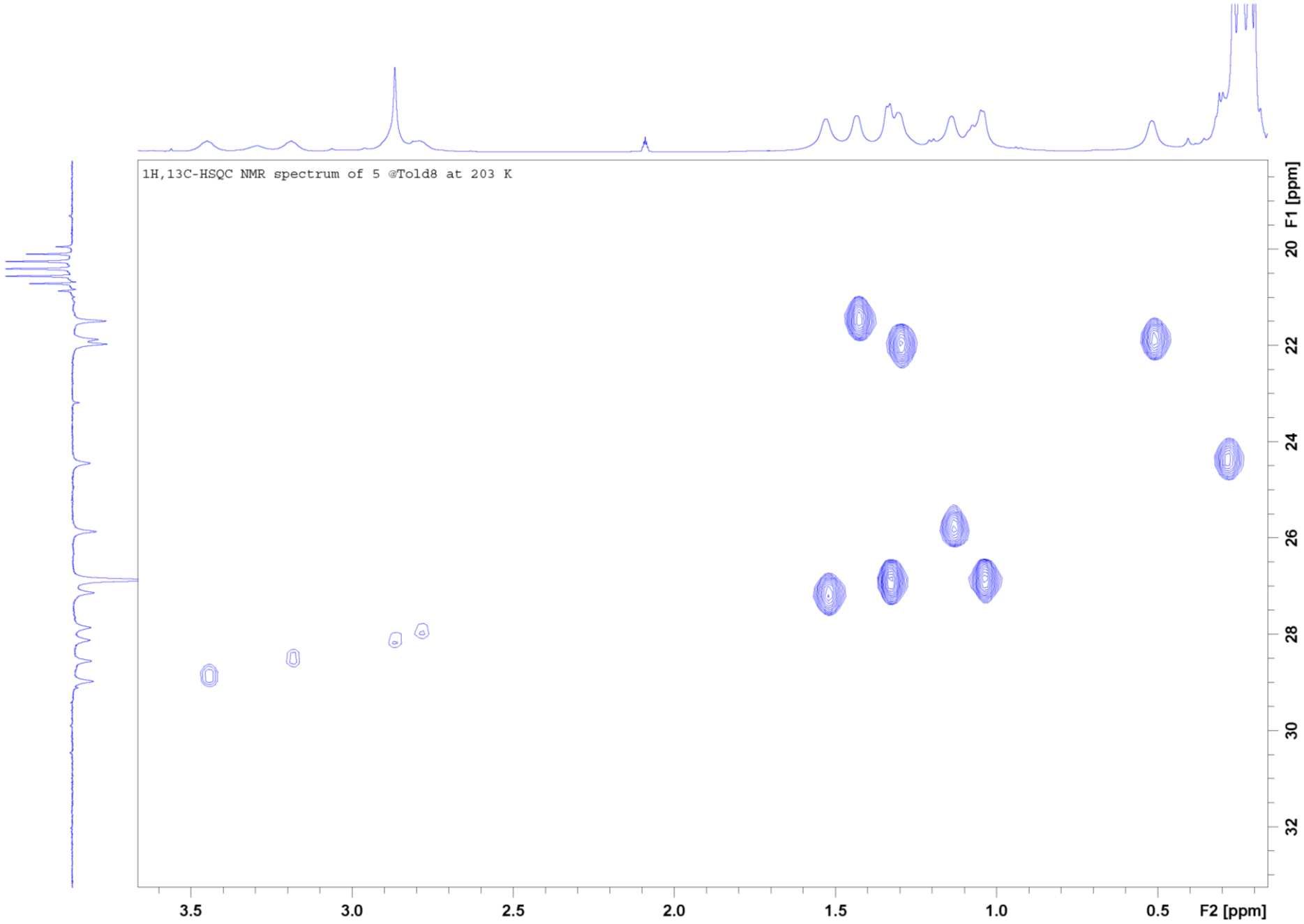

Figure S93. Detail of $^{1}H,^{13}C$-HSQC NMR spectrum of **5** in Tol-d_8, 203 K.

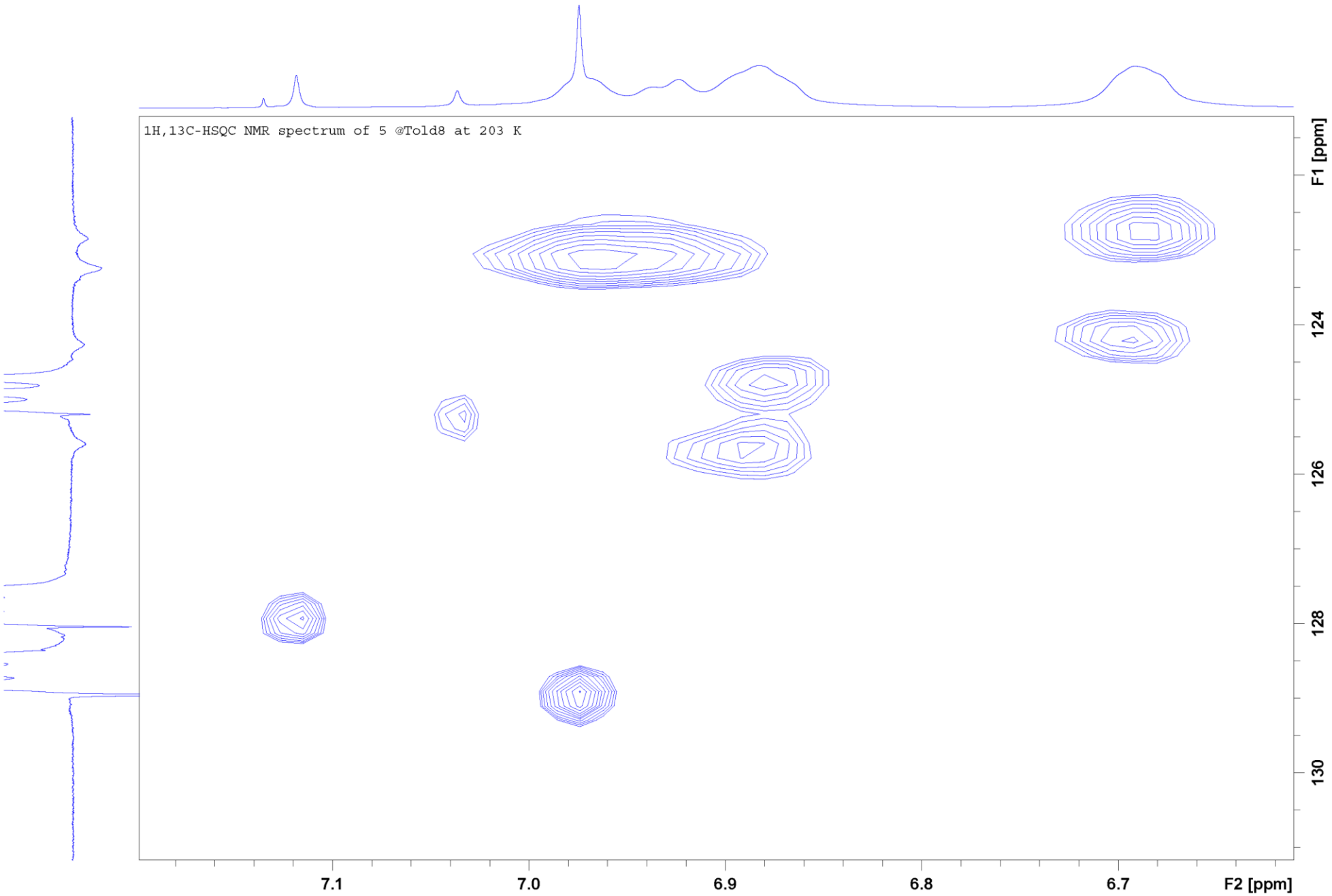

Figure S94. Detail of $^{1}H,^{13}C$-HSQC NMR spectrum of **5** in Tol-d_8, 203 K.

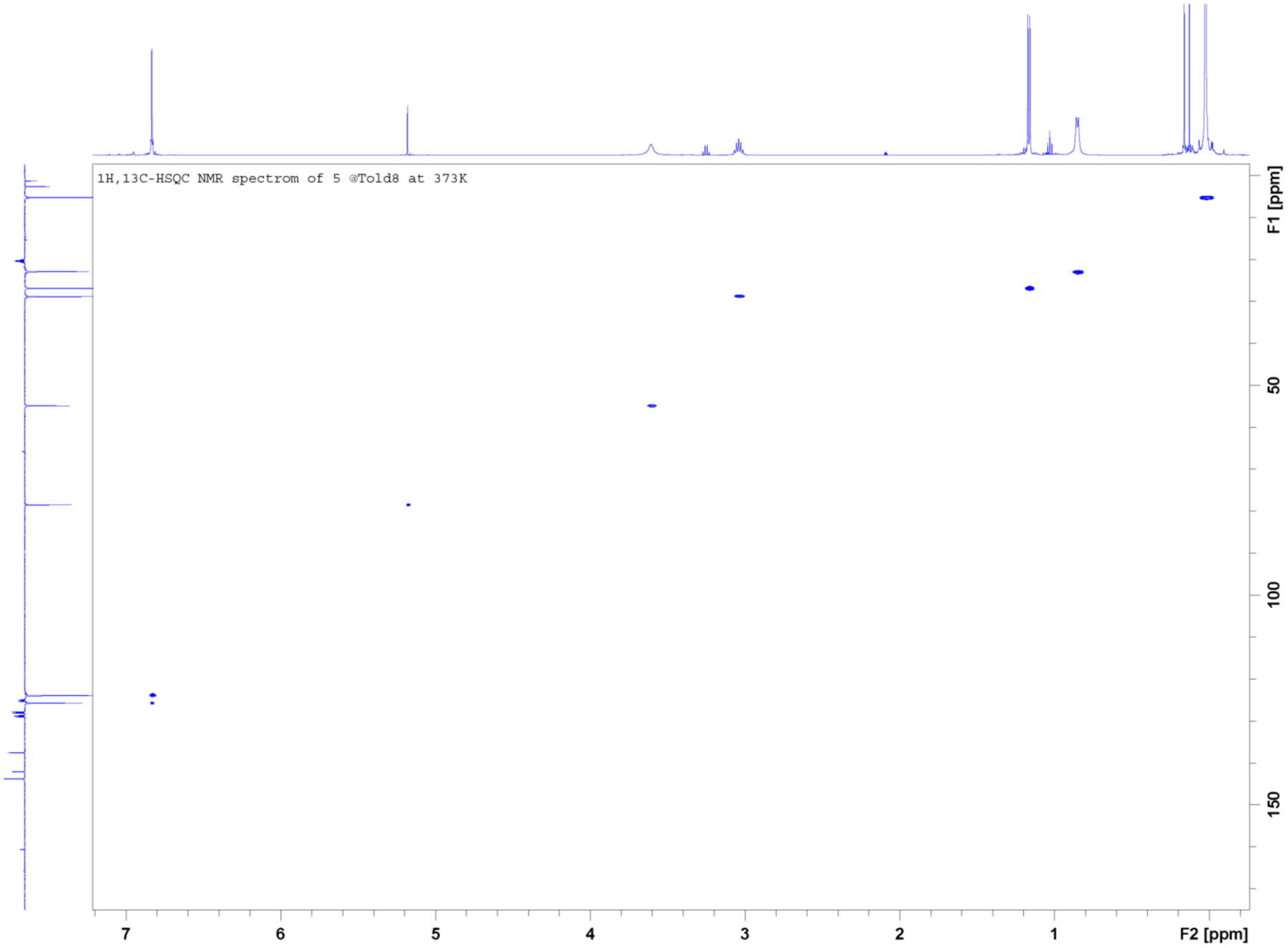

Figure S95. $^{1}H,^{13}C$-HSQC NMR spectrum of **5** in Tol-d_8, 373 K.

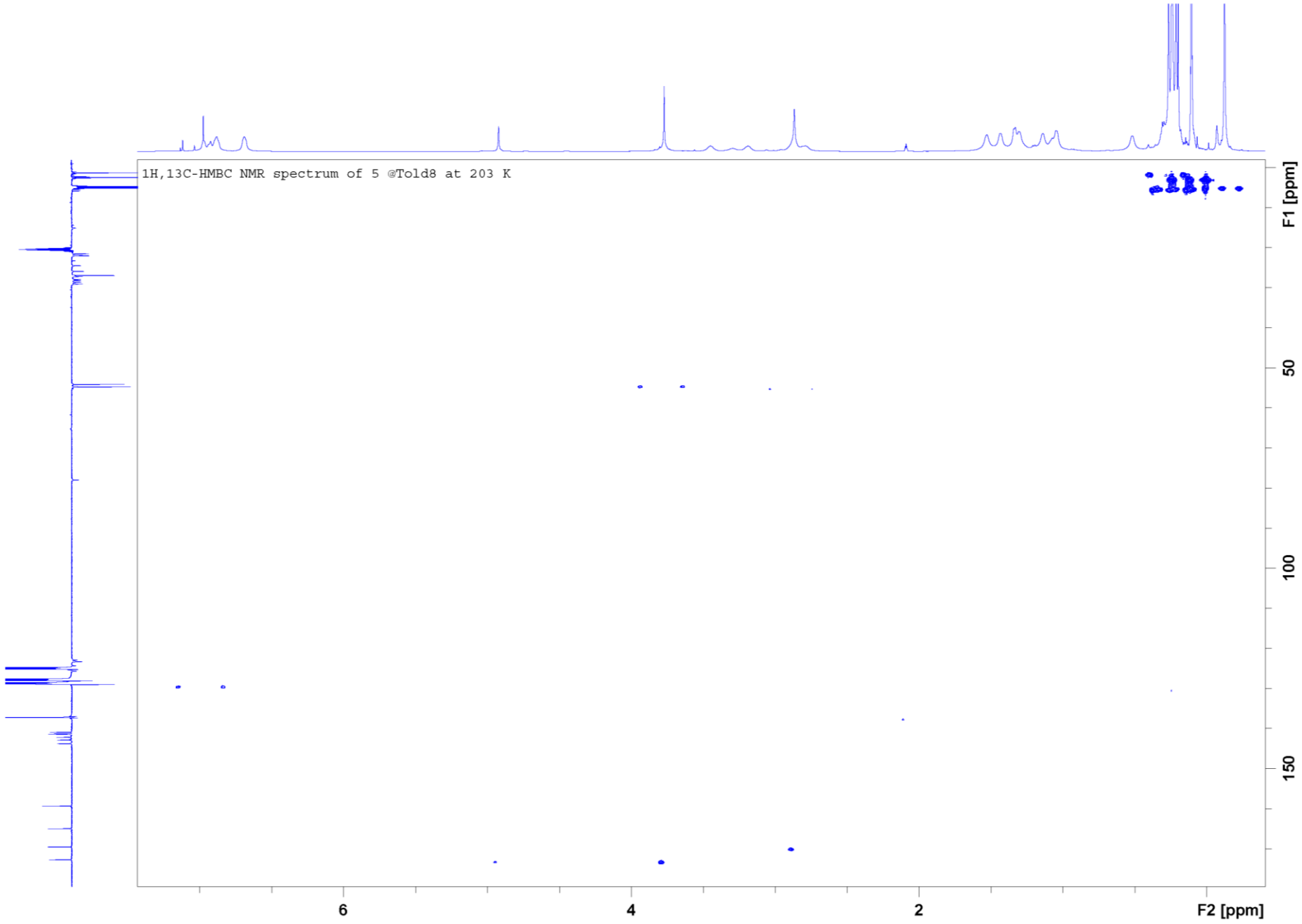

Figure S96. $^{1}H,^{13}C$-HMBC NMR spectrum of **5** in Tol-d_8, 203 K.

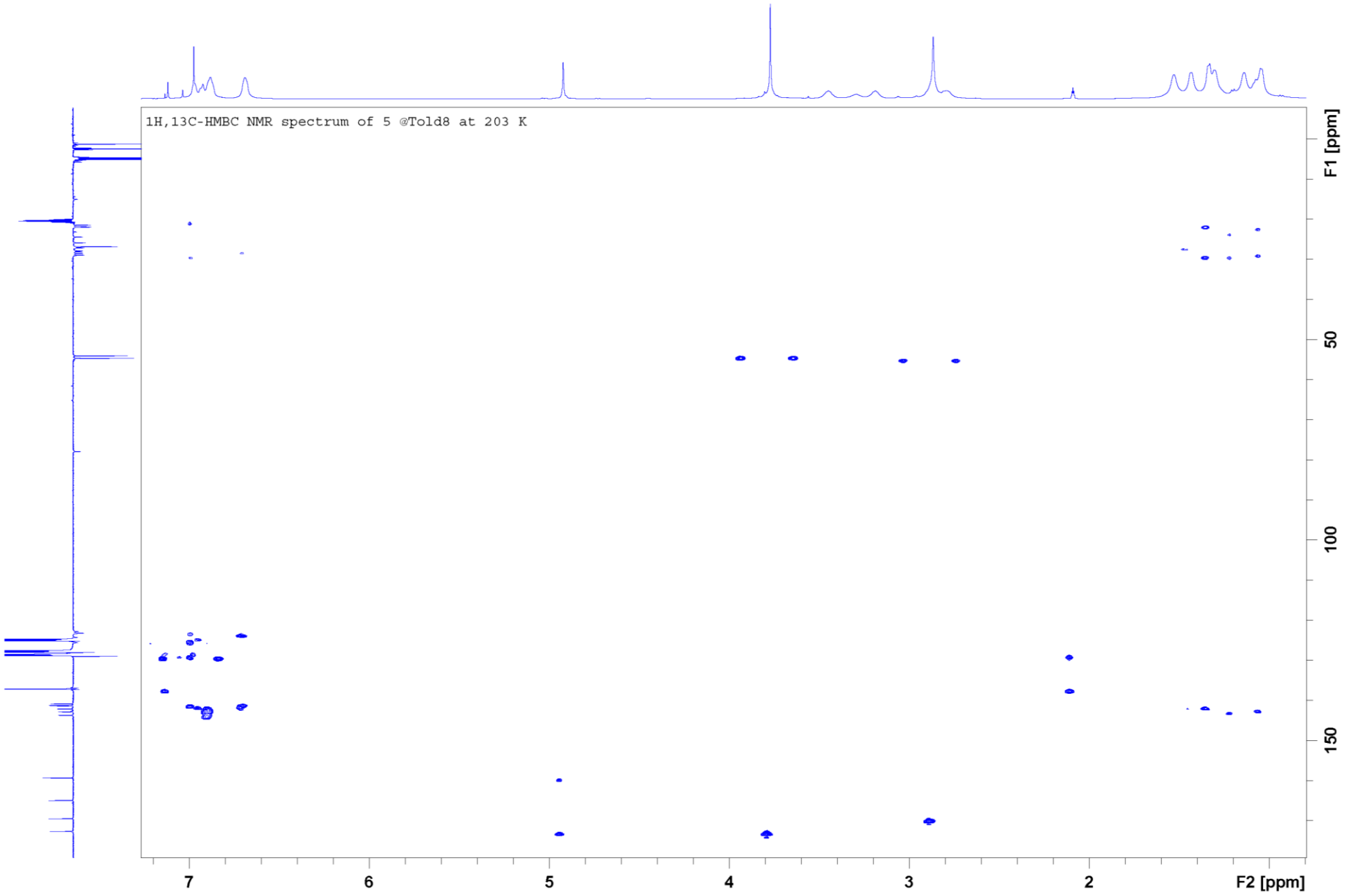

Figure S97. Detail of $^{1}H,^{13}C$-HMBC NMR spectrum of **5** in Tol-d_8, 203 K.

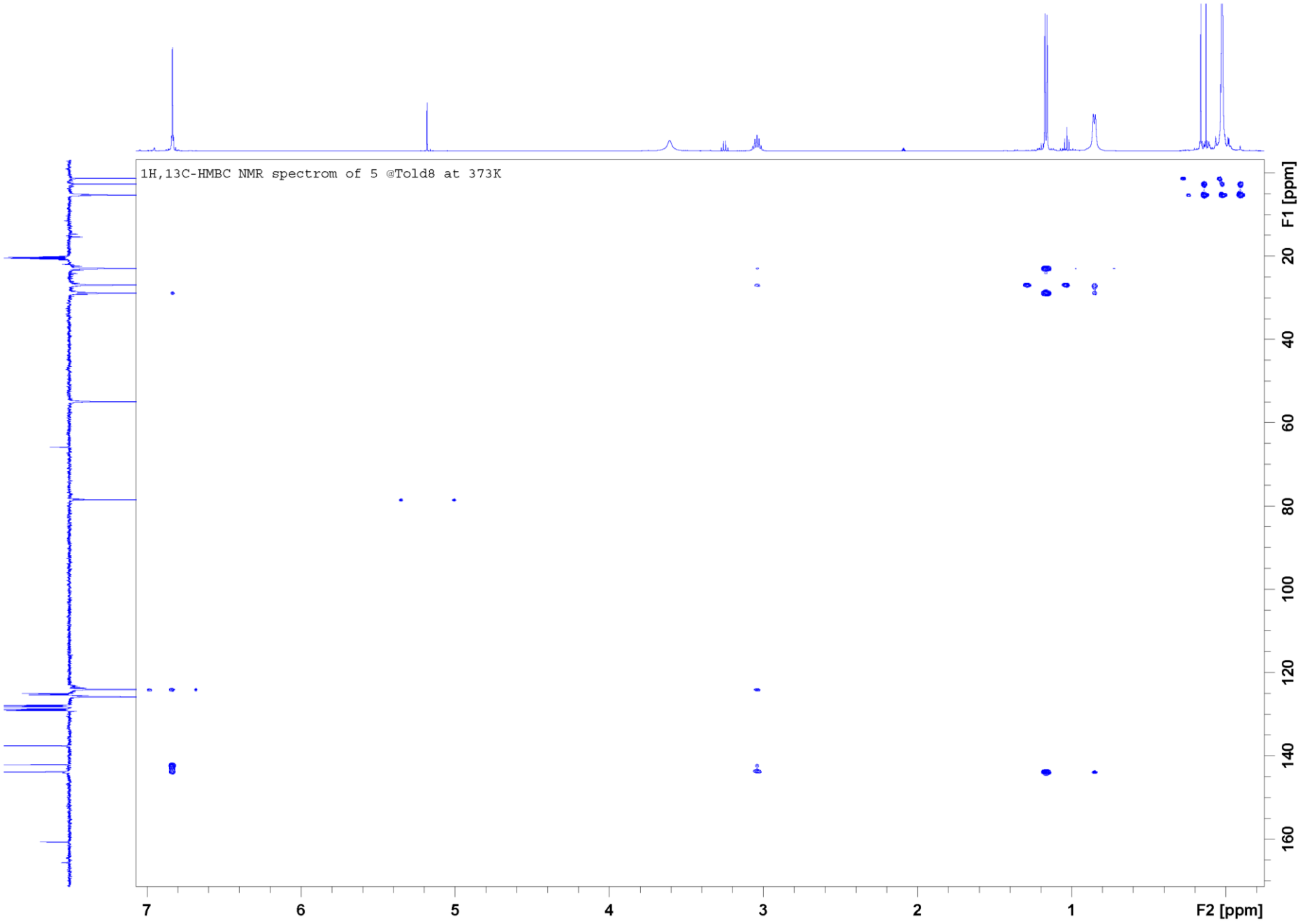

Figure S98. $^{1}H,^{13}C$-HMBC NMR spectrum of **5** in Tol-d_8, 373 K.

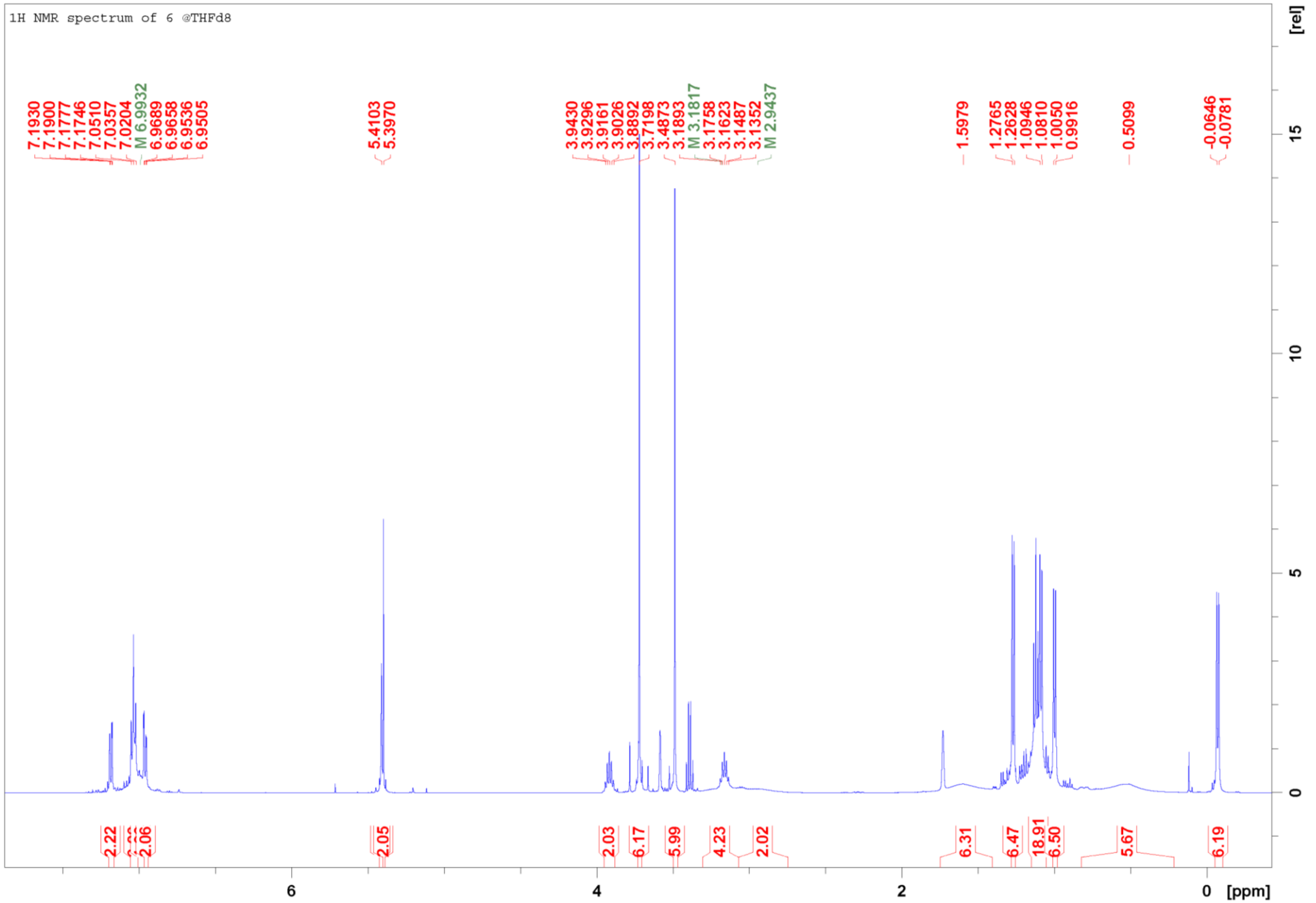

Figure S99. ^{1}H NMR spectrum of **6** in THF-d_8, 295 K.

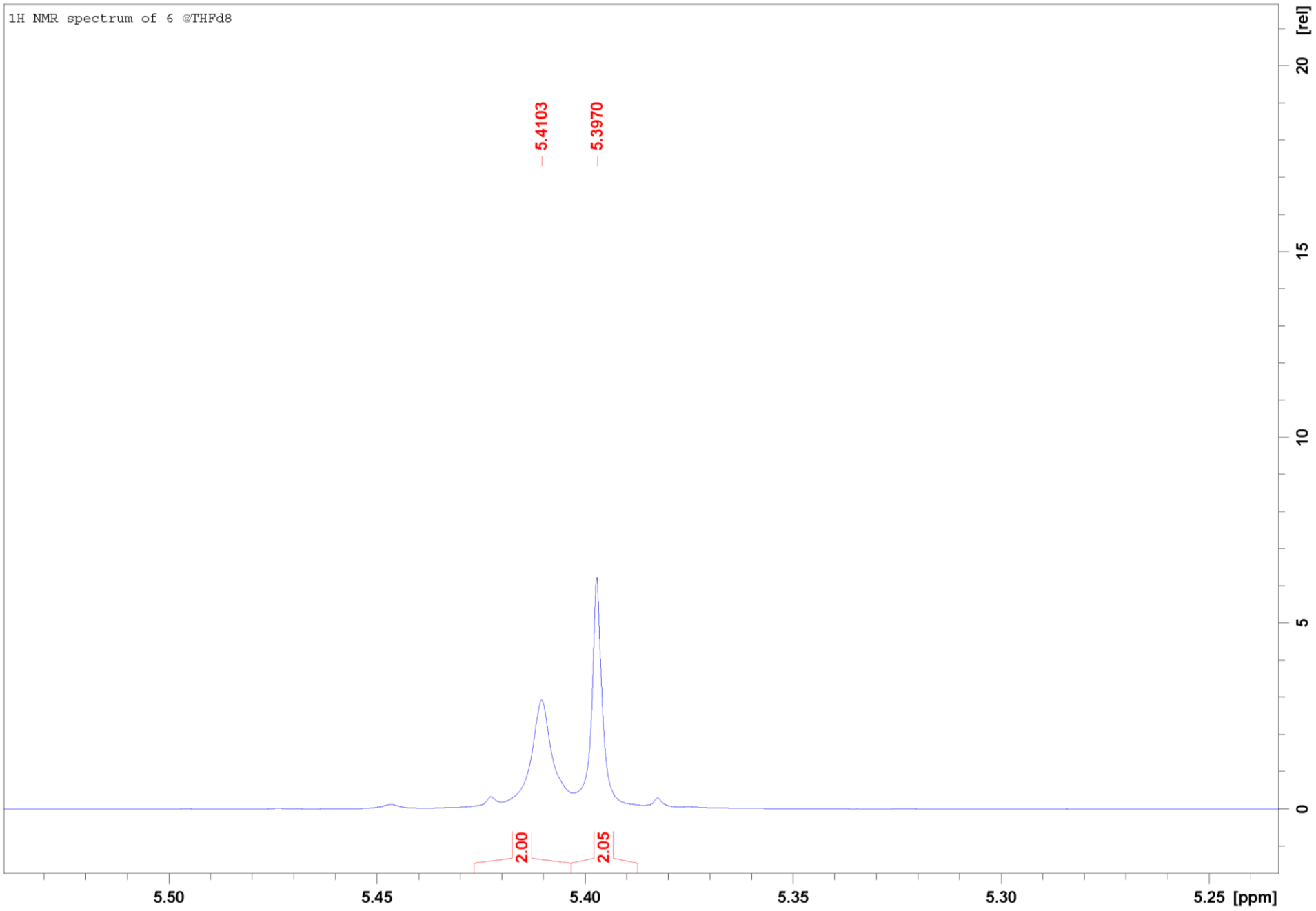

Figure S100. Detail of ^{1}H NMR spectrum of **6** in THF-d_8, 295 K.

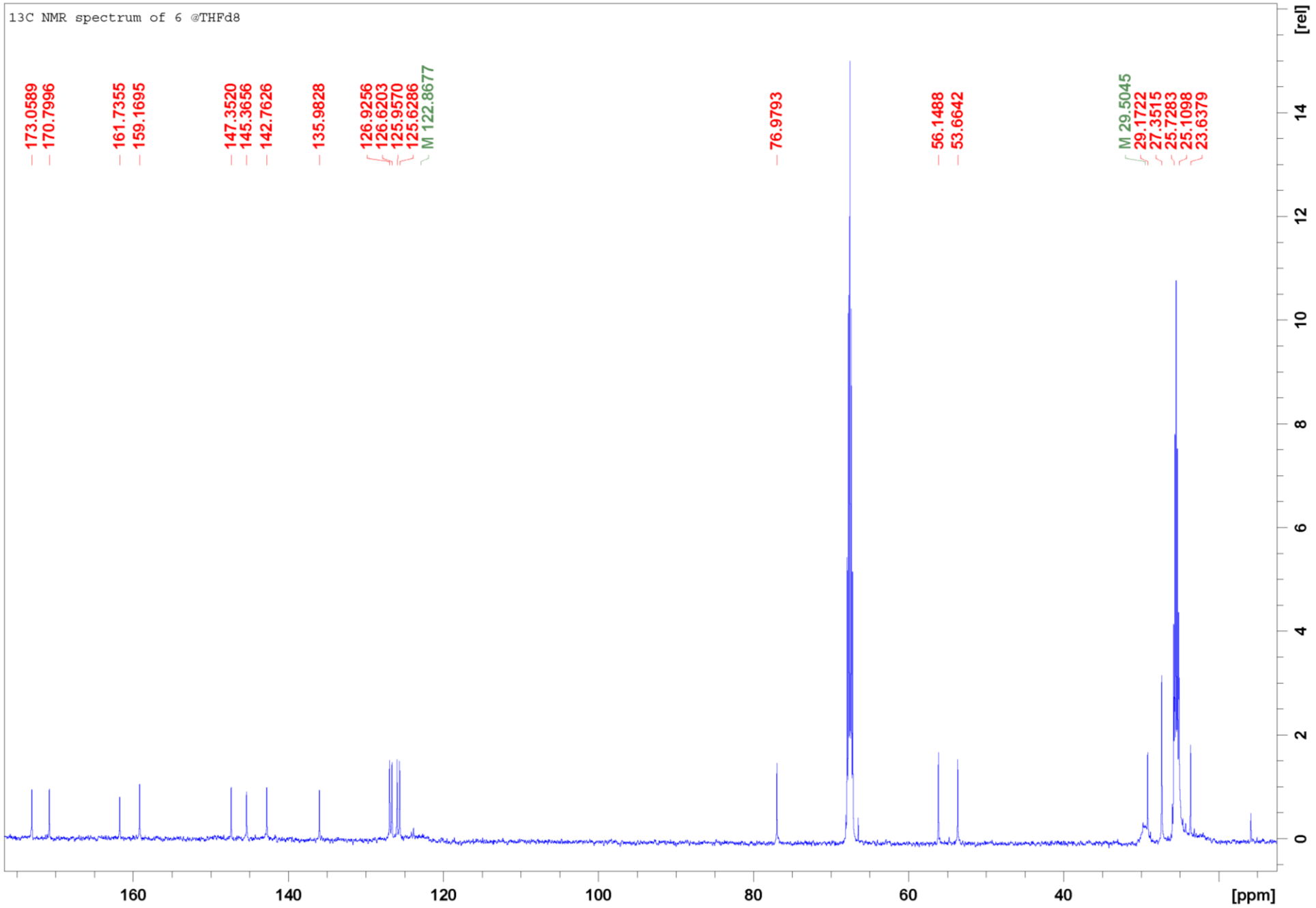

Figure S101. ^{13}C NMR spectrum of **6** in THF-d_8, 295 K.

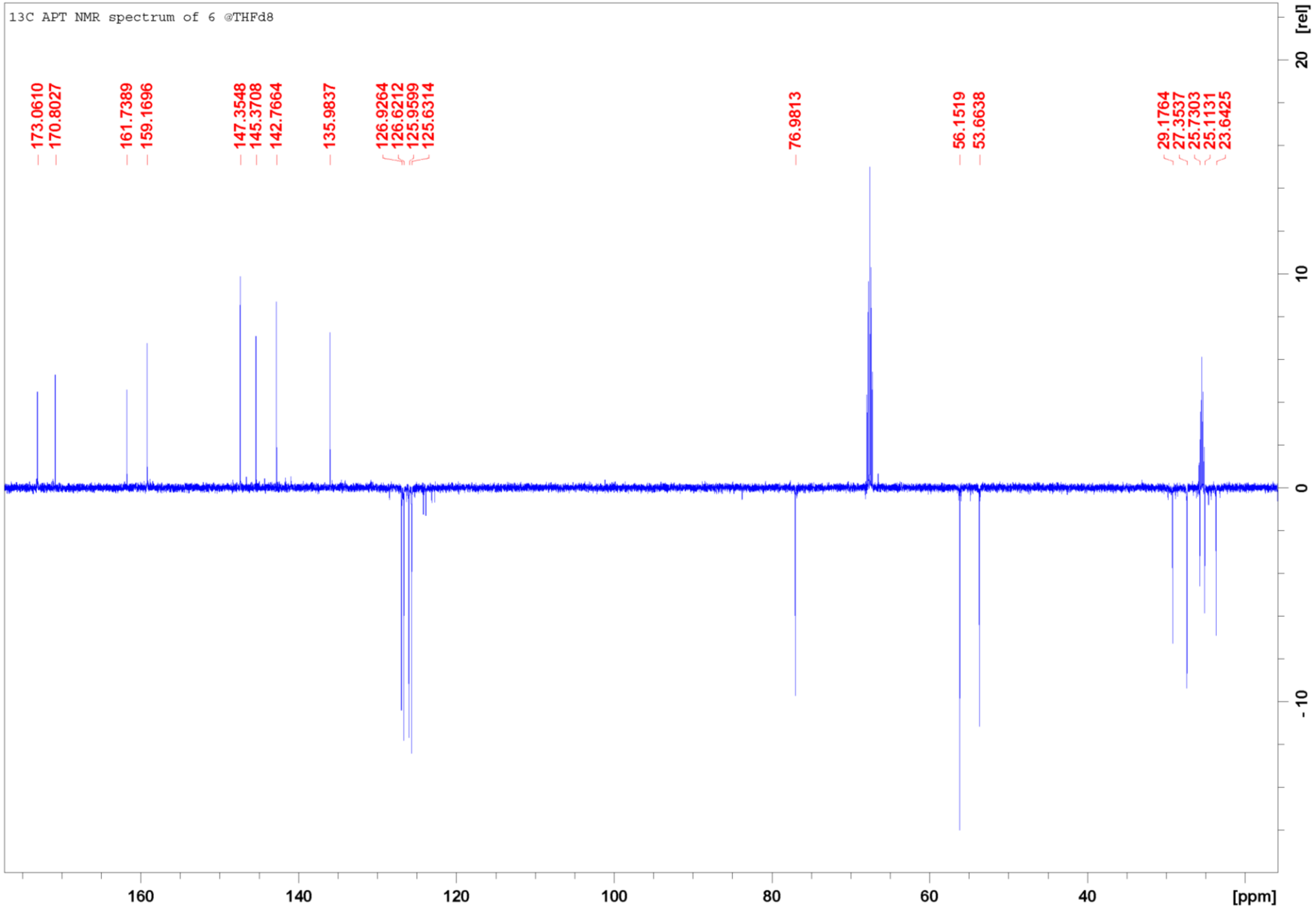

Figure S102. ^{13}C APT NMR spectrum of **6** in THF-d_8, 295 K.

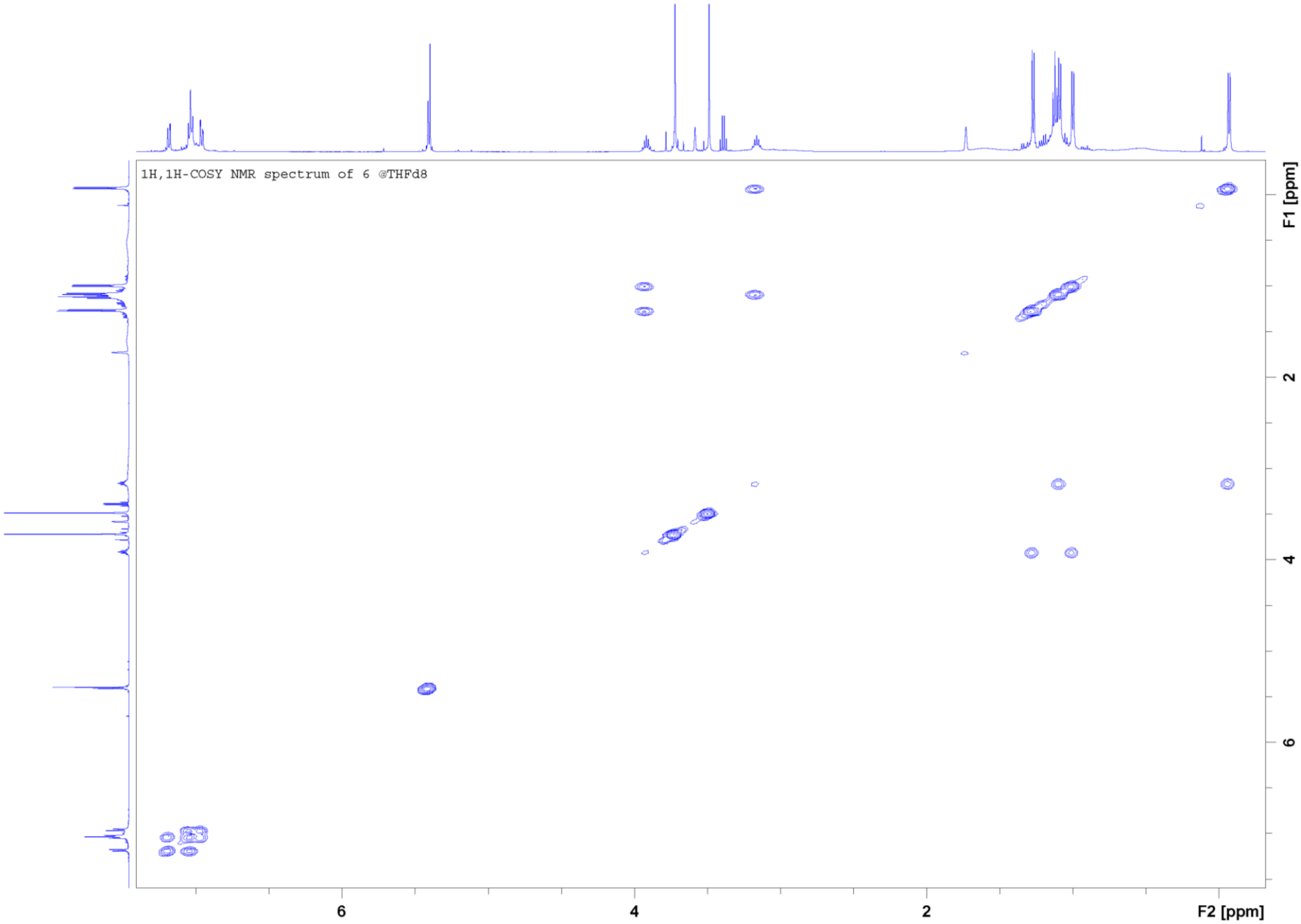

Figure S103. $^{1}H,^{1}H$-COSY NMR spectrum of **6** in THF-d_8, 295 K.

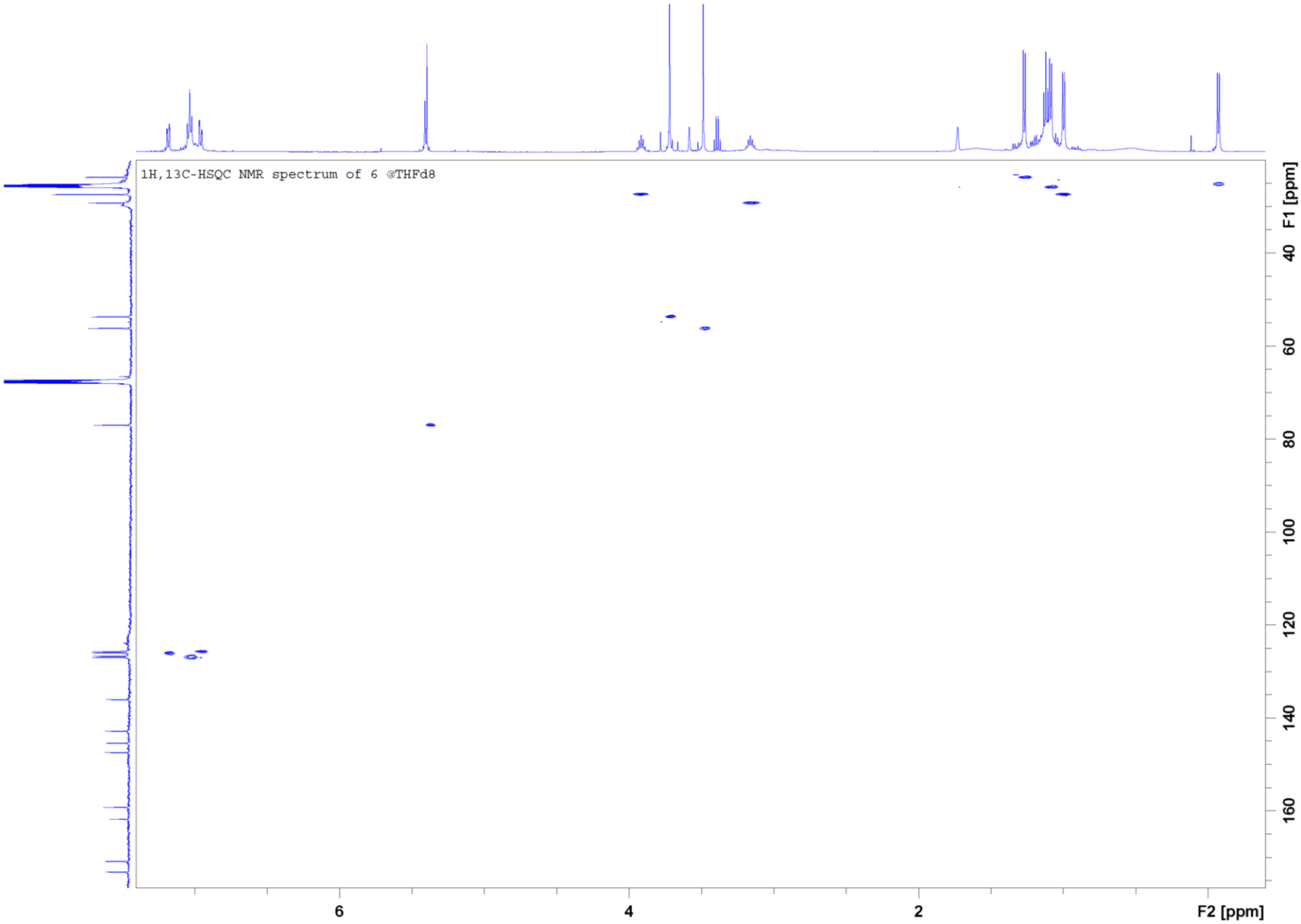

Figure S104. $^{1}H,^{13}C$-HSQC NMR spectrum of **6** in THF-d_8, 295 K.

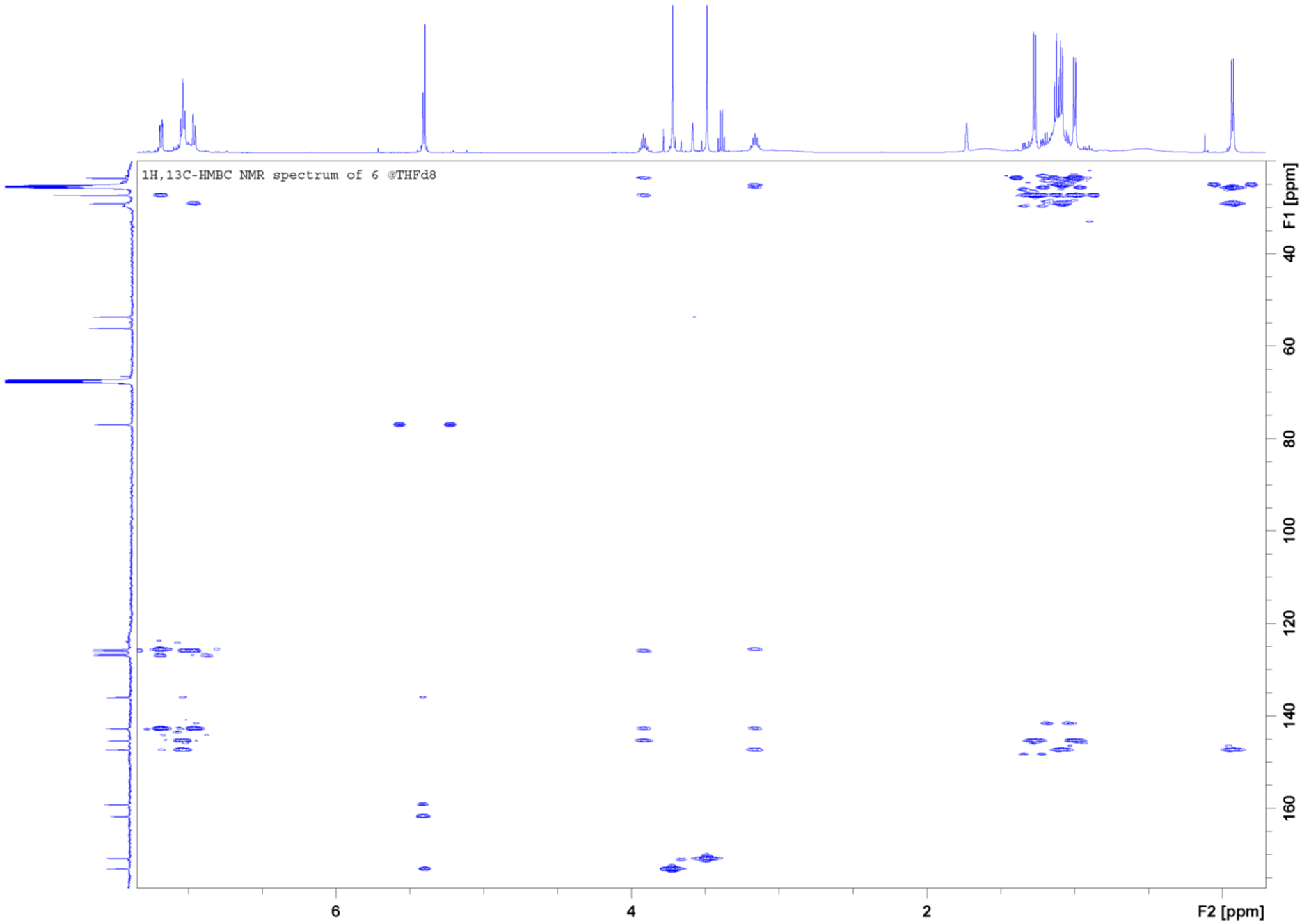

Figure S105. $^{1}H,^{13}C$-HMBC NMR spectrum of **6** in THF-d_8, 295 K.

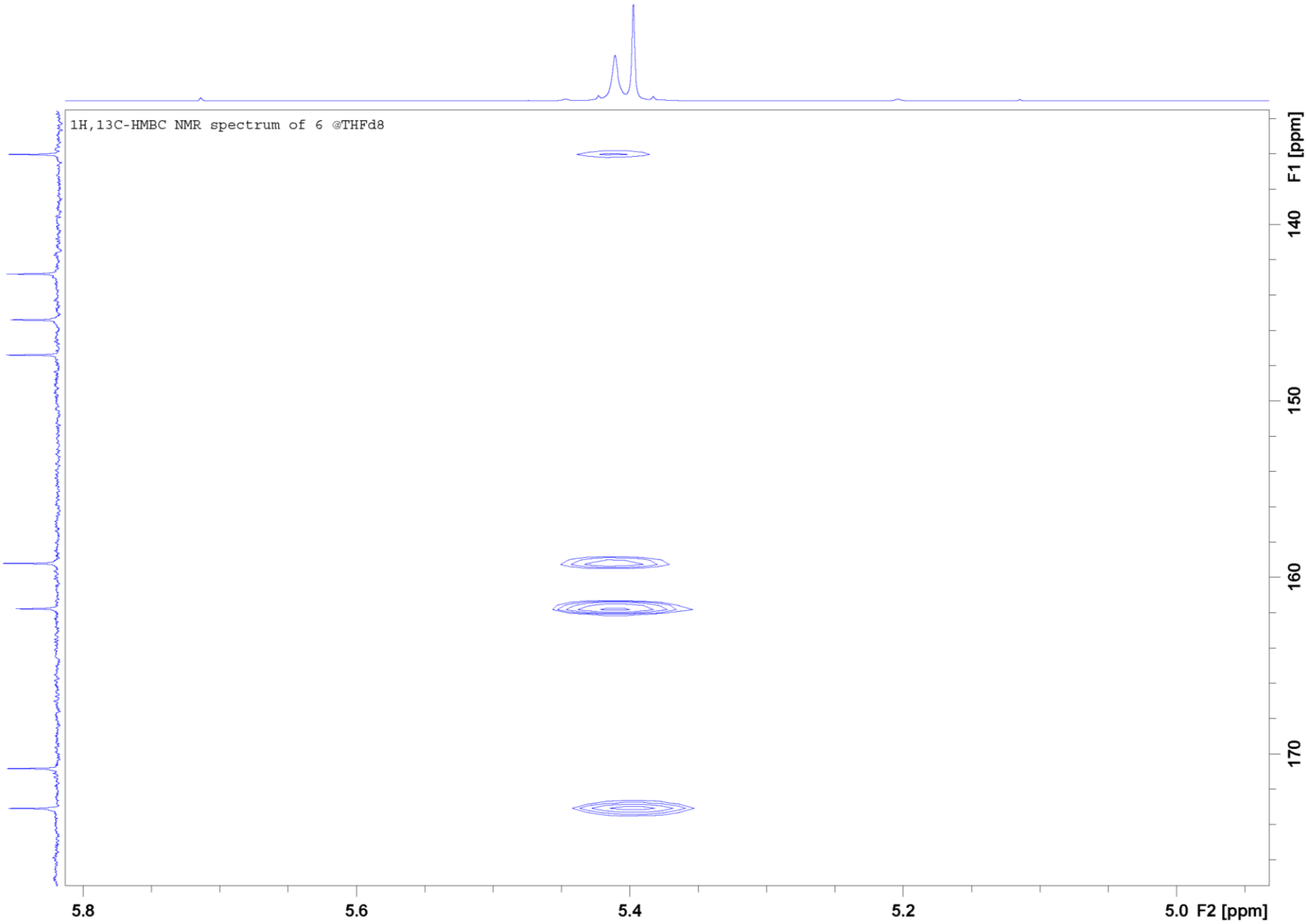

Figure S106. Detail of $^{1}H,^{13}C$-HMBC NMR spectrum of **6** in THF-d_8, 295 K.

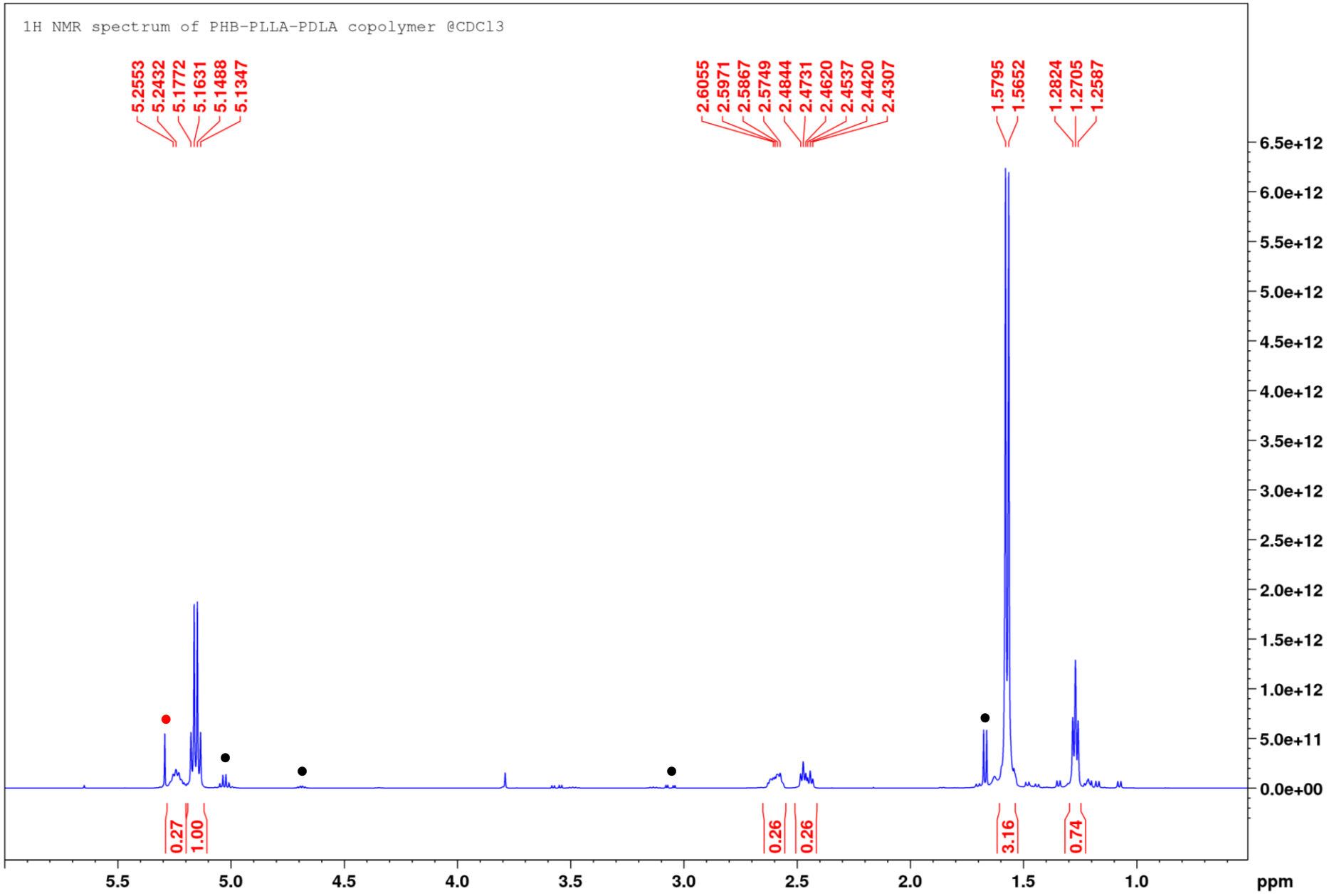

Figure S107. ^{1}H NMR spectrum of **PHB-*b*-PLLA-*b*-PDLA** copolymer (Table 2, entry 6) (crude reaction mixture) in $CDCl_3$, 295 K. Trace signals of CH_2Cl_2 (●) and unreacted monomers (●) are marked.

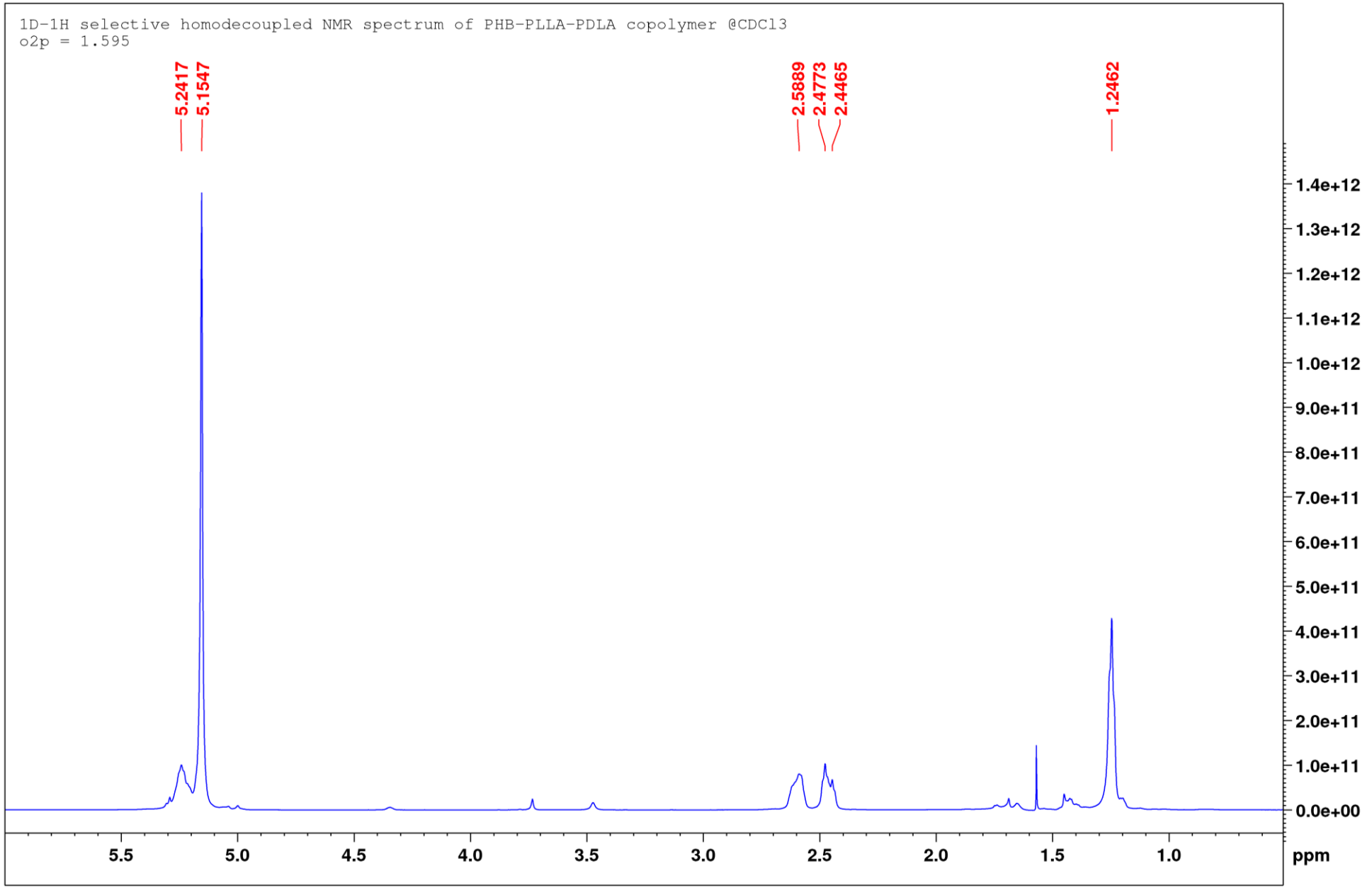

Figure S108. 1D-^{1}H selective homodecoupled NMR spectrum of **PHB-*b*-PLLA-*b*-PDLA** copolymer (Table 2, entry 6) (crude reaction mixture) in $CDCl_3$, 295 K.

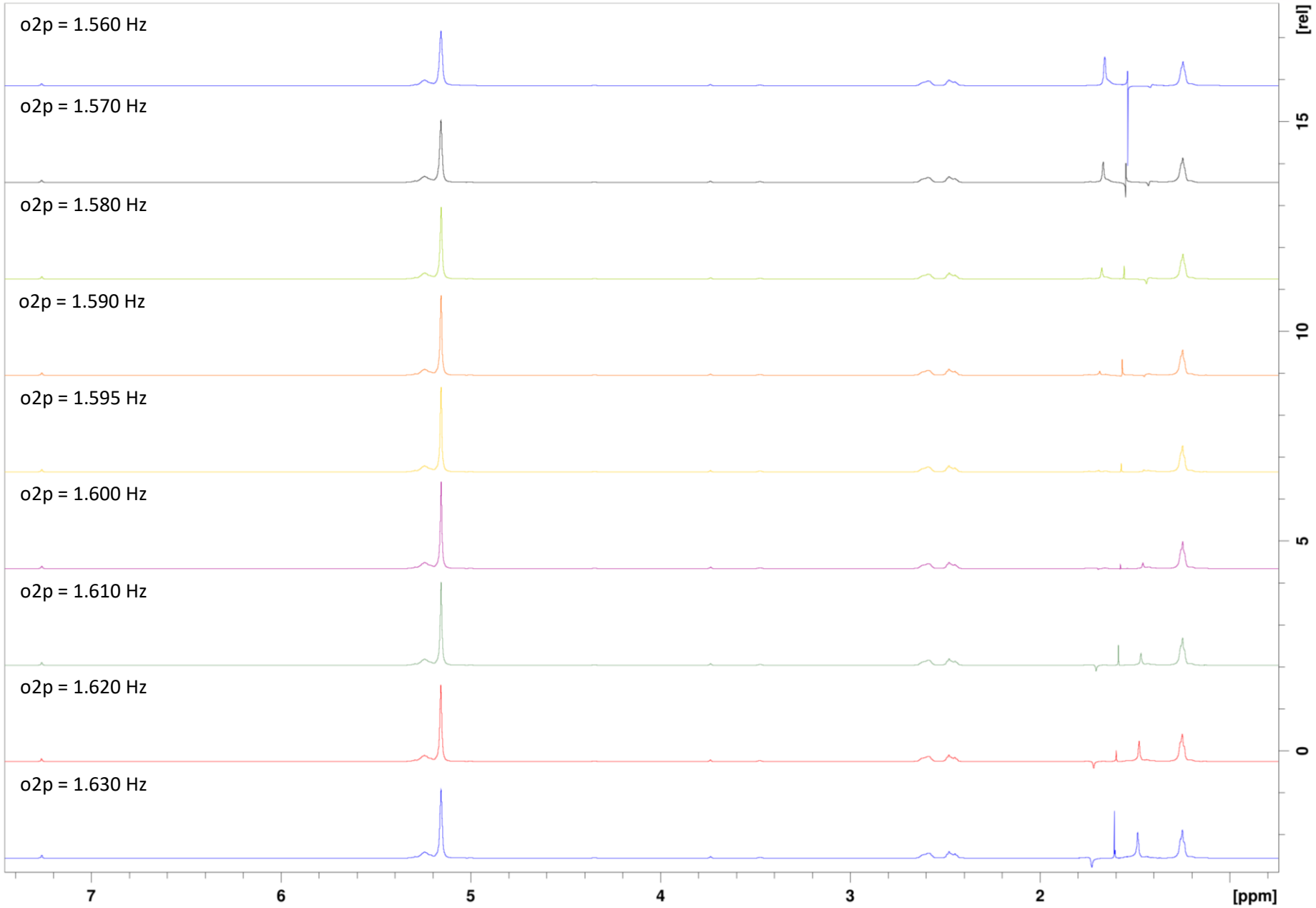

Figure S109. Stacked view of 1D-^{1}H selective homodecoupled NMR spectra of **PHB-*b*-PLLA-*b*-PDLA** copolymer (Table 2, entry 6) (crude reaction mixture) in $CDCl_3$, 295 K, with various o2p parameters.

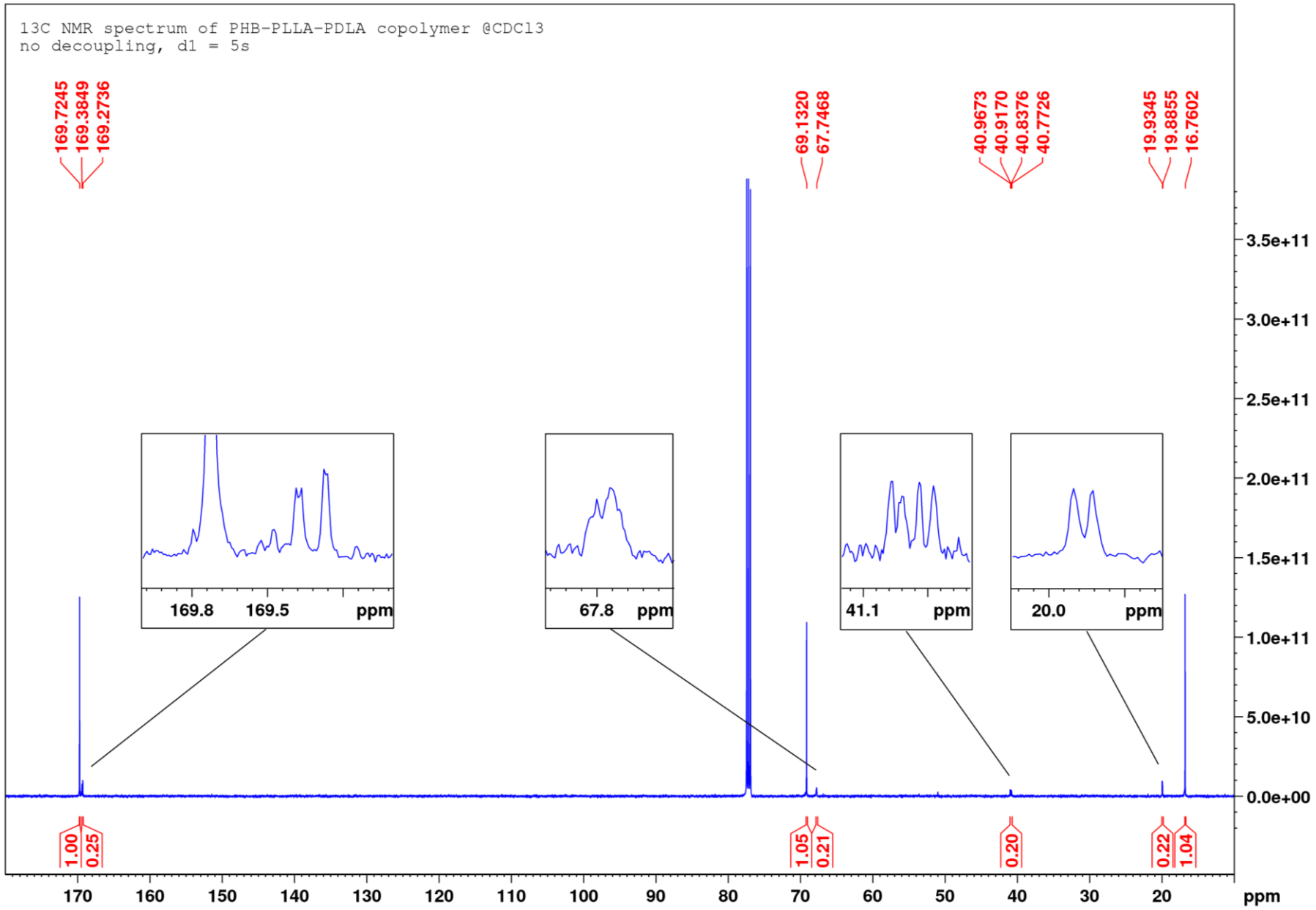

Figure S110. ^{13}C non-decoupled NMR spectrum of **PHB-*b*-PLLA-*b*-PDLA** copolymer (Table 2, entry 6) (crude reaction mixture) in $CDCl_3$, 295 K, with detailed view of multiplets belonging to the PHB part of polymeric chain.

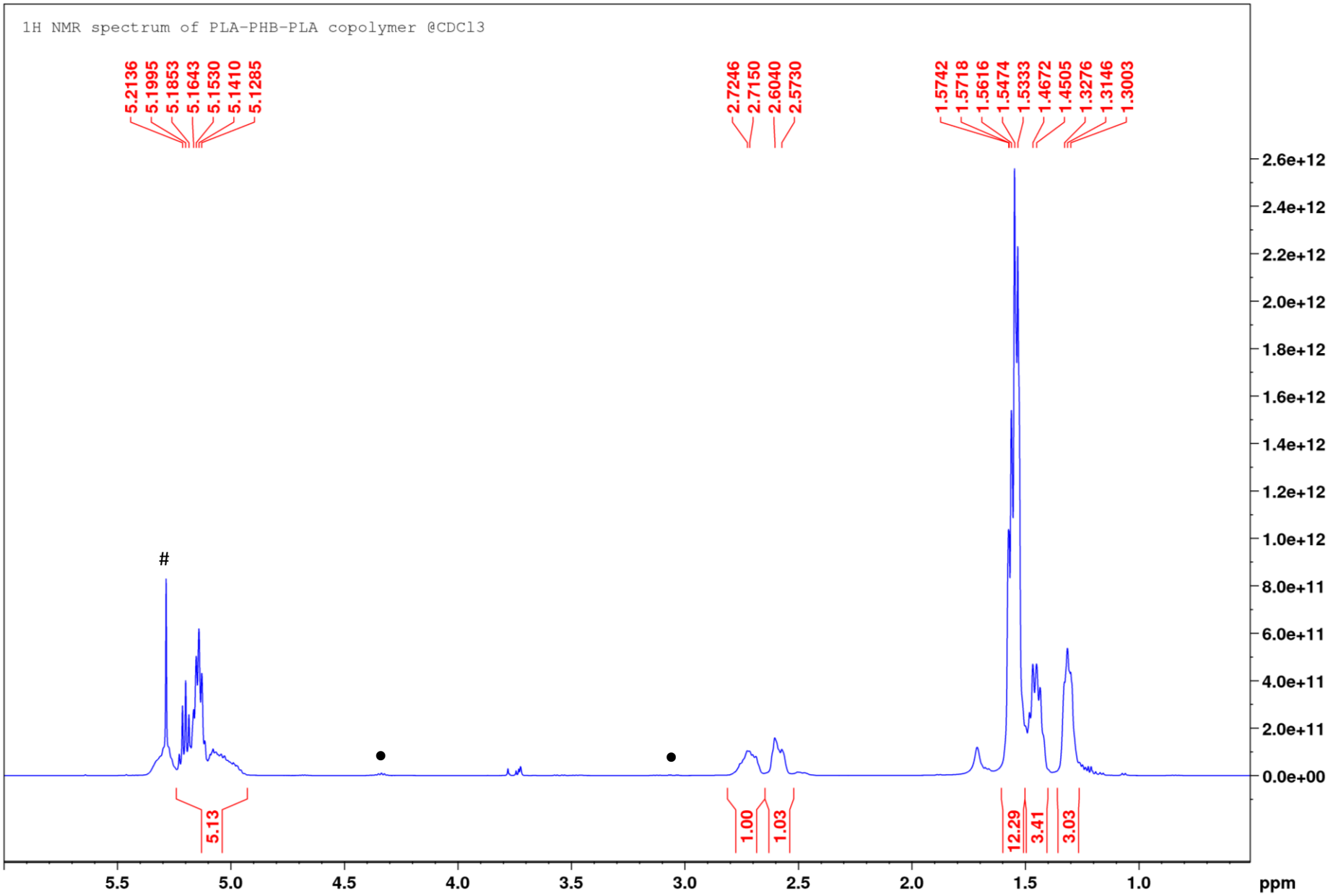

Figure S111. ^{1}H NMR spectrum of **PLA-*b*-PHB-*b*-PLA** copolymer (Table 2, entry 7) (crude reaction mixture) in $CDCl_3$, 295 K. Trace signals of CH_2Cl_2 (#) and unreacted monomers (●) are marked.

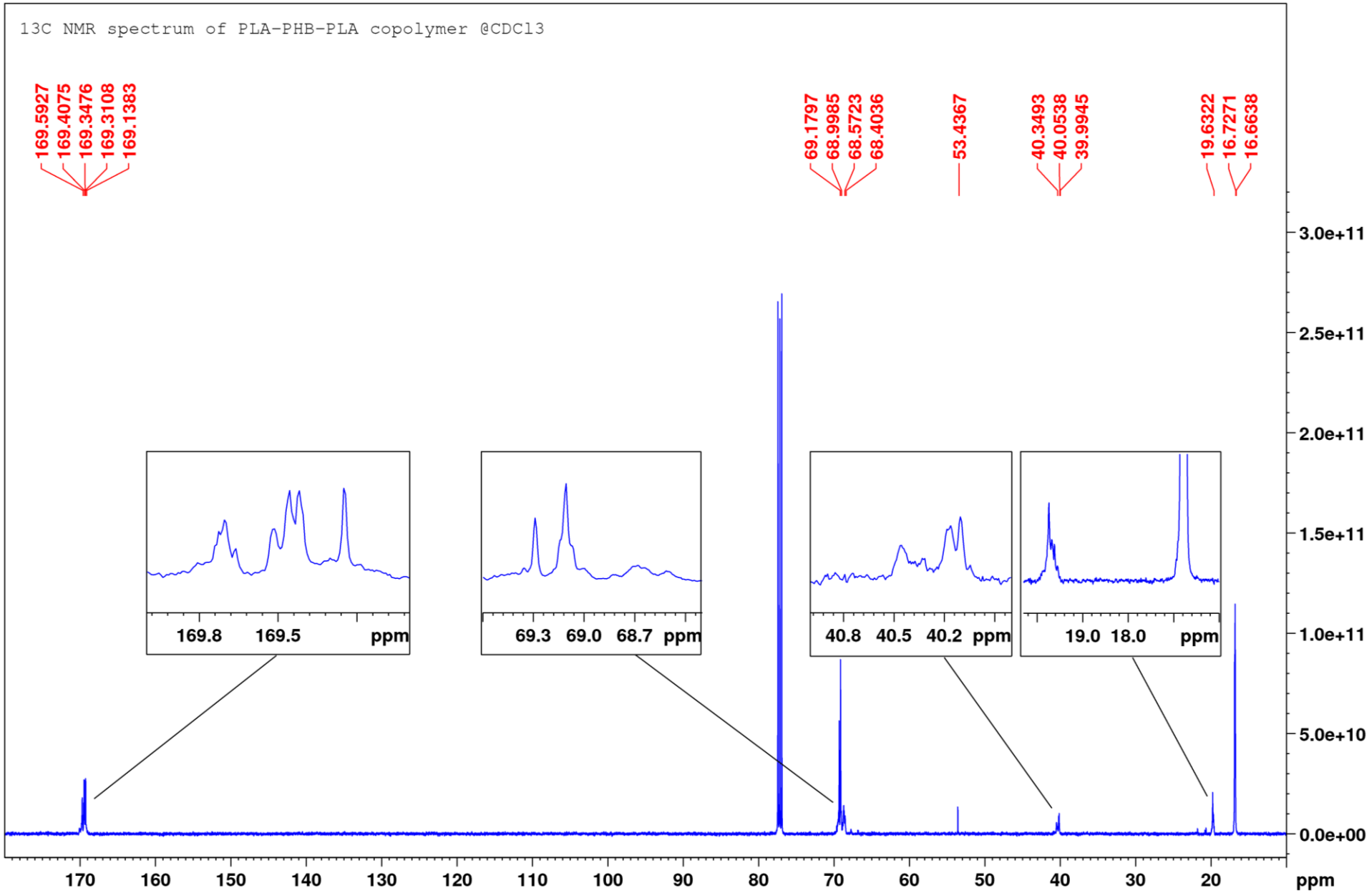

Figure S112. ^{13}C non-decoupled NMR spectrum of **PLA-*b*-PHB-*b*-PLA** copolymer (Table 2, entry 7) (crude reaction mixture) in $CDCl_3$, 295 K, with detailed view of multiplets belonging to the PHB part of polymeric chain.

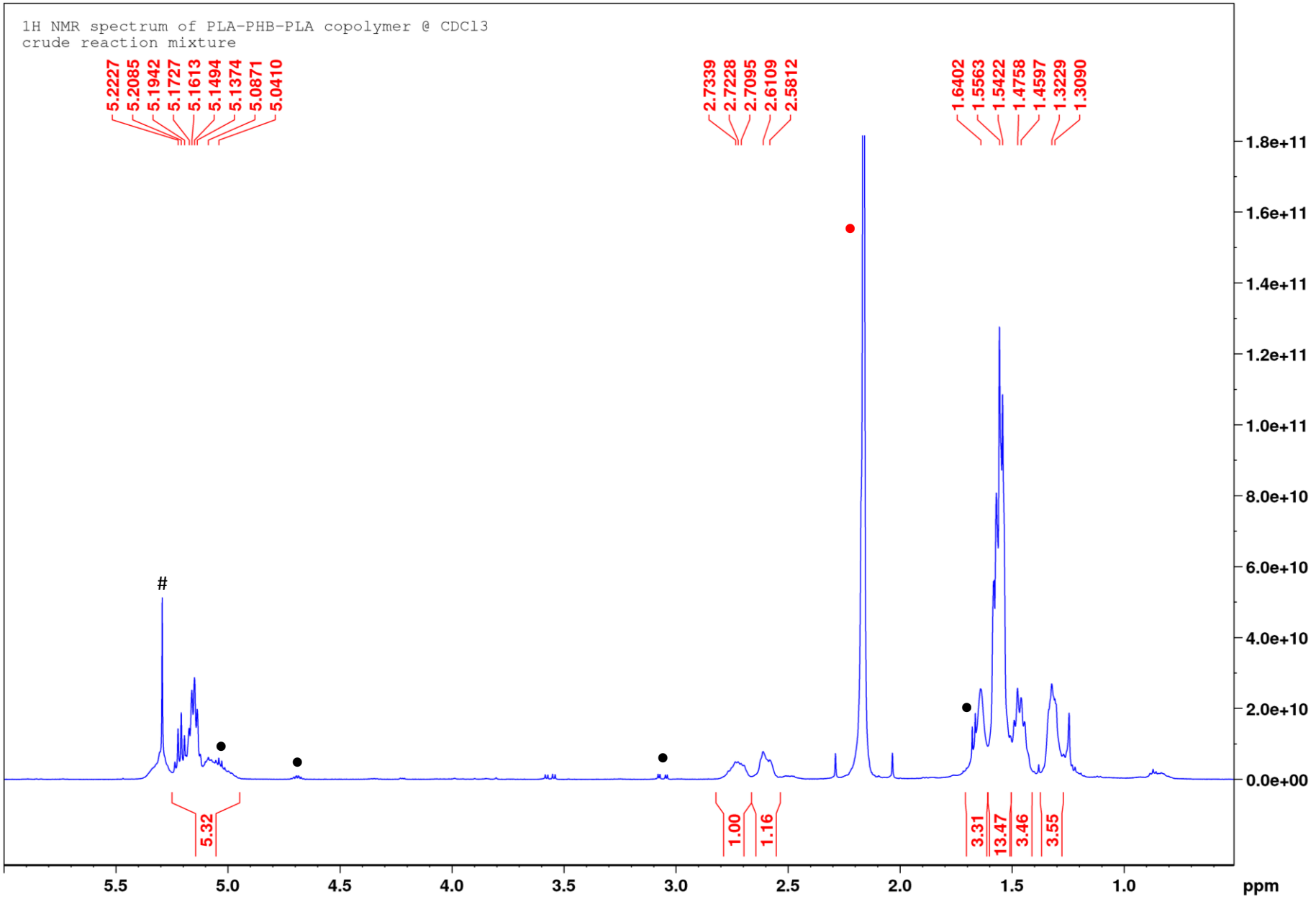

Figure S113. ^{1}H NMR spectrum of **PLA-*b*-PHB-*b*-PLA** copolymer (Table 2, entry 8) (crude reaction mixture) in$CDCl_3$, 295 K. Trace signals of CH_2Cl_2 (#), acetone (●) and unreacted monomers (●) are marked.